SEPTEMBER 2018 Ph. D. in Mechanical Engineering AYTAÇ ŞANLISOY

UNIVERSITY OF GAZIANTEP

GRADUATE SCHOOL OF

NATURAL & APPLIED SCIENCES

AN EXPERIMENTAL INVESTIGATION ON DESIGN AND PERFORMANCE OF PLASMA GASIFICATION SYSTEMS

Ph. D. THESIS

IN

MECHANICAL ENGINEERING

AYTAÇ ŞANLISOY

SEPTEMBER 2018

An Experimental Investigation on Design and Performance of Plasma Gasification Systems

Ph.D. Thesis

in

Mechanical Engineering

University of Gaziantep

Supervisor

Prof. Dr. Melda Özdinç ÇARPINLIOĞLU

by

Aytaç ŞANLISOY

September 2018

REPUBLIC OF TURKEY

UNIVERSITY OF GAZİANTEP

GRADUATE SCHOOL OF NATURAL & APPLIED SCIENCES

DEPARTMENT OF MECHANICAL ENGINEERING

Title of the thesis: An Experımental Investigation on Design and Performance of Plasma Gasification Systems

Name of the student: Aytaç ŞANLISOY

Exam date: September 27th, 2018

Approval of the Graduate School of Natural and Applied Sciences.

Prof. Dr. Ahmet Necmeddin YAZICI

Director

I certify that this thesis satisfies all the requirements as a thesis for the degree of Doctor of Philosophy.

Prof. Dr. M. Sait SÖYLEMEZ

Head of Department

This is to certify that I have read this thesis and that in my opinion it is fully adequate, in scope and quality, as a thesis for the degree of Doctor of Philosophy.

Prof. Dr. Melda Özdinç ÇARPINLIOĞLU

Supervisor

This is to certify that we have read this thesis and that in our consensus opinion it is fully adequate, in scope and quality, as a thesis for the degree of Doctor of Philosophy.

Examining Committee Members:	Signature
Prof. Dr. Beşir ŞAHİN	…………………..
Prof. Dr. Zafer DURSUNKAYA	…………………..
Prof. Dr. Melda Özdinç ÇARPINLIOĞLU	…………………..
Prof. Dr. Veysel ÖZCEYHAN	…………………..
Assoc. Prof. Dr. Emrah ÖZAHİ	…………………..

I hereby declare that all information in this document has been obtained and presented in accordance with academic rules and ethical conduct. I also declare that, as required by these rules and conduct, I have fully cited and referenced all material and results that are not original to this work.

Aytaç ŞANLISOY

ABSTRACT

AN EXPERIMENTAL INVESTIGATION ON DESIGN AND PERFORMANCE OF PLASMA GASIFICATION SYSTEMS

ŞANLISOY, Aytaç

Ph. D. in Mechanical Engineering

Supervisor: Prof. Dr. Melda Özdinç ÇARPINLIOĞLU

September 2018

261 pages

Syngas is produced through gasification of solid fuels. It includes carbonmonoxide (CO), carbondioxide (CO_2), hydrogen (H_2), methane (CH_4) and low amount of hydrocarbon depending on the system operation conditions. In this study, gasification of solid fuels at various flow rate and plasma power by microwave plasma gasification is investigated. All the parameters; temperature, mass and content of syngas, fuel and ash, are measured and the comprehensive thermodynamic analysis of the process are carried out. The MCw gasifier consists of plasma generation system, gasification reactor, fuel-fluid supply system, process output (ash) collection system and measurement/data acquisition chain. The gasification of solid fuels; Russian, South African and Şırnak (Turkey) coals, pine tree and hornbeam sawdust and polyethylene is processed by MCw gasifier. The plasma gasification medium is formed of air and the air flow rate varies between 50 and 100 sL/min, the plasma power varies between 3 kW and 6 kW. According to the experimental results, the syngas temperature alters between 621 °C and 1276 °C. The syngas production varies between 0.66 kg and 1.2 kg. The process energy efficiency (η_{EP}) ranges from 30.8 % to 86.04 %. The system energy efficiency (η_{ES}) changes from 20.6 % to 61.37 %.

Key words: microwave plasma, plasma gasification, coal gasification, waste disposal, syngas, thermodynamic analysis

ÖZET

PLAZMA GAZLAŞTIRMA SİSTEMLERİNİN TASARIM VE PERFORMANSI ÜZERİNE DENEYSEL ARAŞTIRMA

ŞANLISOY, Aytaç

Doktora Tezi, Makine Mühendisliği

Tez Yöneticisi: Prof. Dr. Melda Özdinç ÇARPINLIOĞLU

Eylül 2018

261 sayfa

Katı yakıtların gazlaştırılması ile sentez gaz üretilmektedir. Sentez gazı sistem çalışma şartlarına bağlı olarak karbonmonoksit (CO), karbondioksit (CO_2), hidrojen (H_2), metan (CH_4) ve düşük miktarda hidrokarbonlar içermektedir. Bu çalışmada, mikrodalga plazma gazlaştırma ile katı yakıtların farklı hava debisi ve plazma gücünde ele alarak gazlaştırılması incelenmektedir. Proses parametreleri; sıcaklık, sentez gazı, yakıt ve kül kütlesi, sentez gazı içeriği, yakıt içeriği, kül içeriği ölçülmektedir ve prosesin kapsamlı termodinamik analizi gerçekleştirilmektedir. Katı yakıtların enerji dönüşümünü esas alan MCw gazlaştırıcı; plazma üretim sistemi, gazlaştırma reaktörü, yakıt-akışkan besleme sistemi, proses çıktıları (kül) toplama sistemi ve ölçümleme-veri toplama sistemlerinden oluşmaktadır. MCw gazlaştırıcı ile gürgen ve çam talaşı, Şırnak-Türkiye, Rus ve Güney Afrika kömürü ve polietilen katı yakıtlarının gazlaştırılması gerçekleştirilmiştir. Plazma gazlaşma ortamı hava ile oluşturulmakta olup hava debisi 50 ile 100 sL/dak aralığında, plazma gücü ise 3 ile 6 kW aralığında değiştirilmiştir. Deney sonuçlarına göre, sentez gazı sıcaklığı 621 ℃ ile 1276 ℃ aralığında değişmektedir. Sentez gazı üretimi 0.66 kg ile 1.2 kg aralığında değişmektedir. Proses enerji verimliliği 30.8 % ile 86.04 % aralığında değişmektedir. Sistem enerji verimliliği 20.6 % ile 61.37 % aralığında değişmektedir.

Anahtar kelimeler: mikrodalga plazma, plazma gazlaştırma, kömür gazlaştırma ve atık imhası, sentez gazı, termodinamik analiz

To my family.

ACKNOWLEDGEMENTS

Firstly, I would like to express my sincere gratitude to my advisor Prof. Dr. Melda Özdinç ÇARPINLIOĞLU for the continuous support of my Ph.D study and related research, for her patience, motivation, and immense knowledge. Her guidance helped me in all the time of research and writing of this thesis. I feel honored to that I found opportunity to carry out Phd. Study under her supervision.

Besides my advisor, I would like to express my sincere appreciation to the members of my thesis committee: Prof. Dr. Beşir ŞAHİN and Assoc. Prof. Dr. Emrah ÖZAHİ for their insightful comments and encouragement during thesis period which incented me to widen my research from various perspectives.

My sincere thanks also goes to the Scientific and Technological Research Council of Turkey (TUBITAK) for the financial support under the contract number 115 M 389 that provided me to set up the laboratory and research facilities. Without their precious support it would not be possible to conduct this research.

I sincere thanks to laboratory technician; İbrahim KORKMAZ, graduate students; Halil Melez and Emirhan Tunçbilek, my fellow workmate Taha Tuna GÖKSU for the working together before deadlines, and for all the fun we have had in the last five years. In particular, I am grateful to Prof. Dr. Yahya Erkan AKANSU for enlightening me the first glance of research.

Last but not the least, I would like to thank my wife; Pavlina ŞANLIOY, my son; Adam ŞANLISOY, my father; İsmail ŞANLISOY, my mother; Müjgan ŞANLISOY and my brother; Ali Hayri ŞANLISOY for supporting me spiritually throughout writing this thesis and my life in general.

TABLE OF CONTENTS

LIST OF FIGURES

LIST OF TABLES

Page

LIST OF SYMBOLS AND ABBREVIATIONS

Alphanumeric Symbols

T: temperature

t: time

m: mass

$\dot{m}$: mass flow rate

n: mole number

$\dot{n}$: molar flow rate

W: plasma power

c_p: specific heat at constant pressure

$\bar{c}_p$: molar specific heat at constant pressure

c: specific heat of water

E: energy

h: specific enthalpy

s: specific entropy

$\bar{R}$: universal gas constant

R: gas constant

y: distance from axis of plasma applicator to any position in axis of reactor

h: height of the reactor (Including reactor head)

x: syngas mixture component

S: standard deviation

n: number of samples

x: variable

$\bar{x}$: mean of variable

U: total uncertainty

e1: correction parameter for sulphur

e2: correction parameter for heat resistance

$\dot{\forall}$: volumetric flow rate

M: molar weight

Greek Symbols

η: efficiency

β: coefficient

ρ: density

μ: population mean

$\boldsymbol{v}$: degree of freedom

Subscripts

syn: syngas

in: inlet

g: gasification

E: energy

EP: process energy

ES: system energy

HG: hot gas

CG: cold gas

CcE: carbon conversion efficiency

HcE: hydrogen conversion efficiency

Csyn: carbon in syngas

Cfuel: carbon in fuel

0: ambient state, reference state

ch: chemical

ph: physical

tot: total

i: i component of gas mixture

1: initial

2: final

Atm(s): standard atmosphere (sea level)

Abbreviations

CO: carbon monoxide

H_2: hydrogen

CO_2: carbon dioxide

H_2O: water

CH_4: methane

C: carbon

O: oxygen

H: hydrogen

N: nitrogen

S: sulphur

O_2: oxygen

N_2: nitrogen

C_XH_Y: hydrocarbon

ER: equivalence ratio

HHV: higher heating value

LHV: lower heating value

VSWR: voltage standing wave ratio

Max: maximum

SEM: scanning electron microscope

EDX: energy dispersive X-ray

WI: Wobbe index

RD: relative density

ASTM: American standard test method

ASME: American society of mechanical engineers

B: systematic error

R: random error

U: total uncertainty

CR: Russian coal

CTR: Şırnak (Turkey) coal

CSA: South African coal

PP: polyethylene

HSD: hornbeam sawdust

PSD: pine tree sawdust

M: moisture

VM: volatile matter

FC: fixed carbon

A: ash

P: pressure

V (%): volumetric based

n (%): molar based

m (%): mass based

CCP: content conversion performance

CcE: carbon conversion efficiency

ChE: hydrogen conversion efficiency

H_q: hydrogen quality

MSW: municipal solid waste

CHAPTER I

INTRODUCTION

A variety of materials in the world are processed and used for human needs since the start of industrialization. Despite some of the mass converted into the desired form, the rest is released to the environment as waste. In recent years the recovery from the waste has become significant because of the limited materials in nature and increasing amounts of waste due to increase in the population of the world. Furthermore the available energy demand increased rapidly by the technological developments and the improvements in human comfort. As a result, the necessity of efficient consumption of both the desired forms of mass and energy and high performance recovery make an interest to the scientific community and forced them to investigate and develop new processes for waste management. An unconventional method which is found in plasma gasification systems can be used to convert the waste into an efficient energy form. It utilizes the conversion of a variety of so-called fuels such as industrial, medical or municipal waste types, low grade coals, type of biomasses into syngas which includes mainly CO, H_2 and CO_2. The produced syngas can be used as fuel in combustion systems, for the generation of electricity and for the production of hydrogen.

MCw Gasifier- atmospheric microwave plasma gasifier design, operation and performance characteristics are experimentally investigated in this study. MCw Gasifier is designed and built in Gaziantep University Mechanical Engineering- Fluid Mechanics Laboratory. The operational and proses performance parameters are examined in the lab scaled MCw gasifier. The study is supported by TUBITAK under project number 115 M389. The author of the thesis is the project scholar and the thesis study is performed under the frame of TUBITAK 115 M 389 project (Interim reports (Çarpınlıoğlu and Şanlısoy, 2017; Çarpınlıoğlu and Şanlısoy, 2017; Çarpınlıoğlu and Şanlısoy, 2018)).

MCw GASIFIER is a lab scaled facility which was used to gasify sample fuels such as sawdust, varied graded coals and polyethylene by microwave plasma. As a result of gasification, syngas was produced. Based on syngas temperature, syngas composition and remainder of ash, the waste to energy conversion characteristics are examined at varied power and air flow conditions.

The thesis consists of 7 main chapters which are the introduction, literature review, design construction and calibration of MCw gasifier, fuel characterization, gasification process evaluation, thermodynamic analysis and conclusions. In literature review chapter, recent studies on microwave plasma gasification are given. The definition of thermochemical process, the types of thermochemical processes, gasification process and types of gasification processes, plasma and types of plasma are given. The operation and performance parameters are introduced. The gasification fuel characteristics are also examined. In the design, construction and calibration of MCw gasifier chapter, design and construction details are given and the fundamentals of experimentation are explained. Operating conditions are presented. In the fuel characterization chapter, physical and chemical properties of gasified fuels are examined by proximate and ultimate analysis. The heating value of the fuels are determined. Scanning electron microscope (SEM) and energy dispersive X-ray analyses of the fuels are also performed. In the gasification process evaluation chapter, the amount of produced syngas and ash outputs are presented. The temperature distribution in the reactor, the syngas temperature and the change of temperature are presented at varied plasma powers and air flow rates. The produced syngas content at varied plasma powers, air flow rate and fuels are given. The content of ash is examined by EDX analysis and the content of ash is presented. In the thermodynamic analysis chapter, the performance evaluation parameters; content conversion performance of syngas, ash and hydrogen are defined. Also the hydrogen quality term is introduced. The process, system energy efficiency and hot gas efficiency terms are described for the plasma gasification systems. According to the defined terms, the plasma gasification system is evaluated for the varied fuels, plasma power and air flow rate. In the conclusion chapter, the general conclusions obtained from the experimental study are given.

CHAPTER II

LITERATURE REVIEW

In this chapter, the definition of thermochemical processes and the classification of gasification systems are given. Operation and performance parameters are introduced. Gasification process sequences are defined. In the following section, the plasma is defined, plasma types are classified depending on temperature and thermal equilibrium. In addition, plasma production methods are explained. Thermal plasma gasification systems which are used for the gasification are given as literature survey. In the last subsection, the solid fuel properties and the literature about the fuels are given.

2.1 Definition and classification of gasification process

Gasification is defined as partial oxidization of the material into its elements in case of less than stoichiometric amount of oxidant medium and high temperatures. As a result of the process, syngas is produced which mainly consists of CO, H_2 and CH_4 (Gray, 2014). Syngas content can vary depending on various parameters such as the particle size, supply gas type and flow rate, residence time, type of gasification fuel (material), type of method and etc. Gasification is a thermochemical process. Thermochemical process can be classified as combustion, gasification and pyrolysis as shown in Figure 2.1. The schematic presentation of the thermochemical processes is given in Figure 2.2. (Knoef, 2005).

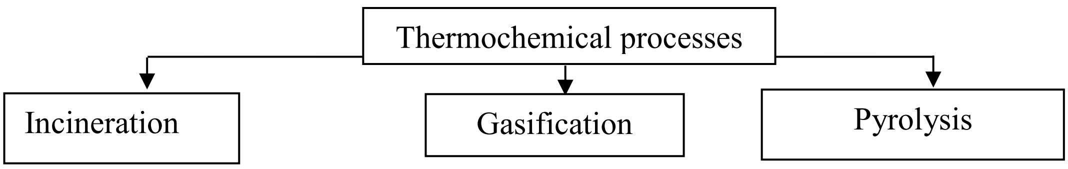

Figure 2.1 Classification of thermochemical processes

2.1.1 Incineration

In incineration process, the materials decompose into their elements in medium where there is stoichiometric or excess amount of oxidant and at high temperature. The process occurs in a temperature range of 850 to 1250°C and generally at atmospheric pressures. Reactant gas is generally air. The main products are CO_2 and H_2O.

2.1.2 Pyrolysis

In this process, the materials decompose into their elements in the absence of oxidant at high temperature. It takes place in the temperature range of 500 to 800°C at atmospheric pressures or over-atmospheric pressures. The products mainly consist of CO, H_2 and CH_4.

2.1.3 Gasification

In gasification process, the materials decompose into their elements in the medium where there is less than stoichiometric amount of oxidant at high temperature. The oxidant can be air, steam, oxygen, nitrogen and etc. The reaction occurs in a temperature range of 550 to 1600°C at varied pressures. As a result of the process, the syngas is produced. The products are mainly consisted of CO, H_2 and CH_4 in syngas.

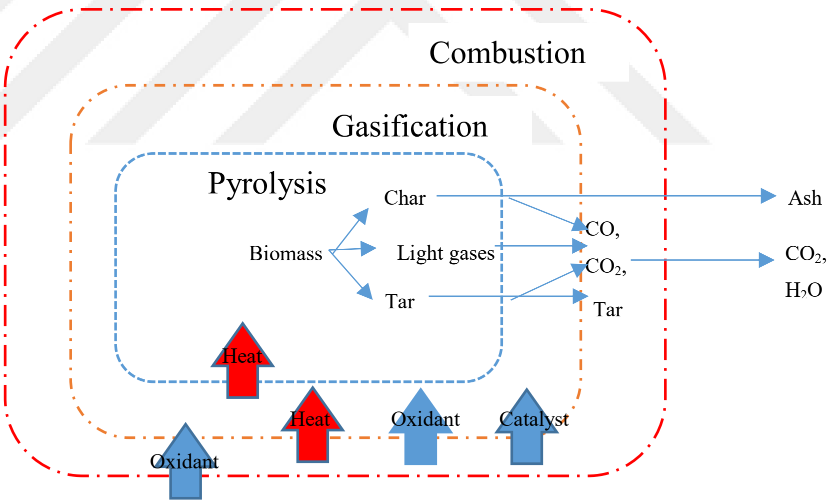

Figure 2.2 Schematic representation of thermochemical processes. (Adopted from Knoef, 2005)

2.1.4 Gasification process

According to the extensive review study of Arena, 2012, gasification process includes a sequence of several exothermic and endothermic reaction steps. In the first step, the materials heat up to 160°C and the water in liquid and vapor phase is separated from the material. The next step is the devolatilization (thermal decomposition) which occurs at temperatures up to 700 °C that includes thermal cracking, heat and mass transfers, releases of light gases such as H_2, CO, CO_2, CH_4 and H_2O, tar and char. Tar is composed of condensable hydrocarbon vapors released as gas and liquid. The char is the remaining of devolatilized material residues. Later the part of the tar is subjected to thermal cracking for conversion to gas and char.

Many reactions occur in the gasification process and these reactions can be classified as the oxidization, steam reaction, hydrogen reaction, carbon monoxide reaction and dehydrogenation (Lin et al., 2014; Lee et al., 2014; Arena, 2012). In tars reaction, heavier hydrocarbons are converted to the simple structured hydrocarbons. The reactions which occur in gasification process are given below.

Oxidization reactions;

Carbon partial oxidization (Equation 2.1)

$$C + O_2 \rightarrow CO_2 \quad (2.1)$$

Carbon oxidization (Equation 2.2)

$$C + \frac{1}{2}O_2 \rightarrow CO \quad (2.2)$$

Hydrogen oxidization (Equation 2.3)

$$H_2 + \frac{1}{2}O_2 \rightarrow H_2O \quad (2.3)$$

Partial oxidization (Equation 2.4)

$$C_xH_y + \frac{1}{2}xO_2 \rightarrow xCO + \frac{1}{2}yH_2 \rightarrow C_XH_Y \quad (2.4)$$

Reactions involving steam;

Water-gas reaction (Equation 2.5)

$$C + H_2O \rightarrow CO + H_2 \quad (2.5)$$

Water-gas shift reaction (Equation 2.6)

$$CO + H_2O \rightarrow CO_2 + H_2 \quad (2.6)$$

Steam reforming (Equation 2.7)

$$C_xH_y + xH_2O \rightarrow xCO + (x + \frac{y}{2})\ H_2O \quad (2.7)$$

Water Decomposition (Equation 2.8)

$$H_2O \rightarrow H_2 + \frac{1}{2}O_2 \tag{2.8}$$

Reactions involving hydrogen;

Hydrogasification (Equation 2.9)

$$C + 2H_2 \rightarrow CH_4 \tag{2.9}$$

Methanation (Equation 2.10)

$$CO + 3H_2O \rightarrow CH_4 + H_2O + \frac{3}{2}O_2 \tag{2.10}$$

Reactions involving carbon monoxide;

Boudouard reaction (Equation 2.11)

$$C + CO_2 \rightarrow 2CO \tag{2.11}$$

Dry reforming (Equation 2.12)

$$C_XH_Y + xCO_2 \rightarrow 2xCO + \frac{y}{2}H_2 \tag{2.12}$$

Tars and hydrocarbons reactions

Carbonization (Equation 2.13)

$$C_XH_Y \rightarrow xC + \frac{y}{2}H_2 \tag{2.13}$$

2.1.5 Operation and Performance parameters

The parameters which affect the gasification performance and the performance evaluation parameters can be summarized as below. (Arena, 2012)

Operation parameters;

Equivalence ratio (ER): it shows the ratio between oxygen content in the oxidant supply to the required of stoichiometric combustion.

Reactor temperature (T_{syn}): Both the magnitude of temperature and temperature profile along the reactor have an importance for both allo-thermal and auto-thermal gasification.

Gasification time (t_g): Depending on the reactor type and design, changing the gas velocity varies gasification time.

Composition of solid fuel: The elemental content, heating value, ash content, volatile matters, moisture content, bulk density and size of the materials crucially affect the performance of the process.

Composition and inlet temperature of oxidant: the type of oxidant and the initial temperature (T_{in}) of oxidant have significant affect in thermodynamic properties of the products.

Performance parameters;

Cold gas efficiency (η_{CG}): The cold gas efficiency (η_{CG}) is the efficiency of the gasification process which denotes the ratio of the output chemical energy of syngas to input chemical energy of fuel. The gases and fuel are assumed to be at the ambient temperature. So, the sensible heat of the materials is neglected. In the thermodynamic analysis section, the cold gas efficiency is evaluated as process efficiency (η_{EP}) and system efficiency (η_{ES}) according to taking account the plasma power.

Hot gas efficiency (η_{HG}): The hot gas efficiency (η_{HG}) is defined as the ratio of sum of chemical and physical energy of syngas to the total energy of the supplied fuel. In this case, the sensible energy of the materials is considered.

Carbon conversion efficiency (CcE): Carbon conversion efficiency (CcE) is defined as the ratio of carbon content of syngas to carbon in fuel supply.

Exergy efficiency (η_{EX}): Exergy efficiency is defined as the ratio of the exergy of syngas to the exergy of the supplied fuel.

Tar content: Tar content is also an important parameter cause of the problems what creates for the process equipment and the use of syngas for applications.

2.1.6 Classification of gasifiers

Gasification process can be classified depending on the heating of reactor, reactor design, reactor pressure, reactor temperature, oxidant type and energy recovery. (Arena, 2012).

In auto-thermal (direct) heating, the reactor is heated up and kept at high temperature by burning a portion of the biomass. However, if the reactor is heated up by an external heat source, the process is called as allo-thermal (indirect) gasification. The gasification process can occur in atmospheric pressures while it can also be pressurized reactors. Generally, the pressurized reactors are more expensive because of the strength requirement of the materials although it operates with higher performance. The conversion can be enhanced and the ash quantity can vary based on reactor temperature.

Reactor design is crucial in conversion and performance of the gasifier. The reactor technologies developed and utilized can be summarized as shown in Figure 2.3. (Arena, 2012).

In fixed bed reactor the biomass is filled to almost all reactor volume and different zones occur depending on the biomass feeding location and the gasification medium. By the sequences, the biomass undergoes drying, pyrolysis, reduction and oxidation reactions. Depending on the feeding place of the biomass and oxidant the fixed bed reactor is classified as updraft or downdraft reactor. In updraft reactor, the materials are fed from the top of the reactor while the oxidant intake is placed at the bottom. The material moves to the oxidants countercurrently. In downdraft reactor, the oxidant and the biomass flow co-currently from top to bottom.

In fluidized bed reactor, the oxidant is blown to the distributor where the biomass is located and it is dispersed in reactor by the blow of air. It can be classified as bubbling fluidized bed and circulating fluidized bed. In bubbling fluidized bed reactor, the superficial velocity is adjusted to a few m/s to overcome the weight and buoyancy force by drag forces. When the superficial velocity is equal to the terminal velocity of the particle, the particles will exhibit fluid-like behavior. It causes a better mixing of the gases and particles which result enhanced heat and mass transfer. In circulating fluidized bed reactor, the superficial velocity is kept higher than the terminal velocity. So, the particles are carried out of the bed by gases. The solid particles are then collected by cyclone and are returned to bed by a downcomer. The regime of the flow varies depending on the superficial velocity and the mass flux. Fluidized bed reactors operate at low temperatures to avoid the melting of ash.

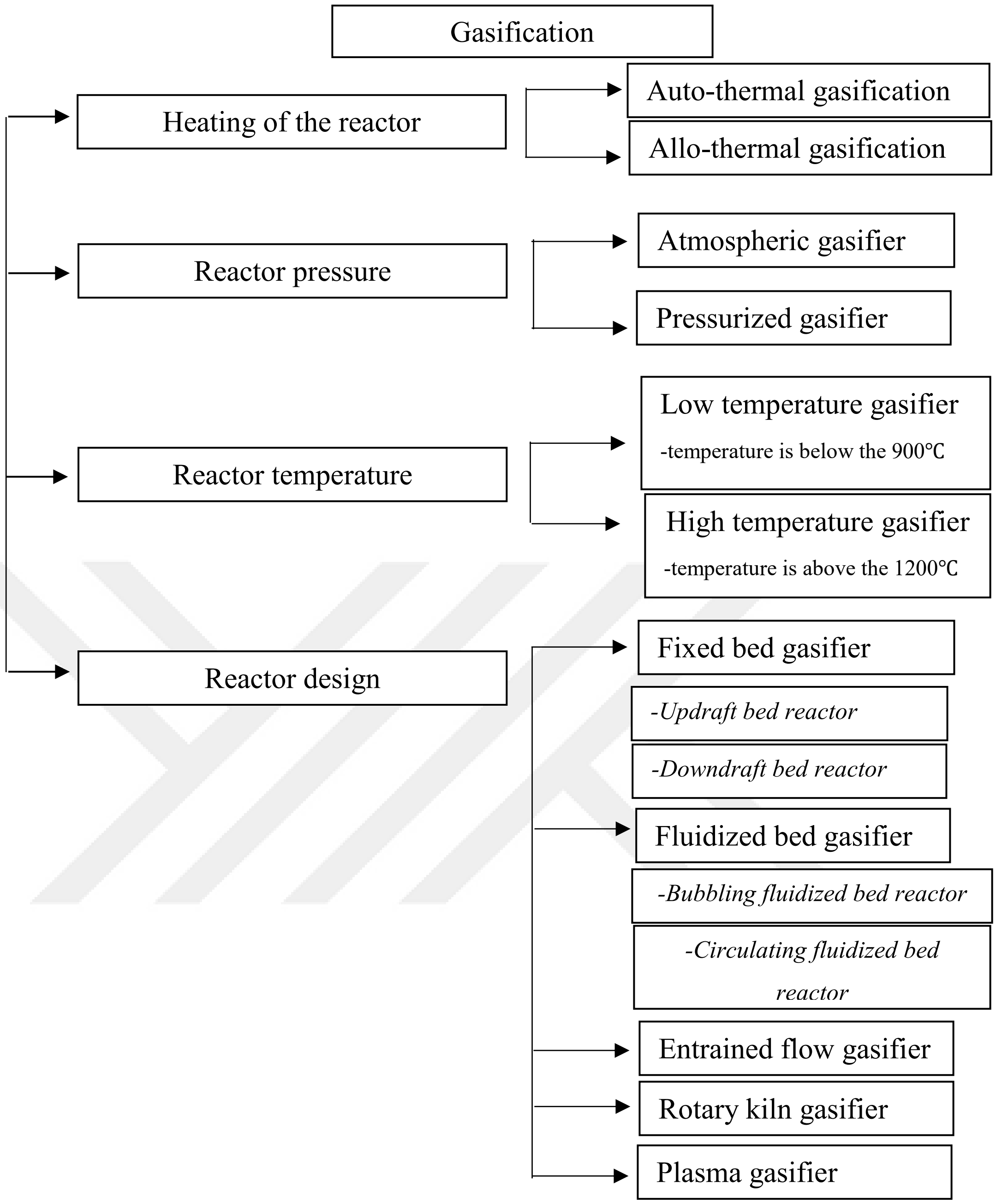

Figure 2.3 Classification of gasification technologies (Arena, 2012).

In entrained flow gasifiers, the fine solid particles are mixed with water to obtain slurry which contains more than 60 % of solid. It is fed into gasifier by pressurized oxygen or air. The turbulent flame at the top of the gasifier burns some of the fuel which provides large amount of heat and converts the rest of fuel into the syngas.

In rotary kiln gasifiers, the solid particles move along a kiln and they are gasified before combustion. It is used in waste incineration reactor.

In plasma gasifiers, the biomass is fed into the gasifier and goes through the plasma medium which has extremely high temperature. As a result of the process, the organic matters are converted into syngas while the inorganic components vitrified into slug.

2.2 Plasma

Plasma, which consists of free electrons, ions, and neutral particles is defined as the fourth state of the matter. Even the plasma includes electrons and charged particles, the plasma is considered as neutral entirely. It is thermally and electrically conductive because of charged particles in plasma. It can be partially ionized as well as fully ionized. While English scientist Sir. William Crookes brought up the fourth state of matter in 1879, American chemist and physicist Irving Langmuir defined ionized gases as plasma first time in 1929 (Roth, 1994). Plasma can occur at different temperatures and densities. While stars are examples for high temperature and dense plasma, the aurora can be example for low temperature and dense plasma. There should be sufficient energy in medium to form plasma from the gas. In addition, energy in medium should be continuous to sustain the plasma. If there is not enough energy to form plasma, the particles will turn to neutral gases. The energy to form the plasma can be electrical, thermal, ultraviolet light and etc. Plasma can form with artificial ways too. Nowadays, plasma in industry is used in many applications such as coating, thin film, gasification, flow control, sterilization, and etc. (Sanlisoy, 2013).

2.2.1 Types of Plasma

Plasma can be classified depending on temperature, thermal equilibrium, discharge methods and etc. In this section, the classification of plasma is given based on the extensive review study of Ruj and Ghosh, 2014 and Bogaerts et al 2002.

2.2.2 Classification of plasma depending on temperature

In general, plasma can be classified as high temperature or low temperature plasma depend on the temperature of the species. Let's denote the electron temperature, ion temperature and gas temperature as $T_{electron}$, T_{ion} and T_{gas}. If the electron temperature is much higher than ion and neutral gas species temperature, the plasma is called low temperature plasma. In case of low temperature plasma, the electron temperature is much higher than the gas and ion spaces as given in equation 2.14.

$$T_{electron} > T_{ion} > T_{gas} \tag{2.14}$$

If the all species are at high temperatures, such as between 4000K (for easy ionized element) and 20000K (for difficult ionized element), the plasma is called high temperature plasma (Bogaerts et al 2002).

2.2.3 Classification of plasma depending on thermal equilibrium

Plasma can be classified depending on the thermal equilibrium of species such as ions, electrons and neutral species. If the species are in thermal equilibrium, all the species should be at the same temperature. Generally, thermal plasma is in thermal equilibrium because the species are at the same temperature. The thermal equilibrium condition can be provided for cold plasma when the plasma space has high pressure. As a result of high pressure, the heat transfer between species can be enhanced and equilibrium can be provided. On the other hand, in the case of non-thermal plasma, the temperature of the species varies. For example, the electrons have high temperature because of the low density and the ions are still at ambient temperature. Generally, this is the characteristics of cold plasma. Pressure, the discharge length or distance between electrodes affect the thermal equilibrium condition.

2.2.4 Classification of plasma depending on discharge method

In this section, the plasma discharge methods are introduced with working principles (Bogaerts et al., 2002).

Direct current discharge: high voltage applied to electrodes and arc is generated in plasma medium. By interaction of plasma gases and generated arc plasma, it breaks down into ions and electrons which cause formation of plasma in medium.

Radio Frequency discharge: In this case, the alternative current is applied between the electrodes, so the electrodes will act as anode for half cycle and cathode for another half cycle. If the electrodes are isolated, the electrodes are gradually charged in half cycle, and partially neutralized in sequence by using RF discharge.

Pulsed glow discharge: In this method, the voltage is applied to electrodes in form of discrete pulses with lengths in order of microseconds. By using microsecond pulses, high peak voltages and currents are applied to the electrodes even the average power consumption is the same with DC or RF discharge.

Dielectric barrier discharge: The dielectric material is located between electrodes or the electrodes are embedded to dielectric material and plasma is formed at desired location. The gap between electrodes varies from a few mm to few cm. In this discharge, many current pulses (filaments) appear.

Corona discharge: At corona discharge, the cathode electrode consists of wire (sharp) geometry. When the voltage is applied to the electrodes, the gases in medium break down into electrons and ions. It is actuated by pulsed signal. The transition from glow to arc occurs if the voltage has long time pulses.

Magnetron discharge: In this discharge, magnetic field and electric field are together are applied to the gases in plasma medium. In this method, the cathode (filament) is located at center of tube surrounded by the anode body which have cavities. The anode body which includes the cathode at the center is packed in a body and evacuated to vacuum pressure. Then the cathode is heated up to approximately 2400 °C to emit free electrons. The cathode is connected to negative pole while the anode is connected to positive pole of DC supplier which causes the acceleration of the electrons towards to anode by electrical field. Because of the magnetic field perpendicular to the path of accelerated electrons, they are forced to make a spiral path leading from cathode to anode body. Anode body includes resonance chambers which bunch the electrons due to resonant effects. One of the resonance chamber is coupled to the antenna located outside the magnetron which converts a portion of kinetic energy into microwave energy which is connected from antenna to waveguide by launcher (Industrial Microwave, 2015).

2.3 Thermal Plasma Gasification

Plasma gasification; powered by an external energy source, operates at very high temperatures in an oxygen starved environment to decompose input waste material down to elemental molecules. Products are syngas and inert vitreous (glass-like) materials. The final products can be used to generate electricity or liquid fuel production. Plasma technology breaks down nearly all the materials excluding the radioactive materials to their elemental form (Gray, 2014). This is the advantage of plasma technology. As a result of high temperature, toxic compounds decompose to harmless chemical elements. In conventional technologies the remaining ash and char should be handled as the final product. Plasma gasification system consists of gasification furnace; feeding system; equipment to handle the slug, ash, tar and char; syngas treatment system; and a monitoring and control system. The temperature of plasma reaches up to 6000 K.

Thermal plasma gasification can be classified depending on the plasma generation, plasma medium and reactor structure. Thermal plasma can be generated by direct current (DC), radio frequency (RF) or microwave signal. Plasma medium can consist of steam, air, oxygen or mixture of these fluids. The MCw reactor structure can be classified depending on the supply of gasification materials such as plasma fixed/moving reactor, plasma entrained-flow reactor, plasma spout-fluid bed reactor (Tang et al., 2013; Ruj and Ghosh, 2014). In plasma fixed bed reactor, the solid fuel is fed into the reactor. It is gasified and the syngas is produced by actuating the plasma generator. In the moving bed reactor, the solid fuels are fed from the top or side of the reactor continuously. When the solid fuel flows through the plasma medium, the organic compounds gasify while the inorganic compounds collected at the bottom of the reactor. In plasma entrained fluid bed reactor, the solid fuel is fed in the tail of the plasma jet. As a result of short residence of solid particles in plasma medium, the rapid heating and quenching obtain. In addition, relatively better mixing and uniform flow structure are obtained in it. In plasma spouting (circulating) fluidized bed, the plasma flow and auxiliary fluid flow are sent into the reactor by a central distributor plate. In this reactor, the superficial velocity is higher than the terminal velocity which causes perfect mixing of gases and particles.

Thermal plasma gasification performance can change depending on the plasma power, reactor temperature, plasma gases flow rate, type of plasma gases and residence time of material in reactor, size of material and moisture content of fuel. The type of the plasma generator, power range of plasma former, oxidants and plasma medium gases, gasification materials, outputs of the reactions are given in Table 2.1. Also, the measurement methods, the major topics of the studies and the results are summarized in tabular form. The results can be briefly explained as; Hrycak et al., 2014; Yoon et al., 2013; Tu et al., 2009 showed the conversion ratio of material into syngas depend on the power consumption of plasma system. If the power level is high, the conversion reaches up to 99 %. Lin et al., 2014 investigated the production of hydrogen by spirulina algae and the production of hydrogen was enhanced by increasing the consumption of microwave power. Hlina et al., 2014 studied the gasification of woody biomass, plastics and oils by 110 kW power plasma system. The gasification of wood performed the best efficiency while the gasification performance of plastic was close to wood gasification. However, the gasification of oil performance was lower. Huang and Tang, 2009 studied the gasification of the tire at particle sizes from 200 µm to 600 µm. The size of the tire was critical on the performance. Increasing the tire size was decreased the gasification performance and the syngas. The conversion of material was between 40 % and 78 %. Lee et al., 2014 investigated two different grades of coal. Low grade coal performed better conversion because of moisture content. Indeed, the conversion performance was decreased by increasing the feeding rate of coal. Uhm et al., 2014 studied low grade Indonesian coal at 1640 °C reactor temperature. The cold gas efficiency reached 84 % in this study. Shin et al., 2013 studied the effect of steam flow to coal flow rate ratio. Increasing the ratio caused the increment in syngas production. Hong et al., 2012 studied the effect of air and steam as supply gases. In the case of steam usage as supply gases, the H_2 production increased while the CO decreased. Yoon and Lee, 2012 studied the location of material supply to the reactor. Supplying fuel close to plasma flame causes to increase holding time of material in the reactor and resulted to increase in hydrogen and syngas production. Using steam as supply gas causes an increase in hydrogen production. However, it reduced the cold gas efficiency and carbon conversion. Rutberg et al., 2011 studied the gasification of the wood includes 20 % moisture by different plasma gases. The air was the simplest and suitable for gasification of wood. Shie et al., 2014 found that the moisture content of rice straw was increasing the CO and H_2 content. Also, the 90 % of syngas content forms in 3 minute operation of the system. Sekiguchi and Orimo, 2004 studied the gasification of polyethylene and supplying steam to the reactor increases the syngas production. The recent developments in thermal plasma gasification systems are presented as conference paper and a journal article later. (Sanlisoy and Carpinlioglu, 2017; Sanlisoy and Carpinlioglu, 2016).

Table 2.1 General review of plasma gasification referring previous experimental studies

	Plasma gasification technologies							
Research team	Type of plasma gasification	Range of plasma power	Type of supplied gases	Type of supplied materials	Measured Outputs	Major topic	Measurement parameters	Solid Result
(Jamróz et al., 2018)	Microwave plasma	1200W-1800W	Nitrogen (30-50L/min)	benzene, toluene, and 1-methylnaphthalene,		Influence of gas flow rate, tar concentration, model tar compound and SC ratio	optical emission spectroscopy, quantitative analysis of the main gaseous by gas chromatography,	The conversion efficiency decreased with increasing tar concentration and gas flow rate while steam addition significantly enhanced it.
Surov et al., 2017	AC Plasma	5-500 kW	Air (21.16-43.33g/s) Steam 1.7(g/s) CO2 CH4	wood, coal and refuse derived fuel (RDF)	CO, H_2, CO_2 CH_4, H_2O, N_2, O_2	43–55 % of H2 + CO production by using wood, coal and RDF.	Proximate-Ultimate analysis, Voltage drop, Reactor Temperature, Gas analysis and gas flow rate	43–55 % of H2 + CO production by using wood, coal and RDF. Conversion is 99 %, selectivity is 98 %, during steam-CO2 plasma reforming of CH4.
(Uhm et al., 2016)	microwave plasma	2 kW	CO2 10-15 L/min	low-grade coal	*C*, *O*, *CO*, *C*2, *O*2 and *CO2*.	The temperature measurement of torch flame by optical spectroscopy. Conversion of CO2 into CO in the plasma torch.	temperature measurement of torch flame light emission spectrum gas chromatography	Efficient conversion of carbon dioxide into carbon monoxide.
Czylkowski et al., 2015	microwave plasma	2 -5.5 kW	CO_2 2700-3900 NL/h N_2 2700-3900 NL/h C_2H_5OH 2 l/h H_2O 2 l/h	Ethanol dry and steam reforming	H_2, N_2, CO, CO_2, O_2, CH_4, C_2H_6, C_2H_4, C_2H_2	Ethanol dry and steam reforming , Hydrogen production by conversion of ethanol	Gas Chromatographs, Fourier transform infrared spectrophotometer	Hydrogen production by conversion of ethanol 751 NL/h of hydrogen production rate 257 NL(H_2)/ kWh energy yield

Table 2.1 (Continued) General review of plasma gasification referring previous experimental studies

Hlina et al., 2014	DC plasma	100-110 kW 200 MJ/kg	H_20 (0.3g/s) Ar (0.2g/s) For ox. CO_2 , H_20	Sawdust, Wood pallets Plastics, Oil	H_2 CO CO_2 CH_4	-Gasification of different biomass materials	-Temperature measurement of reactor -Calorimetric measurements -Gas analysis system	High temperature, low mass flow rate and hydrogen –oxygen plasma resulted high quality synthetic gases. However, in the case of extreme properties of plasma the power consumption is high.
Hrycak et al., 2014	Microwave plasma	0-6 kW	N_2 CO_2 Ar (1500-3900 NL/h)	Ethanol (C_2H_5OH)	H_2 CO CO_2 C_2H_2 (acetylene) CH_4	-Effects of working gases and supplied rates are investigated. -Decrease of working flow rate up to 1500NL/h did not change the performance	-Gas analysis system -Optical emission spectroscopy	Energy efficiency of the hydrogen production should be improved to make the system self-sufficient. Ethanol conversion rate in all cases was more than 99 %.
Lee et al., 2014	DC plasma	118.8 kW	Steam (23kg/h) Argon to protect electrode (1.5m3/h)	Coal (12.5-34.1kg/h)	H_2, CO, CO_2	Moisture content of coal to plasma gasification process in examined.	-Gas Chromatography	Coal which includes more moisture enhances the reaction at high feeding rate. Better conversion of CO, H_2 and cold gas efficiency obtained at low feeding rates of coal.
Lin et al., 2014	Microwave plasma	800-1 kW	Nitrogen 12l/min	Spirulina algae	H_2, CO, CO_2, N_2, CH_4	Effect of microwave power is examined	-Scanning electron microscope -Elemental analyzer -Gas chromatography with TCD and RGA detector	Range of microwave power level can manipulate the hydrogen gas productivity from algae. Heat insulation performance should be improved.

Table 2.1 (Continued) General review of plasma gasification referring previous experimental studies

Shie et al., 2014		10 kW	N_2(10L/min) Steam of water	Municipal solid waste with raw wood (MSW/RW)	H_2, CO, CO_2, CH_4	-Effect of reactor temperature -Effect of steam flow rate to syngas production	-Output gas analysis -Flow measurement of supplied gases -Temperature measurement of the reactor -Output gas analysis -Calorific value analysis	Syngas is increased with increasing temperature without steam. Maximum concentration of H_2 increased by increasing the steam supply. Inorganic components converted into non-leachable and non-hazardous vitrified lava.
Uhm et al., 2014	Microwave plasma	75 kW	Steam	Indonesian brown coal (Low grade)	H_2, CO, CO_2, N_2, H_2O, CH_4		Gas Chromatography	Cold gas efficiency of the hydrogen rich synthetic gas from low grade coal reach up to 84 % at 1640 °C . The moderate sized power plan due to its compact and lightweight design can be useful in rural populated areas.
Yoon et al., 2013	Microwave plasma	2 kW	Nitrogen (15l/min) Oxygen (0-2.6l/min) Steam (0-7.2ml/min)	Glycerol (3g/min)	H_2, CO, CO_2, N_2, CH_4	Affect of O_2/fuel ratio, steam fuel ratio, microwave power, nozzle spray of glycerol and flow rate to syngas composition investigated.	Mass flow controllers Temperature measurement in reactor (k-type and R type thermocouple) Gas chromatograph with Thermal conductive detectors	O_2/fuel ratio should be controlled between 0-0.4 for higher conversion and cold gas efficiency. Increasing H_2O/fuel ratio enhances the H_2 production but it decreases the heating value of syngas. Microwave power increase the performance.

Table 2.1 (Continued) General review of plasma gasification referring previous experimental studies

Shin et al., 2013	Microwave plasma	0-5 kW	Steam (ratio of steam to coal 0.55)	Shenhua Coal Carried by oxygen	H_2, CO, CO_2, CH_4.	Effect of steam to syngas production is investigated Microwave power and gas temperature effect on molecule fraction is examined.		High temperature of plasma torch creates rapid gasification reaction of coal, thereby ensuring a compact plasma system.
Hong et al., 2012	Microwave plasma	4 kW	Oxygen/Air Steam/Air	Brown Coal from Indonesia	H_2, CO, CO_2, CH_4, O_2	Steam plasma torch compared with Oxygen plasma torch and steam plasma torch exhibits excellent performance to syngas generation.	Gas analysis system	Coal gasification system using microwave plasma torch can exist at moderate size due to its compact and lightweight design. It showed excellent gasification performance in a compact operating system.
Yoon and Lee, 2012	Microwave plasma	5 kW	Steam (1.1kg/h) and air (20L/min)	Coal and Charcoal	H_2, CO, CO_2, CH_4	Effect of coal supply location and types of fuel Effect of O2/fuel ratio on syngas production and gasification efficiency	Thermocouples R and K type is used to measure the temperature at reactor. Gas chromatographer with thermal conductive detector.	-Coal gas supplied near plasma flame increases the residence time and contact which causes an increase in hydrogen content and heating value of syngas. -When pure steam plasma generated, the high heating and content of H_2 obtained. However, carbon conversion and cold gas efficiency were lower. -When pure oxygen plasma generated, higher CO and CO_2 content in syngas obtained.

Table 2.1 (Continued) General review of plasma gasification referring previous experimental studies

Rutberg et al., 2011	AC plasma	0MJ/kg-13.3MJ/kg Up to 100 kW	Air, O_2, CO_2, H_20	Wood Residues (20 % moisture)	H_2, CO, CO_2, N_2	Effects of oxidants and supplied rates are investigated. Gasification duration is investigated and the regimes were explained.	-Output gas analysis -Temperature measurement at various stage -Pressure at reactor -Flow measurement of supplied gases -Plasma torch electric characteristics	Gasification by air plasma is most simple and promising method for developing technology of generating syngas from wood and wood residuals for its further application to energy production.
Shie et al., 2010	RF Plasma	10 kW	N_2 (5L/min)	Rice Straw	H_2, CO, CO_2, CH_4	Effect of moisture of rice straw and the temperature of reactor to gaseous product is studied	-Gas chromatographer with TCD -Temperature measurement of reactor	Increasing moisture, the mass yields of H_2 and CO also increased. Almost 90 % of gaseous products appeared in 3 min. Inorganic components converted into non-leachable vitrified lava which is not hazardous.
Tu et al., 2009	RF plasma	357-664W	Nitrogen (200ml/min)	Rice straw	H_2, CO, CH_4, C_2-C_5	Effect of loading power to decompose the combustible solids to syngas.	-Vacuum pressure control in reactor -Temperature measurement at inlet and exit of reactor -Brunauer-Emmett-Teller (BET) surface area measurement -Gas analysis system -Calorimetric measurement system	Energy recovery from pyrolysis of rice straw via RF plasma system increases with increasing the load power.

Table 2.1 (Continued) General review of plasma gasification referring previous experimental studies

Huang and Tang, 2009	RF plasma	1.6-2 kW	Nitrogen (800mL/min)	Tire powder	H_2, CO, CO_2, CH_4	Effect of reactor pressure, supplied power, size of supplied powder tire is examined	-The gas pressure measurement -The gas temperature measurement -Gas chromatography system -Transmission electron microscopy -Photoelectron spectroscopy	Solid conversion ranges from 40 % to 78.4 %. Solid conversion and H_2 concentration is enhanced by increasing the power and reactor pressure Pyrolytic char contains about 85 % carbon.
Tang and Huang, 2007	RF plasma	0-2 kW	Nitrogen Steam	Polyethylene	H_2, CO, CO_2, CH_4	Effect of RF power and reactor pressure to gas temperature, and product gases. Effect of electrode structure Effect of working gases	Pressure measurement of reactor Temperature measurement of reactor Gas analysis system	Different plasma media can create different product gases.
Vaidyanathan et al., 2007	DC plasma	100 kW	Air Helium	Carpet waste USAF BEAR waste base	H_2, CO, O_2, N_2, CH_4, CO_2, H_2O, benzene	Characterization of fuel gas products from the treatment of carpet and USAF BEAR waste	Gas chromatography system with TCD Temperature measurement in reactor	Energy recovery from the waste is one half of the input energy.
Sekiguchi and Orimo, 2004	Microwave plasma	600W	Ar (3.5l/min) H_20 (0-0.71g/min)	Polyethylene	H_2, CO, CO_2, CH_4	Additional steam enhance the syngas. Gasification process depending on reaction time. Steam plasma was effective for the conversion of waste plastics.	Gas analysis system	Additional steam enhances the syngas.

Table 2.1 (Continued) General review of plasma gasification referring previous experimental studies

Sekiguchi and Mori, 2003	Microwave plasma	2.8 kW	Argon Water steam	n-Hexane	H_2, CO, CO_2, H_2O, Solid carbon	Effect of O/C ration to product gases Effect of power to conversion Effect of steam flow rate to conversion	Gas chromatography system Emission spectra system	Production of hydrogen achieved but the conversion is not sufficient. Fuel cell system with plasma reformer evaluated. The efficiency were insufficient. The performance of plasma reformer need improvements.

2.4 Analysis and Modelling of Plasma Gasification Systems

The performance of plasma gasification systems which includes thermochemical processes can be evaluated in terms of thermodynamic analysis. For the modelling of the process, the reactor is chosen as control volume and the conversion efficiencies can be determined regarding to mass conservation. Then the cold gas and hot gas efficiencies and the exergetic efficiency of the process can be described and evaluated for the process. The available information is presented for plasma gasification process modelling in terms of preferred parameters, utilized definitions and comment of the present study in Table 2.2. In the recent studies related to the modelling of plasma gasification process, the following parameters are used for the evaluation of the thermochemical process.

Carbon conversion efficiency ($\mathbf{CcE_{carbon}}$): Carbon conversion efficiency (CcE_{carbon}) is described as the percentage of carbon in syngas to carbon in feedstock as given in equation 2.15. There are different descriptions for the efficiency. The variation occurs because of the mass based (Yoon and Lee, 2012) and mole based definitions (Sekiguchi and Orimo, 2004; Lee et al., 2014).

$$\mathrm{CcE}[\%] = \frac{\dot{n}_{\mathrm{C\ syn}}(\mathrm{kg/s})}{\dot{n}_{\mathrm{C\ fuel}}(\mathrm{kg/s})} \times 100 \qquad (2.15a)$$

$$\mathrm{CcE}[\%] = \frac{\dot{m}_{\mathrm{C\ syn}}(\mathrm{kg/s})}{\dot{m}_{\mathrm{C\ fuel}}(\mathrm{kg/s})} \times 100 \qquad (2.15b)$$

Hydrogen conversion efficiency (HcE): Hydrogen conversion efficiency (HCE) is described as the ratio of mole of hydrogen in syngas to mole of hydrogen in feedstock as shown in equation 2.16a. It can be described also in mass rate form as described in equation 2.16b. (Sekiguchi and Orimo, 2004; Lee et al., 2014).

$$\mathrm{HcE}[\%] = \frac{\dot{n}_{\mathrm{H\ syn}}(\mathrm{mol/s})}{\dot{n}_{\mathrm{H\ fuel}}(\mathrm{mol/s})} \times 100 \qquad (2.16a)$$

$$\mathrm{HcE}[\%] = \frac{\dot{m}_{\mathrm{H\ syn}}(\mathrm{kg/s})}{\dot{m}_{\mathrm{H\ fuel}}(\mathrm{kg/s})} \times 100 \qquad (2.16b)$$

Cold gas efficiency (η_{CG}): The cold gas efficiency (η_{CG}) is the efficiency of the gasification process that denotes the ratio of the output energy of syngas which excludes the sensible energy to input energy of feedstock. There are variations in definition of the terms. In certain studies, the lower heating value is used (Lee et al., 2014; Zhang et al., 2013) while higher heating value is used in other studies (Yoon et al., 2013) as given in equation 2.17. While the higher heating value should be used if the phase of the water is in liquid form, the lower heating value should be considered if the water is in vapor form from the definitions (Çengel and Boles, 2007).

$$\eta_{CG}[\%] = \frac{\dot{m}_{syn}(^{kg}/_{s}) \times (HHV_{syn})(^{kj}/_{kg})}{\dot{m}_{fuel}(^{kg}/_{s}) \times HHV_{fuel}(^{kj}/_{kg}) + \dot{m}_{plasma\ gases} \times E_{plasma\ gases}\left(^{kj}/_{kg}\right) + W_{plasma}} \times 100 \qquad (2.17)$$

Table 2.2 Process parameters utilized definitions for plasma gasification systems

Research group	Parameter	Definition
Yoon and Lee, 2012	Carbon conversion efficiency	$CcE_{carbon}[\%] = \frac{\dot{m}_{C\ in\ syn}(kg/s)}{\dot{m}_{C\ infeedstock}(kg/s)} \times 100$
	Cold gas efficiency	$\eta_{CG}[\%] = \frac{\dot{m}_{syn}(kg/s) \times (HHV_{syn})(^{kj}/_{kg})}{\dot{m}_{feedstock}(kg/s) \times HHV_{feedstock}(^{kj}/_{kg})} \times 100$
Sekiguchi and Orimo, 2004	Conversion for H_2	$H_2 Conversion[\%] = \frac{2P_{H_2}(\text{molar amount of } H_2 \text{ produced})}{4F_{PE}\ (\text{inital molar amount of } C_2H_4)} \times 100$
	Conversion for C	$C\ Conversion[\%] = \frac{P_C(\text{molar amount of C produced})}{2F_{PE}\ (\text{inital molar amount of } C_2H_4)} \times 100$
	Conversion for H_2O based on O element	$H_2O\ Conversion[\%] = \frac{P_{CO}(\text{molar amount of CO produced}) + 2P_{CO_2}(\text{molar amount of } CO_2 \text{ produced})}{2F_{H_2O}(\text{inital molar amount of } C_2H_4)} \times 100$
Lin et al., 2014	Higher heating value of biomass	$HHV(^{kj}/_{kg}) = 33.5[C] + 142.3[H] - 15.4[O] - 14.5[N]$
	The mass flow rate of hydrogen production	$ROP(kg/min) = (\dot{\forall}_{input}(L/min)) \times \left(^{1mole}/_{24.5L}\right) \times x_{H_2} \times \text{molecule weight}(^{kg}/_{mol})$ ROP indicates the rate of production of hydrogen
	Thermal to H_2 efficiency	$\eta_H\% = \frac{\dot{m}_H \times HHV_H(^{kj}/_{kg})}{\dot{m}_N(^{kg}/_{s}) \times q_N(^{kj}/_{kg})}$ $q_N\left(\frac{kJ}{kg}\right) = c_p(h_{out} - h_{in})$ Specific thermal energy rate consumed inside the reactor zone during pyrolysis.
	Carbon conversion	$CcE_{carbon}[\%] = \frac{n_{C\ in\ syn}(mol)}{n_{C\ in\ feedstock}(mol)} \times 100$

Table 2.2 (Continued) Process parameters utilized definitions for plasma gasification systems

Lee et al., 2014	Hydrogen conversion	$\mathrm{HCE}[\%] = \frac{2 \times n_{H\ in\ syn}(mol)}{n_{H\ in\ feedstock}(mol)} \times 100$
	Cold gas efficiency	$\eta_{CG}[\%] = \frac{\dot{m}_{syn}(^{kg}/_{s}) \times \left(LHV_{syn}(^{kj}/_{kg})\right)}{\dot{m}_{feedstock}(^{kg}/_{s}) \times LHV_{feedstock}(^{kj}/_{kg}) + P_{plasma}(kW) \times \eta_{plasma-torch}} \times 100$
	Thermal efficiency of plasma torch	$\eta_{plasma-torch}[\%] = \frac{W_{plasma}(kW) - \left[\dot{m}_{cooling}(^{kg}/_{s}) \times c_p(^{kj}/_{kg.K}) \times (T_{out} - T_{in})(K)\right]}{W_{plasma}(kW)} \times 100$
Sekiguchi and Mori, 2003	Conversion of C_6H_{14}	$\mathrm{Conversion}(H_2O)[\%] = \frac{F_{C_6H_{14}}\ (\text{molar flow rate of } C_6H_{14} \text{ in feed}) - R_{C_6H_{14}}\ (\text{molar flow rate of } C_6H_{14} \text{in product gases})}{F_{C_6H_{14}}\ (\text{molar flow rate of } C_6H_{14} \text{ in feed})} \times 100$
	Conversion of H_2O	$\mathrm{Conversion}(H_2O)[\%] = \frac{F_{H_2O}(\text{molar flow rate of } H_2O \text{ in feed}) - R_{H_2O}(\text{molar flow rate of } H_2O \text{ in product gases})}{F_{H_2O}(\text{molar flow rate of } H_2O \text{ in feed})} \times 100$
	Performance evaluation of fuel cell	$\eta[\%] = \frac{W_{Fuel\ cell}(kW) - W_{plasma}(kW)}{W_{Plasma}(kW)} \times 100$
	Cold gas efficiency	$\eta_{CG}[\%] = \frac{\dot{m}_{syn}(^{kg}/_{s}) \times (LHV_{syn})(^{kj}/_{kg})}{\dot{m}_{MSW}(^{kg}/_{s}) \times LHV_{MSW}(^{kj}/_{kg}) + W_{plasma}(kW) + W_{steam}(kW)} \times 100$

Table 2.2 (Continued) Process parameters utilized definitions for plasma gasification systems

Zhang et al., 2013	Total Energy Efficiency	$\eta_E[\%] = \dfrac{\dot{m}_{syn}(^{kg}/_{s}) \times LHV_{syn}(^{kj}/_{kg}) + \dot{m}_{tar}(^{kg}/_{s}) \times LHV_{tar}(^{kj}/_{kg})}{\dot{m}_{MSW}(^{kg}/_{s}) \times LHV_{MSW}(^{kj}/_{kg}) + W_{plasma}(kW) + W_{steam}(kW)} \times 100$
	Cold gas exergy efficiency	$\eta_{ex-CG}[\%] = \dfrac{\dot{m}_{syn}(^{kg}/_{s}) \times Ex_{ch,syn}(^{kj}/_{kg})}{\dot{m}_{MSW}(^{kg}/_{s}) \times Ex_{ch,MSW}(^{kj}/_{kg}) + \dot{m}_{steam}(^{kg}/_{s}) \times Ex_{ch,steam}(^{kj}/_{kg}) + W_{plasma}(kW)} \times 100$
	Total exergy efficiency	$\eta_{ex}[\%] = \dfrac{\dot{m}_{syn}(^{kg}/_{s}) \times Ex_{ch,syngas}(^{kj}/_{kg}) + \dot{m}_{tar}(^{kg}/_{s}) \times Ex_{ch,tar}(^{kj}/_{kg})}{\dot{m}_{MSW}(^{kg}/_{s}) \times Ex_{ch,MSW}(^{kj}/_{kg}) + \dot{m}_{steam}(^{kg}/_{s}) \times Ex_{ph,steam}(^{kj}/_{kg}) + W_{plasma}(kW)} \times 100$
	Chemical exergy of the municipal solid waste	$Ex_{ch,MSW}(^{kj}/_{kg}) = LHV_{MSW}(^{kj}/_{kg}).\left(\dfrac{1.044 + 0.016(H/C) - 0.3493(O/C)[1 + 0.0531(H/C)] + 0.0493(N/C)}{1 - 0.4124(O/C)}\right)$
	Chemical exergy of the tars	$Ex_{ch,MSW}(^{kj}/_{kg}) = LHV_{tar}(^{kj}/_{kg}).(1.0401 + 0.1728(H/C) + 0.0432(O/C) + 0.2196(S/C)[1 - 2.0628(H/C)])$
	Chemical exergy of syngas	$Ex_{ch}(^{kj}/_{kg}) = \sum_i x_i e_{0(i)}(^{kj}/_{kg}) + R\left(^{kj}/_{kg.K}\right) T_0(K) \sum_i x_i \ln x_i$
	Physical exergy of syngas	$Ex_{ph}\left(^{kj}/_{kg}\right) = (h - h_0)\left(^{kj}/_{kg}\right) - T_0(K)(s - s_0)\left(^{kj}/_{kg.K}\right)$

Table 2.2 (Continued) Process parameters utilized definitions for plasma gasification systems

		$Ex_{ph}\left({}^{kj}/_{kg}\right) = \sum_i x_i \dot{E}x_{ph(i)}\left({}^{kj}/_{kg}\right)$
Kalinci et al., 2011	Total exergy of a material stream	$\dot{E}x_{tot}(kW) = \dot{E}x_{ph}(kW) + \dot{E}x_{ch}(kW)$
	Physical exergy	$\dot{E}x_{ph}(kW) = \dot{m}\left({}^{kg}/_{s}\right)\left[(h - h_0)\left({}^{kj}/_{kg}\right) - T_0(K)(s - s_0)\left({}^{kj}/_{kg.K}\right)\right]$ $\dot{E}x_{ph}(kW) = \sum_i x_i \dot{E}x_{ph(i)}(kW)$
	Chemical exergy	$\dot{E}x_{ch}(kW) = \dot{m}\left({}^{kg}/_{s}\right)\left(\sum_i x_i e_{0(i)}\left({}^{kj}/_{kg}\right) + RT_0 \sum_i x_i \ln x_i \left({}^{kj}/_{kg}\right)\right)$ $e_0\left({}^{kj}/_{kg}\right) = \beta.LHV_{fuel}\left({}^{kj}/_{kg}\right)$ $\beta = \dfrac{1.0412 + 0.2160(H/C) - 0.2499(O/C)[1 + 0.7884(H/C)] + 0.045(N/C)}{1 - 0.3035(O/C)}$
	Higher heating value and Lowe heating value calculations	$HHV\left({}^{Mj}/_{kg}\right) = 0.3491C + 1.1783H + 0.1005S - 0.1034O - 0.0151N - 0.0211ash\ (Mj/kg)$ $LHV\left({}^{Mj}/_{kg}\right) = HHV(1 - H_2O) - 2440(H_2O + 9H)$
	Exergetic efficiency	$\eta_{ex}[\%] = \dfrac{(\dot{E}x)_{output}(kW)}{(\dot{E}x)_{input}(kW)} \times 100$
Janajreh et al., 2013	Cold gas efficiency	$\eta_{CG}[\%] = \dfrac{\dot{m}_{syn}(kg/s) \times (LHV_{syn})\left({}^{kj}/_{kg}\right)}{\dot{m}_{feedstock}(kg/s) \times LHV_{feedstock}\left({}^{kj}/_{kg}\right) + {}^{W_{plasma}(kW)}/_{\eta_{elec.}}} \times 100$
	Chemical exergy	$e_0\left({}^{kj}/_{kg}\right) = \beta.LHV_{fuel}\left({}^{kj}/_{kg}\right)$ $\beta = 1.0438 + 0.0158(H/C) + 0.0813 \quad \text{For } {}^{O}/_{C} \leq 0.5$

Table 2.2 (Continued) Process parameters utilized definitions for plasma gasification systems

		$\beta = \dfrac{1.0414 + 0.0177\left(\frac{H}{C}\right) - 0.3328\left(\frac{O}{C}\right)\left(1 + 0.0537\left(\frac{H}{C}\right)\right)}{1 - 0.402\left(\frac{O}{C}\right)}$ For $0.5 \leq {}^{O}/_{C} \leq 2$
	Exergetic Gasification efficiency	$\eta_{ex}[\%] = \dfrac{\dot{m}_{syn} \times (Ex_{ch,syn} + Ex_{ph,syn}) - \dot{m}_{oxygen} \times Ex_{ch,oxygen} - \dot{m}_{steam} \times (Ex_{ch,steam})}{\dot{m}_{fuel-in}\left({}^{kg}/_{s}\right) \times Ex_{ch,fuel-in}\left({}^{kj}/_{kg}\right) + \dot{m}_{fuel-out}\left({}^{kg}/_{s}\right) \times (Ex_{ch,fuel-out} + Ex_{ph,fuel-out})\left({}^{kj}/_{kg}\right) + W_{plasma}(kW)} \times 100$
Minutillo et al., 2009	Plasma gasification efficiency (cold gas efficiency)	$\eta_{CG}[\%] = \dfrac{\dot{m}_{syn}(kg/s) \times (LHV_{syn})\left({}^{kj}/_{kg}\right)}{\dot{m}_{feedstock}(kg/s) \times LHV_{feedstock}\left({}^{kj}/_{kg}\right) + {}^{(W_{plasma}(kW) + W_{air\ unit}(kW))}/_{\eta_{elec.}}} \times 100$

Hot gas efficiency (η_{HG}): The hot gas efficiency (η_{HG}) is the efficiency of the gasification process that denotes the ratio of the output energy of syngas which includes sensible energy to input energy of feedstock as described in equation 2.18 (Loha et al., 2011).

$$\eta_{HG} = \frac{\dot{m}_{syn} \times \left(HHV_{syngas} + c_{p(syn)}\left(T_{syn} - T_o\right)\right)}{\dot{m}_{fuel} \times HHV_{fuel} + \dot{m}_{plasma\ gases} \times E_{plasma\ gases} + W_{plasma}} \tag{2.18}$$

The higher heating value can be calculated as in given empirical relation 2.19 (Channiwala and Parikh, 2002).

$$HHV = 0.3491C + 1.1783H + 0.1005S - 0.1034O - 0.0151N - 0.0211ash \left(\frac{MJ}{kg}\right) \tag{2.19}$$

Here, the C, H, S, O, N and ash are the weight fractions of carbon, hydrogen, sulphur, oxygen, and nitrogen and ash in the solid fuel respectively. This values are obtained from the ultimate and proximate analyses of the solid fuel.

The lower heating value of the substance can be found by using the equation 2.20. (Finet, 1987).

$$LHV = HHV(1 - H_2O) - 2440(H_2O + 9H) \left(\frac{MJ}{kg}\right) \tag{2.20}$$

In equation 2.20, H_2O is the weight fraction of moisture in fuel.

If syngas is at ambient condition, the higher heating value, HHV is used. On the other hand, if the syngas is at operation condition that is usually higher than evaporation temperature of the water, the lower heating value, LHV should be taken as mentioned in handbook of Çengel and Boles, 2007.

Exergy Efficiency (η_{ex}): The exergy of the stream may have chemical or physical exergy (Kalinci et al., 2011). The exergy of stream can be defined as in equation 2.21.

$$\dot{E}x_{tot} = \dot{E}x_{ph} + \dot{E}x_{ch}\ (kW) \tag{2.21}$$

Physical exergy occurs as a result of pressure and temperature difference between the operation and reference conditions. The physical exergy of the elements of the fuel can be calculated as equation 2.22.

$$\dot{E}x_{ph} = \dot{m}[(h - h_0) - T_0(s - s_0)] \text{ (kW)} \tag{2.22}$$

In equation 2.22, $\dot{m}$ denotes the mass flow rate, h enthalpy of the material at operation condition, h_0 enthalpy of the material at reference state, s entropy at working condition and s_0 entropy at reference state.

The physical exergy of each components of gases spaces can be defined as equation 2.23.

$$\dot{E}x_{ph} = \sum_i x_i \dot{E}x_{ph(i)} \text{ (kW)} \tag{2.23}$$

As a result of chemical reactions, the chemical bonds which bind the atoms together are broken and new ones are formed. The chemical energy formed as a result of the fission or fusion of the chemical bonds. Kotas, 1985, defines the chemical exergy such that "Chemical exergy is equal to the maximum amount of work obtainable when the substance under consideration is brought from the environmental state to the dead state by processes involving heat transfer and exchange of substances only with the environment." Chemical exergy expresses the exergy of a substance at ambient temperature and pressure. The chemical exergy of the gas mixture can be defined as in equation 2.24.

$$\dot{E}x_{ch} = \dot{n}_i \left[\sum_i x_i e_{0(i)} + \bar{R}T_0 \sum_i x_i \ln x_i \right] \text{(kW)} \tag{2.24}$$

Here x_i denotes mole fraction of the compound in gas mixture and e_0 denotes standard chemical exergy. The standard exergy of the product gases can be found in the study of Kotas, 1985. There are uncertainties about the composition of the fuel. Therefore, empirical relations (equation 2.25 and Table 2.3) should be used to calculate the standard chemical exergy.

$$e_0 = \beta.\text{LHV}_{fuel} * 1000 \left(\frac{kJ}{kg}\right) \tag{2.25}$$

β can be determined from the equations given in Table 2.3 that the fuel satisfies restriction.

As a result, the fuel exergy and the product gases exergy can be calculated and the exergetic efficiency can be given as equation 2.26. (Kalinci et al., 2011)

$$\eta_{ex} = \frac{\left(\dot{E}x_{ph} + \dot{E}x_{ch}\right)_{syn}}{\left(\dot{E}x_{ch} + \dot{E}x_{ch}\right)_{fuel} + \dot{E}x_{plasma}} \tag{2.26}$$

Table 2.3 β coefficient equations

Chemical exergy calculations		
Research group	β coefficient	Constrains
Kalinci et al., 2011 (referred to Szargut and Styrylska, 1964)	$\beta = \frac{1.0412+0.2160(H/C)-0.2499(O/C)[1+0.7884(H/C)]+0.045(N/C)}{1-0.3035(O/C)}$	For $\frac{O}{C} \leq 2.67$
Janajreh et al., 2013; Prins et al., 2007 (referred to Szargut and Styrylska, 1964)	$\beta = 1.0438 + 0.0158(H/C) + 0.0813$	for $\frac{O}{C} \leq 0.5$
	$\beta = \frac{1.0414+0.0177\left(\frac{H}{C}\right)-0.3328\left(\frac{O}{C}\right)\left(1+0.0537\left(\frac{H}{C}\right)\right)}{1-0.402\left(\frac{O}{C}\right)}$	For $0.5 \leq \frac{O}{C} \leq 2$
Zhang et al., 2013 (referred to Szargut and Styrylska, 1964)	$\beta = \frac{1.044+0.016(H/C)-0.3493(O/C)[1+0.0531(H/C)]+0.0493(N/C)}{1-0.4124(O/C)}$	For solid fuels
Zhang et al., 2013 (referred to Stepanov, 1995	$\beta = (1.0401 + 0.1728(H/C) + 0.0432(O/C) + 0.2196(S/C)[1 - 2.0628(H/C)])$	For liquid fuels

2.5 Biomass and Coal Description and Properties

The coal and biomass fuel sources are gasified in microwave plasma gasification system in this research. That is why, the coal and biomass characteristics are defined and the properties of them are explained in this section.

2.5.1 Coal

Coal is defined as a combustible fossil fuel that composed of carbon, hydrogen and oxygen. It is a sedimentary rock that its formation begins for 290-360 million years ago in carbon age. Its quality can change depending on the exposed pressure, temperature and formation time which means the organic maturity of it (WCI, 2009). The source of coal energy come from the photosynthesis of died plants which formed the coal in carbon age. Plants in their lifetime capture energy from the sun by photosynthesis. The dead plants decay and form peats in oxygen starved medium such as peat bog. Then the peats get burry by other sediments. Meanwhile, the captured energy from the sun have been stored in chemical form. The peat expose to pressure and temperature which forms the lignite at the beginning of the maturity. By the continuous physical and chemical interaction in many years, the lignite metamorphose to brown coal then to bituminous coal and anthracite.

2.5.2 Classification of Coal

The coal in each metamorphose period from lignite to anthracite has altered physical and chemical properties. Coal quality can be classified as the maturity of coal as shown in Figure 2.4.

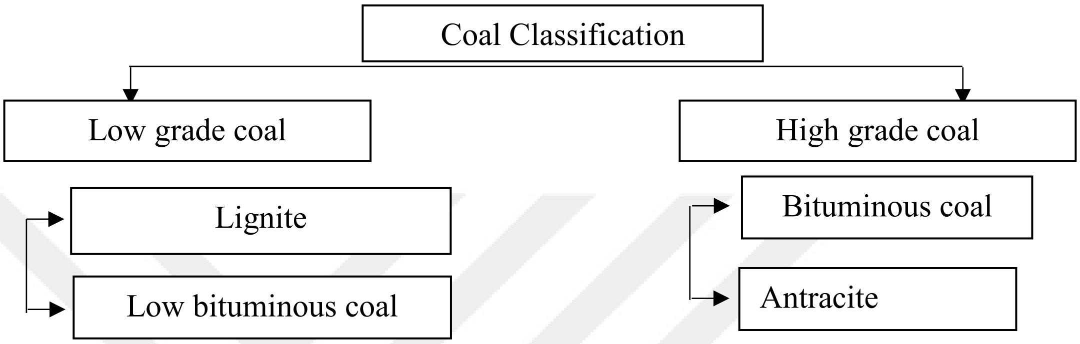

Figure 2.4 Classification of coal resources

2.5.3 Coal reserves, production and consumption

According to BP statistical review of world energy (BP, 2015), there exists 891 billion tons economically feasible coal reserve in the world in 2014 as given in Table 2.4. The coal is evaluated as economically feasible if the mining is possible and production cost of coal is feasible. For this reason, the amount of feasible coal can change depending on the technological developments and the commodity price. The coal reserves decreased 1039 billion tons in 1994 to 909 billion tons in 2004 and 891 billion tons in 2014. The coal reserves in Turkey were 8.7 billion tons in 2014.

Table 2.4 Coal reserves in Turkey and in the world in 2014.

Coal reserves in 2014		(million ton)
World	Low grade coal	403199
	High grade coal	488332
	Total	**891531**
Turkey	Low grade coal	322
	High grade coal	8380
	Total	**8702**
The data were taken from the BP statistical review of world energy (BP, 2015)		

While the production of coal gradually increases, the Chine, USA, India, Australia and South African perform the largest production of coal. The high portion of the produced coal consumes in the countries where it is produced as given in Table 2.5. In 2014, the coal production reached up to 3.9 billion tons, while it was 17.8 million tons in Turkey.

Table 2.5 The Coal production and consumption

	Coal Production (million tons)			Coal Consumption (million tons)		
Years	2004	2009	2014	2004	2009	2014
World	2835.9	3412.7	3933.5	2914.5	3451.9	3881.8
Chine	1106.6	1538.0	1844.6	1125.0	1679.0	1962.4
USA	572.4	540.8	507.8	566.1	496.2	453.4
Russia	132.2	142.3	170.9	99.9	92.2	85.2
India	155.7	210.8	243.5	172.3	250.3	360.2
Australia	197.1	232.6	280.8	50.7	53.4	43.8
South African	137.1	139.7	147.7	86.9	93.8	89.4
Turkey	10.5	17.4	17.8	22.3	30.9	35.9
The data were taken from the BP statistical review of world energy (BP, 2015)						

Coal is used in many sectors such as power plants, iron or steel production, cement factories or as a liquid fuel. Coal is still the biggest source of fuel in power plants and 39 % of electricity is produced by coal powered plants. It is expected to stay in similar level in the following years (WCI, 2009). In addition, the usage of coke coal increases in years in cement factories. While the consumption of coal was 3.9 billion tons in the world, it was 36 million tons in Turkey in 2014.

2.5.4 Biomass

Biomass is a renewable energy source that includes the aquatic and terrestrial vegetation, residues of forestry and agriculture, animal waste and municipal wastes. Biomass is produced from the crops, woods, manure, land fill gases and alcohol fuels.

When the biomass is compared with fossil fuels, both fuels release the carbon monoxide to the environment in the same amount. However, while the biomass releases the carbon monoxide which stored by photosynthesis in recent years, the fossil fuels releases to the environment the carbon monoxide which is captured by plants in carbon age. In biomass burning, the carbon cycle is proceeding, but the carbon captured and embedded to land in carbon age is added to atmosphere by burning the coal (ISRE, 2015).

There are many applications of the biomass utilization in power generation or fuel production. The biomass can be classified as biofuel production or bioenergy production.

2.5.5 Biofuel

In biofuel applications, biomass is converted into liquid fuels which is used as fuel for transportation. The ethanol and biodiesel are commonly used as fuel transportation. Ethanol is formed by fermenting the biomass which includes high carbohydrates. It is produced from starches and sugars. There are also technological developments to produce ethanol from cellulose and hemicellulose and the fibrous material. Moreover, it is also produced from the gasification products (NREL, 2014).

In biodiesel production, the alcohol is combined with vegetable oil, animal fat or recycled oil in the presence of catalyst to form ethyl or methyl ester. The products can be used as additive to conventional fuels or purely in diesel engines (EERE, 2013).

2.5.6 Biopower

Biopower is obtained by converting biomass into heat or electricity forms. Conversion takes place by direct combustion, mixing with fossil fuels or anaerobic digestion. In direct combustion, the biomass is burned and the heat is transferred to fluid via boilers or combustion chambers. Then the fluid accumulates in power generation system to drive the turbine-generator. As a result, the biomass energy is converted into heat and electricity. Another approach is mixing the biomass with fossil fuels and combustion of the mixture in boiler. By this method, the sulphur emission can be reduced and this method is the least-cost usage of renewable energy. In anaerobic digestion, the biomass is decomposed by bacteria in absence of oxygen to form methane and naturel gas (EERE, 2013).

2.5.7 Classification of Biomass

According to Asian Biomass Handbook (Yokoyama and Matsumura, 2008), the biomass can be classified by existence of biomass in nature or depending on the application and usage of biomass. In usage and application categorization, the biomass can be conventional biomass, biomass residues or biomass plantation. While conventional biomass includes the agriculture, forestry, fishery, livestock faming food and etc., biomass residues include forestry, agriculture, livestock residues, straws, municipal wastes and etc. In plantation biomass, biomass is produced by rapid growing creatures such as forestry of eucalyptus, poplar, willow, oil palm, herbaceous farm of sugarcane, switch grass, sorghum, corn, and rapeseed or aquatic farm of algae, hyacinth and giant kelp. In the case of classification of biomass depending on the existence in nature, biomass can be woody biomass which is produced in forestry, herbaceous biomass which produced from grasses and legumes, in farms and fields, or organic wastes which is formed in municipals and livestock. General classification of biomass can be given as shown in Table 2.6.

Table 2.6 Classification of Biomass

Biomass classification	
Woody biomass	By products such as logging process Main products such as trimming the trees In logging process of $1m^3$ wood, $0.36m^3$ blanches and $0,22m^3$ stumps left, and the residue used as biomass energy source.
Herbaceous biomass	Herbaceous biomass include the grasses and legumes.
Sugar and starch crops	Sugar and starch products ferment for the production of ethanol.
Oil producing biomass	Oil producing foods such as soybean, sunflower, rape and palm used for the production of biodiesel.
Animal waste	In farms, the animal wastes are piled or composted to decompose the solid and liquid. The liquid used in farm as fertilizer while the solid contents composted and sold and used in other farms.
Municipal wastes	Organic portion of the municipal waste is recovered to energy by biological and thermal processes.

2.6 Conclusion

The gasification of the fuels and the production of the syngas are the known methods and the industrial application of gasification are in use. The experimental and numerical investigations go on to increase the conversion efficiency, make the system more environmental by reducing the ash output, or using the system in special purposes such as hydrogen production. The plasma gasification is a new way to enhance the performance of gasification process. Because, plasma has extremely high temperatures and the conversion of solid fuel into syngas requires high temperatures. The high conversion performances were achieved by using plasma in gasification applications. However, the investigations are continuing to reveal the effects of each parameters, enhance the performance of the gasification process and reduce the negative environmental impacts. There are many studies on the plasma gasification in literature. However, the potential of consumed and produced energy content of fuels are not revealed in detail. The studies mainly focus on the hydrogen conversion, cold gas efficiency or the conversion performance. However the comparison of the produced syngas energy and the consumed energy to produce the syngas for varied conditions is a gap in the literature. To compare them, the temperature in gasifier, the supplied amounts of air and fuel, produced syngas and ash amount should be measured for each case. Therefore, the experimental set up was designed and constructed to study the thermodynamic assessment of plasma gasification systems. The efficiency parameters regarding to mass and energy content were defined and performance of the plasma gasification system for 6 types of fuels, 3 air flow rate levels and plasma powers between 3 kW and 6 kW are examined.

There are variety of methods to produce the plasma such as DC, RF or microwave plasma (Sanlisoy and Carpinlioglu, 2017). Because of the no electrode erosion, the microwave plasma has advantages when it compared with other generation methods. However, the price of the system is higher when it is compared with others. There are rare studies on microwave plasma. That’s why the microwave plasma generation method is used in this study.

In literature survey chapter; the definition of thermochemical processes and the classification of gasification systems are given in detail. Operation and performance parameters are introduced. The sequences of gasification process are defined. As the gasifier heated by microwave plasma, the basic knowledge about plasma is presented. The plasma is defined, plasma types are classified depending on temperature and thermal equilibrium. In addition, plasma production methods are explained. Thermal plasma gasification systems which are used for the gasification are given as literature survey. The fuels what is used for the gasification are characterized and the literature about the fuels is given.

CHAPTER III

DESIGN CONSTRUCTION AND CALIBRATION OF MCW GASIFIER

Microwave plasma gasification system -MCw Gasifier- consists of the following sub-components; Microwave plasma system, solid waste feeding and fluid supply systems, gasification reactor, process outputs collection system and the measurement - data acquisition system. The properties of each component of the system are explained in detail. Also, the technical details are given in Appendix A.1. The measurement devices, their characteristics and calibrations are given. The revisions in synchronization process of the system are explained by sequence. The process of the experimentation and the data logging procedure are explained in this section. Brief explanation of the experimental system is also given in the presented conference paper (Sanlisoy and Carpinlioglu, 2016). The gasification system is constructed by the support of TUBITAK 115M389 project which is started in October of 2015 and it is going to be completed in October of 2018.

3.1 Microwave Plasma System

In the microwave plasma system, the generation and the transfer of the microwave signal to the reactor are carried out.

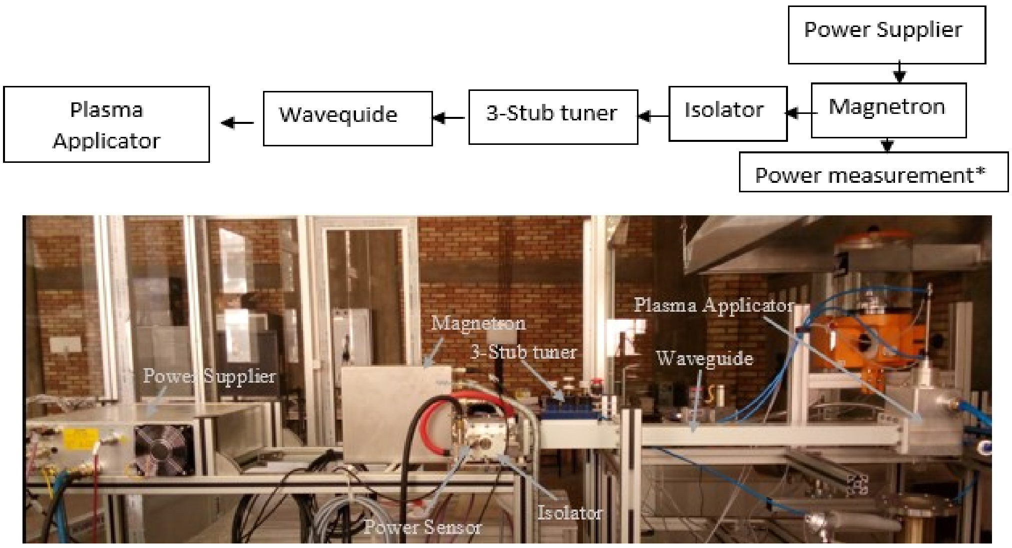

Figure 3.1 Block diagram of microwave plasma system components and presentation of microwave system components

The microwave plasma gasification system consists of a power supplier, a magnetron, an isolator, a stub-tuner, a waveguide and a plasma applicator for the plasma. The magnetron coupled with the power supplier generates the microwave power and the waveguide transfers the signal to the plasma applicator as shown in Figure 3.1.

3.1.1 Microwave Power Supplier

The Muegge MX6000D-110K model 6 kW power supplier is used for the generation of the high voltage for the magnetron head. Also, it is used to control voltage. The system operates via MUEGGE ME0220V-003AB model control software as shown in Figure 3.2. The desired power level can be adjusted by set value. The inputs are given in percentage of the full power scale. The acted power and reflected power are also indicated at the interface. By adjusting the 3-stub tuner, the reflected power can be minimized.

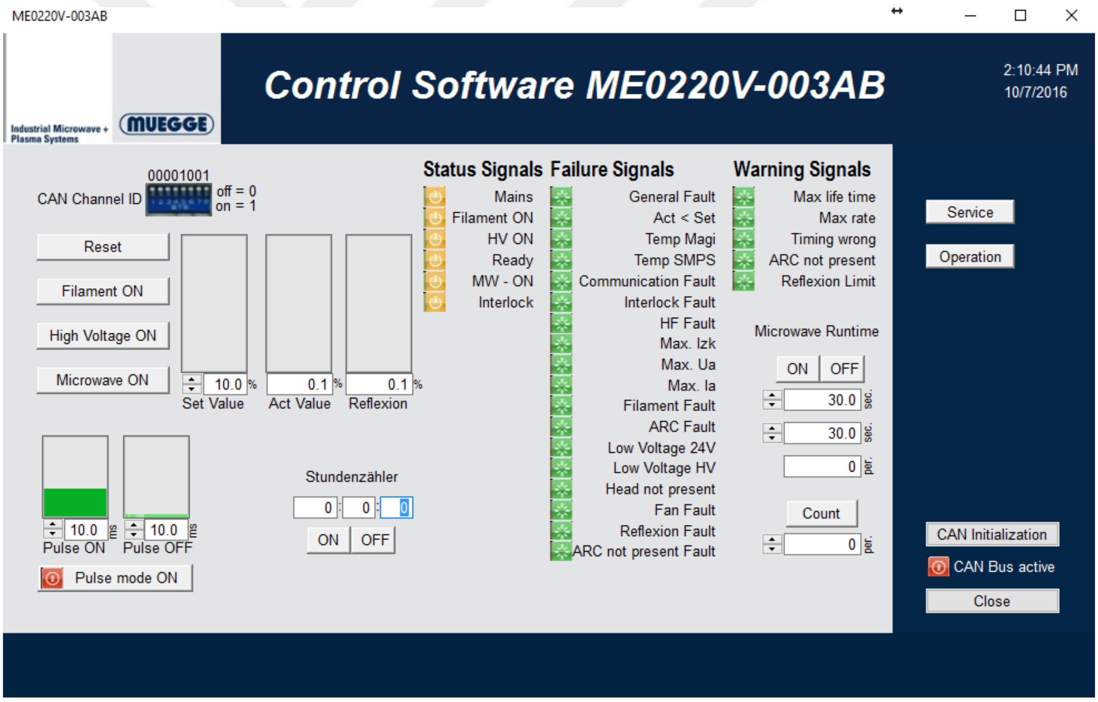

Figure 3.2 The Control software of the Microwave plasma system

3.1.2 Magnetron Head

The Muegge MH6000S-213BF model magnetron head is used as shown in Figure 3.3. The output power can be varied between 0 to 6 kW in the frequency of 2450 MHz. The magnetron is designed for the industrial microwave heating applications. The magnetron uses the Toshiba E3327 model tubed magnet which is packaged magnet type and the sub-electromagnet for stabilizing and controlling the output power is also installed in the tube. The power level is varied by changing the electromagnet current.

The anode is cooled by water at ambient temperature and the output antenna and the filter box are cooled by forced air flow.

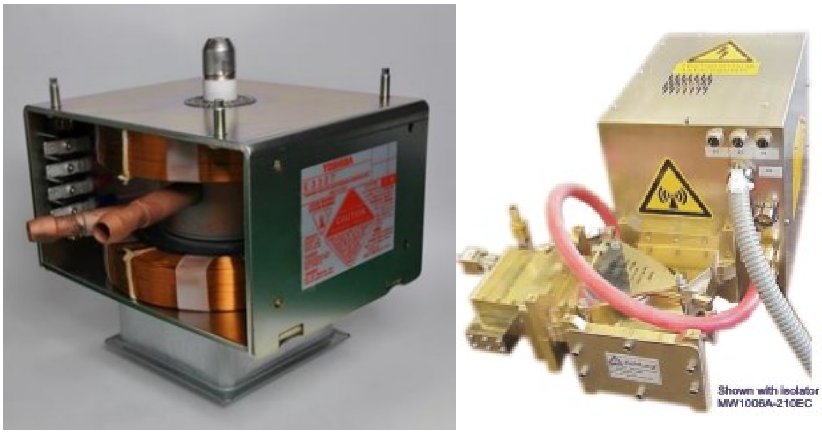

Figure 3.3 Toshiba E3327 model tubed magnet which is integrated by Muegge MH6000S-213BF model magnetron

3.1.3 Isolator

The isolator in Figure 3.4 is used in order to transmit the microwave power in one direction. The part of the output of the magnetron power can be reflected because of mismatching of signal. The reflected power can cause dummy load on magnetron which causes a damage. The isolator prevents the transmitting the reflected power to it in reverse direction. Isolation is a unit of measure (in dB) that states the separation of signal levels on adjacent ports of a device. The greater isolation value, the less interference from a signal on one port presents at the other.

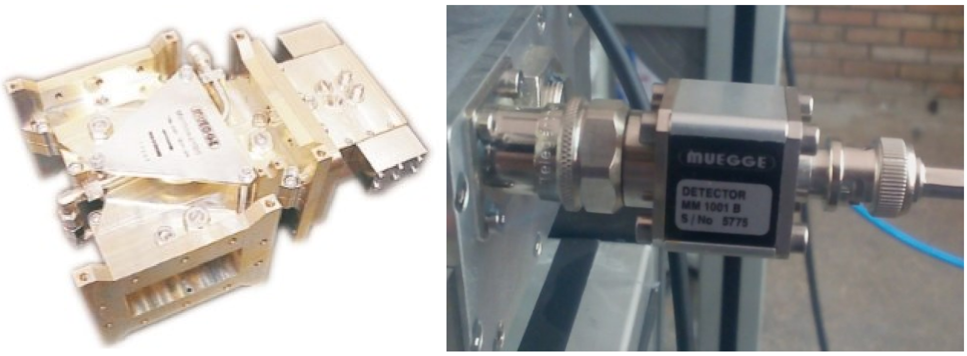

Figure 3.4 Muegge MW1006A-210EC model isolator in connection with Muegge MM1001B-110AB model microwave Detector

The reversed power is controlled by Muegge MM1001B-110AB model microwave detector which is connected to the control software. The reflected power is minimized by adjusting the stub-tuner. Muegge MW1006A-210EC model isolator is used for isolation of magnetron from dummy load. The properties of the isolator are given in Table 3.1.

Table 3.1 Properties of the Isolator

Frequency	2450 MHz
VSWR (Voltage standing wave ratio)	Max. 1.25
Isolation	26 dB
Insertion Loss	0.2 dB
Forward power	6.5 kW
Reflected power	6.5 kW

3.1.4 Stub-tuner

It is designed for load impedance matching in high power microwave heating systems. The stubs come with precision multi turn dial mechanism for tuning adjustment providing a wide range of tuning capability for microwave system of up to 20 kW of forward power at 2450 MHz as given in Table 3.2. The stub tuner is used in order to reduce the Voltage Standing Wave Ratio (VSWR) which is a function of the reflection coefficient. VSWR describes the power reflected from the antenna. The minimum VSWR is 1 which means no reflection (ideal) from the antenna. When an antenna is not matched to the receiver, power is reflected and VSWR is maximized. For the current magnetron the typical VSWR and maximum VSWR are 2.5 and 4. The mismatches are eliminated by using stub-tuner which reduces VSWR in another sense and it makes the impedance matching.

Table 3.2 Properties of the Muegge MW2010A-260EF model Stub-tuner

Frequency	2450MHz
Power	20 kW max.
Tuning capacity	VSWR 10:1

3.1.5 Plasma Applicator

In this component, the microwave power interacts with the plasma gases (air and steam). The plasma is formed inside of quartz tube which is located at the center of the plasma applicator. The microwave signal is transferred from 3 stub tuners to plasma applicator via WR 340 waveguide. It requires air gas flow as a swirl gas up to 200 liters/min and working gas which should be up to the 15 % of the air gas flow rate. The system is cooled by water flow which should be minimum 4 liters/min. The igniter is used in order to start-up the plasma in applicator. The igniter operates by a pneumatic cylinder which is actuated by compressed air. The position of the piston in pneumatic cylinder is detected by proximity sensors. The plasma applicator used in the system is shown in Figure 3.5.

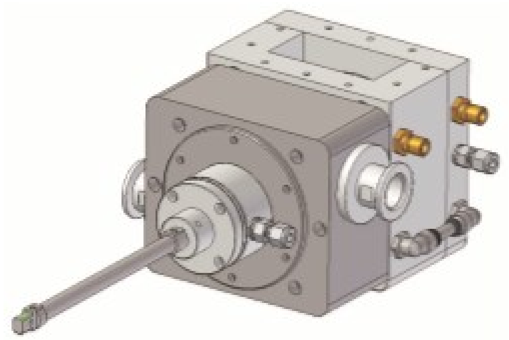

Figure 3.5 Muegge MA6000A-013BB model plasma applicator

3.2 Fluid (Air, Steam) Supply System

The details of the feeding system for steam and air are explained. The solid materials such as powder of coal, sawdust, polyethylene and etc. can be fed into the gasification reactor via a volumetric feeding unit. The KOCH PU-02 model volumetric feeding unit is used in order to feed the solid waste feeding. The amount of solid waste supply rate can be varied from 0 to 2 kg /h. For steam supply, the steam generator with capacity of 6 kg/h steam flow rate at 4 bar gauge pressure and 152 ℃ temperature is used. The required air flow rate is obtained by using Lupamat LKV 30/8 model screw compressor. It generates compressed air which has 8 bar pressure and 4850 l/min flow rate. The required pressure and flow rate are adjusted by using a pressure regulator.

3.2.1 Volumetric Feeding Unit

The KOCH PU-02 model volumetric feeding unit is used in order to feed the solid waste feeding as shown in Figure 3.6.

Figure 3.6 KOCH PU-02 model volumetric feeding unit

It is designed to dose quantities of powdery components. The dosing is effected via the chambers of a feed roller. These are always equally filled. They take the material from the top of the barrel and feed it in metered amounts to the discharge chute. As each chamber has a given volume and the motor runs synchronously, the metered amount is set for the duration of the running time. This time is set via a controller. The amount of solid waste supply rate can be varied from 0 to 2 kg /h.

3.2.2 Compressor

Lupamat LKV 30/8 model single stage screw compressor is used in order to generate compressed air as shown in Figure 3.7. The system generates 4850 L/min flow rate at 8 bar pressure. The compressed air is stored in air tank which has 1m^3 volume. The tank is connected to the compressed air line. The pressure is reduced by using pressure regulator from 8 bar pressure to 4 bar pressure. Then the line is connected to Mass Flow Controller to adjust to the desired flow rate.

Figure 3.7 Lupamat LKV 30/8 model screw compressor with 1m^3 air tank

3.2.3 Steam Generator

Malkan UP100P2E model steam generator with capacity of 6 kg/h steam flow rate at 4.7-5 bar absolute pressure and saturated vapor at 149-152°C temperature as shown in Figure 3.8 used for steam supply. The water is fed into the boiler by pumping system automatically. The water is heated in the boiler by 4.5 kW electrical resistance. The steam generator is connected to the Rotameter to measure the flow rate and adjust to desired level of flow to the reactor.

Figure 3.8 Malkan UP100P2E model steam generator

3.3 Gasification Reactor

Gasification reactor is composed of two sections of cylindrical pipes. The first section is the so-called reduction part comprising the head of the reactor where the diameter is reproduced for the interaction of the water steam by plasma as shown in Figure 3.9.

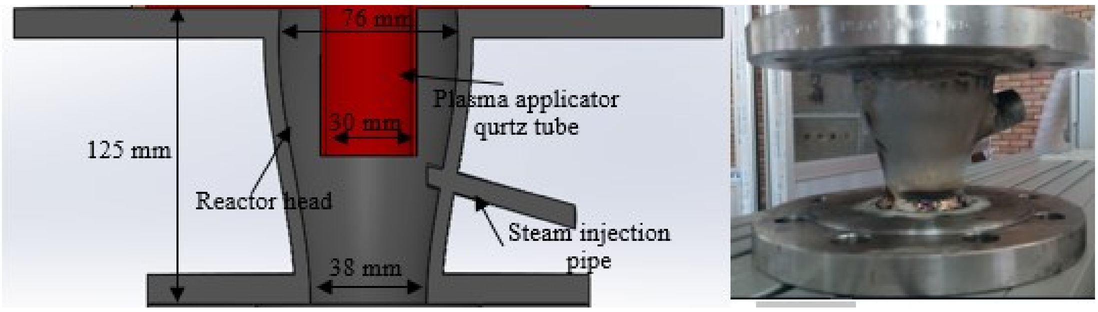

Figure 3.9 Reactor head

The outlet of the plasma applicator has the quartz tube which has 1.5 mm thickness, 30 mm diameter and 200 mm height in the center connected to the head of the reactor. Quartz tube immersion in the head of the reactor is 50 mm. The plasma spout is downward in plasma flame characterization while it was upward in case of gasification process. The other section is the main body of the reactor. The main part is formed of 81mm inner diameter stainless steel pipe which has 3 mm thickness and 500 mm height as shown in Figure 3.10. The reactor includes the holes for thermocouple immersion points.

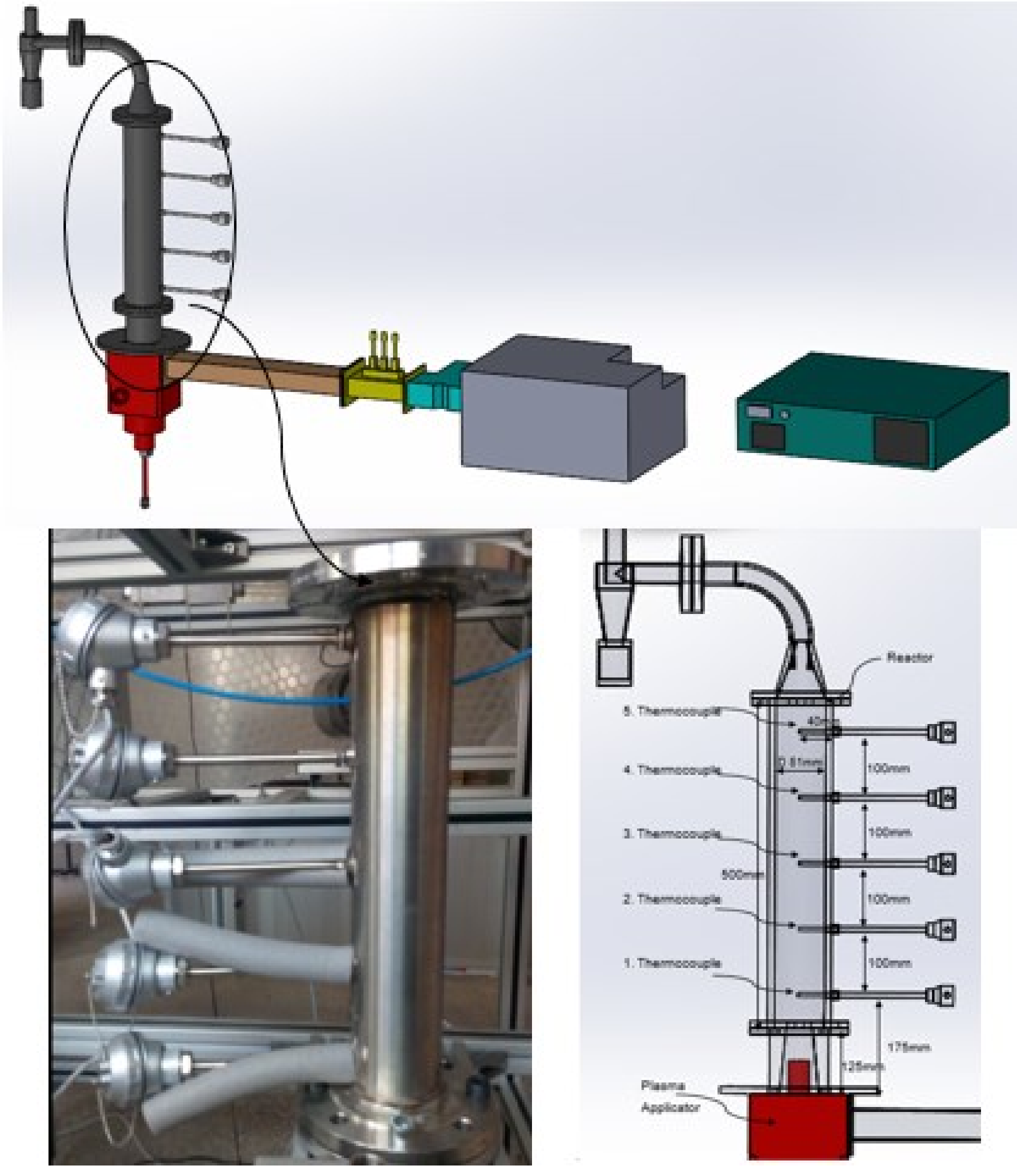

Figure 3.10 Main part of reactor

3.4 Process Output Collection System

As a result of the gasification process, the generated syngas which includes ash and solid particles requires handling process.

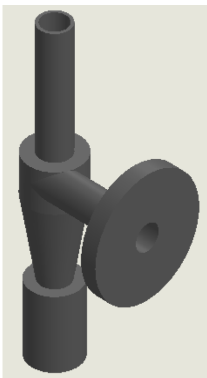

Figure 3.11 Custom-made cyclone filter

Ash and solid particles in the syngas are removed by means of a custom-made cyclone filter as shown in Figure 3.11. The flow which pass through the cyclone filter is estimated to be varying between the 0-15 m^3/h. It is produced by using the components what is available in market. 53mm inner diameter pipe is chosen as a body diameter to satisfy the required flow rate. 53 mm to 28 mm and 28 mm to 21 mm reductions are welded. To satisfy the height of the cylinder, 53 mm inner diameter and 35 mm long pipe weld to one end, nipple which has 21mm diameter are added to another end. At the bottom, the collection unit for ash is prepared. The 28 mm inner diameter pipe which has 150 mm length is immersed into the inside of 53 mm inner diameter pipe by 30 mm.

Table 3.3 Dimensionless parameters for Stairmand model cyclone design (Moore and McFarland, 1990)

	Stairmand model
Body Diameter	1
Inlet height (a/D)	0.5
Inlet width (b/D)	0.2
Outlet length (S/D)	0.5
Gas outlet diameter (De/D	0.5
Cylinder height (h/D)	1.5
Overall height (H/D)	4
Dust outlet diameter (B/D)	0.375

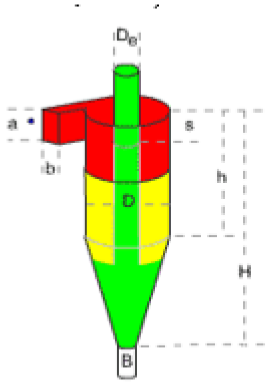

The gap between 53 mm inner diameter pipe and 28 mm inner diameter pipe is filled by welded collar. 28mm inner diameter pipe is welded tangentially to the side of the 53 mm inner diameter pipe where the gases will come by this pipe. The dimensions are nearly the same with the Stairmand model cyclone dimensions (Moore and McFarland, 1990) as given in Table 3.3. For the inlet, instead of rectangular cross section, a circular cross section is used.

3.5 Measurement and Data Acquisition Chain

The each measurement systems for the flow/feed rate, temperature, power consumption, gas analyzing system, proximate and ultimate analysis, SEM/EDX analysis, heating value measurement and mass/volume analysis of fuel are given this section as presented in Figure 3.12.

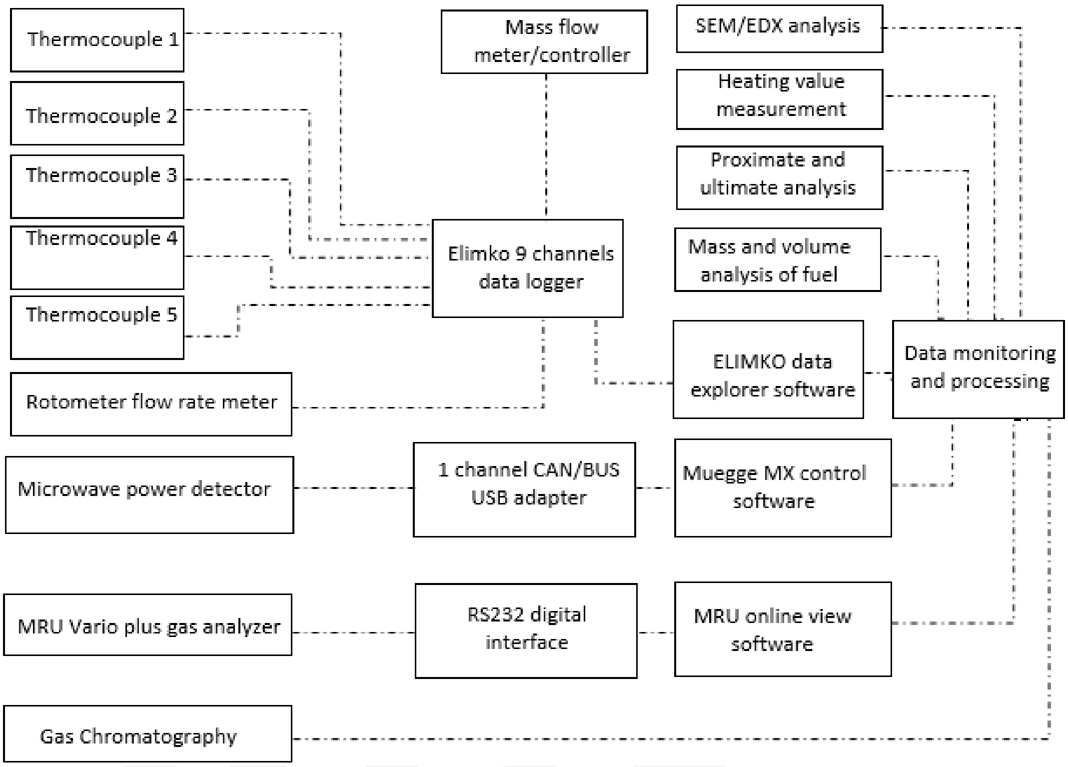

Figure 3.12 The block diagram of the measurement and data acquisition chain

3.5.1 Air Flow rate measurement

For the air flow rate, ALICAT MCR-250SL/MIN-D model mass flow controller as shown in Figure 3.13 is used. It measures the flow rate from 1.25 sL/min up to 250 sL/min. Its accuracy is ± 0.8 % and $\pm$ 0.2 % for reading and full scale respectively. Its repeatability is$\pm$ 0.2 %. It can be operated between -10 to 50°C temperature and up to 10 bar pressures. It can measure the mass flow rate, volumetric flow rate, ambient temperature and pressure. It is also used for the measurement of the ambient conditions.

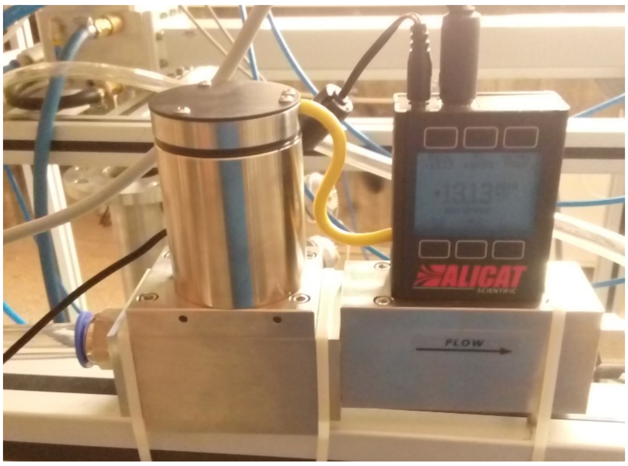

Figure 3.13 ALICAT MCR-250SL/MIN-D model mass flow controller

3.5.2 Steam Flow rate measurement

The steam flow rate is measured by YOKOGAVA RAMC01-A1SS-53L1-E90424/A16/SD model rotameter as shown in Figure 3.14 in the range from 4.5 L/min up to 45 L/min at the 150 °C temperature and 4.75 bar absolute pressure. It is calibrated for the fixed state of the steam generator. However, the steam generator generates the steam at 4.7-5 bar pressure and 149-152°C. The variation in temperature and pressure caused error which was calculated in uncertainty analysis in section 3.9.

Figure 3.14 YOKOGAVA RAMC01-A1SS-53L1-E90424/A16/SD model rotameter

3.5.3 Solid feeding rate measurement

The KOCH PU-02 model volumetric feeding unit is used in order to measure and feed solid material. The device works by taking the material from the top of the barrel and feeds it in precisely metered amounts to the discharge chute. As each chamber has a given volume and the motor runs synchronously, the metered amount is set for the duration of the running time. This time is adjusted via a controller.

3.5.4 Temperature measurement

The thermocouples which are located at measurement positions along the reactor length in the flow direction of plasma. The first measurement location from the plasma applicator's edge is 175 mm away because of the extreme high temperature of the plasma. The height (h) of the reactor which begins from the applicator to the end of the main reactor is 625 mm. 5 thermocouples are used in order to obtain the temperature profile and they are located along the axis of the pipe with 100 mm intervals. The locations of the thermocouples are $y/h = 0.28, 0.44, 0.6, 0.76$ and 0.92. The B type (Pt18Rh-Pt) thermocouple is used with pure alumina coating. Its measuring ability is the temperatures up to 1820°C with an accuracy of ±4°C. The thermocouple sensing edges are immersed at 40 mm perpendicular to the reactor wall such that the measurement inside the plasma flame is possible. The measured inputs are recorded via Elimko E-PR-110 model data acquisition card. It can log analog signal from the device. It has 9 channels. The 5 channels are used to record the temperature measurements. The data logger includes calibration file which is provided by manufacturer and it is used to convert the mV signal outputs to the temperature. Because, the B type thermocouple output voltage signal changes non-linear up to 1000°C. In the laboratory of mechanical engineering department of Gaziantep University, there is not accurate temperature gage for high temperatures. That is the reason why the calibration file of the manufacturer was used instead of preparing our own calibration file.

When the system operated without fuel, the measurement procedure is as follows. Before starting the measurement, the system operated half an hour to provide the steady conditions. Also, the 10 minutes interval is given between two measurements. The temperature measurements are recorded with 1 second sampling period. In case of dosing fuel in the reactor, the continuous temperature measurement is recorded with 1 second intervals. Depending on the process time, the recorded data is varied. The sampling rate in all measurements are 1 data per second. The mean of temperature in each station is calculated by using equation 3.1.

$$\mathrm{T}_{\mathrm{y/h}} = \frac{1}{\mathrm{t_g}} \sum_{\mathrm{t}=1}^{\mathrm{t_g}} \mathrm{T}_{(\mathrm{y,t})} \tag{3.1}$$

The reactor average temperature is determined by using equation 3.2 by taking the average of temperatures in the 5 measurement stations. The average temperature in each measurement location and their average denoted by T_{syn} are presented in Table 3.2.

$$\mathrm{T_{syn}}(°\mathrm{C}) = \left(\mathrm{T}_{\mathrm{y/h}=0.28} + \mathrm{T}_{\mathrm{y/h}=0.44} + \mathrm{T}_{\mathrm{y/h}=0.6} + \mathrm{T}_{\mathrm{y/h}=0.76} + \mathrm{T}_{\mathrm{y/h}=0.92}\right)\Big/5 \quad (°\mathrm{C}) \tag{3.2}$$

3.5.5 Power measurement

The Muegge MM1001B-110AB model microwave power detector is used in order to measure the reflected power. It delivers DC signal as a function of incident microwave power. It is connected to the The Muegge MX model control software for microwave plasma system. The input power can be varied with 1 % steps where the capacity of magnetron is 6 kW. The reflected and the acted power are monitored. The reflected power is minimized and the acted power is maximized by using the power detector. Also, the system operates efficiently by reducing the reflected power.

3.5.6 Data logger

The measured inputs are recorded via Elimko E-PR-110 model data logger. It stores the data to the 8 GB micro SD flash internal. It has USB channels and the data can be transferred via USB to the computer and processed via ELIMKO file explorer and Microsoft Excel. It is also possible to monitor the channels online via ELIMKO data explorer. It can log analog signal from the devices. It has 9 channels. The 5 channels are used in order to record the thermocouples measurements. The other channels are used in order to record each measurement of the steam flow rate, air flow rate, solid feed rate monitoring. Its accuracy for each channel is 0.5 % of reading data. It has 100 ms sampling period for each channels.

3.5.7 Gas analyzing of the syngas

MRU-Various plus model syngas monitoring system as shown in Figure 3.15 is used in order to determine the syngas content.

Figure 3.15 MRU-Various plus model syngas monitoring system

It provides continuous syngas monitoring of the process. It can measure the syngas content of CO, CO_2, CH_4, H_2, and N_2 up to 100 % and O_2 up to 25 %. It uses the nondispersive infrared sensors to measure the CO, CO_2 and CH_4 while it uses the Thermal conductive detector and electrical conductive sensor to measure the H_2 and

O_2 respectively. It has 1 % linearity and repeatability error. It has also 2 % span drift and 0.05 % detection limit. The measurements are recorded by the device which is connected to computer to monitor and data acquisition. The sampling rate is adjusted to 1 data per 2 second. The system records the gas composition continuously. The process time is determined from the gas composition changes at the beginning and at the end of the process. The location of the gas sampling on the reactor is presented in Figure 3.16.

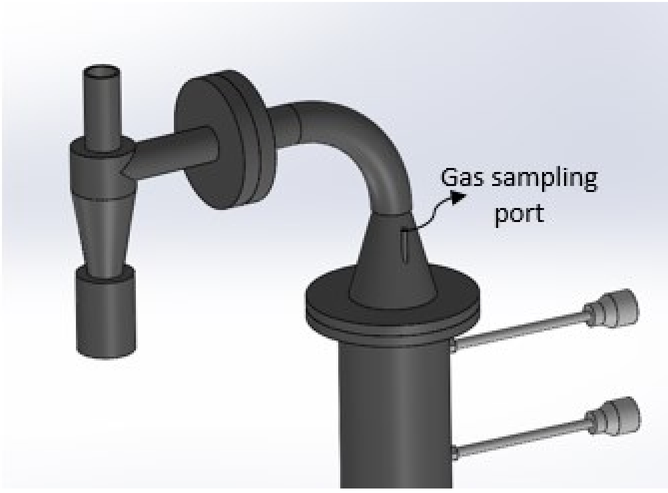

Figure 3.16 Gas sampling port on the reactor

3.5.8 Solid fuel characteristics evaluation

The properties of solid fuels are examined by proximate and ultimate analysis. The heating value of the fuels are measured and calculated. Also, the surface properties are examined by SEM and EDX analysis.

Proximate analysis; the proximate analysis tests are performed by using the oven of Eltra Sulphur content measurement system. The oven of the system is PC-controlled and the temperature in oven can be adjusted to desired temperature. The required mass measurements of the solid fuels for analysis are measured by TP 214 model mass balance device. The proximate analysis are performed according to ASTM D 3172-89 analysis methods. Moisture content, ash content and volatile matters are determined according to D3172, D3174 and D3175 respectively. The detailed calculations and methodology are given in section 4.

Ultimate analysis; the ultimate analysis tests are performed at Şeyh Edebali University central laboratory by service purchase. In the tests, the LECO CHN 628 elementary analyzer system is used. The experiments are performed according to standards given in Table 3.4. Detailed calculations and methodology are given in section 4.

Adiabatic bomb calorimeter; the heating value of the fuels are determined by an adiabatic bomb calorimeter. The tests are performed according to ASME D 5865. The required mass measurements of the solid fuels for analysis are measured by TP 214 model mass balance device. For the temperature measurement in bucket, the Testo 735 model PT100 thermocouple is used. The detailed calculations and methodology are given in section 4.

Table 3.4 The methods and standards can be used for ultimate analysis depending on material

Applied method (ASME)	Measured parameters	Material
D5291	C ,H, N	Oils
D5373/MTH A	C ,H, N	Coals
D1552	S	Oil and petroleum products
D4239	S	Coals
D5016	S	Coals and ash
29541	C,H,N	Solid mineral fuels
19579	S	Solid mineral fuels

SEM/EDX analysis; The Scanning electron microscope (SEM) and EDX analysis of the solid fuels and ash components of the products are performed at Gaziantep University SEM laboratory by service purchase. JEOL 6390LV Scanning Electron Microscope with EDX detector is used in the analysis.

3.6 Preliminary studies of Plasma Calibration

The heating in the reactor is performed by Microwave plasma system and the temperature in the reactor varies with the plasma flame properties. However, the plasma flame characteristic is not visible in the gasification process. That is why, the plasma flame characteristics should be investigated for the optimum performance of the plasma gasification systems. For the gasification performance, the high temperature and the distribution of the plasma flame in the reactor are essential. The effects of the power, air flow rate and steam flow rate on plasma flame shape, temperature distribution and magnitude are investigated in this section. The given results are presented in conference and published in journal (Sanlisoy and Carpinlioglu, 2017; Sanlisoy and Carpinlioglu, 2016). The system is operated at varied air flow rate, steam flow rate and microwave power level. The plasma flame pictures are taken for the each case. The pictures are captured by the Sony Cybershot DSC-W220 12.1 Digital Camera. The camera is hold perpendicular to the plasma applicator. The distance from applicator to the camera is approximately 2 m. The dimensions of the plasma in Figures are analyzed by using Origin Pro 8.5.1 program. The Figures are captured by digitizer tool of the Origin Pro 8.5.1. For this purpose the pictures are taken perpendicular as much as possible to the plasma applicator. Each picture size is calibrated to the known dimensions in the pictures. The measured dimensions have approximate results which are extracted from digitizer.

In case of supplying just air to the reactor, the plasma flame characteristics are examined from the exit of plasma applicator. On the other hand, in case of supplying air and steam to the reactor, the flame characteristics are examined from the exit of reactor head. Because, the steam flow is supplied to the reactor from the side of reactor head. The supplying steam flow from the plasma applicator is tested. However, the saturated steam damps the plasma flame. After that, the supplying steam from the side of reactor is tested and the results are presented in steam-air supplying section.

Effects of Parameters on Plasma Flame Shape in Case of Air supplying: The properties of the air plasma are presented in the Table 3.5. When air flow rate is 50 sL/min, the diameter of the plasma is nearly the same up to 0.6 kW. Increasing power causes enlargement in the diameter when the power is between 0.6 kW and 3 kW. More increment in power from 3 kW to 3.6 kW does not cause a change in the diameter. However, the length of the plasma flame rises from 59 mm to 123.5 mm by gradually increasing power. The length of the plasma cannot be read after 1.5 kW, because its length increases to 123.5 mm which matches with the lower section of the reactor. Also, the plasma tail is unclear to observe. When the flow rate is increased up to 100 sL/min, the change in plasma shape is observed. While it is pointed end, it turns to the spread shape. The diameter of the plasma is nearly same up to 1.8 kW. Increasing power causes enlargement in the diameter when the power is between 1.8 W and 2.7 kW. Increasing power from 2.7 kW to 3.6 kW causes no change in the diameter. However, the length of the plasma flame rises from 59 mm to 131.5 mm by gradually increasing power. The length of the plasma cannot be read after 3.6 kW because of similar manners for 50 sL/min air flow rate.

Table 3.5 Plasma properties (Size and shape of the plasma)

50 sL/min air flow rate				100 sL/min air flow rate			
Power (W_{plasma}) (W)	Length (L) (mm)	Diameter (D) (mm)	Shape of plasma	Power (W_{plasma}) (W)	Length (L) (mm)	Diameter (D) (mm)	Shape of plasma
300	56.6	13.5	spreading	300	60.5	15	spreading
600	57.7	13.	spreading	600	59	15	spreading
900	65.4	14.6	spreading	900	59	15	spreading
1200	122	15.1	pointed end	1200	72.5	15.6	spreading
1500	123.5	17	pointed end	1500	72	15.9	spreading
1800	not estimated	20.7	pointed end	1800	77.8	15.9	spreading
2100	not estimated	18.6	pointed end	2100	80	16.5	spreading
2400	not estimated	18.8	pointed end	2400	82.3	17.1	spreading
2700	not estimated	19.1	pointed end	2700	89.3	18.2	spreading
3000	not estimated	20.2	pointed end	3000	92.1	17.8	spreading
3300	not estimated	19.9	pointed end	3300	101.2	18.1	spreading
3600	not estimated	20.4	pointed end	3600	131.5	17.4	spreading
3900	-	-		3900	not estimated	17.8	pointed end
4200	-	-		4200	not estimated	17.8	pointed end

Figure 3.17 shows that the increasing power causes more intensive and bigger plasma. The plasma flame spreads along the reactor axis after 0.9 kW in case of 50 sL/min air flow rate. By increasing the power, both the diameter and length of the plasma increase. Also its intensity increases.

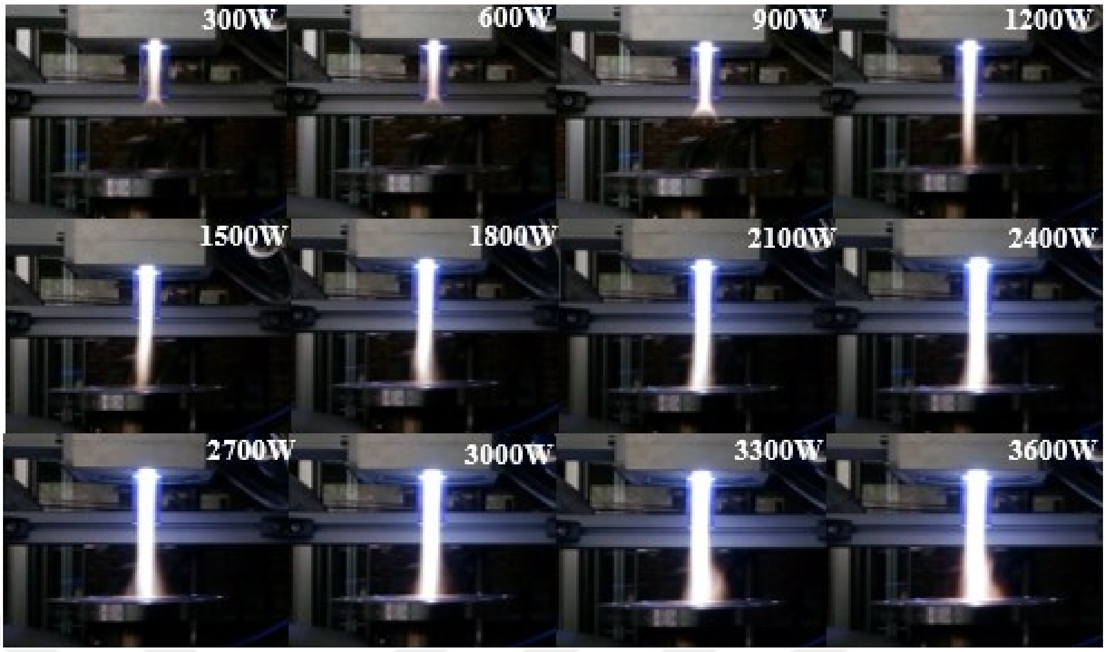

Figure 3.17 Effects of microwave power on plasma performance in case of 50 sL/min air flow rate

In Figure 3.18, the effects of power change in plasma are investigated when the air flow rate is in 100 sL/min. In this case, the plasma volume is spread after 1.8 kW power. When it is compared by 50 sL/min air flow rate, the similar plasma volume is observed at much higher power levels.

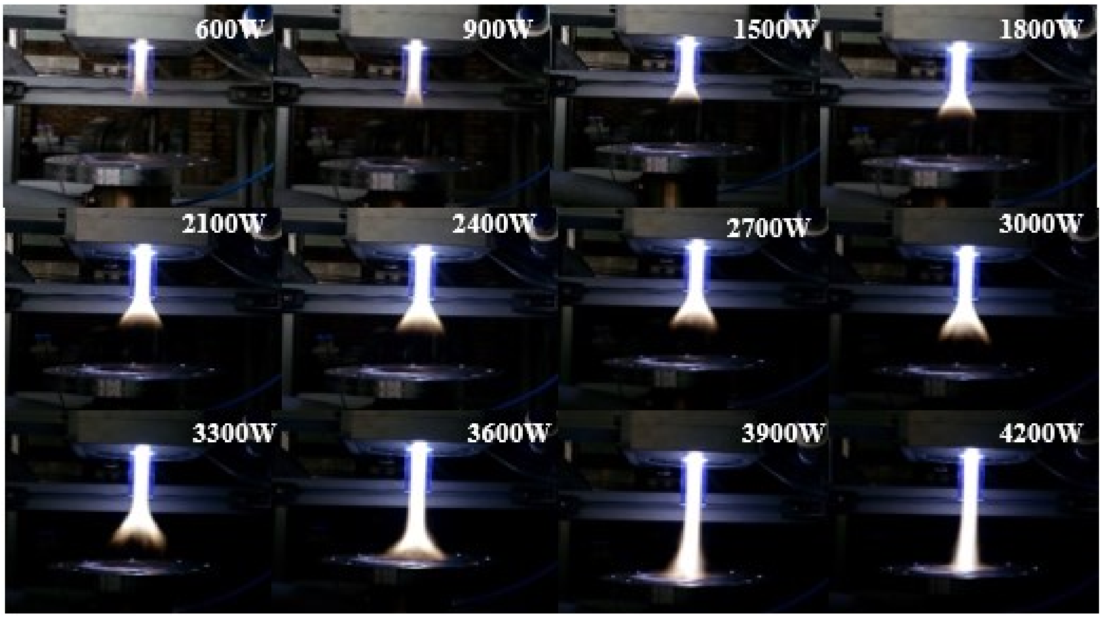

Figure 3.18 Effects of microwave power on plasma performance in case of 100 sL/min air flow rate

In Figure 3.19, the flow rate of the air is varied at 3.6 kW plasma power to reveal the effects of air flow rate. The results clearly show that the flow rate has inversely proportional relation by plasma volume. The reason is, the instant energy is shared by the flow in the applicator. The similar trend is given in the study of Leins (Leins, 2010) where the power is proportional and flow rate has inversely proportional effect on plasma diameter and length respectively.

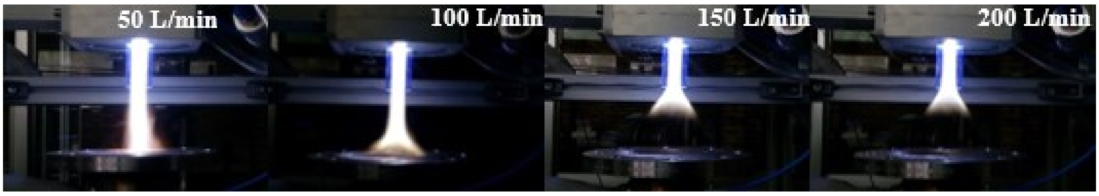

Figure 3.19 Effects of the air flow rate on plasma performance in case of 3600W plasma power

Effects of Parameters on Plasma Flame Shape in Case of Air-Steam supplying: The geometrical properties of the air-steam plasma are presented in the Table 3.6. The plasma flame pictures are taken at the exit of reactor head. The plasma flame diameter and length are 28 mm and 120 mm respectively at 0.6 kW in case of 50 sL/min of air flow. The plasma flame increases to 42.8 mm diameter and 251.5 mm length by increasing power to 6 kW. In case of 50 sL/min air flow and 9 L/min water vapor, the plasma flame diameter and length are 20.8 mm and 71.7 mm respectively at 0.6 kW.

Table 3.6 Plasma properties in case of usage of water vapor

Power (W_{plasma}) (W)	Length (L) (mm)	Diameter (D) (mm)	Power (W_{plasma}) (W)	Length (L) (mm)	Diameter (D) (mm)
50 sL/min air			50 sL/min air-9 sL/min water vapor		
600	120	28	600	71.7	20.8
1200	140	28.9	1200	83.2	21.5
2100	143.4	30	2100	97	24.2
2400	149.9	33	2400	125.7	34
3000	202.2	36.4	3000	150.4	33.3
3600	251.5	42.8	3600	178.9	33.6
50 sL/min air-18 sL/min water vapor			50 sL/min air-27 sL/min water vapor		
600	40	7.5	600	-	-
1200	57	15.8	1200	25.7	6.8
2100	62.5	17.3	2100	28.9	11.9
2400	75.6	21.4	2400	64.8	17.4
3000	84.8	26.5	3000	102	23.4
3600	125	27.4	3600	128.9	27.8

The plasma flame increases to 33.6 mm diameter and 178.9 mm length by increasing power to 6 kW. In case of 50 sL/min air flow and 18 L/min water vapor, the plasma flame diameter and length are 7.5 mm and 40 mm respectively at 0.6 kW. The plasma flame increases to 27.4 mm diameter and 125 mm length by increasing power to 6 kW. In case of 50 sL/min of air and 27 L/min vapor, the plasma flame could not spread from the reactor head at 0.6 kW. It has 6.8 mm diameter and 25.7 mm length at 0.6 kW. The plasma flame increases to 27.8 mm diameter and 128.9 mm length by increasing power to 6 kW. Results clearly showed that, the plasma flame diameter and length are increases by increasing power. While it has 42.8 mm diameter and 251.5 mm length in case of without steam and 50 sL/min air, it reduces to 27.8 mm diameter and 128.9 mm length by using 27 L/min steam flow rate and 50 L/min air flow rate. The diameter of the plasma flame decrease 35 % and its length decreases almost 50 %. The plasma flame characteristics at the exit of reactor head in case of 50 sL/min air flow rate is given in Figure 3.20. It is seen that the increasing power causes more intensive and larger plasma. The plasma flame spreads along the reactor axis after 600 W in case of 50 sL/min air flow rate. By increasing the power, both the diameter and length of the plasma increase. Also its intensity increases.

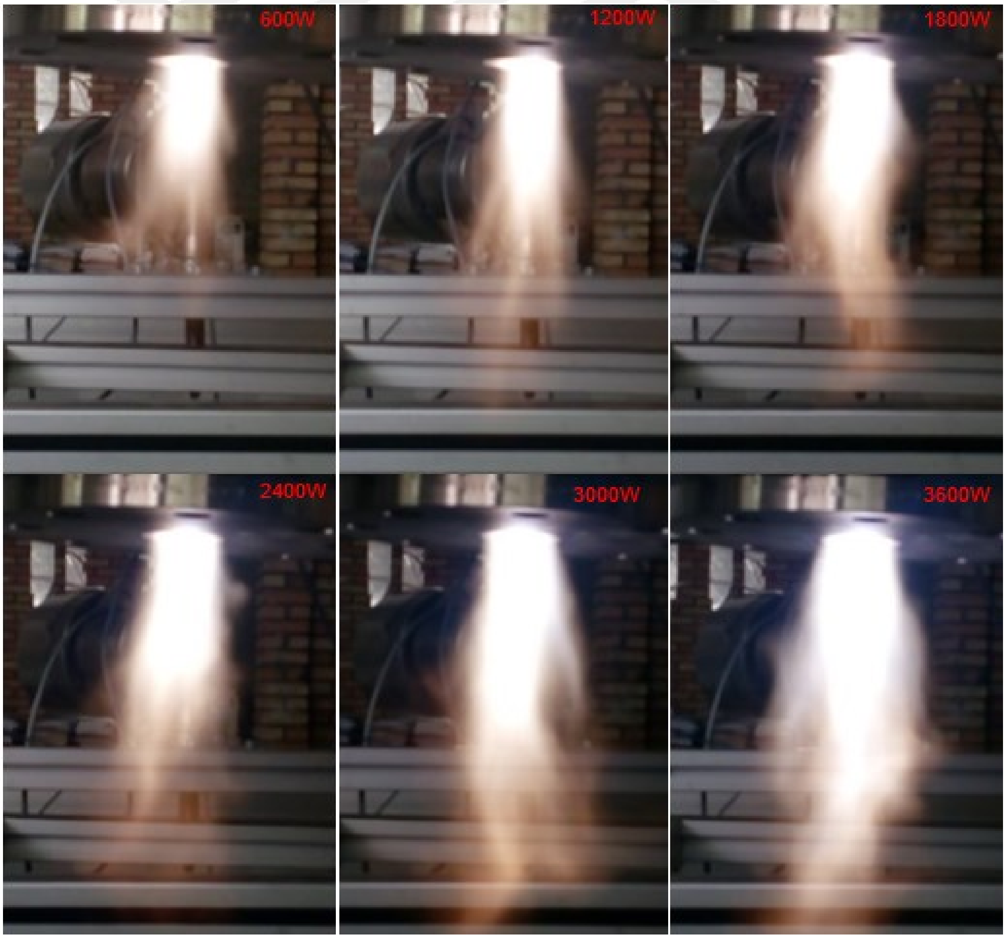

Figure 3.20 Effects of microwave power on plasma flame in case 50 sL/min air flow rate

Figure 3.21 shows the plasma flame characteristics at the exit of reactor head in case of 50 sL/min air flow rate and 9 L/min water steam flow rate. It is seen that the increasing power causes more intensive and bigger plasma. However, the addition of water vapor to the reactor suppresses the plasma flame and reduces the diameter and length of plasma flame. The plasma flame spreads along the reactor by increasing the power. Both the diameter and length of the plasma increase by increasing the power. Also its intensity increases and the color of plasma changes from orange color to the blue.

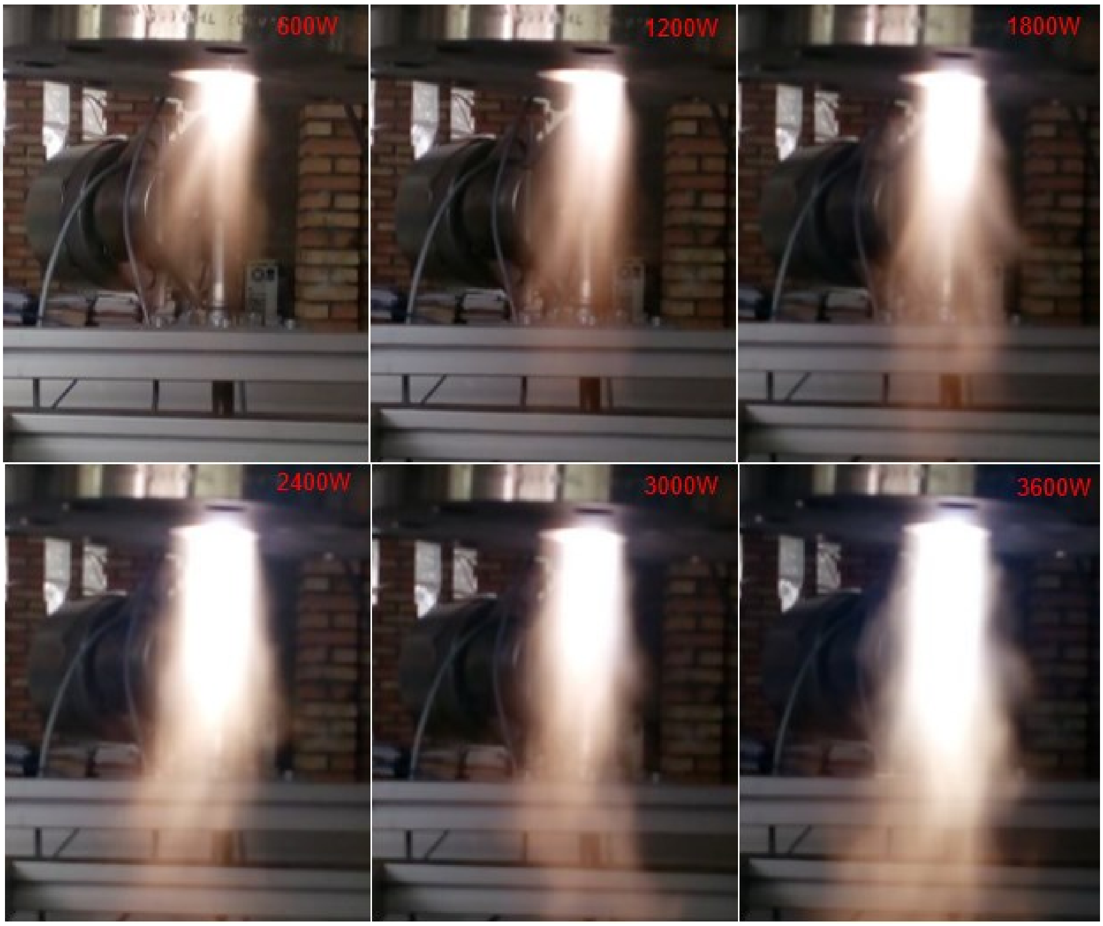

Figure 3.21 Effects of microwave power on plasma flame in case of 9 L/min water steam and 50 sL/min air flow rate

Figure 3.22 shows the plasma flame characteristics at the exit of reactor head in case of 50 sL/min air flow rate and 18 L/min water steam flow rate. It is seen that the increasing power causes more intensive and bigger plasma. However, the increment of water vapor flow rate suppresses more the plasma flame, reduces the diameter and length of plasma flame and changes the plasma color to more orange. The plasma flame spreads along the reactor by increasing the power. Both the diameter and length of the plasma increase by increasing the power. Also its intensity increases and the color of plasma changes from orange color to the blue.

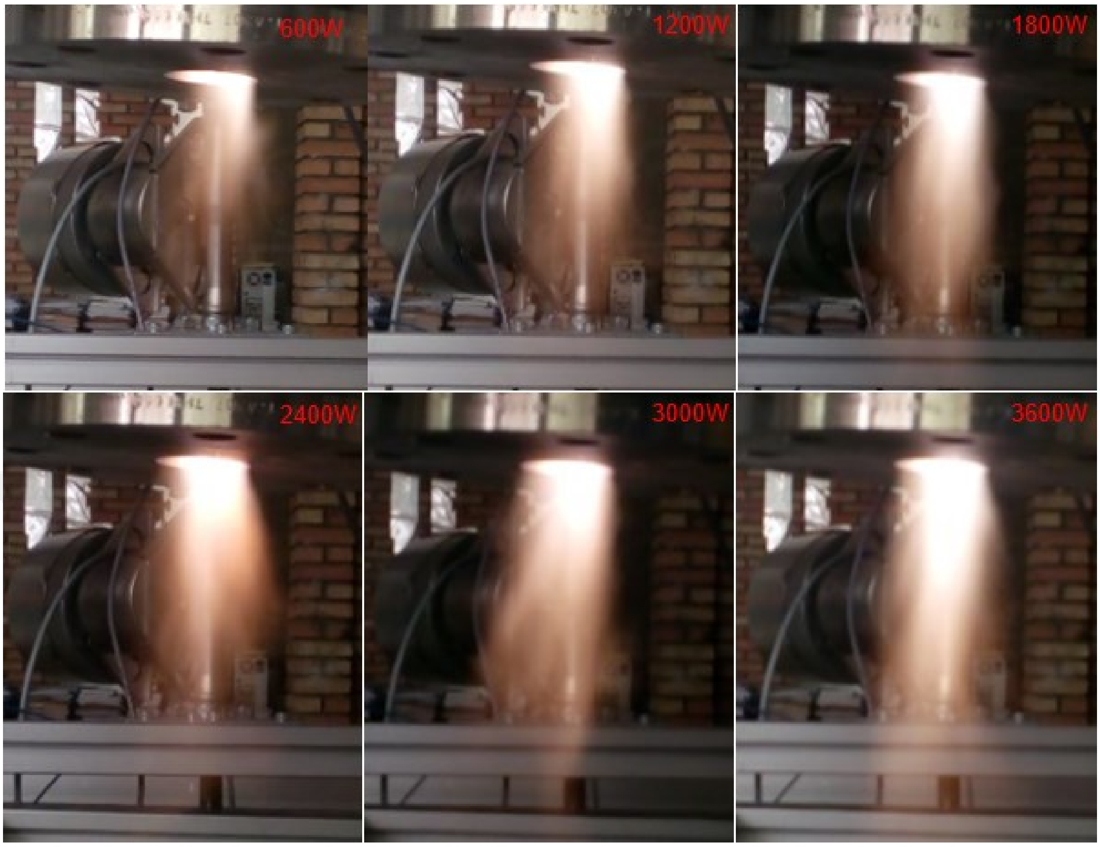

Figure 3.22 Effects of microwave power on plasma flame in case of 18 L/min water steam and 50 s L/min air flow rate

Figure 3.23 shows the plasma flame characteristics at the exit of reactor head in case of 50 sL/min air flow rate and 27 L/min water steam flow rate. It is seen that the plasma flame starts to spreads along the reactor by power levels of 1.8 kW and it spreads along the reactor by increasing the power. The reason of the plasma flame suppress may be the heating capacity of water. Because of the high heating capacity of water, the plasma power become insufficient to spread the plasma. The plasma flame is suppressed more and more by increasing the flow rate of the water vapor. Increasing water vapor flow rate suppresses more the plasma flame, reduces the diameter and length of plasma flame and changes the plasma color to more orange. Both the diameter and length of the plasma increase by increasing the power. Also its intensity increases and the color of plasma changes from orange color to the blue by increasing the power.

Figure 3.23 Effects of microwave power on plasma flame in case of 27 L/min water steam and 50 sL/min air flow rate

Gasification Reactor Temperature Measurements: The temperature distributions in gasification reactor are investigated in this section. The temperature variations by changing the power level between 1.8 kW-6 kW are examined in case of 50 sL/min and 100 sL/min air flow rates. In Figure 3.24, the temperature distribution is presented in case of 50 sL/min air flow rate. The thermocouple which is located at y/h=0.28 (closest measurement point to plasma flame) measures the highest temperature $T_{y/h=0.28} = 718$ °C at 1.8 kW power. By varying the power from 1.8 kW to 6 kW, the temperature at y/h=0.28 ($T_{y/h=0.28}$) is increased from 718 °C to 1265 °C. From the region of the plasma flame to downward, the temperature decreases gradually. The minimum measured temperature is 281 °C at y/h=0.92 ($T_{y/h=0.92}$) and 1.8 kW power which is the most distant measurement point from the plasma flame. It varies from 281°C to 710 °C by increasing the power from 1.8 kW to 6 kW. The average temperature (T_{syn}) in the reactor increases from 480 °C at 1.8 kW power to 1018 °C at 6 kW power.

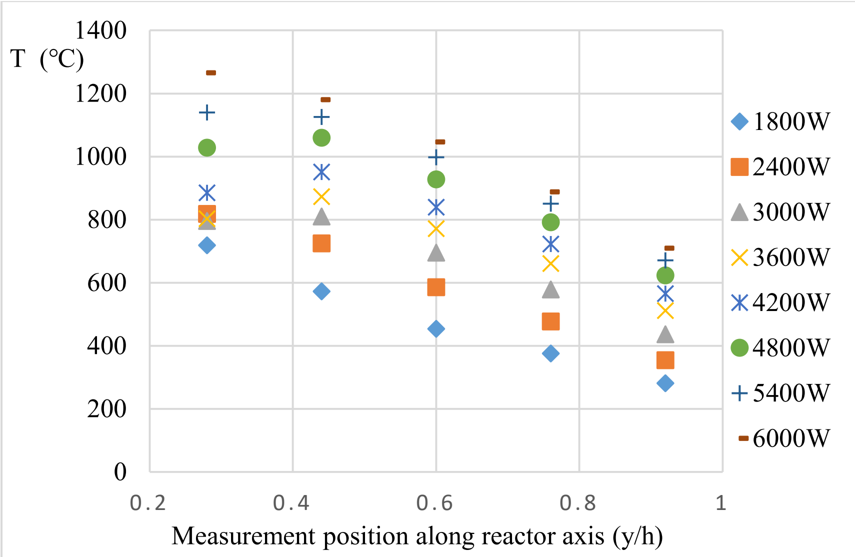

Figure 3.24 Temperature distribution in the gasification reactor in case of 50 sL/min air flow rate

In Figure 3.25, the temperature distribution is presented in case of 100 sL/min air flow rate. The thermocouple which is located at y/h=0.28 (closest measurement point to plasma flame) measures the highest temperature $T_{y/h=0.28} = 483$ °C at 1.8 kW power. By varying the power from 1.8 kW to 6 kW the temperature at y/h=0.28($T_{y/h=0.28}$) increases from 483 to 1275 °C. From the region of the plasma flame to downward, the temperature decreases gradually. The minimum temperature, at 260 °C is measured at the y/h=0.92 ($T_{y/h=0.92}$) which is the most distant measurement point from the plasma flame.

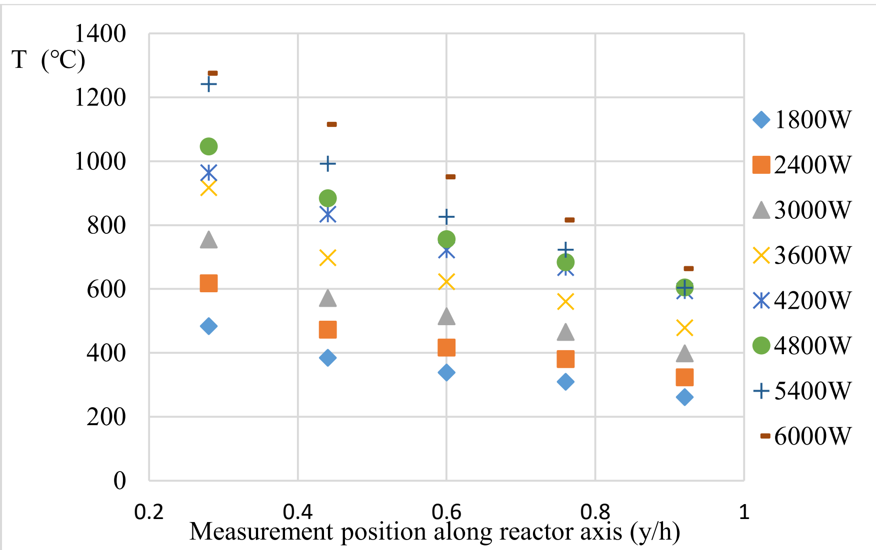

Figure 3.25 Temperature distribution in the gasification reactor in case of 100 sL/min air flow rate

It varies from 260 °C to 663 °C by increasing the power from 1.8 kW to 6 kW at the y/h=0.92 ($T_{y/h=0.92}$). The average temperature (T_{syn}) in the reactor increases from 348 °C at 1.8 kW power to 918 °C at 6 kW power.

Increasing the air flow rate causes the shortening of the length of the plasma as observed in pictures. This also causes the reduction in temperature. The average temperature (T_{syn}) reduces from 1018 °C to 918 °C when the air flow rate is increased from 50 sL/min to 100 sL/min. The reason of temperature reduction may be the reduction of the plasma intensity. However, the higher flow rate causes the reduction in temperature gradient along the axis. The temperature distribution is more uniform at 100 sL/min air flow rate. This is also an expected result. It is clear that when the plasma has spreading shape, the temperature is lower and more uniform. In case of pointed end plasma, the temperature is higher and its gradient is higher.

3.7 Changes in the system design and the applications

In this section, the problems that occurred during the system installation and experimentation are explained. The revisions were mainly for the reactor design of the MCw gasification reactor and the gas analysis system.

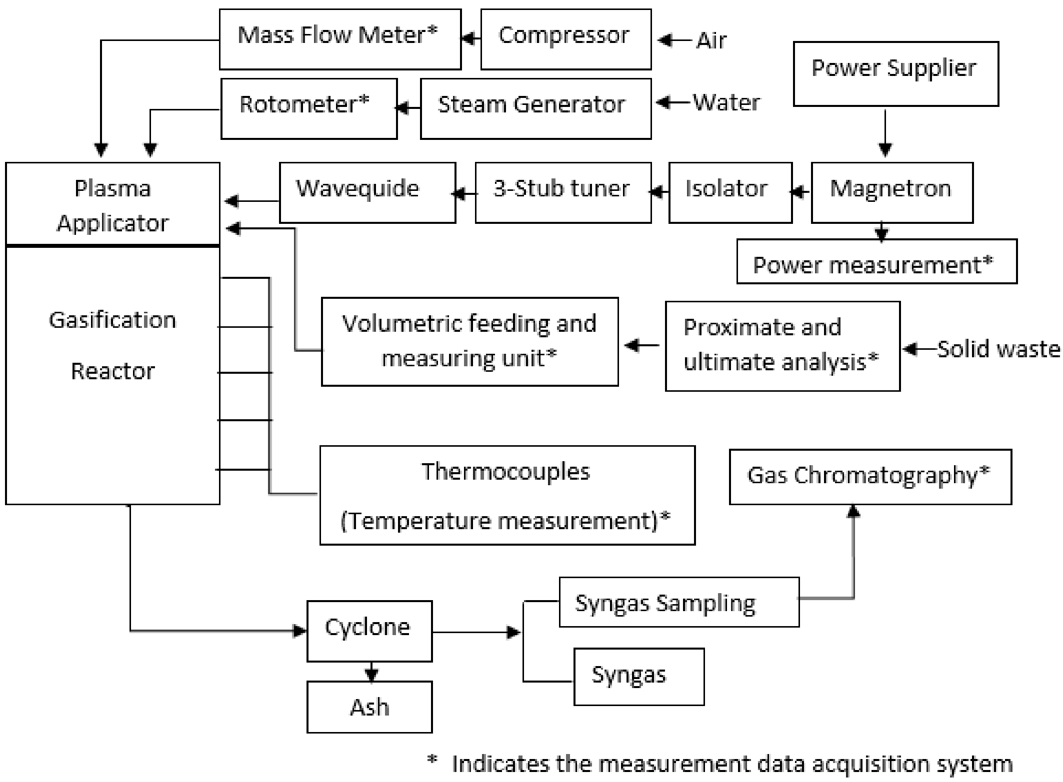

Figure 3.26 The first proposed experimental set-up

The first proposed experimental setup was presented in Figure 3.26. The occurred problems and the solutions of the problems are given below;

1-Solid fuel feeding to reactor; It was proposed to feed the solid fuels by fuel supply system. However, the pressure in reactor was higher when compared with the pressure in the barrel of the feeder. So, fuel particles were reversed.

As a solution, the fuel supply system was isolated from the leakages of air in storage place. Also, the air flow is by-passed. By this way, the reactor and the feeder became in same pressure. The solid feeding location had to be changed by these modifications.

2-Solid fuel feeding location; It was proposed to feed the solid particles by reactor head fuel feeding port. However, it was changed to satisfy the equilibrium of pressure in solid feeder and reactor.

The solid fuels were mixed with air and supplied to the system by plasma applicator air inlet port to satisfy equilibrium of pressure in reactor and solid fuel feeder. The new proposed system configuration is given in Figure 3.27.

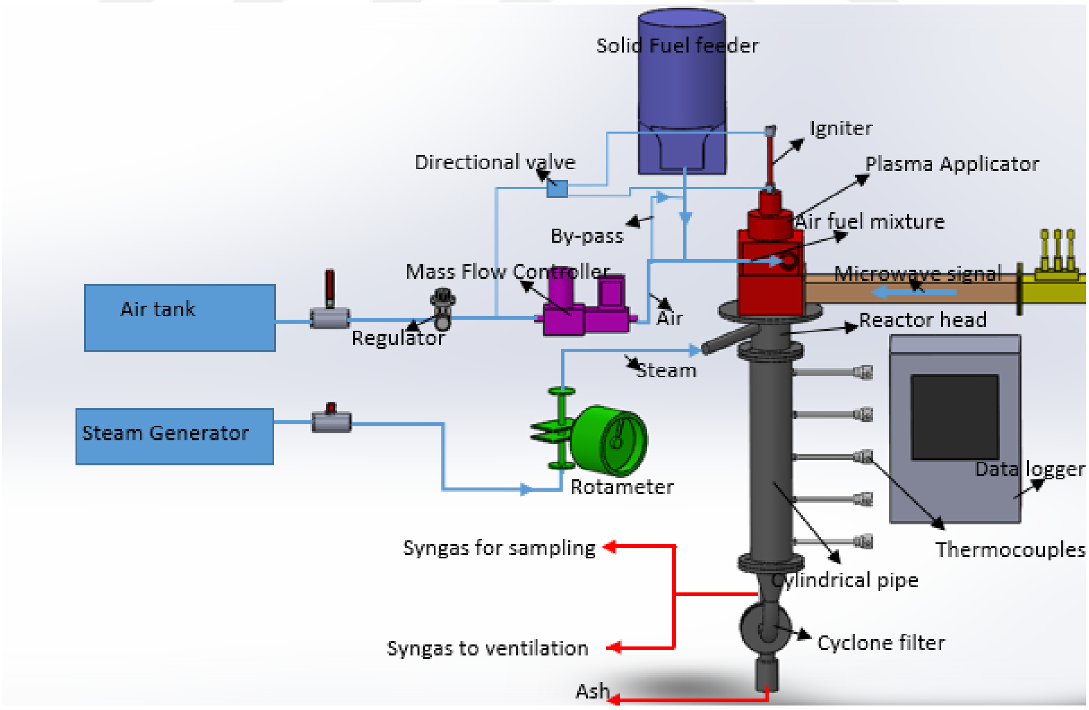

Figure 3.27 The revised experimental set-up to overcome the feeding of the solid fuel

3-Direction of the plasma flame; the production and control of microwave flame plasma was specified under atmospheric conditions as given in section 3.6. Then the plasma applicator is connected to the reactor head. By the modifications explained in previous section, the solid fuel feeding is also provided when the system is operated. However, the syngas production was not achieved because of the air amount was much higher than the fuel in reactor. The gases are without color. The products are mainly consist of CO_2, O_2 and N_2. The gas content is 20 % CO_2, 1- 2 % CO, 10 % O_2, and 65 % N_2. Although the fuel feeding rate is adjusted to feed the maximum solid fuel and the air flow rate reduced to 50 sL/min, the syngas production was not achieved. In case of reducing air flow rate to the less than 50 sL/min, the swirling flow does not occur in plasma applicator. So, the quartz glass in the center of the applicator melt. It is caused because of high energy density in it. As a result, the minimum air flow rate and maximum fuel feeding rate were restricted. To overcome these problems, the reactor is dosed by certain amount of solid fuel (250 g) and then the plasma is activated instead of simultaneous feeding and plasma operation. In this case, the produced gas content is similar to the simultaneous solid fuel feeding and plasma operation. After a while of the operation of the plasma, the reactor was opened and the solid fuels were checked. It is observed that the plasma flame interact just the fuels at top of the reactor. The reaction was not occurred in whole reactor because the plasma was in contact just in the upper side of the gasifier. The plasma applicator and reactor assembly were reversed to spread the reaction to whole reactor. The gasifier connected from bottom and then the reactor and at the top the cyclone filter were located. The reactor were filled with solid fuel and then the reaction processes were performed by producing high amount of smoke. By this way, the solid feeder was just used to dose the reactor. The simultaneous solid fuel feeding and plasma gasification system operation were cancelled.

4- Moisture content of fuel and water vapor supply; it was proposed to use air and water vapor as oxidant in the reactor. However, the experiences with sawdust gasification show that the moisture in the reactor causes to stop plasma flame in the reactor. Because the sawdust interaction with plasma flame and the moisture in sawdust produces water drop in the reactor and these drops stop the plasma flame in the applicator. Also, the quartz glass become dirty and wet which affects the transmission of microwave signal and increases significantly reflected power. Another effect of moisture is that it leaks to the magnetron through waveguide and it reduces the durability of magnetron. The deformed quartz glass is presented in Figure 3.28. Because of these circumstances, the water steam usage as oxidant were cancelled.

Figure 3.28 Deformed quartz glass because of low air flow rate input and moisture content of fuel

5-Gas analysis; the food engineering laboratory has the gas chromatography system and the system was designed to analyze the liquid sample by using the auto sampler and FTIR detector. On the other hand, the system can be operated for syngas analysis with TCD too. Just, it needs revisions such as changing the column, assembling to inlet port an auto valve and etc. However, the tools was not exist in food engineering. The available columns in food engineering were on trial. As a result, an available packed column for the syngas analysis application could not found. Another problem was the injection of the sample. The gas tight syringe was used to inject the syngas sample to the inlet port. Because of manual injection, in each case the sample was injected at varied pressures. As a result of the missing components of the gas analyzer, the analyzer gave the varied retention time and peak amplitude for the same amount of the injected pure CO instead of the same peak and retention time. After that, the syngas analyzing system was rented from a commercial company in Adana. Samples were measured by using the MRU vario plus gas monitoring system. The last version of the system set-up is given in Figure 3.29.

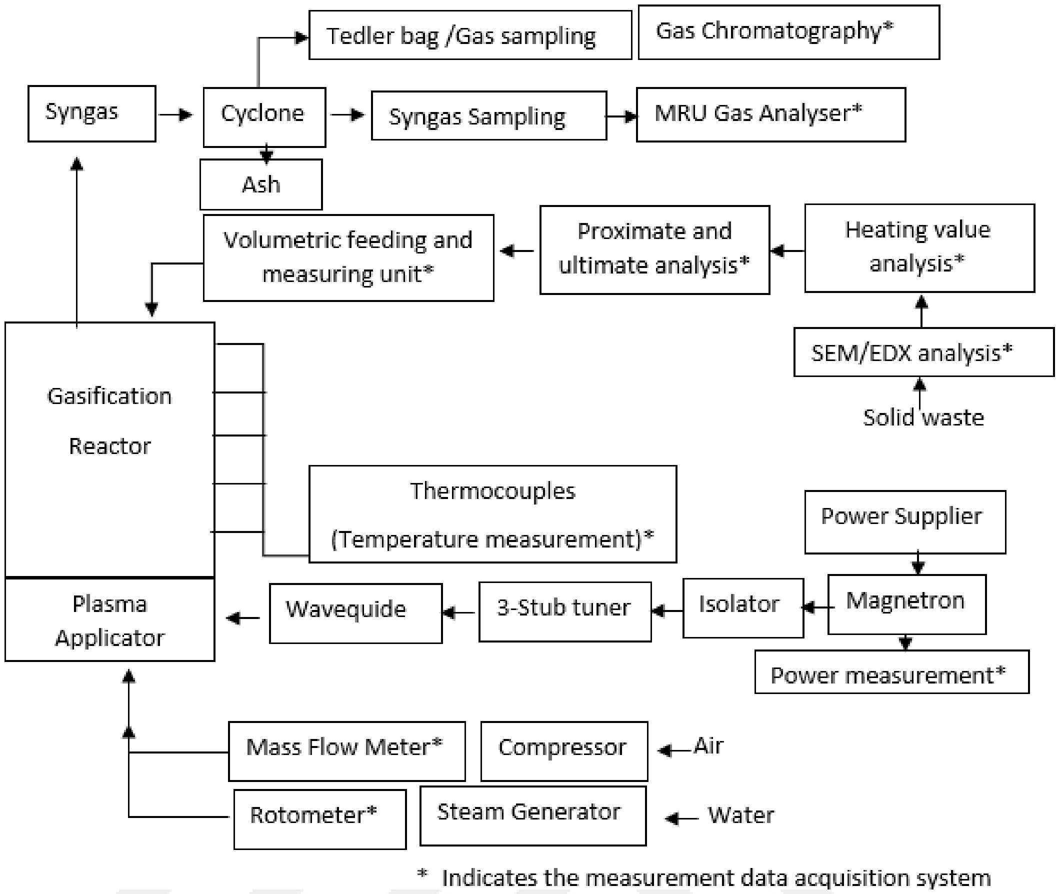

Figure 3.29 The last version of MCw gasifier after modifications and the block diagram of operation.

3.8 Presentation of Experimentation

The operational work of system is carried out by usage of air as oxidant for 6 different fuels at varied powers between 3000 W and 6000 W. 50 sL/min, 75 sL/min and 100 sL/min air flow rates are the operational range of air flow rate. The independent parameters and their ranges are given in Table 3.7. The power for the operation of the system is chosen above 3000W because of the flame characteristics and also the low power applications has reverse effects on magnetron of microwave plasma system. In each case, 250 g fuel is dosed to the reactor. The fuels are dosed to reactor before the operation of plasma. The plasma applicator is located at the bottom of the reactor and plasma flame is injected to the fuels from the bottom.

The produced syngas is cleaned by cyclone filter which is located at the top of the reactor. The cleaned syngas is sampled and the content of the syngas is monitored by using the MRU-Various plus model syngas monitoring system with 2s sampling frequency. The start and end of the process are determined by syngas monitoring system. At the beginning and end of the process, the gas content is just consist of air.

Table 3.7 The independent parameters and their ranges

Experiment method	Varied parameters
Ultimate and Proximate analysis	6 type of solid fuels; HSD, PSD, CR, CSA, CTR and PP.
Heating value analysis	6 type of solid fuels; HSD, PSD, CR, CSA, CTR and PP.
SEM/EDX analysis	6 type of solid fuels; HSD, PSD, CR, CSA, CTR and PP. Ash of 6 type of solid fuels; HSD, PSD, CR, CSA, CTR and PP.
Temperature measurement	3 different flow rates; 50 sL/min, 75 sL/min and 100 sL/min. Different power levels; from 0 to 6 kW.
MRU vario plus Gas analyzer	3 different flow rates; 50 sL/min, 75 sL/min and 100 sL/min. 6 different power levels; 3 kW, 3.6 kW,4.2 kW, 4.8 kW, 5.4 kW and 6kW.

3.9 The Operation and Data Logging Procedure

The temperature, air flow rate, syngas content and the applied microwave power are measured during the experimentation. While the air flow rate and power parameters are independent of the process and adjusted just before the experimentation, the temperature and the syngas content are depending on variables to the process. They are acquired and recorded. The block diagram of the software is given in Figure 3.30.

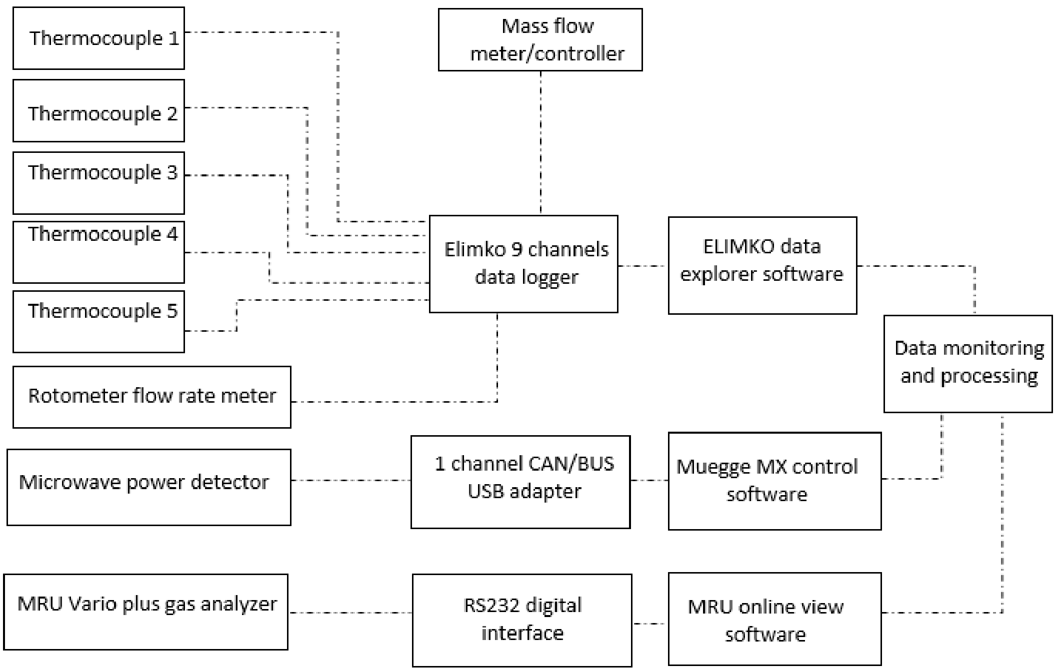

Figure 3.30 The block diagram of the data logging system

The methodology for the data collection is altered in each stage of the experimentation. Here, the methods are divided into the operation and data logging for the plasma flame temperature in case of the empty reactor and the operation and the data logging for the temperature measurement and gas analyzer during the gasification process.

The operation and data logging for the plasma flame temperature in case of empty reactor;

1- The air compressor is operated to pressurize the air tank to 8 bar.

2- The cooling water valves for the power supplier, magnetron and plasma applicator are opened.

3- The air flow rate is adjusted to desired level by mass flow controller and the air is supplied to the plasma applicator. The air flow rate should not be less than 50 sL/min.

4- The data logger is opened to log and monitor the temperature and flow rates. The data is logged by sampling rate of 1 sample per 1 second continuously.

5- The Muegge MX control software is initialized.

6- In the program, the CAN initialization is activated and the CAN BUS active icon turns from red to green color. It shows that the computer and the device are connected. If the system works properly, the “main” icon also turns from yellow to green. If there is a mistake, it is seen in red color.

7- The “reset” icon is pressed to reset the device.

8- The “filament on” icon is pressed to open the filament. When it is ready, the filament on icon in status signal turns from yellow to green. If it shows red, there is error.

9- The “High voltage on” icon is pressed to open the high voltage. When it is ready, “High voltage on” and “Ready” icons in status signal turn from yellow to green. If it shows red, there is error.

10- Before opening the Microwave signal, it is adjusted to low values such as 10 %.

11- The “Microwave on” icon is pressed to open the microwave. When it is ready, “Microwave on” icon in status signal turns from yellow to green. If it shows red, there is error.

12- In the failure signals, all icons should turn to green color. Otherwise, if the red color is seen in any icon, the related error should be fixed before the operation.

13- By opening the microwave power, the acted power and reflected powers are measured and monitored in the program.

14- The power level is increased to 30 % or 40 % of full range. Then, the pneumatic button to operate the igniter is activated. If the plasma flame is not occurred, the stub tuners are turned. Then the igniter button is activated again. The trials in each case are less than 5 times. If the flame is not generated, the stub tuners are turned for new setting. The flame is generated by the trial-errors.

15- When the plasma flame is generated, the sound of plasma can be heard or the reflected power decreases in the control software.

16- By using stub tuners, the reflected power is adjusted to minimum value (close to zero).

17- The desired microwave power is adjusted by “set value” icon. In each change of power, the reflected power changes. If it increases, the new settings to stub tuners are required.

18- By using the mass flow meter, the atmospheric pressure and temperature are recorded.

19- The system is operated 20 minutes to bring the reactor steady conditions.

20- The start time is recorded and the end time is recorded after 5 minutes. In each parameter change, the time is recorded. A 5 minute interval is given for the reactor to reach new steady conditions. After 10 minutes of operation from the parameter change time, the time is recorded again. The first half of 10 minutes is considered as interval time and the last half of the 10 minutes is the measurement time. There are 300 seconds. It means that there are 300 measurements for each station.

21- To shut down the system; the set value is lowered in steps until the power is zero. The microwave is turned off by pressing “Microwave on”, then pressing the “High Voltage on” to close the High voltage, then pressing “Filament on” to close the filament. The cooling water valves are shut off. The air flow rate is adjusted to zero and compressed air valve is shut off.

22- The logged data are exported to Microsoft Excel program and the data at recorded time periods are extracted and Tables for each cases are created regarding to time of operation.

23- For each case, the average of temperature in each station are calculated as given in equation 3.5.

$$T = \frac{1}{300}\sum_{t=1}^{300} T_{(t)} \qquad (3.5)$$

The operation and data logging for the temperature measurement and gas analyzer during the gasification process;

The first 17 steps explained in previous section are repeated in this operation too. In case of the gasification process, both the temperature and syngas analyzing data are acquired.

1- The plasma is generated in the reactor without any fuel. The system is operated for 20 minutes to heat up the reactor and provide steady conditions in reactor.

2- The plasma is shut off by repeating the method in line 21 in previous section and the cyclone filter is reassembled. The 250 g solid fuel is dosed to the reactor. The cyclone filter is mounted to the reactor again.

3- The detector of the MRU syngas analyzer is connected to the top of the reactor as shown in Figure 3.16. The gas analyzer is adjusted to measure the CO, CO_2, CH_4, H_2, O_2 and N_2 simultaneously. The sampling rate is 1 data per 2 seconds.

4- Step 6-17 in previous section is repeated to generate the plasma. By operation of plasma flame, the percentage of O_2 decreases and the percentage of CO and percentage of H_2 increase. The gas composition change is taken as starting time of the process and the time is recorded.

5- The time when the gas composition is taken from the analyzer is approximately the same with air, it is considered as the end of the process. This time is recorded.

6- To close the system; the set value is lowered by steps until the power is zero. The microwave is closed by pressing to “Microwave on”, then pressed to the “High Voltage on” to close the High voltage, then pressed to “Filament on” to close the filament. The cooling water valves are shut off. The air flow rate is adjusted to zero and compressed air valve is shut off.

7- The minimum and maximum operation times for the each case are altered between 420 and 1020 seconds. The data which is logged by MRU online software is exported to Microsoft Excel. The durations of the processes are estimated and the average of each case is calculated by equation 3.6.

$$\mathrm{CO} = \frac{2}{\mathrm{t_g}} \sum \mathrm{CO_{(t)}} \tag{3.6a}$$

$$\mathrm{CO_2} = \frac{2}{\mathrm{t_g}} \sum \mathrm{CO_{2(t)}} \tag{3.6b}$$

$$\mathrm{H_2} = \frac{2}{\mathrm{t_g}} \sum \mathrm{H_{2(t)}} \tag{3.6c}$$

$$\mathrm{CH_4} = \frac{2}{\mathrm{t_g}} \sum \mathrm{CH_{4(t)}} \tag{3.6d}$$

$$\mathrm{O_2} = \frac{2}{\mathrm{t_g}} \sum \mathrm{O_{2(t)}} \tag{3.6e}$$

$$\mathrm{N_2} = \frac{2}{\mathrm{t_g}} \sum \mathrm{N_{2(t)}} \tag{3.6f}$$

8- The temperature measurement data which are logged by Elimko data explorer software are exported to Microsoft Excel. The start and end of the process times (explained in step 4 and 5) are recorded and the temperature variations according to process time tables are generated for each case.
For each case, the average of temperature in each station is calculated as given in equation 3.7.

$$T = \frac{1}{t_g} \sum_{t=1}^{t_g} T_{(t)} \tag{3.7}$$

9- Ash content after the handling the solid fuels is collected at the cyclone filter.

3.10 Conclusion

MCw plasma gasification system was installed and operated as proposed. Firstly the plasma generation system was taken into operation. The measurement and the data logging systems were mounted to the system and the calibration of them were performed. The plasma flame characteristics in the atmospheric conditions were examined. Then, the fluid supply systems and solid fuel feeding systems were operated.

In the operation of the system, there were several problems to feed the fuel to the reactor. The problems are solved by the following ways.

-Solid fuel feeding method

The fuel supply system was isolated from the leakages of air in storage place. Also, the air flow is by-passed. By this way, the reactor and the feeder pressures were equalized. The solid feeding location had to be changed by these modifications. As a result, the reversing of solid particles in the feeder is prevented.

-Solid fuel feeding location

The solid fuels were mixed with air and supplied to the system by plasma applicator air inlet port to satisfy equilibrium of pressure in reactor and solid fuel feeder. The new proposed system configuration is given in Figure 3.27.

-Gasification process and syngas production problem

In case of steady state operation, the syngas production was not achieved because of amount of air was much higher than the fuel in reactor. Although, the fuel feeding rate is adjusted to feed the maximum solid fuel and the air flow rate reduced to 50 sL/min, the syngas production was not achieved. In case of reducing air flow rate to the less than 50 sL/min, the swirling flow does not occur in plasma applicator. So, the quartz glass in the center of the applicator melt. It is caused because of high energy density in it. As a result, the minimum air flow rate and maximum fuel feeding rate were restricted.

To overcome these problems, the reactor is dosed by certain amount of solid fuel (250 g) and then the plasma is activated instead of simultaneous feeding and plasma operation. In this case, the produced gas content is similar to the simultaneous solid fuel feeding and plasma operation. After a while of operation of plasma, the reactor was opened and the solid fuels were checked. It is observed that the plasma flame interacts just the fuels at top of the reactor. The reaction was not occurred in whole reactor because the plasma was in contact just in the upper side of the gasifier. The plasma applicator and reactor assembly were reversed to spread the reaction to whole reactor. The gasifier was connected from the bottom and then the reactor at the top the cyclone filter were located. The reactor was filled with solid fuel and then the reaction processes were performed by producing high amount of smoke. By this way, the solid feeder was just used to dose the reactor. The simultaneous solid fuel feeding and plasma gasification system operation were cancelled.

-The usage of steam as oxidant was cancelled because of problems that occurred in the plasma generation system.

The air supplying and generation of air plasma were carried out. The temperature distribution in the gasifier was presented. The uncertainty of measurement systems were determined in in Appendix A.2 and the following experimentation plan was given in Table 3.7.

CHAPTER IV

FUEL CHARACTERIZATION

In this chapter, 6 different type of solid fuels Russian coal (CR), South African coal (CSA), Şırnak coal (CTR), pine tree sawdust (PSD), hornbeam sawdust (HSD) and polyethylene (PP) properties are presented. The physical properties of the fuels were examined. The proximate and ultimate analysis of the solid fuels were carried out to see the content of the solid fuels. The heating value of the solid fuels were calculated by using the empirical equations and the results of the experiments.

4.1 Sample Preparation

6 different solid fuels; Russian coal (CR), South African coal (CSA), Şırnak coal (CTR), pine tree sawdust (PSD), hornbeam sawdust (HSD) and polyethylene (PP) were prepared for the gasification process. Each of them was pulverized to granular sizes except the polyethylene. Polyethylene was similar in shape and size with lentil. While the coals were screened by 0.1 mm particle size, the sawdust was screened to 1 mm particle size. At least 5 kg for each sample was prepared for the gasification process.

Table 4.1 Density and size of the solid fuels for the gasification process

Solid fuel	Particle sizes (mm)	Density (kg/m3)
Russian coal (CR)	0.1	701.03
South African coal (CSA)	0.1	749.79
Şırnak Coal (CTR)	0.1	929.79
Hornbeam sawdust (HSD)	1	230.07
Pine sawdust (PSD)	1	218.87
Polyethylene (PP)	-	211,86

In Table 4.1, the particle sizes and the density of them are given. Each sample was meshed to the desired size as given in the Table 4.1. While coals have much higher density, the densities of two sawdust and polyethylene are closer to each other. From coals, the Sırnak coal has the highest density with approximately 930 kg/m^3.

4.2 Proximate Analysis

Proximate analysis indicates the contents of the moisture, volatile matter, fixed carbon and ash in the fuels in percentage by weight. Proximate analysis was performed according to ASTM D 3172-89 method. The moisture content, volatile matter and ash content are measured according to ASTM D3173, D3175 and D3174 methods, respectively.

Moisture content (M): moisture content is determined by removing the water from the sample fuel by specified method without causing any chemical change in fuel. Approximately, 1 g of fine powdered coal is weighed in crucible covered by lid. Crucible-lid is placed inside oven where the temperature is maintained at 105 to 110 ℃ for 1 hour. Then sample is taken out and weighed. Loss in weight is giving the moisture content in the fuel. The moisture content can be determined by using equation 4.1.

$$\mathrm{M}(\%) = \frac{\text{Initial weight} - \text{final weight of the sample}}{\text{Initial weight of the sample}} \times 100 \tag{4.1}$$

Volatile Matter (VM): the volatile matter is determined by holding the dried fuel sample in oven where the temperature maintained 925 ℃ $\pm$ 25℃ for 7 minute. Then the sample is weighted again. The losses in weight of dry fuel sample gives the volatile components. The percentage of the volatile matters can be calculated as equation 4.2.

$$\mathrm{VM}\ (\%) = \frac{\text{Initial weight} - \text{final weight of the sample}}{\text{Initial weight of the sample}} \times 100 \tag{4.2}$$

Ash content (A): Rest of the fuel sample in crucible after the volatile matter measurements held in oven without using lid at 700◦ C + 50℃ for two hours. After the burning of the fuel, the residue in the crucible gives the ash content. The amount is measured and percentage ash is determined by using equation 4.3.

$$\mathrm{A}\ (\%) = \frac{\text{Residual weight of the sample}}{\text{Initial weight of the sample}} \times 100 \tag{4.3}$$

Fixed carbon (FC): the difference between the initial weight of the sample and the sum of the moisture, volatile matter and ash gives the fixed carbon content. The percentage of the fixed carbon can be determined by using equation 4.4.

$$FC(\%) = 100 - \% \text{ of } (\mathrm{M} + \mathrm{VM} + \mathrm{A}) \quad (4.4)$$

Table 4.2 Results on proximate analysis of the solid fuels

Solid fuel	Moisture (M) (%)	Volatile matter (VM) (%)	Fixed carbon (FC) (%)	Ash (A) (%)
Russian coal (CR)	3.15	23.51	67.46	5.87
South African coal (CSA)	3.40	25.94	55.94	14.71
Şırnak Coal (CTR)	0.85	36.67	21.05	41.43
Hornbeam sawdust (HSD)	17.39	72.58	10.02	0.69
Pine sawdust (PSD)	21.35	69.54	8.53	0.58
Polyethylene (PP)	0.19	94.90	0.91	5.44

In Table 4.2, the proximate analysis results are given in terms of moisture, volatile matter, fixed carbon and ash contents. While coals include less moisture in the level of 3 %, sawdust includes moisture in the level of 20 %. The moisture content decreases the heating value content. Similar results are presented for the volatile matter. While the volatile matter content is approximately 26 % for coals, it jumps to the 70 % level for sawdust. For polyethylene, the high percentage of the content (94.9 %) includes the volatile matters. The high volatile matter content means that the high proportion of the fuel distill over as gas or vapor. It burns with the long flame, high smoke and has the adverse effect on the heating value. The fixed carbon content is desired for the higher heating value and this is the highest for the Russian coal which includes 67.46 %. Then the South African coal has the 56 % fixed carbon. The Sırnak coal has less than 21 % and sawdust have approximately the 10 % fixed carbon. The ash content is not combustible matter and it reduces the heating value of the fuel. The results show that Russian coal has the lowest ash with 5.87 % while the South African coal has 14.71 % and Sırnak coal has the 41.43 % ash content. The sawdust has the ash content less than 1 %.

4.3 Ultimate Analysis

Ultimate analysis gives the elementary composition of carbon (C), hydrogen (H), oxygen (O), nitrogen (N) and sulphur (S) in percentage by weight. Ultimate analysis should be carried out for the solid fuels. These experiments is being conducted in Bilecik Şeyh Edebali University central research laboratory by service procurement. The solid fuel samples were transferred to the laboratory. They use LECO CHN 628 model analyzer to perform the experiments. The LECO CHN628 utilizes pure oxygen in the furnace to complete combustion and recovery of the elements of interest. Carrier gas sweeps the combustion gas to separate infrared cells utilized for the detection of H_2O and CO_2, while a thermal conductivity cell is used for the detection of nitrogen.

Table 4.3 Ultimate analysis of the solid fuels

Solid fuel	Carbon (C) (%)	Hydrogen (H) (%)	Oxygen (O) (%)	Nitrogen (N) (%)	Sulphur (S) (%)
Russian coal (CR)	66.81	4.49	21.72	1.00	0.11
South African coal (CSA)	62.56	4.08	17.61	0.64	0.40
Şırnak Coal (CTR)	42.18	3.75	5.96	0.35	6.33
Hornbeam sawdust (HSD)	36.15	6.24	56.92	0.00	0.00
Pine sawdust (PSD)	39.66	6.45	53.30	0.00	0.00
Polyethylene (PP)	69.6	10.26	16.14	0.00	0.00

In Table 4.3, the ultimate analyze results are presented. While the hydrogen and carbon content constitute the heating value, the oxygen, nitrogen, Sulphur and ash contents decrease the heating value of the fuel. The polyethylene has the highest carbon and hydrogen content in solid fuels with the contents of 69.6 % carbon and 10.26 % hydrogen. On the other hand, the sawdust have relatively less carbon and hydrogen in the fuels with contents of 36.15 % and 39.66 % for carbon and 6.24 % and 6.45 % for hydrogen in the hornbeam and pine sawdust relatively. In coals, the Russian coal (66.81 % carbon, 4.49 % hydrogen) and the South African coal (62.56 % carbon, 4.08 % hydrogen) have similar carbon and hydrogen content, but the Sırnak coal (42.18 % carbon, 3.75 % hydrogen) has relatively less carbon and hydrogen content.

4.4 Heating Value of the Solid Fuels

The heating value of the fuels are determined by using adiabatic bomb calorimeter. In this method, solid fuel samples are screened to 1 mm size and 1 g sample is taken for analysis. The heat resistance coil is measured and coiled to heat up and ignite the coal sample. The fuel sample capsule are produced by press where the coil part of wire stayed inside the capsule. Then the ends of wire coil is assembled to the heater electrodes. The coal sample with wire which is connected to poles of heater is located in crucible. The crucible is located in the bomb tank. The bomb tank is filled by compressed oxygen which has 10 bar pressure. Then the bomb tank is immersed into 2.5 Liter water in bucket. The electric cable is connected to the cable ports of the bomb tank. The thermocouple is also immersed in the water bucket to monitor the temperature variation. The water in bucket has a mixer to get uniform temperature. When ignition starts, the temperature is measured and time counter is started. The electric current is applied to the wire coil in coal until the current is shorted. The maximum temperature of water and time taken to get maximum temperature are recorded. Then the Higher heating value (HHV) is calculated by using equation 4.5. The heating value of coals and sawdust are measured by this method. However, the tests could not perform to the polyethylene due to the structure of the polyethylene.

$$HHV = \frac{m_{water} * c * (T_2 - T_1) - e_1 - e_2}{m_{fuel\ sample}} \quad (4.5)$$

m_{water} is the amount of water in bucket, c is the specific heat of water (4.187 kJ/kg°C), T_1 is the corrected initial temperature, T_2 is the corrected final temperature, e_1 is the correction parameter for the Sulphur in sample, e_2 is the correction parameter for the heat resistance wire and $m_{fuel\ sample}$ is the weight of the fuel sample. e_1 and e_2 are neglected for the calculation because of the very small amounts of values for this experimentation.

The heating value of fuels were also calculated by using empirical equations described by Channiwala and Parikh, 2002 for the calculation of HHV and described by Finet, 1987 for calculation the LHV in equation 4.6 and equation 4.7 respectively. Heating value of 6 solid fuels are evaluated by these empirical equations.

$$\mathrm{HHV} = 0.3491\mathrm{C} + 1.1783\mathrm{H} + 0.1005\mathrm{S} - 0.1034\mathrm{O} - 0.0151\mathrm{N} - 0.0211\mathrm{ash}\left(\frac{\mathrm{MJ}}{\mathrm{kg}}\right) \quad (4.6)$$

$$\mathrm{LHV} = \mathrm{HHV}(1 - \mathrm{H_2O}) - 2440(\mathrm{H_2O} + 9\mathrm{H})\left(\frac{\mathrm{MJ}}{\mathrm{kg}}\right) \quad (4.7)$$

In the Table 4.4, the measured and calculated heating values are presented. While coals have greater higher heating value (HHV) when compared with sawdust, the Sırnak coal has the lowest heating value in the coal types. The Russian and South African coal have also similar heating values. This is also result of similar carbon and hydrogen contents in ultimate analysis. The higher heating value (HHV) of the polyethylene is not available to measure by the adiabatic bomb calorimeter. The heating value of polyethylene (PP) is calculated by using equation 4.6 and 4.7. The elementer compositions are determined by proximate and ultimate analysis. Also, the empirical equation results are compared with adiabatic bomb calorimeter tests and the percentage of error is determined by using equation 4.8.

$$\text{Error \%} = \frac{\text{Adiabatic bomb calorimeter} - \text{Empirical equation}}{\text{Adiabatic bomb calorimeter}} \times 100 \qquad (4.8)$$

Table 4.4 Heating value of the solid fuel samples

Solid fuel	Adiabatic bomb calorimeter	Empirical equation		
	HHV (kJ/kg)	HHV (kJ/kg)	LHV (kJ/kg)	ERROR (%)
Russian coal (CR)	31336	26240	24351	16
South African coal (CSA)	30759	24546	22733	20
Şırnak Coal (CTR)	19954	18284	17284	8
Hornbeam sawdust (HSD)	21353	14072	9831	34
Pine sawdust (PSD)	17942	15922	10585	11
Polyethylene (PP)	-	34633	32310	

4.5 Conclusion

In this chapter, the physical and chemical properties of the solid fuels what are used for the gasification are given in detail. The details about the size of the solid particles, the densities of the fuels are presented. The proximate and the ultimate analysis of the fuels are required to see the content of fuel and determine the heating value of each fuel. The contents of the fuels are examined by the proximate and the ultimate analysis. The heating value of the fuels are measured by the experimental methods and calculated by the empirical equations using the proximate and the ultimate analysis. The SEM analysis are also performed to reveal the characteristics of fuels. Also, the elemental composition of fuels is determined by EDX analysis. The details of these tests are presented in Appendix A.3. The brief presentation of the results are given in Table 4.5.

Table 4.5 The brief presentation of results of solid fuel characteristics

	Density	Proximate analysis		Ultimate analysis		Adiabatic bomb calorimeter	Empirical heating value calculation		EDX analysis	
HSD	701.03	M(%)	17.39	C(%)	36.15	21352.90	HHV (kJ/kg)	14072.47	C(%)	49.31
		VM(%)	72.58	H(%)	6.24				O(%)	47.5
		FC(%)	10.02	O(%)	56.92		LHV (kJ/kg)	9830.65	S(%)	0.39
		A(%)	0.69	N(%)	0				Others (%)	2.8
				S(%)	0					
PSD	749.79	M(%)	21.35	C(%)	39.66	17941.66	HHV (kJ/kg)	15921.67	C(%)	53.95
		VM(%)	69.54	H(%)	6.45				O(%)	44.31
		FC(%)	8.53	O(%)	53.3		LHV (kJ/kg)	10585.04	S(%)	0.27
		A(%)	0.58	N(%)	0				Others (%)	1.47
				S(%)	0					
CR	929.79	M(%)	3.15	C(%)	66.81	31336.05	HHV (kJ/kg)	26240.19	C(%)	71.29
		VM(%)	23.51	H(%)	4.49				O(%)	19.3
		FC(%)	67.46	O(%)	21.72		LHV (kJ/kg)	24350.76	S(%)	0.49
		A(%)	5.87	N(%)	1				Others (%)	8.92
				S(%)	0.11					
CSA	230.07	M(%)	3.40	C(%)	62.56	30758.85	HHV (kJ/kg)	24546.44	C(%)	71.64
		VM(%)	25.94	H(%)	4.08				O(%)	19.14
		FC(%)	55.94	O(%)	17.61		LHV (kJ/kg)	22732.93	S(%)	0.67
		A(%)	14.71	N(%)	0.64				Others (%)	8.55
				S(%)	0.4					
CTR	218.87	M(%)	0.85	C(%)	42.18	19954.03	HHV (kJ/kg)	18284.11	C(%)	60.71
		VM(%)	36.67	H(%)	3.75				O(%)	20.51
		FC(%)	21.05	O(%)	5.96		LHV (kJ/kg)	17284.45	S(%)	6.51
		A(%)	41.43	N(%)	0.35				Others (%)	12.27
				S(%)	6.33					
PP	211,86	M(%)	0.19	C(%)	69.6	-	HHV (kJ/kg)	34633.44	C(%)	82.38
		VM(%)	94.90	H(%)	10.26				O(%)	11.05
		FC(%)	0.91	O(%)	16.14		LHV (kJ/kg)	32309.91	S(%)	0.14
		A(%)	5.44	N(%)	0				Others (%)	6.43
				S(%)	0					

CHAPTER V

GASIFICATION PROCESS EVALUATION

In this chapter, general overview about the evaluation of the gasification process is given. The gasification results of the fuels in the case of 50, 75 and 100 sL/min air flow rate and varied powers between 3 kW and 6 kW are presented for each fuel type. Then the effects of power, air flow rate and fuel type on temperature distribution in the gasification reactor are given. The Energy Dispersive X-ray (EDX) analysis of 6 different solid fuel ashes at 3 kW and 6 kW power, 50 sL/min and 100 sL/min air flow rate are performed.

5.1 Methodology for data acquisition and processing

The data acquisition procedure for the temperature and the syngas analysis is given in Section 3.12. In this section, the data acquisition and processing procedure are explained in detail. As it is mentioned in section 3.12, the sampling rate for the temperature measurement is 1 s while it is 2 s for the gas analyzing. The supplied solid fuel is measured and dosed to reactor via volumetric feeder. The air flow rate is measured and supplied by a mass flow controller. The acquired raw data is stored and proceeded by the methods explained below.

Mass balance in the reactor: While the air and solid fuel are input of the reactor the ash and syngas are the outputs of the reactor. As the inputs and outputs amount are parameter for the thermodynamic analysis, the unit of all parameters is converted to SI unit system. The air flow rate is measured by mass flow controller in units of sL/min. The measured standard volumetric flow rate ($\dot{\forall}$) (standard conditions) is converted to mass (m_{air}) by using equation 5.1. The produced syngas is determined by extracting ash amount from the supplied air and solid fuel. The produced syngas ($\mathrm{m}_{\mathrm{syngas}}$) is determined by equation 5.2. The amount of air, fuel supply and the produced syngas and ash amounts are presented in Table 5.1 for each case.

$$m_{air}(kg) = \left(\dot{\forall}(^{sL}/_{min}) . \frac{P_{atm(s)}(kPa)}{R_{air}(\frac{kPa.m^3}{kg.K}).T_s(K)} \right) . t_g\ (s) \tag{5.1}$$

$$m_{syngas}(kg) = m_{air}(kg) + m_{fuel}(kg) - m_{ash}(kg) \tag{5.2}$$

Table 5.1 Presentation of inputs and the outputs to the reactor in each case

	Power (W)	t_g (s)	m_{ash} (kg)	m_{fuel} (kg)	m_{air} (kg)	m_{syngas} (kg)	M_{syngas} (kg /kmol)
Hornbeam sawdust -50 sL/min	3000	880	0.00216	0.25	0.87	1.12	29.88
	3600	820	0.00208		0.81	1.06	28.87
	4200	800	0.00196		0.79	1.04	28.30
	4800	720	0.00189		0.71	0.96	28.15
	5400	680	0.00184		0.67	0.92	27.77
	6000	600	0.00183		0.59	0.84	27.25
Hornbeam sawdust -75 sL/min	3000	720	0.00234	0.25	0.71	0.96	30.63
	3600	650	0.00222		0.64	0.89	29.87
	4200	630	0.00209		0.62	0.87	29.32
	4800	600	0.00201		0.59	0.84	29.15
	5400	540	0.00196		0.53	0.78	28.42
	6000	500	0.00191		0.49	0.74	27.92
Hornbeam sawdust -100 sL/min	3000	640	0.0026	0.25	0.63	0.88	30.83
	3600	600	0.00249		0.59	0.84	30.12
	4200	560	0.00235		0.55	0.80	30.01
	4800	520	0.00226		0.51	0.76	29.65
	5400	450	0.00218		0.44	0.69	29.09
	6000	420	0.00212		0.41	0.66	28.64
Pine tree sawdust -50 sL/min	3000	880	0.00282	0.25	0.87	1.12	29.85
	3600	840	0.00259		0.83	1.08	29.21
	4200	800	0.00245		0.79	1.04	28.69
	4800	720	0.00226		0.71	0.96	28.35
	5400	680	0.00198		0.67	0.92	27.96
	6000	600	0.00174		0.59	0.84	27.07
Pine tree sawdust -75 sL/min	3000	720	0.00338	0.25	0.71	0.96	30.07
	3600	680	0.00307		0.67	0.92	30.14
	4200	600	0.00286		0.59	0.84	29.51
	4800	560	0.00278		0.55	0.80	29.32
	5400	520	0.00244		0.51	0.76	28.64
	6000	460	0.00212		0.45	0.70	28.28

Table 5.1 (Continued) Presentation of inputs and the outputs to the reactor in each case

Pine tree sawdust - 100 sL/min	3000	640	0.00482	0.25	0.63	0.88	31.14
	3600	600	0.00443		0.59	0.84	29.82
	4200	580	0.00401		0.57	0.82	29.64
	4800	540	0.00357		0.53	0.78	29.12
	5400	510	0.00314		0.50	0.75	28.83
	6000	440	0.00301		0.43	0.68	28.38
Russian coal - 50 sL/min	3000	1020	0.05232	0.25	1.01	1.20	32.07
	3600	960	0.05018		0.95	1.15	31.87
	4200	920	0.04822		0.91	1.11	31.67
	4800	840	0.04538		0.83	1.03	31.55
	5400	800	0.04116		0.79	1.00	31.29
	6000	740	0.03927		0.73	0.94	31.17
Russian coal - 75 sL/min	3000	820	0.06321	0.25	0.81	1.00	32.83
	3600	790	0.05812		0.78	0.97	32.78
	4200	750	0.05463		0.74	0.94	32.50
	4800	700	0.04622		0.69	0.89	32.40
	5400	680	0.04366		0.67	0.88	32.32
	6000	620	0.04084		0.61	0.82	32.27
Russian coal - 100 sL/min	3000	740	0.0738	0.25	0.73	0.91	33.52
	3600	710	0.06874		0.70	0.88	33.47
	4200	680	0.06126		0.67	0.86	33.33
	4800	660	0.05619		0.65	0.84	33.22
	5400	640	0.05131		0.63	0.83	32.99
	6000	620	0.04701		0.61	0.81	32.82
South African coal - 50 sL/min	3000	1010	0.05621	0.25	1.00	1.19	31.55
	3600	970	0.05323		0.96	1.15	31.47
	4200	910	0.05115		0.90	1.10	31.35
	4800	870	0.04834		0.86	1.06	31.19
	5400	780	0.04623		0.77	0.97	30.88
	6000	760	0.04418		0.75	0.96	30.88
South African coal - 75 sL/min	3000	800	0.06843	0.25	0.79	0.97	32.40
	3600	760	0.06431		0.75	0.94	32.46
	4200	720	0.05929		0.71	0.90	32.24
	4800	660	0.05632		0.65	0.84	31.99
	5400	630	0.05188		0.62	0.82	31.96
	6000	600	0.04977		0.59	0.79	31.96
South African coal - 100 sL/min	3000	740	0.07767	0.25	0.73	0.90	32.96
	3600	700	0.07332		0.69	0.87	32.78
	4200	670	0.06998		0.66	0.84	32.82
	4800	630	0.06527		0.62	0.81	32.54
	5400	590	0.06215		0.58	0.77	32.37
	6000	550	0.05887		0.54	0.73	32.26

Table 5.1 (Continued) Presentation of inputs and the outputs to the reactor in each case

Şırnak (Turkey) coal - 50 sL/min	3000	880	0.06947	0.25	0.87	1.05	31.25
	3600	840	0.06623		0.83	1.01	31.10
	4200	820	0.05817		0.81	1.00	31.04
	4800	800	0.05664		0.79	0.98	30.93
	5400	780	0.05244		0.77	0.97	30.60
	6000	760	0.04926		0.75	0.95	30.64
Şırnak (Turkey) coal – 75 sL/min	3000	710	0.07798	0.25	0.70	0.87	32.10
	3600	680	0.07312		0.67	0.85	31.85
	4200	670	0.06917		0.66	0.84	31.83
	4800	640	0.06643		0.63	0.81	31.65
	5400	620	0.06376		0.61	0.80	31.34
	6000	600	0.06054		0.59	0.78	31.21
Şırnak (Turkey) coal -100 sL/min	3000	690	0.09177	0.25	0.68	0.84	33.07
	3600	650	0.08612		0.64	0.81	32.84
	4200	620	0.07421		0.61	0.79	32.92
	4800	600	0.06952		0.59	0.77	32.65
	5400	580	0.066		0.57	0.76	32.17
	6000	540	0.06301		0.53	0.72	32.11
Polyethylene - 50 sL/min	3000	660	0.0021	0.25	0.65	0.90	27.84
	3600	640	0.00201		0.63	0.88	27.68
	4200	600	0.00187		0.59	0.84	27.55
	4800	580	0.00163		0.57	0.82	27.10
	5400	560	0.00144		0.55	0.80	26.89
	6000	520	0.00116		0.51	0.76	26.37
Polyethylene - 75 sL/min	3000	620	0.00402	0.25	0.61	0.86	28.17
	3600	600	0.00386		0.59	0.84	28.10
	4200	580	0.00361		0.57	0.82	27.95
	4800	570	0.00334		0.56	0.81	27.67
	5400	540	0.00299		0.53	0.78	27.49
	6000	520	0.00239		0.51	0.76	27.30
Polyethylene - 100 sL/min	3000	600	0.00613	0.25	0.59	0.84	28.48
	3600	580	0.00559		0.57	0.82	28.25
	4200	580	0.0052		0.57	0.82	28.14
	4800	560	0.00485		0.55	0.80	28.01
	5400	540	0.00443		0.53	0.78	27.79
	6000	520	0.00401		0.51	0.76	27.58

Reactor Temperature: The reactor temperature is measured by 5 thermocouples which are located at y/h=0.28, 0.44, 0.6, 0.76 and 0.92. In each station, the samples are acquired by 1 sample per second. The mean of temperature in each station ($T_{y/h}$) is calculated by using equation 5.3.

$$\mathrm{T_{y/h}} = \frac{1}{\mathrm{t_g}} \sum_{\mathrm{t=1}}^{\mathrm{t_g}} \mathrm{T_{(y,t)}} \tag{5.3}$$

The reactor average temperature (T_{syn}) is determined by equation 5.4 by taking the average of temperatures of the 5 measurement stations. The average temperature in each measurement location ($T_{y/h}$) and their average (T_{syn}) are presented in Table 5.2.

$$\mathrm{T_{syn}}(°\mathrm{C}) = {\left(\mathrm{T_{y/h=0.28}} + \mathrm{T_{y/h=0.44}} + \mathrm{T_{y/h=0.6}} + \mathrm{T_{y/h=0.76}} + \mathrm{T_{y/h=0.92}}\right)}\Big/_{5} \;\; (°\mathrm{C}) \tag{5.4}$$

Table 5.2 Presentation of temperature for each measurement location in each case (Temperature measurement uncertainty is 13°C)

	Power (W)	t_g (s)	T_0 (°C)	$T_{y/h=0.28}$ (°C)	$T_{y/h=0.44}$ (°C)	$T_{y/h=0.6}$ (°C)	$T_{y/h=0.76}$ (°C)	$T_{y/h=0.92}$ (°C)	T_{syn} (°C)
Hornbeam sawdust – 50 sL/min	3000	880	30.79	921	909	794	655	515	759
	3600	820		950	989	877	761	579	831
	4200	800		1046	1078	970	825	657	915
	4800	720		1184	1195	1060	884	712	1007
	5400	680		1349	1253	1129	962	786	1096
	6000	600		1476	1325	1236	1014	825	1175
Hornbeam sawdust - 75 sL/min	3000	720	31.8	894	815	665	567	450	678
	3600	650		951	1006	793	668	558	795
	4200	630		1151	1003	913	807	687	912
	4800	600		1156	1156	1019	867	719	983
	5400	540		1377	1123	1017	958	796	1054
	6000	500		1432	1311	1131	997	857	1146
Hornbeam sawdust - 100 sL/min	3000	640	32.2	831	686	574	540	474	621
	3600	600		1045	824	717	656	569	762
	4200	560		1119	977	838	795	707	887
	4800	520		1257	1009	875	793	749	937
	5400	450		1342	1146	951	817	785	1008
	6000	420		1456	1273	1078	951	886	1129
Pine tree sawdust - 50 sL/min	3000	880	30.79	937	917	797	661	516	766
	3600	840		951	992	879	757	578	831
	4200	800		1047	1088	973	829	651	918
	4800	720		1205	1216	1065	900	714	1020
	5400	680		1361	1275	1139	971	779	1105
	6000	600		1447	1349	1215	1017	818	1169
Pine tree sawdust - 75 sL/min	3000	720	31.4	902	819	659	562	454	679
	3600	680		951	989	807	680	562	798
	4200	600		1101	1005	929	786	675	899
	4800	560		1166	1157	1010	898	722	991
	5400	520		1380	1153	1054	964	789	1068
	6000	460		1444	1322	1133	1005	858	1152

Table 5.2 (Continued) Presentation of temperature for each measurement location in each case (Temperature measurement uncertainty is 13℃)

Pine tree sawdust - 100 sL/min	3000	640	32.1	855	692	594	536	470	630
	3600	600		1031	801	723	651	579	757
	4200	580		1097	968	841	793	712	882
	4800	540		1197	1018	875	803	756	930
	5400	510		1370	1146	960	827	826	1026
	6000	440		1434	1284	1097	940	884	1128
Russian coal - 50 sL/min	3000	1020	33.4	997	1006	867	718	538	825
	3600	960		1016	1088	956	823	629	902
	4200	920		1109	1193	1048	906	705	992
	4800	840		1283	1319	1158	1001	776	1107
	5400	800		1429	1410	1239	1056	834	1194
	6000	740		1585	1479	1314	1115	889	1276
Russian coal - 75 sL/min	3000	820	32.9	976	876	712	611	494	734
	3600	790		1061	1054	877	739	611	868
	4200	750		1181	1090	1011	855	733	974
	4800	700		1267	1226	1116	971	784	1073
	5400	680		1487	1297	1155	1021	857	1163
	6000	620		1570	1408	1230	1092	932	1246
Russian coal - 100 sL/min	3000	740	32.2	915	704	636	567	482	661
	3600	710		1114	856	760	684	579	799
	4200	680		1175	1010	892	819	712	922
	4800	660		1271	1080	934	841	775	980
	5400	640		1502	1205	1013	888	847	1091
	6000	620		1547	1362	1174	1005	930	1204
South African coal - 50 sL/min	3000	1010	33.2	988	1004	860	720	533	821
	3600	970		1005	1084	949	820	632	898
	4200	910		1102	1186	1042	899	699	985
	4800	870		1278	1315	1153	993	774	1103
	5400	780		1418	1399	1229	1047	831	1185
	6000	760		1572	1474	1304	1103	882	1267
South African coal - 75 sL/min	3000	800	33.4	973	871	704	606	490	729
	3600	760		1056	1045	870	733	609	862
	4200	720		1191	1047	1003	849	730	964
	4800	660		1257	1214	1106	961	776	1063
	5400	630		1481	1247	1142	1008	855	1147
	6000	600		1557	1385	1220	1083	926	1234
South African coal - 100 sL/min	3000	740	33.4	908	710	630	562	480	658
	3600	700		1105	849	754	679	575	793
	4200	670		1159	1007	886	813	707	914
	4800	630		1279	1073	929	832	771	977
	5400	590		1429	1200	1003	880	844	1071
	6000	550		1534	1351	1164	1001	918	1193
Şırnak (Turkey) coal - 50 sL/min	3000	880	30.4	972	990	846	707	524	808
	3600	840		989	1070	934	808	620	884
	4200	820		1093	1160	1025	887	685	970
	4800	800		1267	1289	1129	979	762	1086
	5400	780		1400	1373	1213	1035	817	1167
	6000	760		1545	1450	1278	1087	868	1246

Table 5.2 (Continued) Presentation of temperature for each measurement location in each case (Temperature measurement uncertainty is 13°C)

Şırnak (Turkey) coal -75 sL/min	3000	710	31.3	957	856	695	594	480	716
	3600	680		1035	1026	850	715	594	844
	4200	670		1200	1034	984	839	708	953
	4800	640		1241	1194	1080	944	755	1043
	5400	620		1449	1217	1117	992	832	1121
	6000	600		1539	1356	1192	1057	902	1210
Şırnak (Turkey) coal -100 sL/min	3000	690	32.5	885	687	615	548	469	641
	3600	650		1086	829	742	668	552	775
	4200	620		1134	981	858	793	689	891
	4800	600		1247	1051	907	818	745	954
	5400	580		1417	1176	986	864	816	1052
	6000	540		1483	1306	1145	978	887	1160
Polyethylene - 50 sL/min	3000	660	33.1	956	974	832	690	516	793
	3600	640		965	1053	919	789	610	867
	4200	600		1066	1141	1000	866	674	949
	4800	580		1267	1268	1111	956	750	1070
	5400	560		1377	1350	1193	1009	803	1147
	6000	520		1520	1427	1236	1060	847	1218
Polyethylene - 75 sL/min	3000	620	32.8	933	835	678	584	472	700
	3600	600		1010	1021	830	704	584	830
	4200	580		1180	1017	967	814	696	935
	4800	570		1221	1174	1053	929	743	1024
	5400	540		1426	1187	1099	975	818	1101
	6000	520		1502	1334	1163	1031	887	1183
Polyethylene - 100 sL/min	3000	600	32.2	870	670	605	539	461	629
	3600	580		1068	815	729	651	547	762
	4200	580		1115	964	843	779	677	876
	4800	560		1216	1034	892	805	732	936
	5400	540		1379	1156	962	849	803	1030
	6000	520		1445	1284	1116	954	872	1134

Gas analysis: The MRU-Various plus model syngas monitoring system detects the syngas components in volumetric based percentage. The data are collected at a rate of 1 sample per 2 seconds. The average of each gas component percentage is determined by using equation 5.5 in volumetric base.

$$CO\ (V\,\%) = \frac{2}{t_g}\sum CO_{(t)} \tag{5.5a}$$

$$CO_2(V\,\%) = \frac{2}{t_g}\sum CO_{2(t)} \tag{5.5b}$$

$$H_2(V\,\%) = \frac{2}{t_g}\sum H_{2(t)} \tag{5.5c}$$

$$CH_4(V\,\%) = \frac{2}{t_g}\sum CH_{4(t)} \tag{5.5d}$$

$$O_2(V\,\%) = \frac{2}{t_g}\sum O_{2(t)} \tag{5.5e}$$

$$N_2(V\,\%) = \frac{2}{t_g}\sum N_{2(t)} \tag{5.5f}$$

The syngas content percentages in volumetric based are identical with the molar based percentages of syngas mixture from Dalton / Amagat model as given in equation 5.6.

$$\frac{n_i}{n_{syn}} = \frac{\forall_i}{\forall_{syn}} = \frac{P_i}{P_{syn}} \tag{5.6}$$

So, the relation between molar percentage and volumetric percentage can be given as equation 5.7. The volumetric/molar percentage of gas components in syngas is presented in Table 5.3.

$$CO\ (n\,\%) = CO\ (V\,\%) \tag{5.7a}$$

$$CO_2(n\,\%) = CO_2\ (V\,\%) \tag{5.7b}$$

$$H_2(n\,\%) = H_2\ (V\,\%) \tag{5.7c}$$

$$CH_4(n\,\%) = CH_4\ (V\,\%) \tag{5.7d}$$

$$O_2(n\,\%) = O_2\ (V\,\%) \tag{5.7e}$$

$$N_2(n\,\%) = N_2\ (V\,\%) \tag{5.7f}$$

Table 5.3 Presentation of molar based syngas content distribution for each cases (MRU vario plus system results)

	Power (W)	t_g (s)	O_2,%	CO_2,%	CO,%	H_2,%	CH_4,%	N_2,%
Hornbeam sawdust- 50 sL/min	3000	880	0.68	16.79	7.33	2.35	1.87	70.97
	3600	820	0.77	13.80	8.97	4.43	1.83	70.19
	4200	800	0.81	11.34	9.23	5.12	1.81	71.69
	4800	720	0.69	11.28	14.2	5.63	1.83	66.37
	5400	680	0.83	10.89	15.27	6.87	1.8	64.34
	6000	600	0.88	10.49	18.95	8.65	1.81	59.22
Hornbeam sawdust- 75 sL/min	3000	720	0.92	21.32	5.40	2.20	2.08	68.08
	3600	650	0.96	19.84	6.83	4.18	2.11	66.08
	4200	630	1.01	18.12	6.44	5.26	2.13	67.04
	4800	600	0.96	17.45	7.62	5.47	2.17	66.33
	5400	540	0.88	14.26	9.17	6.31	2.15	67.23
	6000	500	1.02	12.49	12.21	7.17	2.16	64.95

Table 5.3 (Continued) Presentation of molar based syngas content distribution for each cases (MRU vario plus system results)

Hornbeam sawdust- 100 sL/min	3000	640	1.20	22.30	4.71	1.94	2.33	67.52
	3600	600	1.22	21.12	5.42	3.98	2.28	65.98
	4200	560	1.26	20.84	5.94	4.24	2.26	65.46
	4800	520	1.32	19.97	6.38	5.12	2.21	65.00
	5400	450	1.28	17.65	7.96	5.86	2.17	65.08
	6000	420	1.34	16.42	9.61	6.83	2.19	63.62
Pine tree sawdust - 50 sL/min	3000	880	0.82	18.20	8.30	3.20	2.17	67.31
	3600	840	0.86	15.91	8.88	4.30	2.13	67.92
	4200	800	0.85	14.87	9.69	5.6	2.21	66.78
	4800	720	0.88	13.19	12.7	5.84	2.28	65.11
	5400	680	0.91	11.27	14.82	6.21	2.25	64.54
	6000	600	0.90	10.22	17.35	8.98	2.23	60.33
Pine tree sawdust- 75 sL/min	3000	720	0.84	19.56	7.12	3.18	2.19	67.11
	3600	680	0.87	20.43	9.73	3.47	2.22	63.28
	4200	600	0.99	19.16	11.21	5.12	2.23	61.29
	4800	560	1.03	18.83	12.84	5.63	2.26	59.41
	5400	520	1.01	16.12	14.17	6.57	2.28	59.85
	6000	460	1.08	16.01	17.21	7.88	2.29	55.53
Pine tree sawdust- 100 sL/min	3000	640	0.89	24.80	6.51	2.18	2.51	63.11
	3600	600	0.97	19.62	7.23	4.06	2.49	65.63
	4200	580	1.04	18.56	8.12	4.18	2.38	65.72
	4800	540	1.07	16.32	9.11	4.83	2.34	66.33
	5400	510	1.02	15.18	9.68	5.23	2.3	66.59
	6000	440	1.05	14.23	10.96	6.38	2.31	65.07
Russian coal- 50 sL/min	3000	1020	2.38	28.62	45.04	1.68	1.38	20.90
	3600	960	2.47	27.32	46.38	1.71	1.27	20.85
	4200	920	2.6	26.13	46.21	1.82	1.21	22.03
	4800	840	2.54	25.56	47.16	1.94	1.15	21.65
	5400	800	2.62	24.02	48.28	2.02	1.11	21.95
	6000	740	2.67	23.32	48.03	2.08	1.04	22.86
Russian coal- 75 sL/min	3000	820	3.21	33.06	42.14	1.62	1.43	18.54
	3600	790	3.16	32.84	43.73	1.67	1.38	17.22
	4200	750	3.36	31.18	44.21	1.76	1.37	18.12
	4800	700	3.32	30.64	45.84	1.83	1.34	17.03
	5400	680	3.28	30.27	46.17	1.91	1.35	17.02
	6000	620	3.33	30.12	47.08	2.03	1.29	16.15
Russian coal- 100 sL/min	3000	740	5.12	36.24	38.60	1.13	1.58	17.33
	3600	710	5.21	36.01	39.21	1.21	1.56	16.80
	4200	680	5.16	35.18	40.48	1.27	1.45	16.46
	4800	660	5.24	34.53	40.22	1.33	1.42	17.26
	5400	640	5.31	33.22	41.18	1.42	1.38	17.49
	6000	620	5.40	32.16	42.02	1.46	1.36	17.60
South African coal- 50 sL/min	3000	1010	2.24	25.47	39.18	1.75	1.35	30.01
	3600	970	2.35	24.86	38.96	1.76	1.23	30.84
	4200	910	2.42	24.30	39.28	1.89	1.19	30.92
	4800	870	2.31	23.52	38.67	2.04	1.10	32.36
	5400	780	2.44	21.62	41.52	2.10	1.09	31.24
	6000	760	2.56	21.69	40.83	2.18	1.01	31.73

Table 5.3 (Continued) Presentation of molar based syngas content distribution for each cases (MRU vario plus system results)

South African coal- 75 sL/min	3000	800	2.92	30.75	38.35	1.81	1.37	24.80
	3600	760	2.88	31.20	39.79	1.87	1.31	22.94
	4200	720	3.09	29.93	40.23	1.97	1.34	23.43
	4800	660	3.02	28.50	41.71	2.05	1.30	23.42
	5400	630	3.05	28.45	42.01	2.14	1.28	23.06
	6000	600	3.06	28.61	42.84	2.27	1.21	21.99
South African coal- 100 sL/min	3000	740	4.45	33.70	33.20	1.73	1.37	25.54
	3600	700	4.64	32.77	34.50	1.85	1.36	24.88
	4200	670	4.54	33.07	35.22	1.94	1.26	23.97
	4800	630	4.72	31.42	35.39	2.03	1.24	25.20
	5400	590	4.73	30.56	37.06	2.17	1.20	24.28
	6000	550	4.91	29.91	38.24	2.23	1.18	23.52
Şırnak (Turkey) coal- 50 sL/min	3000	880	2.30	23.43	36.83	1.54	1.57	34.32
	3600	840	2.42	22.38	37.40	1.59	1.39	34.83
	4200	820	2.49	22.11	37.31	1.68	1.32	35.08
	4800	800	2.50	21.63	37.51	1.83	1.27	35.26
	5400	780	2.51	19.67	37.78	1.91	1.27	36.85
	6000	760	2.59	19.95	36.74	1.92	1.29	37.50
Şırnak (Turkey) coal- 75 sL/min	3000	710	3.11	28.59	33.15	1.58	1.52	32.04
	3600	680	3.26	26.85	34.41	1.60	1.34	32.54
	4200	670	3.36	26.76	33.21	1.67	1.25	33.75
	4800	640	3.37	25.74	34.14	1.78	1.22	33.75
	5400	620	3.39	24.00	34.01	1.89	1.23	35.48
	6000	600	3.49	23.34	33.44	1.94	1.32	36.47
Şırnak (Turkey) coal- 100 sL/min	3000	690	4.82	34.31	26.52	1.63	1.55	31.17
	3600	650	4.89	32.76	28.22	1.67	1.38	31.09
	4200	620	5.14	33.18	28.56	1.70	1.28	30.14
	4800	600	5.32	31.67	28.67	1.85	1.25	31.24
	5400	580	5.39	28.80	28.56	1.95	1.26	34.03
	6000	540	5.59	28.48	29.42	1.96	1.35	33.19
Polyethylene- 50 sL/min	3000	660	1.12	16.21	19.62	9.80	2.12	51.13
	3600	640	1.18	15.30	20.11	9.91	2.01	51.49
	4200	600	1.32	14.62	20.67	10.03	1.98	51.38
	4800	580	1.44	13.01	21.31	10.80	1.94	51.50
	5400	560	1.43	12.54	21.94	11.32	1.95	50.82
	6000	520	1.52	11.21	22.27	12.56	1.86	50.58
Polyethylene- 75 sL/min	3000	620	1.99	20.12	16.44	11.12	1.95	48.38
	3600	600	1.96	19.88	16.91	11.28	1.88	48.09
	4200	580	1.98	19.56	17.23	11.67	1.89	47.67
	4800	570	1.97	18.27	17.44	12.01	1.77	48.54
	5400	540	2.03	17.94	18.12	12.51	1.73	47.67
	6000	520	2.01	17.32	18.54	12.89	1.63	47.61
Polyethylene- 100 sL/min	3000	600	2.39	22.16	14.12	11.21	2.03	48.09
	3600	580	2.41	21.88	15.05	11.87	2.21	46.58
	4200	580	2.47	21.64	15.23	12.08	2.34	46.24
	4800	560	2.55	21.43	15.61	12.43	2.45	45.53
	5400	540	2.63	21.12	15.87	12.96	2.67	44.75
	6000	520	2.68	20.16	16.32	13.14	2.81	44.89

The syngas content percentages in molar based are converted to mass based by using equation 5.8. The syngas molecular weight is calculated by equation 5.9. The mass based syngas content distribution in percentage is given in Table 5.4.

$$CO\ (m\ \%) = \frac{(CO(n\ \%).M_{CO})}{\left(\sum Syngas(n\ \%).M_{syngas}\right)}.100 \quad (5.8a)$$

$$CO_2\ (m\ \%) = \frac{\left(CO_2\ (n\ \%).M_{CO_2}\right)}{\left(\sum Syngas(n\ \%).M_{syngas}\right)}.100 \quad (5.8b)$$

$$H_2\ (m\ \%) = \frac{\left(H_2(n\ \%).M_{H_2}\right)}{\left(\sum Syngas(n\ \%).M_{syngas}\right)}.100 \quad (5.8c)$$

$$CH_4\ (m\ \%) = \frac{\left(CH_4(n\ \%).M_{CH_4}\right)}{\left(\sum Syngas(n\ \%).M_{syngas}\right)}.100 \quad (5.8d)$$

$$O_2\ (m\ \%) = \frac{\left(O_2\ (n\ \%).M_{O_2}\right)}{\left(\sum Syngas(n\ \%).M_{syngas}\right)}.100 \quad (5.8e)$$

$$N_2\ (m\ \%) = \frac{\left(N_2\ (n\ \%).M_{N_2}\right)}{\left(\sum Syngas(n\ \%).M_{syngas}\right)}.100 \quad (5.8f)$$

$$\sum Syngas(n\ \%).M_{syngas} = CO(n\ \%).M_{CO} + CO_2\ (n\ \%).M_{CO_2} + H_2(n\ \%).M_{H_2} + CH_4(n\ \%).M_{CH_4} + O_2\ (n\ \%).M_{O_2} + N_2\ (n\ \%).M_{N_2} \quad (5.9)$$

Table 5.4 Presentation of mass based syngas content distribution for each cases (MRU vario plus system results)

	Power(W)	t_g (s)	O_2,%	CO_2,%	CO,%	H_2,%	CH_4,%	N_2,%
Hornbeam sawdust- 50 sL/min	3000	880	0.73	24.73	6.87	0.16	1.00	66.51
	3600	820	0.85	21.03	8.70	0.31	1.02	68.09
	4200	800	0.92	17.63	9.13	0.36	1.02	70.93
	4800	720	0.78	17.63	14.12	0.40	1.04	66.02
	5400	680	0.96	17.25	15.39	0.49	1.04	64.86
	6000	600	1.04	16.94	19.48	0.64	1.06	60.86
Hornbeam sawdust- 75 sL/min	3000	720	0.96	30.63	4.94	0.14	1.09	62.24
	3600	650	1.03	29.22	6.40	0.28	1.13	61.94
	4200	630	1.10	27.20	6.15	0.36	1.16	64.03
	4800	600	1.05	26.34	7.32	0.38	1.19	63.72
	5400	540	0.99	22.08	9.04	0.44	1.21	66.24
	6000	500	1.17	19.68	12.25	0.51	1.24	65.15
Hornbeam sawdust- 100 sL/min	3000	640	1.25	31.82	4.28	0.13	1.21	61.32
	3600	600	1.30	30.85	5.04	0.26	1.21	61.34
	4200	560	1.34	30.55	5.54	0.28	1.20	61.07
	4800	520	1.42	29.63	6.02	0.35	1.19	61.38
	5400	450	1.41	26.70	7.66	0.40	1.19	62.64
	6000	420	1.50	25.22	9.39	0.48	1.22	62.19

Table 5.4 (Continued) Presentation of mass based syngas content distribution for each cases (MRU vario plus system results)

Pine tree sawdust- 50 sL/min	3000	880	0.88	26.83	7.78	0.21	1.16	63.13
	3600	840	0.94	23.97	8.51	0.29	1.17	65.11
	4200	800	0.95	22.80	9.46	0.39	1.23	65.17
	4800	720	0.99	20.47	12.54	0.41	1.29	64.30
	5400	680	1.04	17.74	14.84	0.44	1.29	64.64
	6000	600	1.06	16.60	17.95	0.66	1.32	62.40
Pine tree sawdust- 75 sL/min	3000	720	0.89	28.62	6.63	0.21	1.17	62.48
	3600	680	0.92	29.83	9.04	0.23	1.18	58.80
	4200	600	1.07	28.57	10.64	0.35	1.21	58.16
	4800	560	1.12	28.26	12.26	0.38	1.23	56.74
	5400	520	1.13	24.77	13.85	0.46	1.28	58.51
	6000	460	1.22	24.91	17.04	0.56	1.30	54.98
Pine tree sawdust- 100 sL/min	3000	640	0.91	35.05	5.85	0.14	1.29	56.75
	3600	600	1.04	28.95	6.79	0.27	1.34	61.62
	4200	580	1.12	27.55	7.67	0.28	1.28	62.09
	4800	540	1.18	24.66	8.76	0.33	1.29	63.78
	5400	510	1.13	23.16	9.40	0.36	1.28	64.66
	6000	440	1.18	22.06	10.81	0.45	1.30	64.19
Russian coal- 50 sL/min	3000	1020	2.37	39.26	39.32	0.10	0.69	18.25
	3600	960	2.48	37.71	40.74	0.11	0.64	18.32
	4200	920	2.63	36.31	40.86	0.11	0.61	19.48
	4800	840	2.58	35.65	41.86	0.12	0.58	19.21
	5400	800	2.68	33.78	43.20	0.13	0.57	19.64
	6000	740	2.74	32.92	43.14	0.13	0.53	20.53
Russian coal- 75 sL/min	3000	820	3.13	44.31	35.95	0.10	0.70	15.81
	3600	790	3.08	44.08	37.35	0.10	0.67	14.71
	4200	750	3.31	42.21	38.09	0.11	0.67	15.61
	4800	700	3.28	41.61	39.62	0.11	0.66	14.72
	5400	680	3.25	41.21	40.00	0.12	0.67	14.75
	6000	620	3.30	41.07	40.85	0.13	0.64	14.01
Russian coal- 100 sL/min	3000	740	4.89	47.57	32.24	0.07	0.75	14.48
	3600	710	4.98	47.34	32.80	0.07	0.75	14.06
	4200	680	4.95	46.44	34.01	0.08	0.70	13.83
	4800	660	5.05	45.74	33.90	0.08	0.68	14.55
	5400	640	5.15	44.30	34.95	0.09	0.67	14.84
	6000	620	5.27	43.12	35.85	0.09	0.66	15.02
South African coal- 50 sL/min	3000	1010	2.27	35.53	34.78	0.11	0.69	26.63
	3600	970	2.39	34.76	34.67	0.11	0.63	27.44
	4200	910	2.47	34.11	35.08	0.12	0.61	27.62
	4800	870	2.37	33.17	34.71	0.13	0.57	29.05
	5400	780	2.53	30.80	37.65	0.14	0.56	28.32
	6000	760	2.66	30.90	37.01	0.14	0.52	28.77
South African coal- 75 sL/min	3000	800	2.89	41.75	33.14	0.11	0.68	21.43
	3600	760	2.84	42.28	34.32	0.12	0.65	19.79
	4200	720	3.07	40.85	34.94	0.12	0.67	20.35
	4800	660	3.03	39.19	36.51	0.13	0.65	20.49
	5400	630	3.05	39.17	36.80	0.13	0.64	20.20
	6000	600	3.07	39.39	37.53	0.14	0.61	19.27

Table 5.4 (Continued) Presentation of mass based syngas content distribution for each cases (MRU vario plus system results)

South African coal- 100 sL/min	3000	740	4.33	45.00	28.20	0.10	0.67	21.70
	3600	700	4.53	43.98	29.47	0.11	0.66	21.25
	4200	670	4.43	44.34	30.05	0.12	0.62	20.45
	4800	630	4.64	42.49	30.46	0.13	0.61	21.68
	5400	590	4.67	41.54	32.06	0.13	0.59	21.00
	6000	550	4.87	40.79	33.19	0.14	0.59	20.42
Şırnak (Turkey) coal- 50 sL/min	3000	880	2.36	32.99	33.00	0.10	0.80	30.75
	3600	840	2.49	31.66	33.68	0.10	0.72	31.36
	4200	820	2.57	31.34	33.66	0.11	0.68	31.64
	4800	800	2.58	30.77	33.96	0.12	0.66	31.91
	5400	780	2.62	28.29	34.58	0.12	0.67	33.72
	6000	760	2.70	28.65	33.58	0.13	0.67	34.27
Şırnak (Turkey) coal- 75 sL/min	3000	710	3.10	39.18	28.91	0.10	0.76	27.95
	3600	680	3.28	37.09	30.25	0.10	0.67	28.61
	4200	670	3.38	36.99	29.21	0.10	0.63	29.69
	4800	640	3.41	35.80	30.20	0.11	0.62	29.87
	5400	620	3.46	33.70	30.39	0.12	0.63	31.70
	6000	600	3.58	32.91	30.00	0.12	0.68	32.71
Şırnak (Turkey) coal- 100 sL/min	3000	690	4.67	45.64	22.45	0.10	0.75	26.39
	3600	650	4.77	43.89	24.06	0.10	0.67	26.51
	4200	620	5.00	44.35	24.29	0.10	0.62	25.63
	4800	600	5.22	42.68	24.59	0.11	0.61	26.79
	5400	580	5.36	39.40	24.87	0.12	0.63	29.63
	6000	540	5.57	39.03	25.66	0.12	0.67	28.94
Polyethylene - 50 sL/min	3000	660	1.29	25.62	19.74	0.70	1.22	51.43
	3600	640	1.36	24.32	20.34	0.72	1.16	52.09
	4200	600	1.53	23.35	21.01	0.73	1.15	52.23
	4800	580	1.70	21.12	22.02	0.80	1.15	53.21
	5400	560	1.70	20.52	22.85	0.84	1.16	52.92
	6000	520	1.84	18.71	23.65	0.95	1.13	53.72
Polyethylene - 75 sL/min	3000	620	2.26	31.42	16.34	0.79	1.11	48.08
	3600	600	2.23	31.13	16.85	0.80	1.07	47.92
	4200	580	2.27	30.79	17.26	0.84	1.08	47.76
	4800	570	2.28	29.06	17.65	0.87	1.02	49.12
	5400	540	2.36	28.71	18.46	0.91	1.01	48.55
	6000	520	2.36	27.91	19.01	0.94	0.96	48.82
Polyethylene - 100 sL/min	3000	600	2.69	34.23	13.88	0.79	1.14	47.27
	3600	580	2.73	34.08	14.92	0.84	1.25	46.17
	4200	580	2.81	33.84	15.15	0.86	1.33	46.01
	4800	560	2.91	33.67	15.61	0.89	1.40	45.52
	5400	540	3.03	33.43	15.99	0.93	1.54	45.08
	6000	520	3.11	32.16	16.57	0.95	1.63	45.57

5.2 The evaluation of quantity of syngas to supplied air, ash and fuel

The produced syngas (m_{syngas}) to the supplied air (m_{air}) depending on plasma power is presented in Figure 5.1 for hornbeam sawdust (HSD), pine tree sawdust (PSD), Russian coal (CR), South African coal (CSA), Şırnak (Turkey) coal (CTR), polyethylene (PP) at 50 sL/min air flow rate. While the ratio of syngas to air (m_{syngas}/m_{air}) is the highest for polyethylene (PP), the lowest ratio occurs for coals. The same amount of fuel is dosed to the reactor and the air supply rate is constant. However, the gasification of coals are longer than the polyethylene (PP). So, this is the reason why the ratio of syngas to air (m_{syngas}/m_{air}) is lower for coals and higher for polyethylene (PP). The maximum ratio increases from 1.38 at 3 kW to 1.49 at 6 kW for polyethylene (PP), while the minimum ratio increases from 1.19 at 3 kW to 1.29 at 6 kW at 50 sL/min air flow rate for the Russian coal (CR).

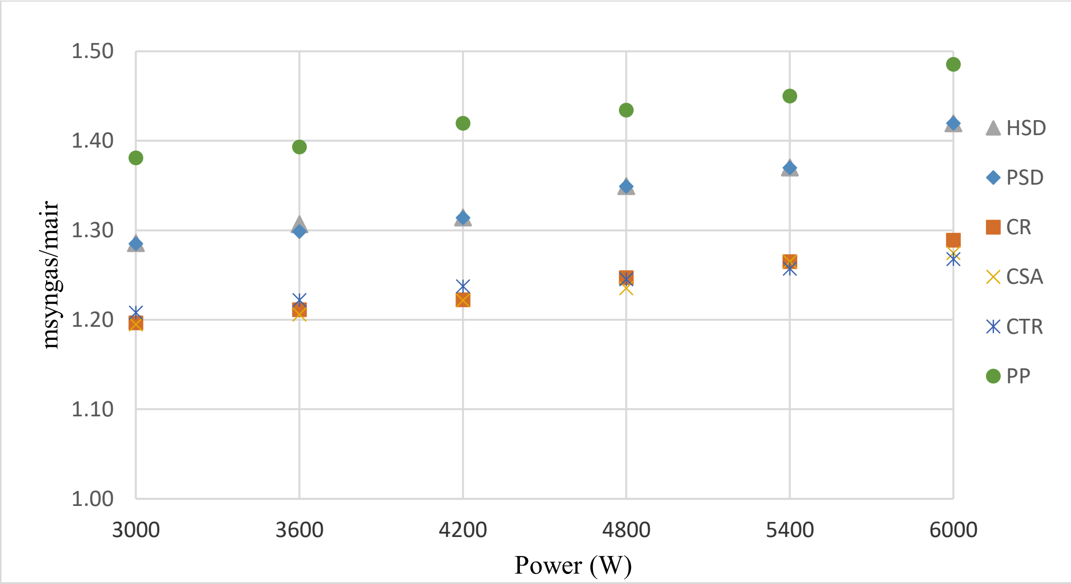

Figure 5.1 The ratio of syngas to the supplied air flow rate depending on plasma power at 50 sL/min air flow rate

The ratio of produced syngas (m_{syngas}) to the supplied air (m_{air}) depending on plasma power is presented in Figure 5.2 for hornbeam sawdust (HSD), pine tree sawdust (PSD), Russian coal (CR), South African coal (CSA), Şırnak (Turkey) coal (CTR), polyethylene (PP) at 75 sL/min air flow rate. The increment of air flow rate is accelerated the gasification process. While the time required to complete the process is decreased, the supplied air amount to reactor increases. As a result, the ratio of syngas to air (m_{syngas}/m_{air}) decreases by increasing the air flow rate. The ratio of the syngas to air supply (m_{syngas}/m_{air}) at 3 kW is varied between 1.15 and 1.27, while it is between 1.21 and 1.36 at 6 kW power. By increasing the power, the ratio varies more depending on fuel. The minimum ratio occurs for Şırnak (Turkey) coal (CTR) as 1.21 and the highest ratio occurs for pine tree sawdust as 1.36 at 6 kW power. It is directly related with the gasification process time and supplied air rate.

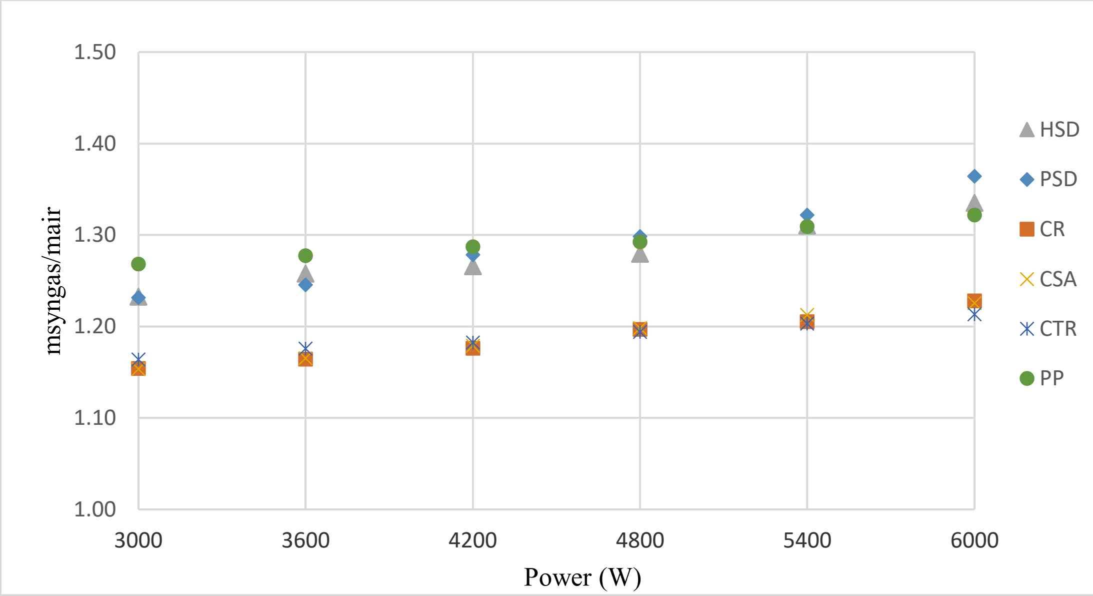

Figure 5.2 The ratio of syngas to the supplied air flow rate depending on plasma power at 75 sL/min air flow rate

The ratio of produced syngas (m_{syngas}) to the supplied air (m_{air}) depending on plasma power is presented in Figure 5.3 for hornbeam sawdust (HSD), pine tree sawdust (PSD), Russian coal (CR), South African coal (CSA), Şırnak (Turkey) coal (CTR), polyethylene (PP) at 100 sL/min air flow rate. The ratio of the syngas to air supply (m_{syngas}/m_{air}) at 3 kW is varied between 1.12 for Şırnak (Turkey) coal (CTR) and 1.21 for polyethylene (PP). The deviation of the ratios depending on fuels increases by increasing the power to 6 kW. At this power, the Russian coal has the lowest ratio 1.17 while the ratio of Hornbeam sawdust is the maximum with 1.30.

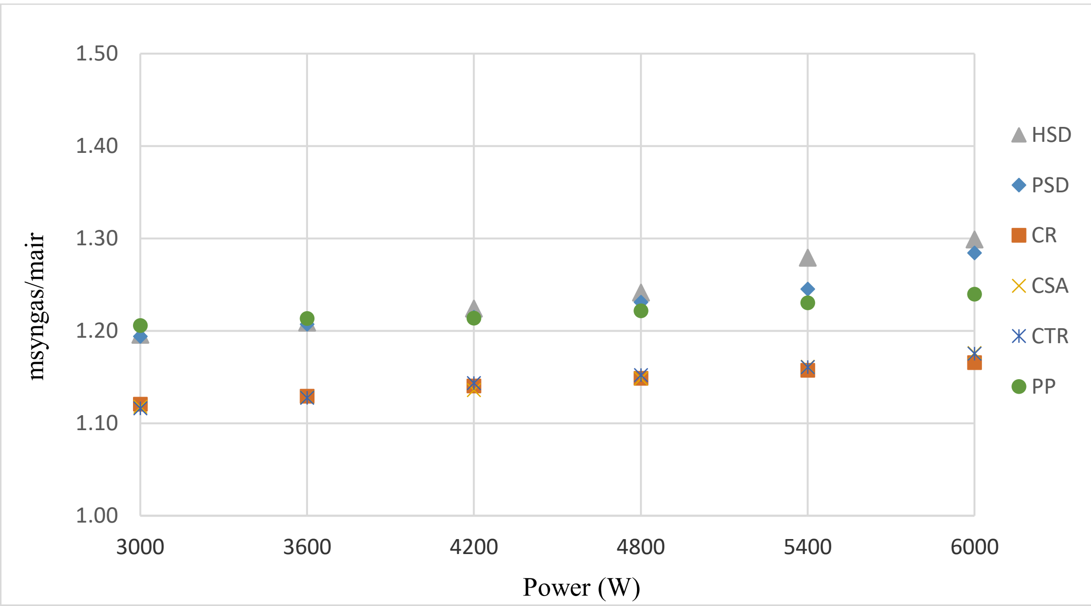

Figure 5.3 The ratio of syngas to the supplied air flow rate depending on plasma power at 100 sL/min air flow rate

The ratio of produced syngas (m_{syngas}) to the supplied fuel (m_{fuel}) depending on plasma power is presented in Figure 5.4 for hornbeam sawdust (HSD), pine tree sawdust (PSD), Russian coal (CR), South African coal (CSA), Şırnak (Turkey) coal (CTR), polyethylene (PP) at 50 sL/min air flow rate. The ratio of the syngas to fuel supply (m_{syngas}/m_{fuel}) at 3 kW is varied between 3.6 for polyethylene (PP) and 4.82 for Russian coal (CR). While the ratio of syngas to fuel (m_{syngas}/m_{fuel}) is the lowest for polyethylene, the highest ratio occurs for Russian Coal (CR). The same amount of fuel is dosed to the reactor and the air supply rate is constant. However, while the duration of gasification for Russian coal (CR) is longest, the gasification duration of polyethylene is the shortest. So, this is the reason why the ratio of syngas to air (m_{syngas}/m_{fuel}) is lower for polyethylene and higher for Russian coal (CR). The ratio of the syngas to air supply (m_{syngas}/m_{fuel}) reduces by increasing the plasma power. Also, the variation of the ratios depending on fuels is decreasing. At 6 kW plasma power, the Russian coal (CR) has 3.76 ratio while the polyethylene (PP) is 3.05.

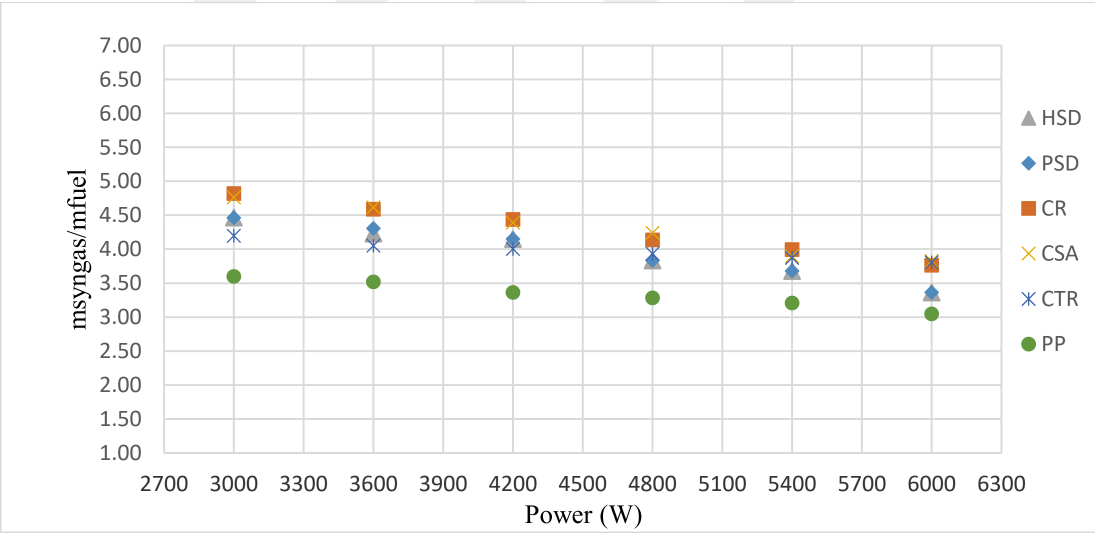

Figure 5.4 The ratio of syngas to the supplied fuel rate depending on plasma power at 50 sL/min air flow rate

The ratio of produced syngas (m_{syngas}) to the supplied fuel (m_{fuel}) depending on plasma power is presented in Figure 5.5 for hornbeam sawdust (HSD), pine tree sawdust (PSD), Russian coal (CR), South African coal (CSA), Şırnak (Turkey) coal (CTR), polyethylene (PP) at 75 sL/min air flow rate. The increment of air flow rate is accelerated the gasification process. While the time required to complete the process is decreased, the supplied air amount to reactor increases. As a result, the ratio of syngas to fuel (m_{syngas}/m_{fuel}) increases by increasing the air flow rate. It decreases by increasing the plasma power. The ratio of the syngas to fuel supply (m_{syngas}/m_{fuel}) at 3 kW is varied between 4.65 and 5.60, while it is between 3.71 and 4.51 depending on fuel type at 6 kW power. The minimum ratio occurs for pine tree sawdust as 3.71 at 6 kW power, while the highest ratio occurs for Russian coal (CR) as 5.6 at 3kW power.

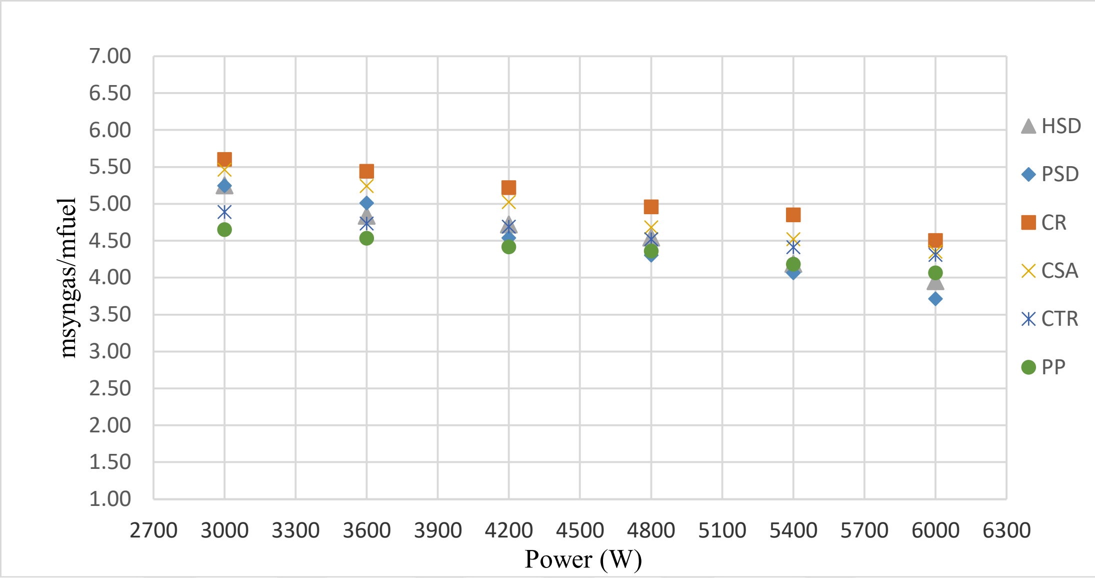

Figure 5.5 The ratio of syngas to the supplied fuel rate depending on plasma power at 75 sL/min air flow rate

The ratio of produced syngas (m_{syngas}) to the supplied fuel rate (m_{fuel}) depending on plasma power is presented in Figure 5.6 for hornbeam sawdust (HSD), pine tree sawdust (PSD), Russian coal (CR), South African coal (CSA), Şırnak (Turkey) coal (CTR), polyethylene (PP) at 100 sL/min air flow rate.

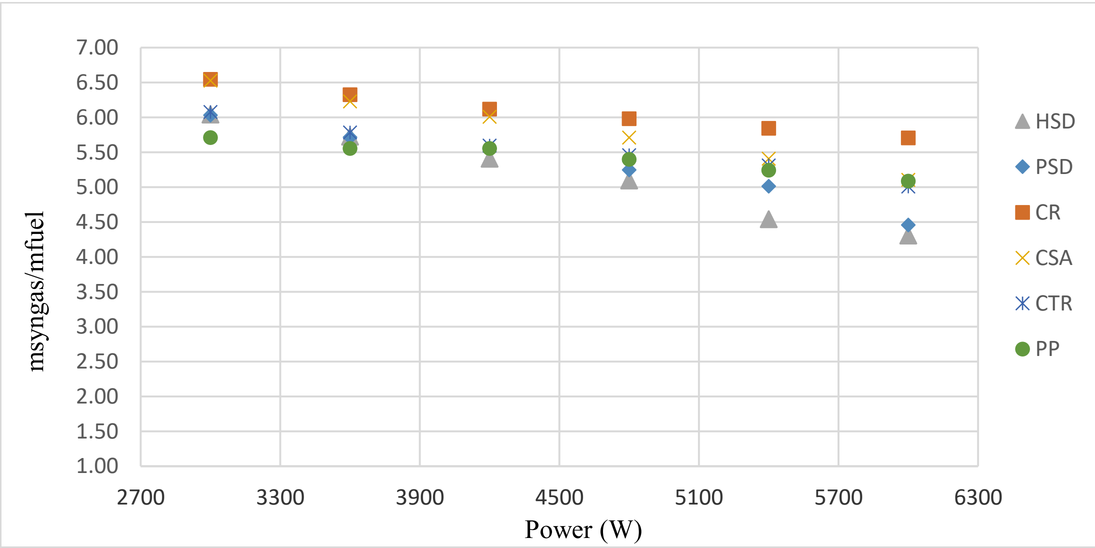

Figure 5.6 The ratio of syngas to the supplied fuel rate depending on plasma power at 100 sL/min air flow rate

The ratio of the syngas to fuel supply (m_{syngas}/m_{fuel}) at 3 kW is varied between 5.71 and 6.55, while it is between 4.31 and 5.71 depending on fuel type at 6 kW power. The minimum ratio occurs for hornbeam sawdust as 4.31 at 6 kW power, while the highest ratio occurs for Russian coal (CR) as 6.55 at 3kW power. The deviation of the ratios depending on fuels increase by increasing the power to 6 kW.

The ratio of ash (m_{ash}) to the supplied fuel (m_{fuel}) depending on plasma power is presented in Figure 5.7 for hornbeam sawdust (HSD), pine tree sawdust (PSD), Russian coal (CR), South African coal (CSA), Şırnak (Turkey) coal (CTR), polyethylene (PP) at 50 sL/min air flow rate. While the ash to fuel rate of hornbeam sawdust, pine tree sawdust and polyethylene is below the 0.01, it is varied between 0.1571 and 0.2779 for the coals. The ash amount decreases by increasing the plasma power.

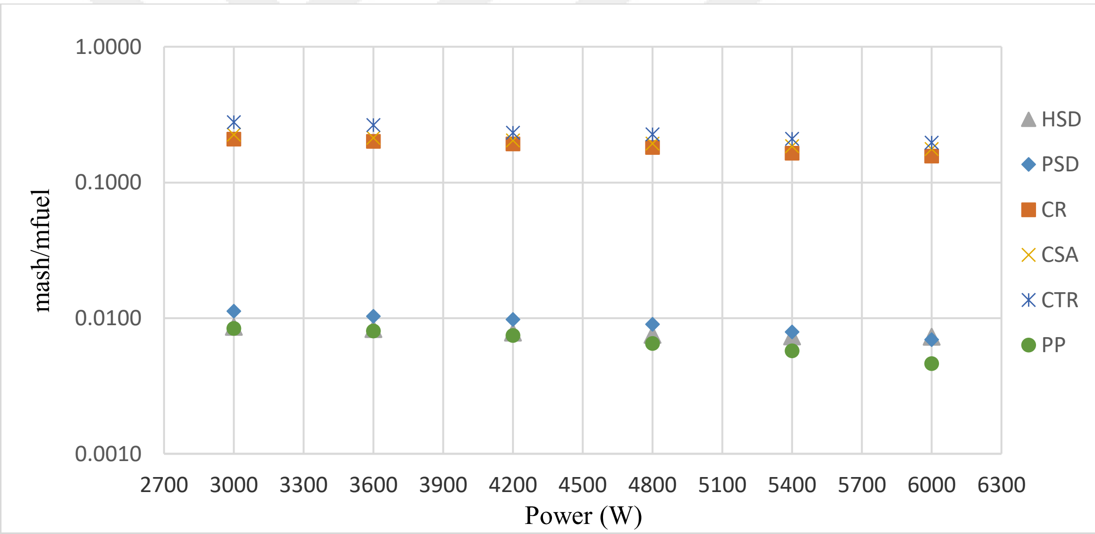

Figure 5.7 The ratio of ash to the supplied fuel rate depending on plasma power at 50 sL/min air flow rate

The ratio of ash (m_{ash}) to the supplied fuel (m_{fuel}) depending on plasma power is presented in Figure 5.8 for hornbeam sawdust (HSD), pine tree sawdust (PSD), Russian coal (CR), South African coal (CSA), Şırnak (Turkey) coal (CTR), polyethylene (PP) at 75 sL/min air flow rate. While the ash to fuel rate of hornbeam sawdust, pine tree sawdust and polyethylene is below the 0.02, it is varied between 0.1634 and 0.3119 for the coals. The rate of ash to fuel increases by raising the air flow rate from 50 to 75 sL/min. The ash amount decreases by increasing the plasma power from 3kW to 6kW.

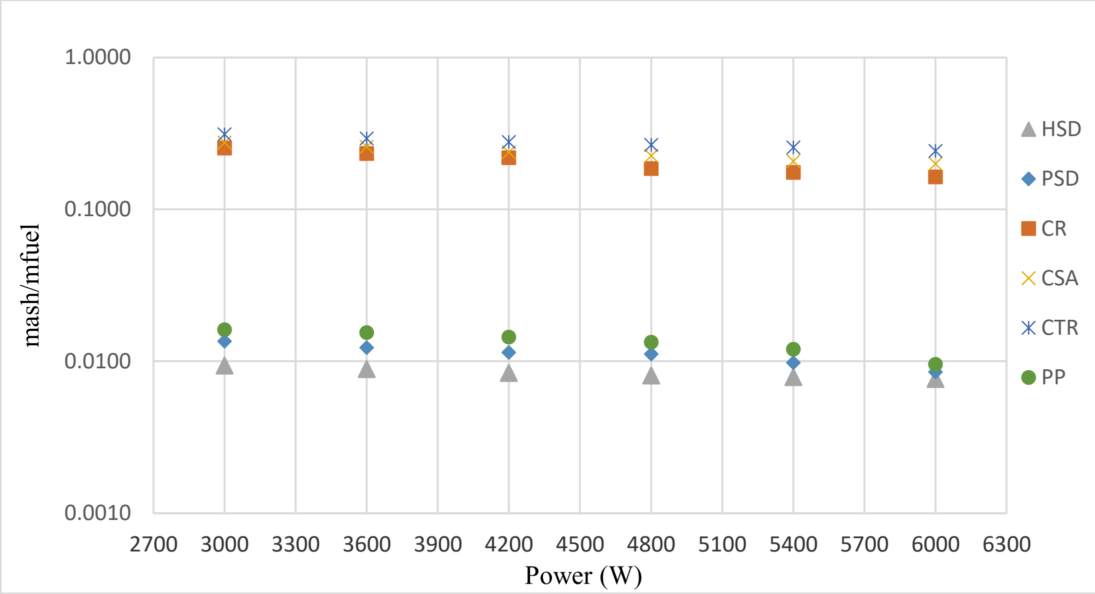

Figure 5.8 The ratio of ash to the supplied fuel rate depending on plasma power at 75 sL/min air flow rate

The ratio of ash (m_{ash}) to the supplied fuel (m_{fuel}) depending on plasma power is presented in Figure 5.9 for hornbeam sawdust (HSD), pine tree sawdust (PSD), Russian coal (CR), South African coal (CSA), Şırnak (Turkey) coal (CTR), polyethylene (PP) at 100 sL/min air flow rate.

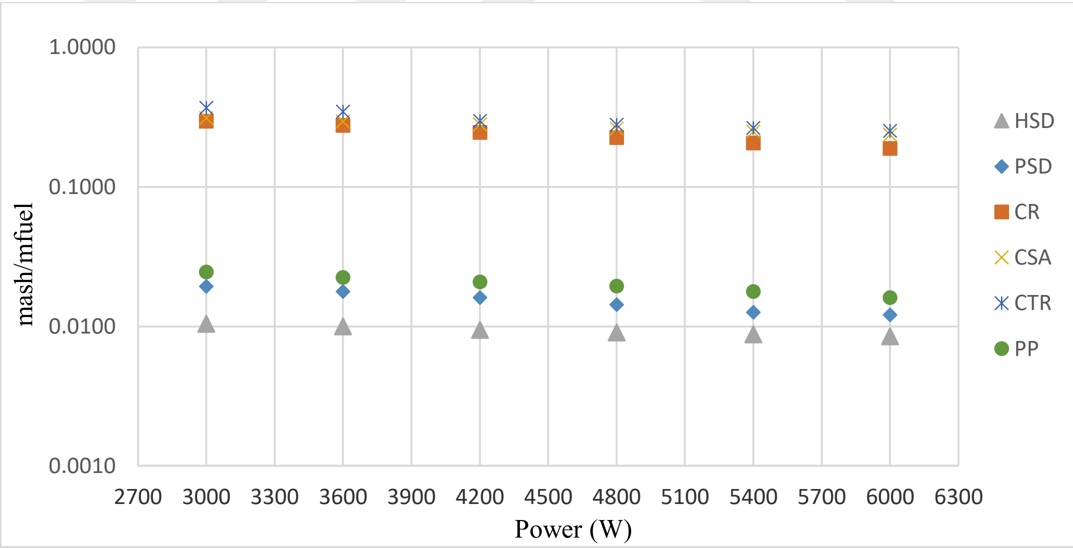

Figure 5.9 The ratio of ash to the supplied fuel rate depending on plasma power at 100 sL/min air flow rate

While the ash to fuel rate of hornbeam sawdust, pine tree sawdust and polyethylene is below the 0.03, it is varied between 0.1880 and 0.3671 for the coals. The rate of ash to fuel increases by raising the air flow rate from 75 to 100 sL/min. The ash amount decreases by increasing the plasma power from 3 kW to 6 kW.

5.3 Effects of Power, air flow rate and fuels on temperature distribution

In Figure 5.10, the temperature distribution along the gasifier is presented for hornbeam sawdust (HSD), pine tree sawdust (PSD), Russian coal (CR), South African coal (CSA), Şırnak (Turkey) coal (CTR), polyethylene (PP) and without fuel (WF) at power levels of 3 kW, 3.6 kW, 4.2 kW, 4.8 kW, 5.4 kW and 6 kW and 50s L/min air flow rate.

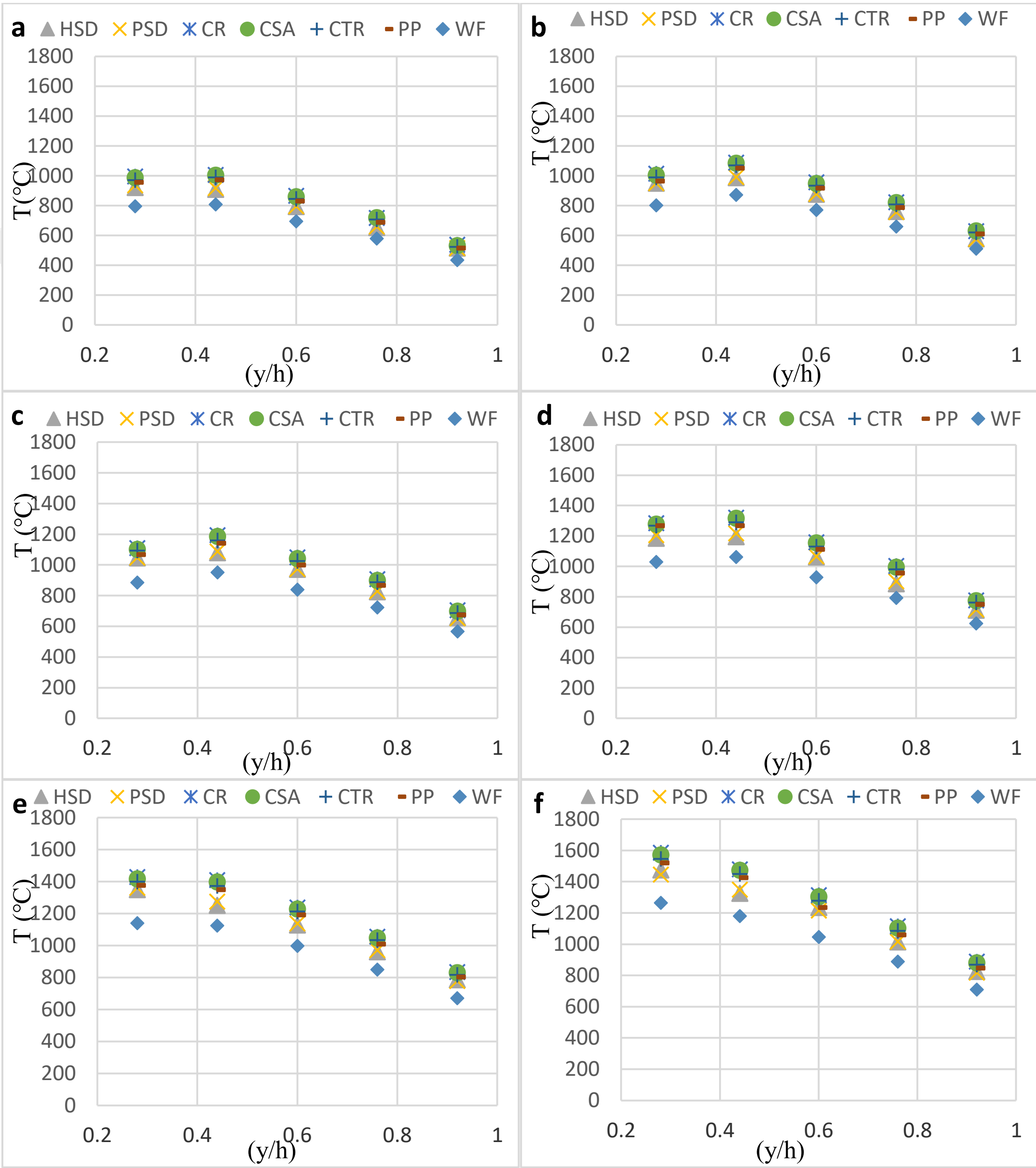

Figure 5.10 Effects of power on temperature distribution in the reactor in case of 50 sL/min air flow rate, a: 3 kW, b: 3.6 kW, c: 4.2 kW, d: 4.8 kW, e: 5.4 kW, f: 6 kW

In each case of usage of hornbeam sawdust (HSD) and pine tree sawdust (PSD) at 50 sL/min air flow, the average temperature in the gasifier (T_{syn}) increases in range between 12.00 % and 13.41 % in all power cases of hornbeam sawdust (HSD) and in range between 12.92 % and 13.62 % in all power cases of pine tree sawdust (PSD) respectively when it is compared to without fuel (WF) case. Similarly, in each case of usage of Russian coal (CR) at 50 sL/min air flow, the average temperature in the gasifier (T_{syn}) increases between 19.66 % and 20.23 %, in each case of usage of South African coal (CSA) at 50 sL/min air flow, the average temperature in the gasifier (T_{syn}) increases between 19.23 % and 19.65 % and in each case of usage of Şırnak (Turkey) coal (CTR) at 50 sL/min air flow, the average temperature in the gasifier (T_{syn}) increases between 17.92 % and 18.37 % when it is compared with the without fuel (WF) case respectively. Also, in case of usage of polyethylene (PP) at 50 sL/min air flow, the average temperature in the gasifier ($\mathrm{T_{syn}}$) increases between 16.42 % and 17.21 % when it is compared with the without fuel (WF) case. The temperature in the reactor rises by increment of power. In gasifier at 50 sL/min air flow rate, the highest measured temperature is 1585°C in case of 6 kW power and at $y/h = 0.28$ in Russian coal (CR).

In Figure 5.11, the temperature distribution along the gasifier is given for hornbeam sawdust (HSD), pine tree sawdust (PSD), Russian coal (CR), South African coal (CSA), Şırnak (Turkey) coal (CTR), polyethylene (PP) and without fuel (WF) at power levels of 3 kW, 3.6 kW, 4.2 kW, 4.8 kW, 5.4 kW and 6 kW and 75 sL/min air flow rate. In each case of usage of hornbeam sawdust (HSD) and pine tree sawdust (PSD) at 75 sL/min air flow, the average temperature in the gasifier (T_{syn}) increases in range between 7.73 % and 19.85 % in all power cases of hornbeam sawdust (HSD) and in range between 8.07 % and 20.33 % in all power cases of pine tree sawdust (PSD) respectively when it is compared to without fuel (WF) case. Similarly, in each case of usage of Russian coal (CR) at 75 sL/min air flow, the average temperature in the gasifier (T_{syn}) increases between 15.52 % and 26.33 %, in each case of usage of South African coal (CSA) at 75 sL/min air flow, the average temperature in the gasifier (T_{syn}) increases between 14.94 % and 25.62 % and in each case of usage of Şırnak (Turkey) coal (CTR) at 75 sL/min air flow, the average temperature in the gasifier (T_{syn}) increases between 13.09 % and 24.09 % when it is compared with the without fuel (WF) case respectively.

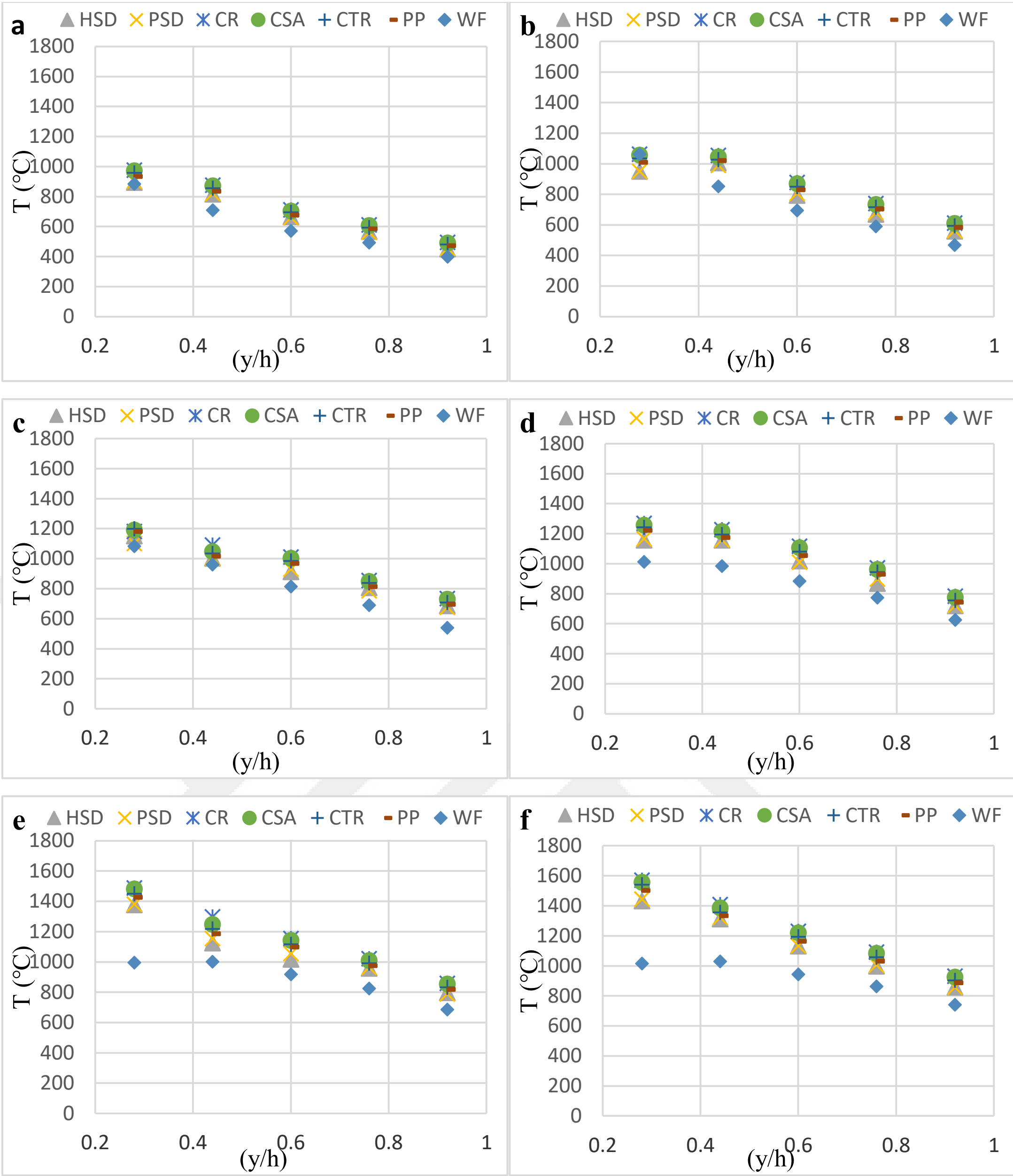

Figure 5.11 Effects of power on temperature distribution in the reactor in case of 75 sL/min air flow rate, a: 3 kW, b: 3.6 kW, c: 4.2 kW, d: 4.8 kW, e: 5.4 kW, f: 6 kW

Also, in case of usage of polyethylene (PP) at 75 sL/min air flow, the average temperature in the gasifier (T_{syn}) increases between 11.58 % and 22.43 % when it is compared with the without fuel (WF) case. The temperature in the reactor rises by increment of power. In gasifier at 75 sL/min air flow rate, the highest measured temperature is 1570°C in case of 6 kW power and at $y/h = 0.28$ in Russian coal (CR).

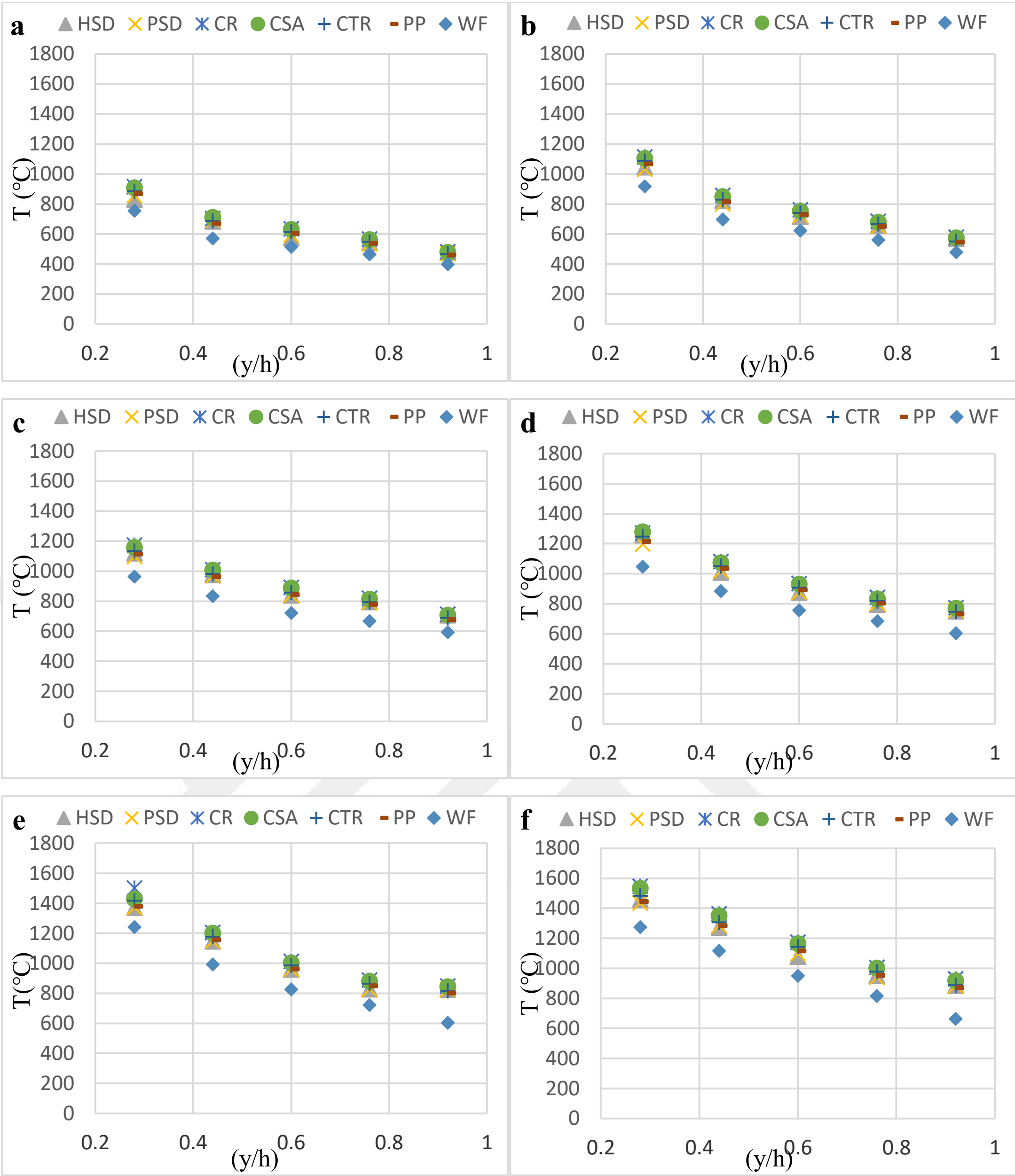

Figure 5.12 Effects of power on temperature distribution in the reactor in case of 100 sL/min air flow rate, a: 3 kW, b: 3.6 kW, c: 4.2 kW, d: 4.8 kW, e: 5.4 kW, f: 6 kW

In Figure 5.12, the temperature distribution along the gasifier is given for hornbeam sawdust (HSD), pine tree sawdust (PSD), Russian coal (CR), South African coal (CSA), Şırnak (Turkey) coal (CTR), polyethylene (PP) and without fuel (WF) at power levels of 3 kW, 3.6 kW, 4.2 kW, 4.8 kW, 5.4 kW and 6 kW and 100 sL/min air flow rate. In each case of usage of hornbeam sawdust (HSD) and pine tree sawdust (PSD) at 100 sL/min air flow, the average temperature in the gasifier (T_{syn}) increases in range between 12.91 % and 15.17 % in all power cases of hornbeam sawdust (HSD) and in range between 13.48 % and 14.54 % in all power cases of pine tree sawdust (PSD) respectively when it is compared to without fuel (WF) case.

Similarly, in each case of usage of Russian coal (CR) at 100 sL/min air flow, the average temperature in the gasifier (T_{syn}) increases between 18.00 % and 19.92 %, in each case of usage of South African coal (CSA) at 100 sL/min air flow, the average temperature in the gasifier (T_{syn}) increases between 17.34 % and 19.23 % and in each case of usage of Şırnak (Turkey) coal (CTR) at 100 sL/min air flow, the average temperature in the gasifier (T_{syn}) increases between 15.16 % and 16.90 % when it is compared with the without fuel (WF) case respectively. Also, in case of usage of polyethylene (PP) at 100 sL/min air flow, the average temperature in the gasifier (T_{syn}) increases between 13.69 % and 15.08 % when it is compared with the without fuel (WF) case. The temperature in the reactor rises by increment of power. In gasifier at 100 sL/min air flow rate, the highest measured temperature is 1547°C in case of 6 kW power and at $y/h = 0.28$ in Russian coal (CR).

5.4 Gasification results of Hornbeam Sawdust

The temperature distribution and the produced syngas fractions for the gasification of hornbeam sawdust are investigated in this section. The temperature variations are examined by changing the power level between 3 kW-6 kW in case of 50 sL/min, 75 sL/min and 100 sL/min air flow rate. Then the syngas content fractions are examined by changing the power level between 3 kW – 6 kW in case of 50 sL/min, 75 sL/min and 100 sL/min air flow rate.

In Figure 5.13, the temperature distribution is presented at varied powers in case of feeding of 50 sL/min air flow rate and initially 250 gr hornbeam sawdust dosed to the reactor. The thermocouple which is located at y/h=0.28 (closest measurement point to plasma flame) has highest temperature $T_{y/h=0.28} = 921°C$ at 3 kW power. The temperature at y/h=0.28 ($T_{y/h=0.28}$) increases from 921 to 1476 °C by increasing the power from 3 kW to 6 kW. The temperature decreases gradually from region of the plasma flame to downward.

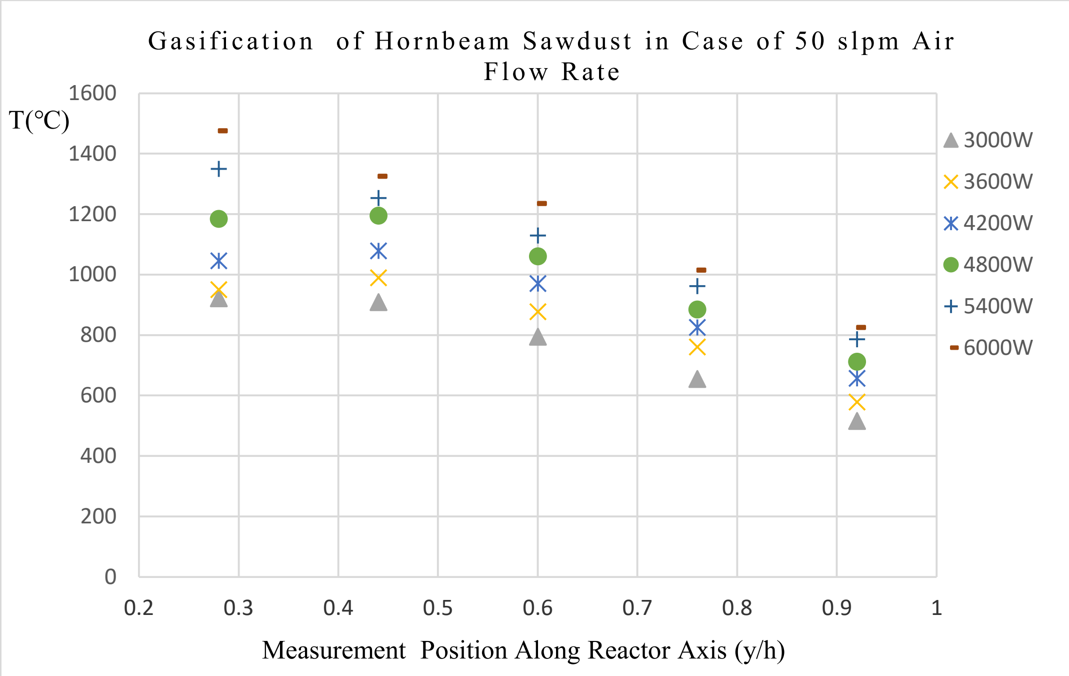

Figure 5.13 The temperature distribution for the gasification of hornbeam sawdust (HSD) in case of 50 sL/min air flow rate

The minimum temperature is measured 515 °C at the y/h=0.92 ($T_{y/h=0.92}$) and 3 kW power which is the most distant measurement point from the plasma flame. It varies from 515 to 825 °C by increasing the power from 3 kW to 6 kW. The average temperatures in the reactor (T_{syn}) are 758°C , 830°C, 915°C, 1006°C, 1095°C, 1175°C at 3 kW, 3.6 kW, 4.2 kW, 4.8 kW, 5.4 kW and 6 kW plasma power respectively. The average temperature increases by increasing plasma power. Because, the increment of plasma power increases the energy density in the reactor.

In Figure 5.14, the temperature distribution in the reactor is given at varied powers in case of 75 sL/min air flow rate input and initially 250 gr hornbeam sawdust dosed to the reactor. The thermocouple at y/h=0.28 which is closest to plasma flame has highest temperature $T_{y/h=0.28}$ = 894°C at 3 kW power. The temperature at y/h=0.28 ($T_{y/h=0.28}$) rises from 894 to 1432 °C by increasing the power from 3 kW to 6 kW. The temperature reduces gradually from region of the plasma flame to downward. The minimum temperature is measured 450 °C at the y/h=0.92 ($T_{y/h=0.92}$) and 3 kW power which is the most distant measurement point from the plasma flame. It varies from 450 to 857 °C by increasing the power from 3 kW to 6 kW. The average temperatures in the reactor (T_{syn}) are 678°C , 795°C, 911°C, 983°C, 1054°C and 1145°C at 3 kW, 3.6 kW, 4.2 kW, 4.8 kW, 5.4 kW and 6 kW plasma power respectively. The average temperature increases by increasing plasma power. Because, the increment of plasma power rises the energy density in the reactor.

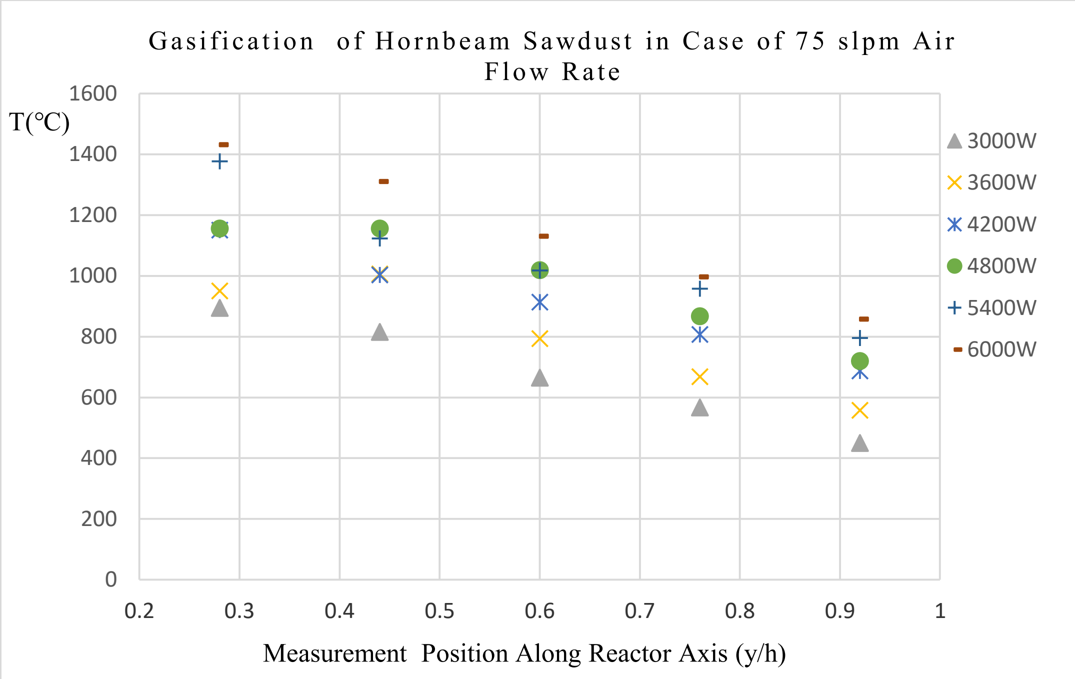

Figure 5.14 The temperature distribution for the gasification of hornbeam sawdust (HSD) in case of 75 sL/min air flow rate

The magnitude of the temperature decreases by increasing the flow rate from 50 to 75 sL/min. Because, the increment of air flow rate lowers the energy density in reactor. However, the temperature in the reactor becomes more uniform. The deviation of temperature from point y/h=0.28 ($T_{y/h=0.28}$) to y/h= 0.92 ($T_{y/h=0.92}$) at 6 kW plasma power and 50 sL/min air flow rate is 650°C, while it is 574°C at 6 kW plasma power and 75 sL/min air flow rate.

The variation of temperature with power is given in case of 100 sL/min air flow rate feeding and initially 250 gr hornbeam sawdust dosed to the reactor in Figure 5.15. The closest thermocouple to plasma flame located at y/h=0.28 ($T_{y/h=0.28}$) has highest temperature 830°C at 3 kW power. The temperature at y/h=0.28 ($T_{y/h=0.28}$) goes up from 830°C to 1456 °C by increasing the power from 3 kW to 6 kW. The temperature lessens progressively from region of the plasma flame to downward. The lowest temperature is measured 474 °C at the y/h=0.92 ($T_{y/h=0.92}$) and 3 kW power which is the outmost measurement point from the plasma flame. It varies from 474 to 886 °C by increasing the power from 3 kW to 6 kW. The average temperatures (T_{syn}) in the reactor are 620°C , 762°C, 887°C, 936°C, 1008°C and 1128°C at 3 kW, 3.6 kW, 4.2 kW, 4.8 kW, 5.4 kW and 6 kW plasma power respectively. The average temperature goes up by increasing plasma power. Because, the increment of plasma power rises the energy density in the reactor.

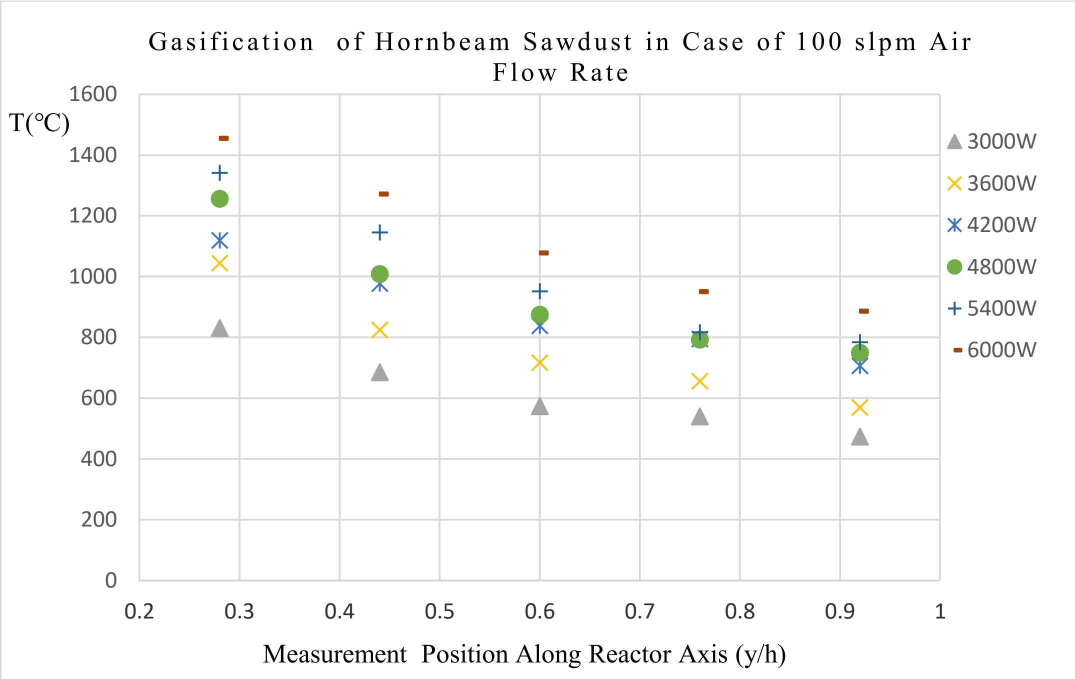

Figure 5.15 The temperature distribution for the gasification of hornbeam sawdust (HSD) in case of 100 sL/min air flow rate

The magnitude of the temperature decreases by increasing the flow rate from 75 to 100 sL/min too. Because, the increment of air flow rate reduces the energy density in reactor. The temperature in the reactor at 100 sL/min air flow rate becomes slightly more uniform when it is compared with 75 sL/min air flow rate. The variation of temperature between y/h=0.28 ($T_{y/h=0.28}$) and y/h= 0.92 ($T_{y/h=0.92}$) at 6 kW plasma power and 75 sL/min air flow rate is 574°C, while it is 569°C at 6 kW plasma power and 100 sL/min air flow rate.

In Figure 5.16, the fraction of syngas is presented in case of gasification of hornbeam sawdust (HSD) at 50 sL/min air flow rate and power levels between 3 kW-6 kW. As a result of the process, the O_2 in syngas stays below 0.9 % in all power levels. The CO_2 gradually decreases by increasing power from 16.79 % at 3 kW to 10.49 % at 6 kW. In contrast to that, the CO and H_2 increase by increasing the power. The CO increases from 7.33 % to 18.95 % and H_2 increases from 2.35 % to 8.65 % by increasing power from 3 kW to 6 kW. The CH_4 stays in the level of 1.8 % in all power cases. The rest of the mixture is considered as N_2 that reduces by increasing power from 70.97 % to 59.22 %.

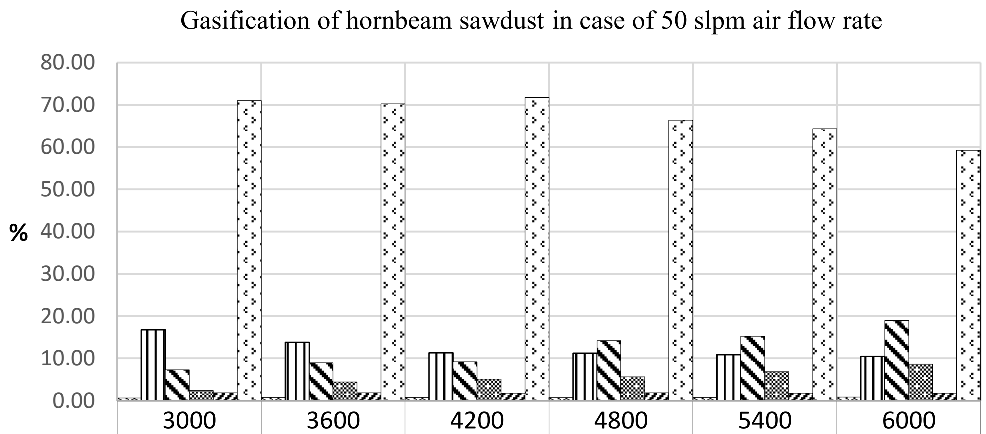

	3000	3600	4200	4800	5400	6000
O2	0.68	0.77	0.81	0.69	0.83	0.88
CO2	16.79	13.80	11.34	11.28	10.89	10.49
CO	7.33	8.97	9.23	14.2	15.27	18.95
H2	2.35	4.43	5.12	5.63	6.87	8.65
CH4	1.87	1.83	1.81	1.83	1.8	1.81
N2	70.97	70.19	71.69	66.37	64.34	59.22

Figure 5.16 The produced syngas fractions for the gasification of hornbeam sawdust (HSD) in case of 50 sL/min air flow rate.

In Figure 5.17, the syngas content distribution as percentage is given in case of gasification of hornbeam sawdust (HSD) at 75 sL/min air flow rate and power levels between 3 kW – 6 kW. Similar trend is observed as in 50 sL/min air flow rate. The O_2 in syngas stays in level of 1 % in all power levels. The CO_2 gradually reduces by increment of power from 21.32 % at 3 kW to 12.49 % at 6 kW. On the other hand, the CO and H_2 go up from 5.40 % to 12.21 % and 2.2 % to 7.17 % respectively by increasing power from 3 kW to 6 kW. The CH_4 remains almost constant in the level of 2.1 % in all power cases. The remainder of syngas, N_2 reduces by increasing power from 68.08 % to 64.95 %.

The gasification results are shown in case of gasification of hornbeam sawdust (HSD) at 100 sL/min air flow rate and power levels between 3 kW – 6 kW in Figure 5.18. The results are as follows. The O_2 in syngas increases from 1.2 % to 1.34 % by increasing plasma power. Unlike the CO_2 gradually decreases from 22.3 % to 16.42 % by increasing power from 3 kW to 6 kW, the CO and H_2 increase from 4.71 % to 9.61 % and from 1.94 % to 6.83 % respectively by increasing power from 3 kW to 6 kW.

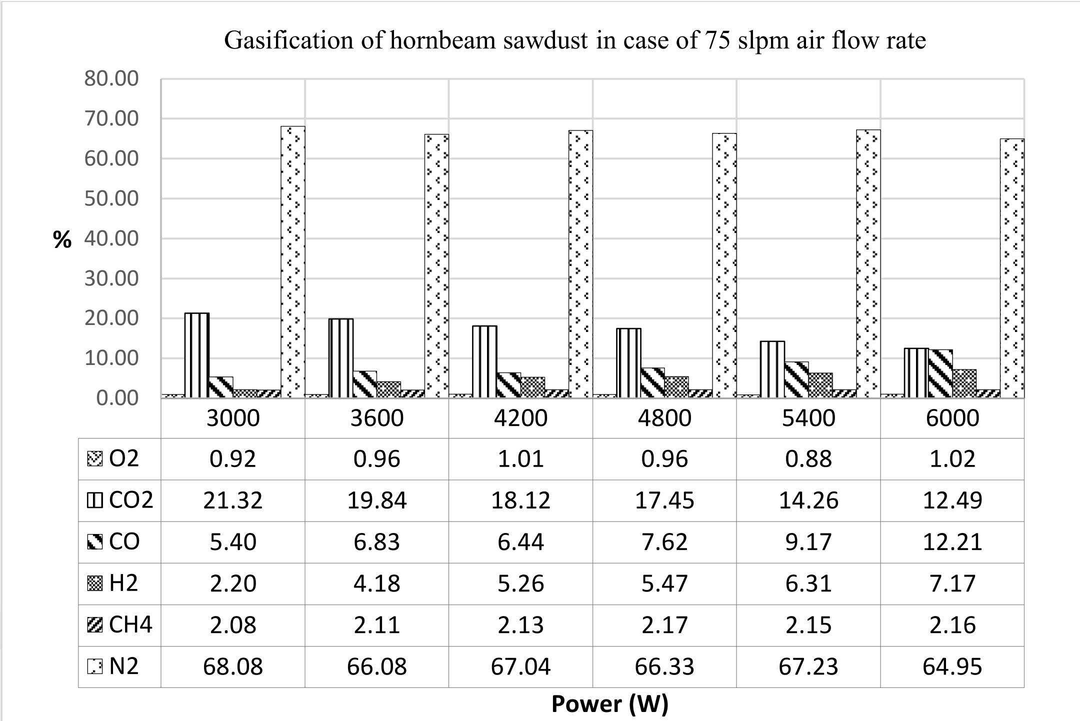

	3000	3600	4200	4800	5400	6000
O2	0.92	0.96	1.01	0.96	0.88	1.02
CO2	21.32	19.84	18.12	17.45	14.26	12.49
CO	5.40	6.83	6.44	7.62	9.17	12.21
H2	2.20	4.18	5.26	5.47	6.31	7.17
CH4	2.08	2.11	2.13	2.17	2.15	2.16
N2	68.08	66.08	67.04	66.33	67.23	64.95

Figure 5.17 The produced syngas fractions for the gasification of hornbeam sawdust (HSD) in case of 75 sL/min air flow rate

The CH_4 reduces from 2.33 % to 2.19 % by increasing the plasma power. The remainder of syngas considered as N_2 that reduces by increasing power from 67.52 % to 63.62 %.

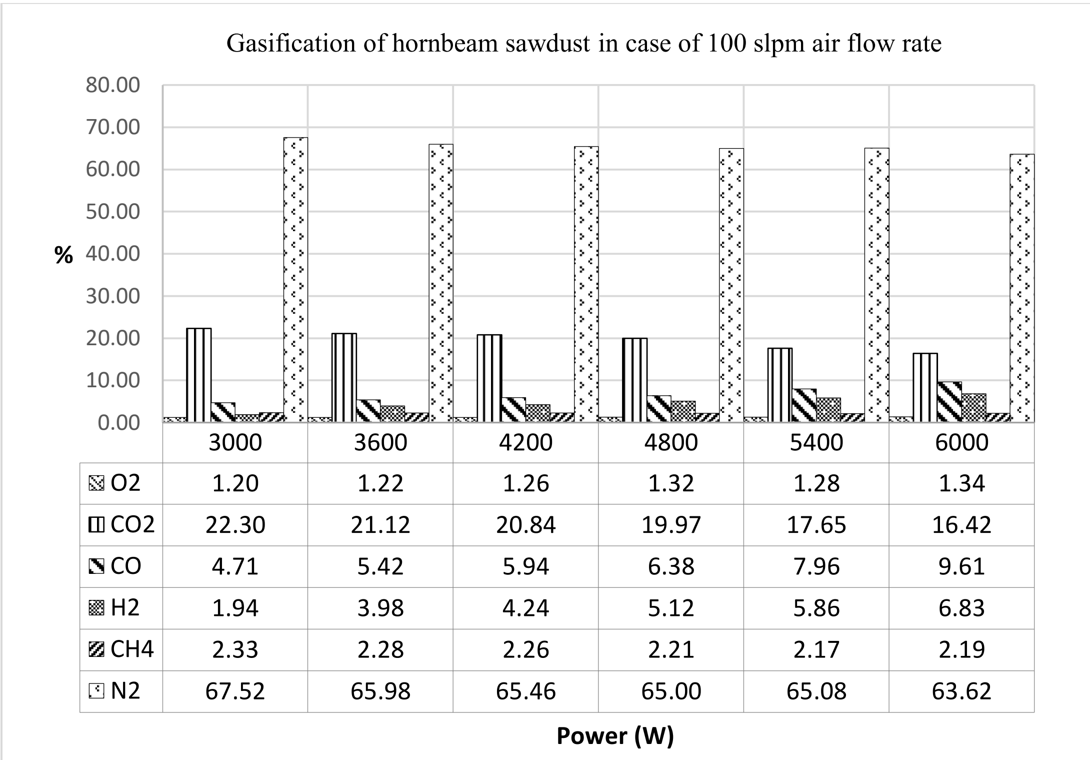

	3000	3600	4200	4800	5400	6000
O2	1.20	1.22	1.26	1.32	1.28	1.34
CO2	22.30	21.12	20.84	19.97	17.65	16.42
CO	4.71	5.42	5.94	6.38	7.96	9.61
H2	1.94	3.98	4.24	5.12	5.86	6.83
CH4	2.33	2.28	2.26	2.21	2.17	2.19
N2	67.52	65.98	65.46	65.00	65.08	63.62

Figure 5.18 The produced syngas percentages for the gasification of hornbeam sawdust (HSD) in case of 100 sL/min air flow rate

The air flow rate on syngas fraction has essential importance when the results compared for 50, 75 and 100 sL/min air flow rate. The increase in flow rate has a reverse effect on CO percentage. The CO decreases from 18.95 % to 9.61 % by increasing air flow rate from 50 sL/min to 100 sL/min at 6 kW power. Likewise, H_2 percentage reduces by increasing flow rate. It is 8.65 % for 50 sL/min air flow rate, 7.17 % for 75 sL/min air flow rate and 6.83 % for 100 sL/min air flow rate for 6 kW power. However, the CO_2 increases from 10.49 % to 16.42 %, the CH_4 increases from 1.81 % to 2.19 % and the O_2 increases from 0.88 % to 1.34 % by increasing flow rate from 50 to 100 sL/min air flow rate at 6 kW power. The N_2 in syngas mixture fluctuates between 59.22 % and 64.95 % by increasing flow rate from 50 to 100sL/min air flow rate at 6 kW power. Syngas fractions change with similar way by increasing the flow rate in different power levels.

5.5 Gasification of Pine tree Sawdust

The variation of temperature and the distribution of produced syngas content for the gasification of pine tree sawdust are analyzed in this section. The temperature variation is investigated by changing the power level between 3 kW-6 kW in case of 50 sL/min, 75 sL/min and 100sL/min air flow rate. Then the distribution of syngas content is examined by changing the power level between 3 kW-6 kW in case of 50 sL/min, 75 sL/min and 100 sL/min air flow rate.

The variation of temperature by change of power is presented in case of 50 sL/min air flow rate feeding and initially 250 gr pine tree sawdust dosing to the reactor in Figure 5.19. The closest thermocouple to plasma flame which is located at y/h=0.28 has highest temperature $T_{y/h=0.28} = 937°C$ at 3 kW power. The temperature at y/h=0.28 ($T_{y/h=0.28}$) goes up from 937 to 1447 °C by increasing the power from 3 kW to 6 kW. The temperature reduces progressively from region of the plasma flame to downward. The lowest measured temperature is 516 °C at the y/h=0.92 ($T_{y/h=0.92}$) and 3 kW power which is the outmost measurement point from the plasma flame. It rises from 516 to 818 °C by increasing the power from 3 kW to 6 kW. The average temperatures in the reactor (T_{syn}) are 765°C , 831°C, 917°C, 1019°C, 1105°C and 1169°C at 3 kW, 3.6 kW, 4.2 kW, 4.8 kW, 5.4 kW and 6 kW plasma power respectively. The average temperature increases by increasing plasma power. Because, the increment of plasma power increases the energy density in the reactor.

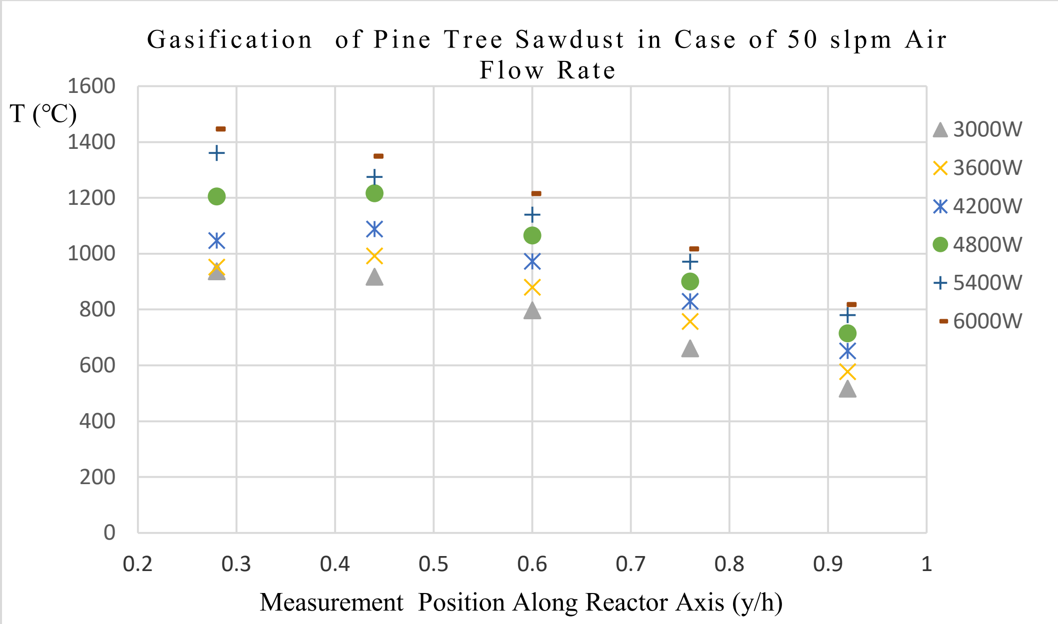

Figure 5.19 The temperature distribution for the gasification of pine tree sawdust (PSD) in case of 50 sL/min air flow rate

The temperature distribution by change of power is given in case of 75 sL/min air flow rate feeding and initially 250 gr pine tree sawdust dosed to the reactor in Figure 5.20. The closest thermocouple to the plasma flame which is located at y/h=0.28 has highest temperature $T_{y/h=0.28}$ = 902°C at 3 kW power. The temperature at y/h=0.28 ($T_{y/h=0.28}$) goes up from 902 to 1444 °C by increasing the power from 3 kW to 6 kW. The temperature declines gradually from region of the plasma flame to downward. The minimum temperature is measured 453 °C at the y/h=0.92 ($T_{y/h=0.92}$) and 3 kW power which is the farthest measurement point from the plasma flame. It rises up from 453 to 857 °C by increasing the power from 3 kW to 6 kW. The average temperatures in the reactor (T_{syn}) are 679°C, 798°C, 899°C, 990°C, 1068°C and 1152°C at 3 kW, 3.6 kW, 4.2 kW, 4.8 kW, 5.4 kW and 6 kW plasma power respectively. The average temperature increases by increasing plasma power. Because, the increment of plasma power rises the energy density in the reactor.

The average temperature goes down by increasing the air flow rate from 50 to 75 sL/min. Because, the increment of air flow rate lowers the energy density in reactor. However, the temperature in the reactor becomes more uniform. The difference of temperature between y/h=0.28 ($T_{y/h=0.28}$) and y/h= 0.92 ($T_{y/h=0.92}$) at 6 kW plasma power and 50 sL/min air flow rate is 628°C, while it is 586°C at 6 kW plasma power and 75 sL/min air flow rate.

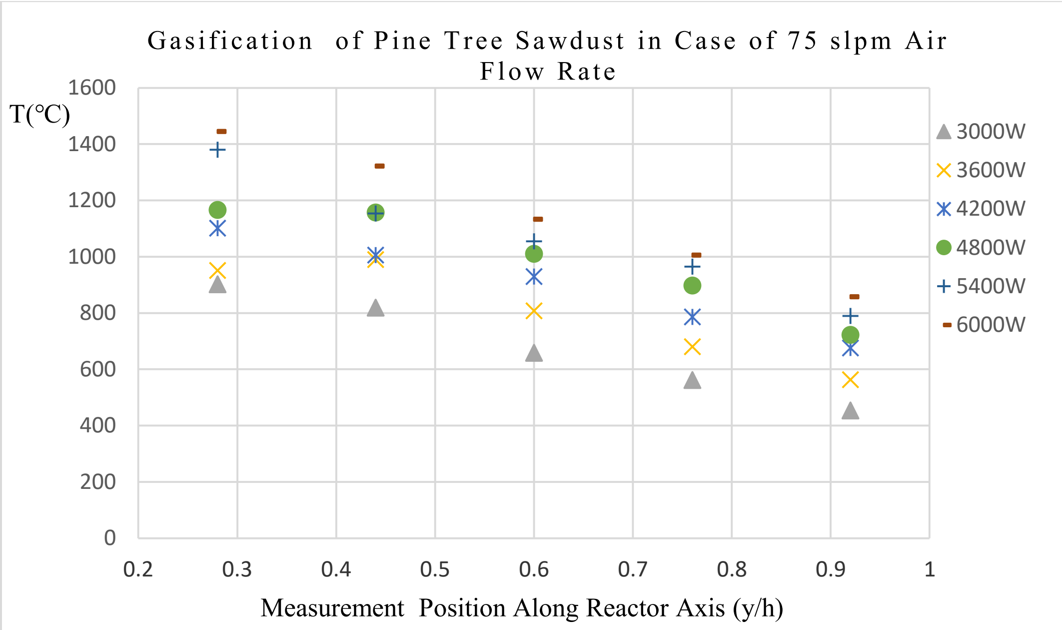

Figure 5.20 The temperature distribution for the gasification of pine tree sawdust (PSD) in case of 75 sL/min air flow rate

The variation of temperature by increasing power is given in in Figure 5.21 in case of 100 sL/min air flow rate and initially 250 gr pine tree sawdust dosed to the reactor. The nearest thermocouple to the plasma flame which is located at y/h=0.28 ($T_{y/h=0.28}$) has highest temperature $T_{y/h=0.28}$ = 855°C at 3 kW power. The temperature at y/h=0.28 ($T_{y/h=0.28}$) increases from 855 to 1434 °C by increasing the power from 3 kW to 6 kW. The temperature reduces gradually from region of the plasma flame to downward. The lowest temperature is measured 470 °C at the y/h=0.92 ($T_{y/h=0.92}$) and 3 kW power which is the most distant measurement point from the plasma flame. It goes up from 470 to 883 °C by increasing the power from 3 kW to 6 kW. The average temperatures in the reactor (T_{syn}) are 629°C , 756°C, 882°C, 929°C, 1026°C and 1127°C at 3 kW, 3.6 kW, 4.2 kW, 4.8 kW, 5.4 kW and 6 kW plasma power respectively. The average temperature goes up by increasing plasma power. Because, the increment of plasma power rises the energy density in the reactor.

The average temperature (T_{syn}) reduces by increasing the flow rate from 75 to 100 sL/min too. Because, the increment of air flow rate reduces the energy density in reactor. The temperature in the reactor at 100 sL/min air flow rate varied less than in case of 75 sL/min air flow rate. The variation of temperature between y/h=0.28 ($T_{y/h=0.28}$) and y/h= 0.92 ($T_{y/h=0.92}$) is 586°C at 6 kW plasma power and 75 sL/min air flow rate, while it is 550°C at 6 kW plasma power and 100 sL/min air flow rate.

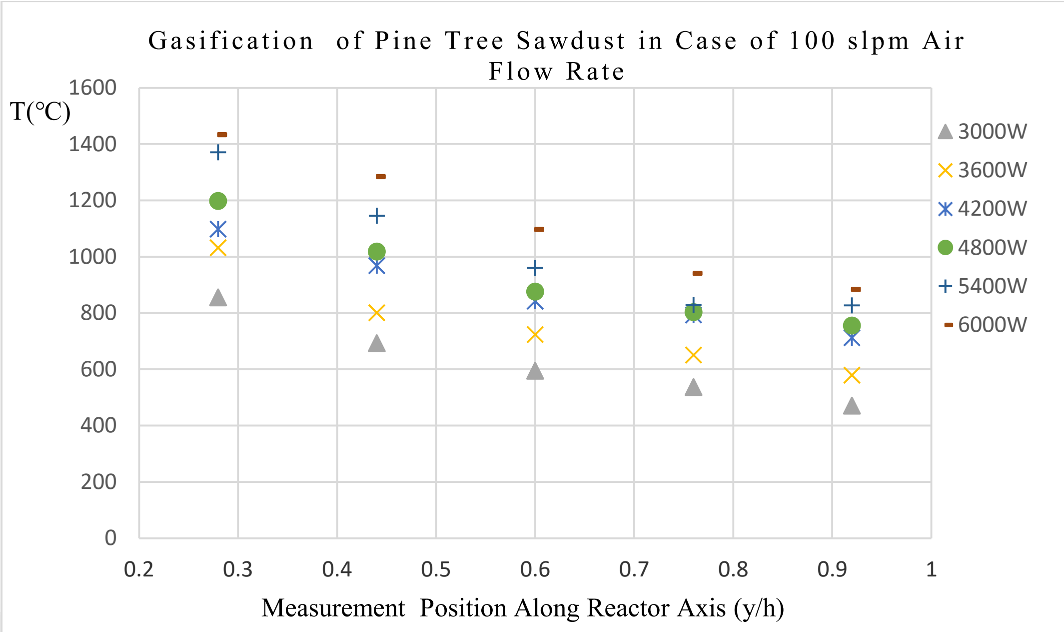

Figure 5.21 The temperature distribution for the gasification of pine tree sawdust (PSD) in case of 100 sL/min air flow rate

The distribution of syngas content by changing power is shown in Figure 5.22 in case of gasification of pine tree sawdust (PSD) at 50 sL/min air flow rate and power levels between 3-6 kW. As a result of the process, the O_2 in syngas stay below 0.91 % in all power levels.

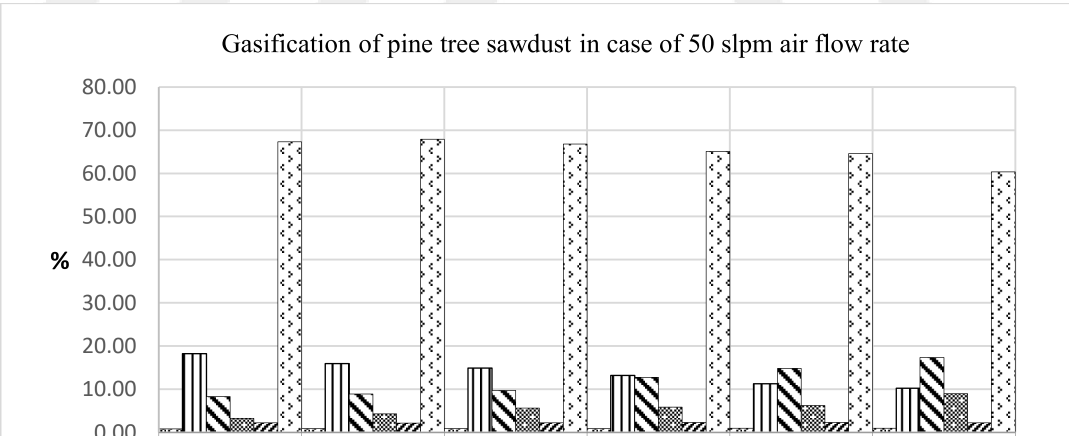

	3000	3600	4200	4800	5400	6000
O2	0.82	0.86	0.85	0.88	0.91	0.90
CO2	18.20	15.91	14.87	13.19	11.27	10.22
CO	8.30	8.88	9.69	12.7	14.82	17.35
H2	3.20	4.30	5.6	5.84	6.21	8.98
CH4	2.17	2.13	2.21	2.28	2.25	2.23
N2	67.31	67.92	66.78	65.11	64.54	60.33

Power (W)

Figure 5.22 The produced syngas percentages for the gasification of pine tree sawdust (PSD) in case of 50 sL/min air flow rate

The CO_2 gradually goes down by increasing power from 18.20 % at 3 kW to 10.22 % at 6 kW although the CO and H_2 rise by increasing the power. The CO and H_2 go up from 8.30 % to 17.35 % and from 3.2 % to 8.98 % respectively by increasing power from 3 kW to 6 kW. The CH_4 varies between 2.13 % and 2.28 %. The remainder of the syngas, N_2 reduces from 67.31 % to 60.33 % by increment of power from 3 kW to 6 kW.

The variation of syngas by power change in case of gasification of pine tree sawdust (PSD) at 75 sL/min air flow rate and power levels between 3-6 kW is presented in Figure 5.23. The O_2 in syngas remains in level of 1.08 % in all power levels. The CO_2 lessens by increasing power from 19.56 % at 3 kW to 16.01 % at 6 kW. However, the CO and H_2 rise by increasing the power. The CO and H_2 rise from 7.12 % to 17.21 % and from 3.18 % to 7.88 % respectively by increasing power from 3 kW to 6 kW. Likewise, the CH_4 slightly augments from 2.19 % to 2.29 % by increasing power from 3 kW to 6 kW. The rest of syngas, N_2 reduces from 67.11 % to 55.53 % by increasing power from 3 kW to 6 kW.

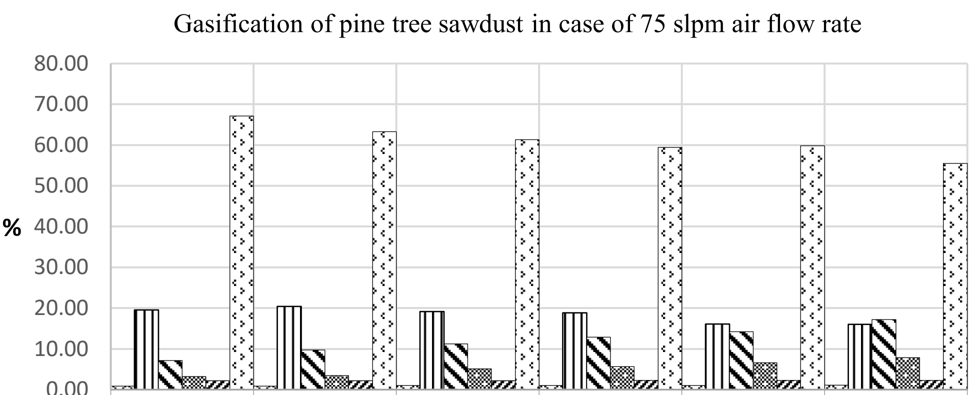

	3000	3600	4200	4800	5400	6000
O2	0.84	0.87	0.99	1.03	1.01	1.08
CO2	19.56	20.43	19.16	18.83	16.12	16.01
CO	7.12	9.73	11.21	12.84	14.17	17.21
H2	3.18	3.47	5.12	5.63	6.57	7.88
CH4	2.19	2.22	2.23	2.26	2.28	2.29
N2	67.11	63.28	61.29	59.41	59.85	55.53

Power (W)

Figure 5.23 The produced syngas percentages for the gasification of pine tree sawdust (PSD) in case of 75 sL/min air flow rate

The fraction of syngas variation depending on power between 3 kW – 6 kW in case of gasification of pine tree sawdust (PSD) at 100 sL/min air flow rate is given in Figure

5.24. The O_2 in syngas fluctuates between 0.89 % and 1.07 % in power levels between 3 kW – 6 kW. Despite the CO_2 gradually reduces by increment of power from 24.8 % at 3 kW to 14.23 % at 6 kW, the CO rises from 6.51 % to 10.96 % and H_2 increases from 2.18 % to 6.38 % by increasing power from 3 kW to 6 kW. The CH_4 goes down from 2.51 % to 2.31 % by increasing plasma power from 3 kW to 6 kW. The rest of syngas, N_2 fluctuates between 63.11 % and 66.59 % by increasing power from 3 kW to 6 kW.

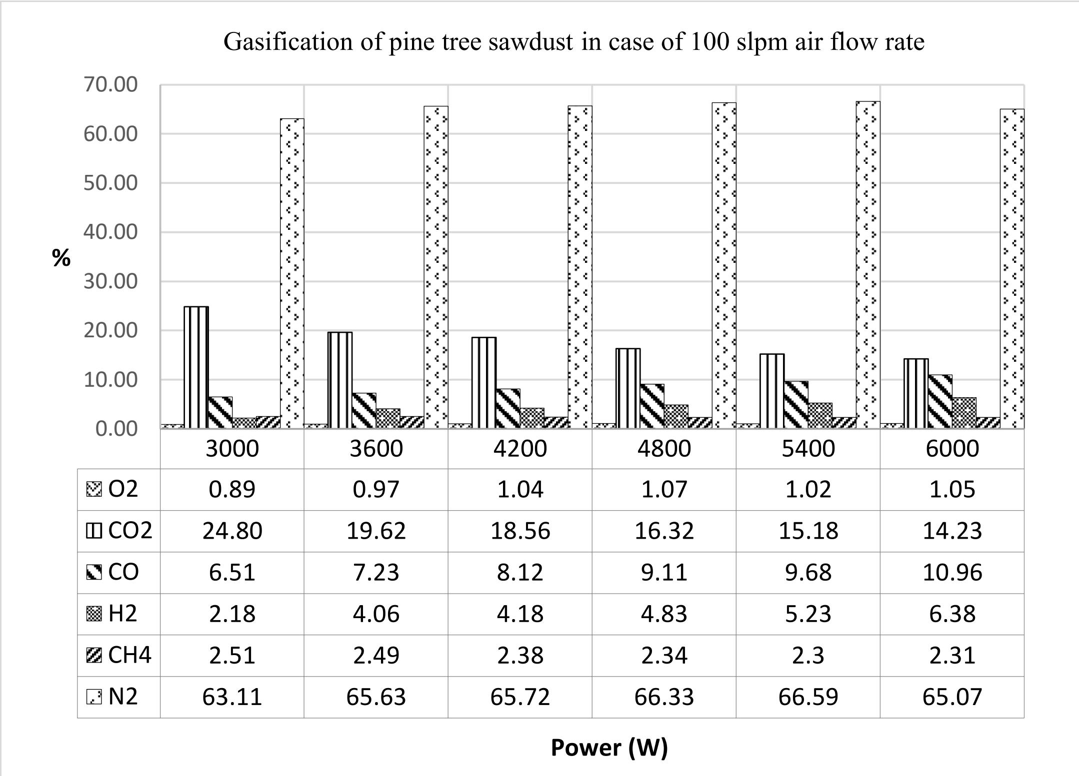

	3000	3600	4200	4800	5400	6000
O2	0.89	0.97	1.04	1.07	1.02	1.05
CO2	24.80	19.62	18.56	16.32	15.18	14.23
CO	6.51	7.23	8.12	9.11	9.68	10.96
H2	2.18	4.06	4.18	4.83	5.23	6.38
CH4	2.51	2.49	2.38	2.34	2.3	2.31
N2	63.11	65.63	65.72	66.33	66.59	65.07

Figure 5.24 The produced syngas percentages for the gasification of pine tree sawdust (PSD) in case of 100 sL/min air flow rate

Also, the air flow rate effects the syngas content distribution. The effect of air flow rate on syngas content is investigated by comparing the syngas content distribution at 50, 75 and 100 sL/min flow rate in case of gasification of pine tree sawdust (PSD) at varied power level from 3 kW to 6 kW. Increasing of flow rate has a reverse effect on CO which goes down from 17.35 % to 10.96 % by increasing flow rate from 50 sL/min to 100 sL/min at 6 kW power. Likewise, H_2 lowers by increasing flow rate. It diminishes from 8.98 % to 6.38 % by raising the air flow rate from 50 sL/min, to 100 sL/min for 6 kW power. Meanwhile, the CO_2 fluctuates between 10.22 % and 16.01 % by increasing flow rate from 50 to 100 sL/min at 6 kW power. Similarly, the O_2 in syngas mixture fluctuates between 0.9 % and 1.08 % by increasing flow rate from 50 sL/min to 100 sL/min at 6 kW power. The CH_4 slightly rises from 2.23 % to 2.31 % by increasing flow rate from 50 to 100 sL/min at 6 kW power. The N_2 in syngas mixture fluctuates between 55.53 % and 60.33 % by increasing air flow rate from 50 to 100 sL/min at 6 kW power. Syngas fractions change with similar way by increasing the flow rate in different power levels.

5.6 Gasification of Russian Coal

The temperature in the gasifier and the syngas content distribution depending on power and flow rate for the gasification of Russian coal are given in this section. The temperature distributions in gasifier are examined by changing the power level between 3 kW-6 kW in case of 50 sL/min, 75 sL/min and 100sL/min air flow rate. Then the syngas contents are examined by changing the power level between 3 kW-6 kW in case of 50 sL/min, 75 sL/min and 100 sL/min air flow rate.

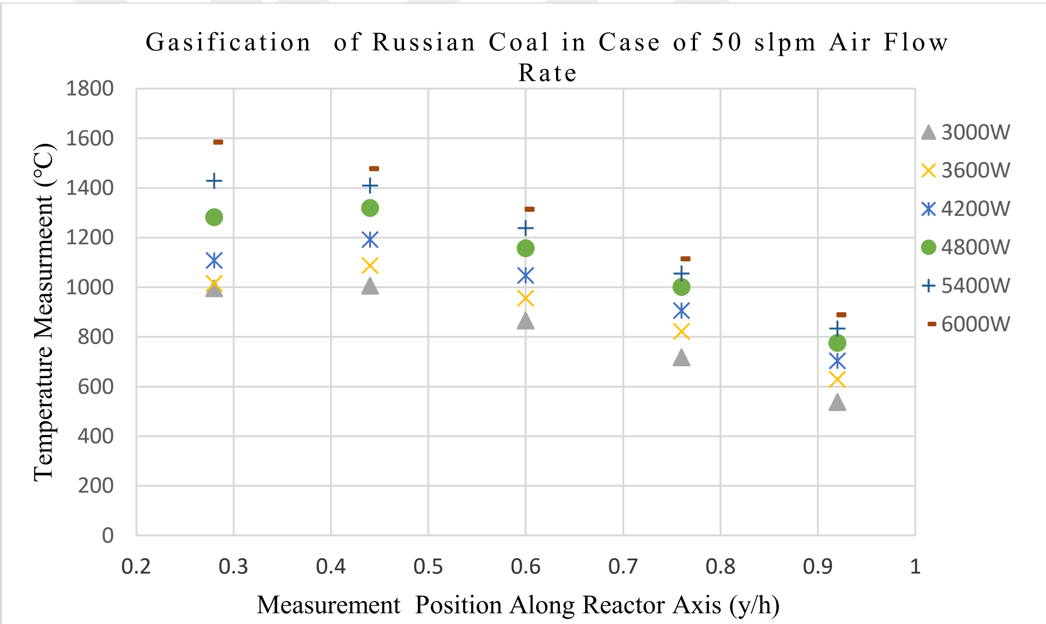

Figure 5.25 The temperature distribution for the gasification of Russian coal (CR) in case of 50 sL/min air flow rate

The temperature distribution depending on power level in case of 50 sL/min air flow rate input and initially 250 gr Russian coal (CR) dosed to the reactor are presented in Figure 5.25. The closest thermocouple to the plasma flame which is located at y/h=0.28 has highest temperature $T_{y/h=0.28} = 997°C$ at 3 kW power. The temperature at y/h=0.28 ($T_{y/h=0.28}$) rises from 997 °C to 1585 °C by increasing the power from 3 kW to 6 kW. The temperature reduces gradually from region of the plasma flame to downward. The lowest temperature is measured 538°C at the y/h=0.92 ($T_{y/h=0.92}$) and

3 kW power which is the most distant measurement point from the plasma flame. It rises from 538 to 889 °C by increasing the power from 3 kW to 6 kW. The average temperatures in the reactor (T_{syn}) are 825°C , 902°C, 992°C, 1107°C, 1193°C and 1276°C at 3 kW, 3.6 kW, 4.2 kW, 4.8 kW,5.4 kW and 6 kW plasma power respectively. The average temperature increases by increasing plasma power. Because, the increment of plasma power increases the energy density in the reactor.

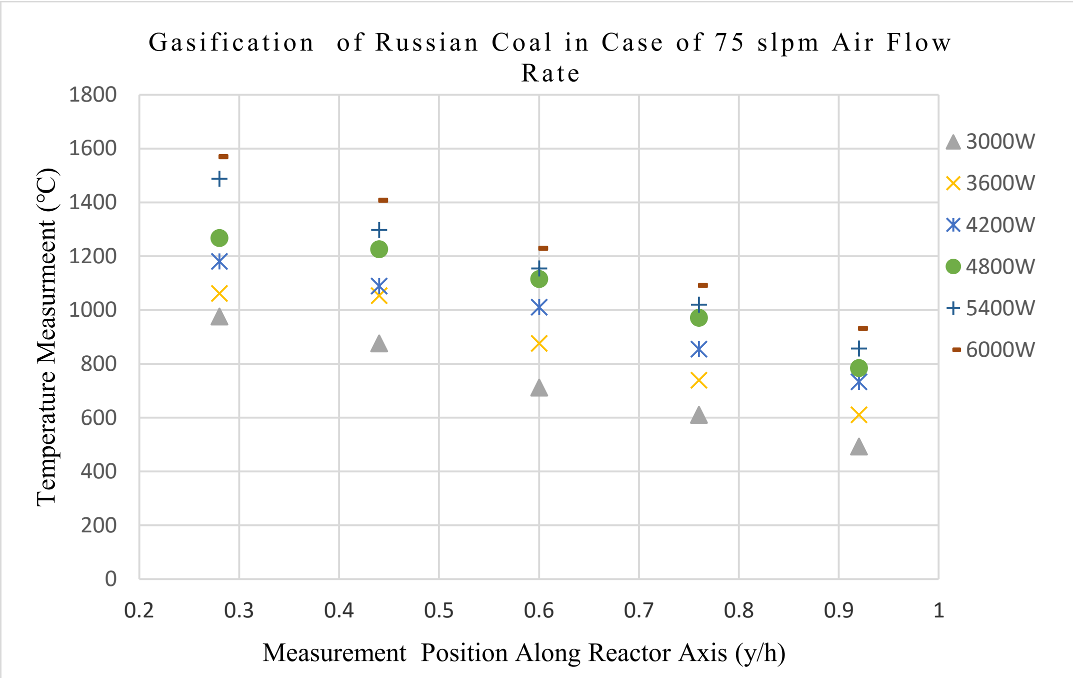

Figure 5.26 The temperature distribution for the gasification of Russian coal (CR) in case of 75 sL/min air flow rate

The temperature distribution in case of 75 sL/min air flow rate input and initially 250 gr Russian coal dosed to the reactor is given at varied power levels in Figure 5.26. The closest thermocouple to the plasma flame which is located at y/h=0.28 has highest temperature $T_{y/h=0.28}$ = 976°C at 3 kW power. The temperature at y/h=0.28 ($T_{y/h=0.28}$) goes up from 976°C to 1570°C by increasing the power from 3 kW to 6 kW. The temperature goes down gradually from region of the plasma flame to downward. The minimum measured temperature is 493 °C at the y/h=0.92 ($T_{y/h=0.92}$) and 3 kW power which is the outmost measurement point from the plasma flame. It goes up from 493 to 931 °C by increasing the power from 3 kW to 6 kW. The average temperatures in the reactor (T_{syn}) are 733°C, 868°C, 973°C, 1073°C, 1163°C and 1246°C at 3 kW, 3.6 kW, 4.2 kW, 4.8 kW, 5.4 kW and 6 kW plasma power respectively. The average temperature increases by increasing plasma power. Because, the increment of plasma power rises the energy density in the reactor.

The magnitude of the average temperature lowers by increasing the air flow rate from 50 to 75 sL/min. Because, the increment of air flow rate lowers the energy density in reactor. However, the temperature gradient in the reactor reduces. The difference of temperature at point y/h=0.28 ($T_{y/h=0.28}$) and y/h= 0.92 ($T_{y/h=0.92}$) at 6 kW plasma power and 50 sL/min air flow rate is 695°C, while it is 638°C at 6 kW plasma power and 75 sL/min air flow rate.

The variation of temperature by changing power in gasifier depending on power in case of 100 sL/min air flow rate input and initially 250 gr Russian coal (CR) dosed to the reactor is shown in Figure 5.27. The closest thermocouple to the plasma flame which is located at y/h=0.28 has highest temperature $T_{y/h=0.28} = 915°C$ at 3 kW power. The temperature at y/h=0.28 ($T_{y/h=0.28}$) goes up from 915 °C to 1547 °C by increasing the power from 3 kW to 6 kW. The temperature reduces gradually from region of the plasma flame to downward. The lowest temperature is measured 482 °C at the y/h=0.92 ($T_{y/h=0.92}$) and 3 kW power which is the farthest measurement point from the plasma flame. It varies from 482 to 930 °C by increasing the power from 3 kW to 6 kW. The average temperatures in the reactor (T_{syn}) are 660°C , 798°C, 921°C, 980°C, 1091°C and 1203°C at 3 kW, 3.6 kW, 4.2 kW, 4.8 kW, 5.4 kW and 6 kW plasma power respectively. The average temperature goes up by increasing plasma power. Because, the increment of plasma power rises the energy density in the reactor.

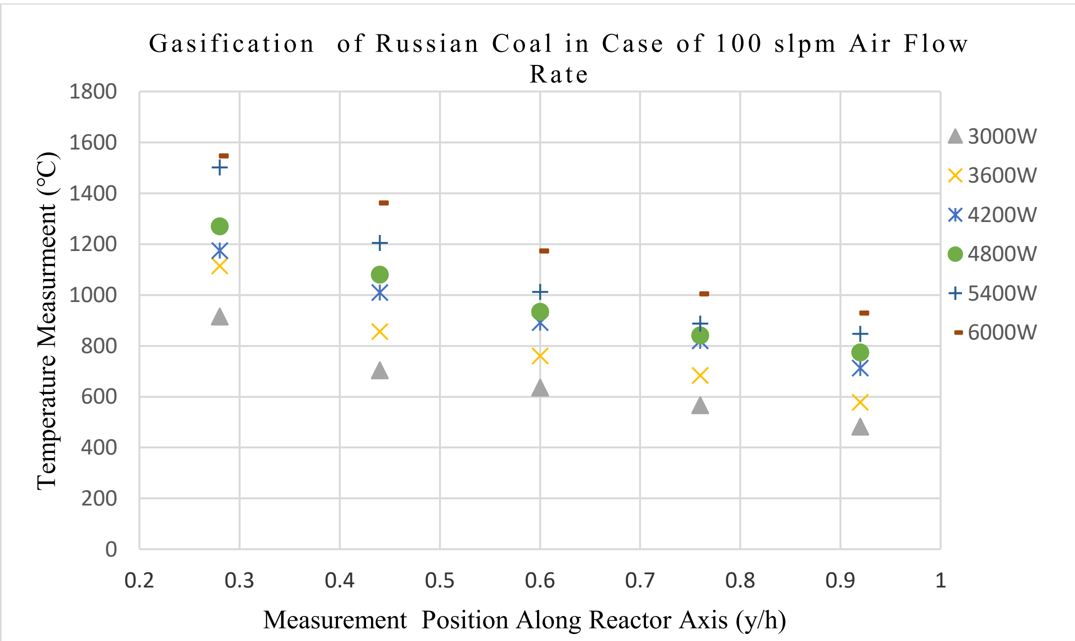

Figure 5.27 The temperature distribution for the gasification of Russian coal (CR) in case of 100 sL/min air flow rate

The magnitude of the temperature reduces by increasing the flow rate from 75 to 100 sL/min too. Because, the increment of air flow rate reduces the energy density in reactor. The temperature in the reactor at 100 sL/min air flow rate becomes slightly more uniform when it is compared with 75 sL/min air flow rate. The variation of temperature at point y/h=0.28 ($T_{y/h=0.28}$) and y/h= 0.92 ($T_{y/h=0.92}$) at 6 kW plasma power and 75 sL/min air flow rate is 638℃, while it is 617℃ at 6 kW plasma power and 100 sL/min air flow rate.

The content of syngas is presented in case of gasification of Russian coal (CR) at 50 sL/min air flow rate and power levels between 3 kW and 6 kW in Figure 5.28. The CO_2 is gradually reduces by increasing power from 28.62 % at 3 kW to 23.32 % at 6 kW. Also, The CH_4 goes down from 1.38 % to 1.04 % by increment of power from 3 kW to 6 kW. In contrast to that, The O_2 in syngas rise from 2.38 % at 3 kW to 2.67 % at 6 kW. Similarly, the CO in syngas mixture rises from 45.04 % to 48.03 % and H_2 rises from 1.68 % to 2.08 % by increasing power from 3 kW to 6 kW. The remainder of syngas, N_2 rises by increasing power from 20.9 % to 22.86 % by increasing power from 3 kW to 6 kW.

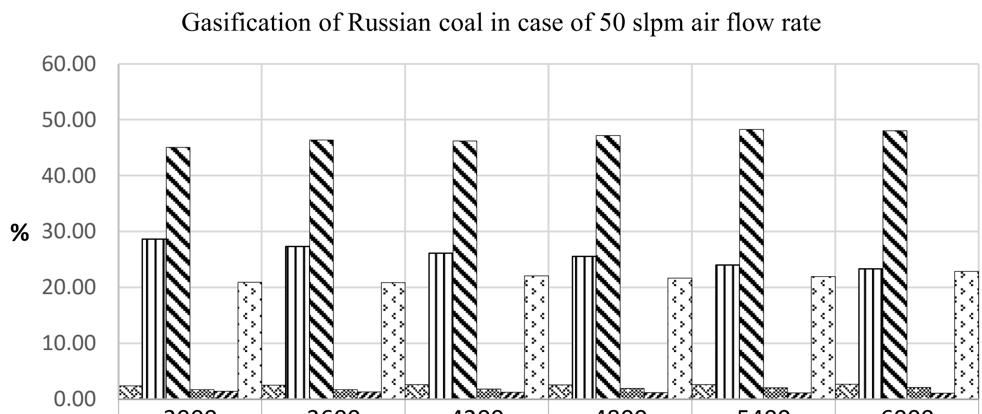

	3000	3600	4200	4800	5400	6000
O2	2.38	2.47	2.6	2.54	2.62	2.67
CO2	28.62	27.32	26.13	25.56	24.02	23.32
CO	45.04	46.38	46.21	47.16	48.28	48.03
H2	1.68	1.71	1.82	1.94	2.02	2.08
CH4	1.38	1.27	1.21	1.15	1.11	1.04
N2	20.90	20.85	22.03	21.65	21.95	22.86

Power (W)

Figure 5.28 The produced syngas percentages for the gasification of Russian coal (CR) in case of 50 sL/min air flow rate

The fraction of syngas mixture components are given in case of gasification of Russian coal (CR) at 75 sL/min air flow rate and power levels between 3 kW – 6 kW in Figure 5.29. The O_2 in syngas fluctuates between 3.16 % and 3.36 % in power levels between 3 kW – 6 kW. Despite the CO_2 slightly lowers by increasing power from 33.06 % at 3 kW to 30.12 % at 6 kW, the CO and H_2 rise from 42.14 % to 47.08 % and from 1.62 % to 2.03 % respectively by increasing power from 3 kW to 6 kW. On the other hand, the CH_4 reduces from 1.43 % to 1.29 % by increasing power from 3 kW to 6 kW. The rest of the syngas mixture, N_2 reduces from 18.54 % to 16.15 % by increment of power from 3 kW to 6 kW.

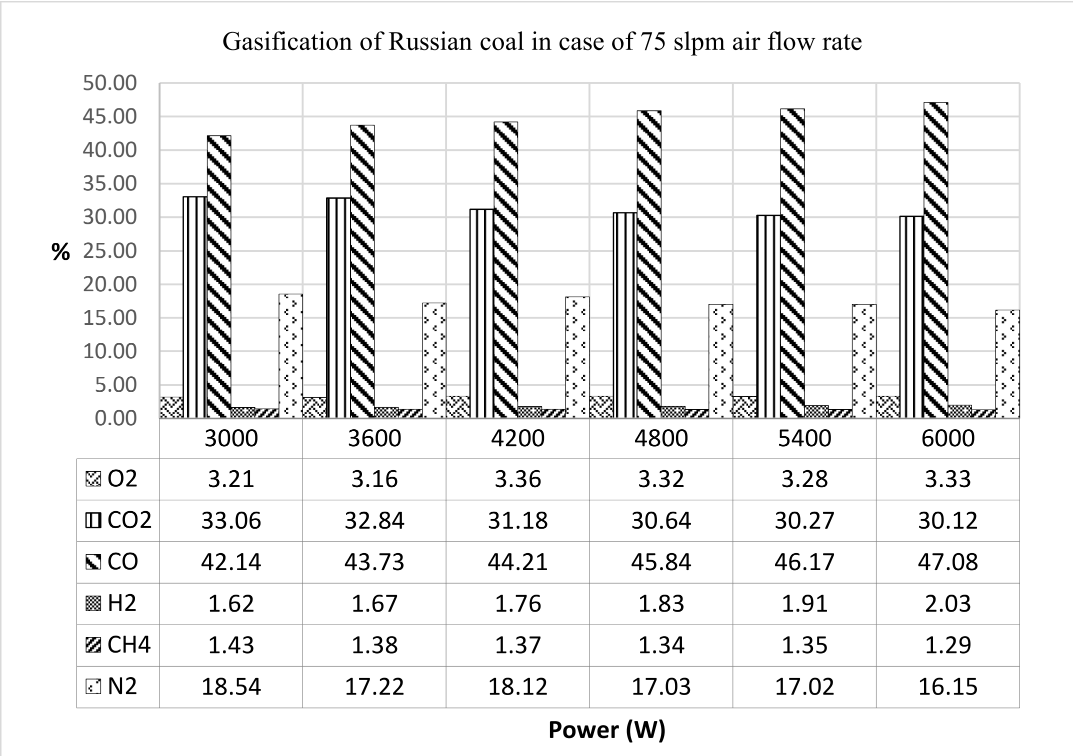

	3000	3600	4200	4800	5400	6000
O2	3.21	3.16	3.36	3.32	3.28	3.33
CO2	33.06	32.84	31.18	30.64	30.27	30.12
CO	42.14	43.73	44.21	45.84	46.17	47.08
H2	1.62	1.67	1.76	1.83	1.91	2.03
CH4	1.43	1.38	1.37	1.34	1.35	1.29
N2	18.54	17.22	18.12	17.03	17.02	16.15

Figure 5.29 The produced syngas percentages for the gasification of Russian coal (CR) in case of 75 sL/min air flow rate

The variation of content of syngas mixture depending on power between 3 kW – 6 kW is shown in Figure 5.30 in case of gasification of Russian coal (CR) at 100 sL/min air flow rate. The O_2 in syngas gently rises from 5.12 % to 5.4 % by changing power from 3 kW to 6 kW. Also, the CO and H_2 go up from 38.6 % to 42.02 % and from 1.13 % to 1.46 % respectively by increasing power from 3 kW to 6 kW. On the other hand, the CO_2 gradually goes down by increasing power from 36.24 % at 3 kW to 32.16 % at 6 kW. Likewise, The CH_4 lowers from 1.58 % to 1.36 % by increasing power from 3 kW to 6 kW. The remainder of syngas mixture, N_2 fluctuates between 16.46 % and 17.60 % in power levels between 3 kW and 6 kW.

The cases at 50, 75 and 100 sL/min air flow rate in case of gasification of Russian coal (CR) at varied power level from 3 kW to 6 kW is compared to reveal the effects of air flow rate on syngas conversion. The increase in flow rate has a reverse effect on CO. It lowers from 48.03 % to 42.02 % by increasing flow rate from 50 sL/min to 100 sL/min at 6 kW power. Likewise, H_2 diminishes from 2.08 % to 1.46 % by raising the flow rate from 50 sL/min, to 100 sL/min for 6 kW power. Meanwhile, the CO_2 in syngas rises from 23.32 % to 32.16 % by increasing flow rate from 50 to 100 sL/min at 6 kW power. Also, the CH_4 and O_2 in syngas mixture rise from 1.04 % to 1.36 % and from 2.67 % to 5.4 % respectively by increasing flow rate from 50 to 100 sL/min at 6 kW power. The N_2 in syngas mixture fluctuates between 16.15 % and 22.86 % by increasing flow rate from 50 to 100 sL/min at 6 kW power. Syngas fractions change with similar way by increasing the flow rate in different power levels.

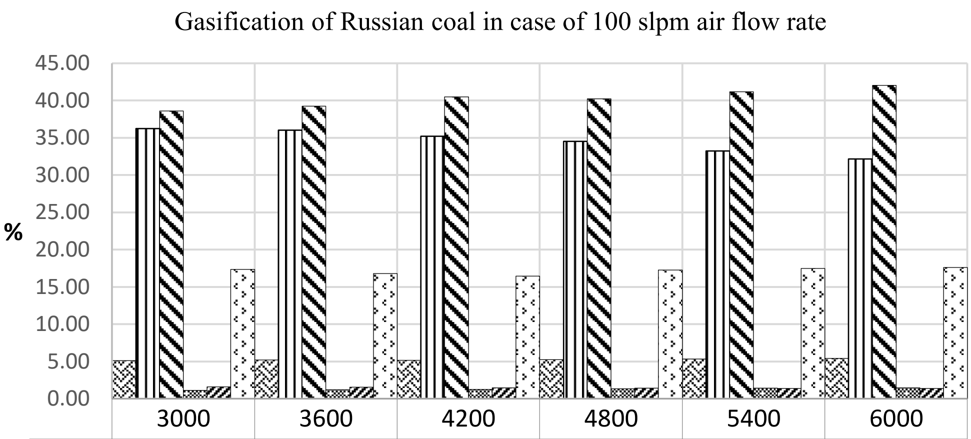

	3000	3600	4200	4800	5400	6000
O2	5.12	5.21	5.16	5.24	5.31	5.40
CO2	36.24	36.01	35.18	34.53	33.22	32.16
CO	38.60	39.21	40.48	40.22	41.18	42.02
H2	1.13	1.21	1.27	1.33	1.42	1.46
CH4	1.58	1.56	1.45	1.42	1.38	1.36
N2	17.33	16.80	16.46	17.26	17.49	17.60

Power (W)

Figure 5.30 The produced syngas percentages for the gasification of Russian coal (CR) in case of 100 sL/min air flow rate

When the gasification of Russian coal (CR) compared with the gasification of sawdust, the following results can deduce from the comparison. The CO and CO_2 content in syngas increase essentially because of the coal include higher amount of Carbon (Table 3). On the other hand, the CH_4 and H_2 decreased dramatically. The reason of it is the coal include less Hydrogen (Table 3) when it is compared with sawdust. The produced syngas content is directly proportional with the content of fuel.

5.7 Gasification of South African Coal

The temperature distribution and the produced syngas percentages for the gasification of South African coal (CSA) are investigated in this section. The temperature variations are examined by changing the power level between 3 kW-6 kW and 50 sL/min - 100 sL/min air flow rate. After that, the syngas content distributions are studied by changing the power level between 3 kW-6 kW in case of 50 sL/min, 75 sL/min and 100 sL/min air flow rate.

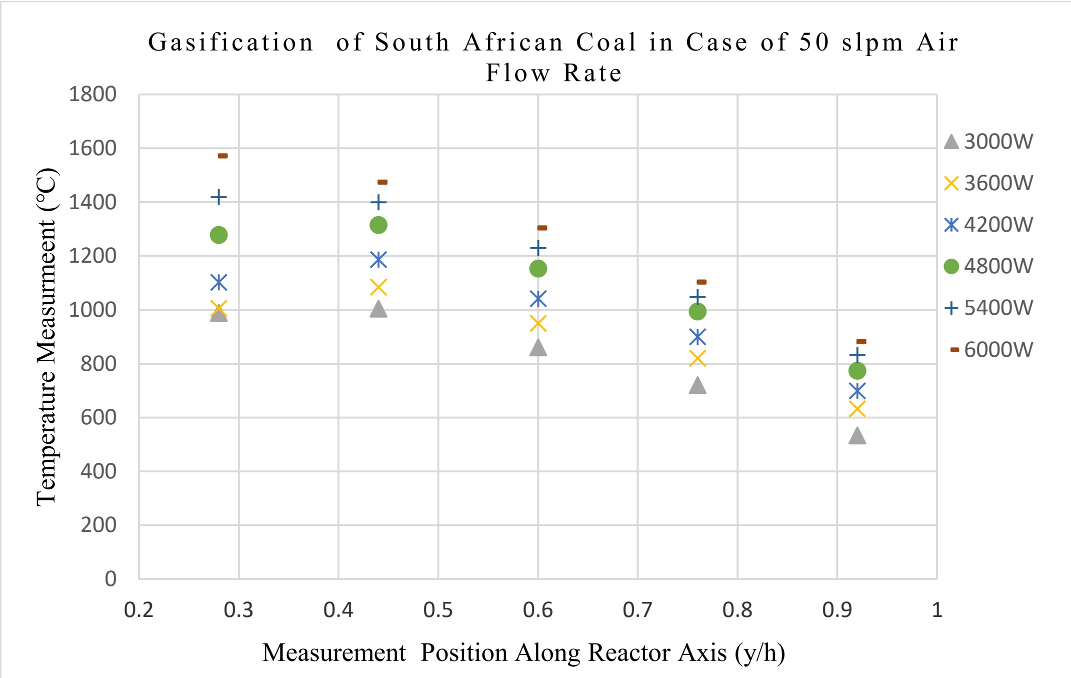

Figure 5.31 The temperature distribution for the gasification of South African coal (CSA) in case of 50 sL/min air flow rate

The temperature distribution depending on power in case of 50 sL/min air flow rate input and initially 250 gr South African coal (CSA) dosed to the reactor are presented in Figure 5.31. The nearest thermocouple to the plasma flame (at y/h=0.28) has highest temperature $T_{y/h=0.28} = 988°C$ at 3 kW power. The temperature at y/h=0.28 ($T_{y/h=0.28}$) rises from 988 °C to 1572 °C by increasing the power from 3 kW to 6 kW. The temperature in gasifier reduces gradually from region of the plasma flame to outmost. The lowest measured temperature is 533°C at the y/h=0.92 ($T_{y/h=0.92}$) and 3 kW power which is the farthest point from the plasma flame. It varies from 533 to 881 °C by increasing the power from 3 kW to 6 kW. The average temperatures in the reactor (T_{syn}) are 821°C , 898°C, 985°C, 1102°C, 1184°C and 1266°C at 3 kW, 3.6 kW, 4.2 kW, 4.8 kW, 5.4 kW and 6 kW plasma power respectively. The average temperature goes up by increasing plasma power. Because, the increment of plasma power rises the energy density in the reactor.

The temperature distribution at varied powers is given in Figure 5.32 in case of 75 sL/min air flow rate input and initially 250 gr South African coal (CSA) dosed to the reactor. The closest thermocouple to plasma flame which is located at y/h=0.28 has highest temperature $T_{y/h=0.28}$ = 973°C at 3 kW power. The temperature at y/h=0.28 ($T_{y/h=0.28}$) rises from 973 to 1557°C by increasing the power from 3 kW to 6 kW. The temperature goes down gradually from region of the plasma flame to downward. The minimum temperature is measured 489 °C at the y/h=0.92 ($T_{y/h=0.92}$) and 3 kW power which is the outmost point from the plasma flame. It changes from 489 to 925 °C by increasing the power from 3 kW to 6 kW. The average temperatures in the reactor (T_{syn}) are 728°C, 862°C, 963°C, 1062°C, 1146°C and 1234°C at 3 kW, 3.6 kW, 4.2 kW, 4.8 kW, 5.4 kW and 6 kW plasma power respectively. The average temperature increases by increasing plasma power. Because, the increment of plasma power increases the energy density in the reactor.

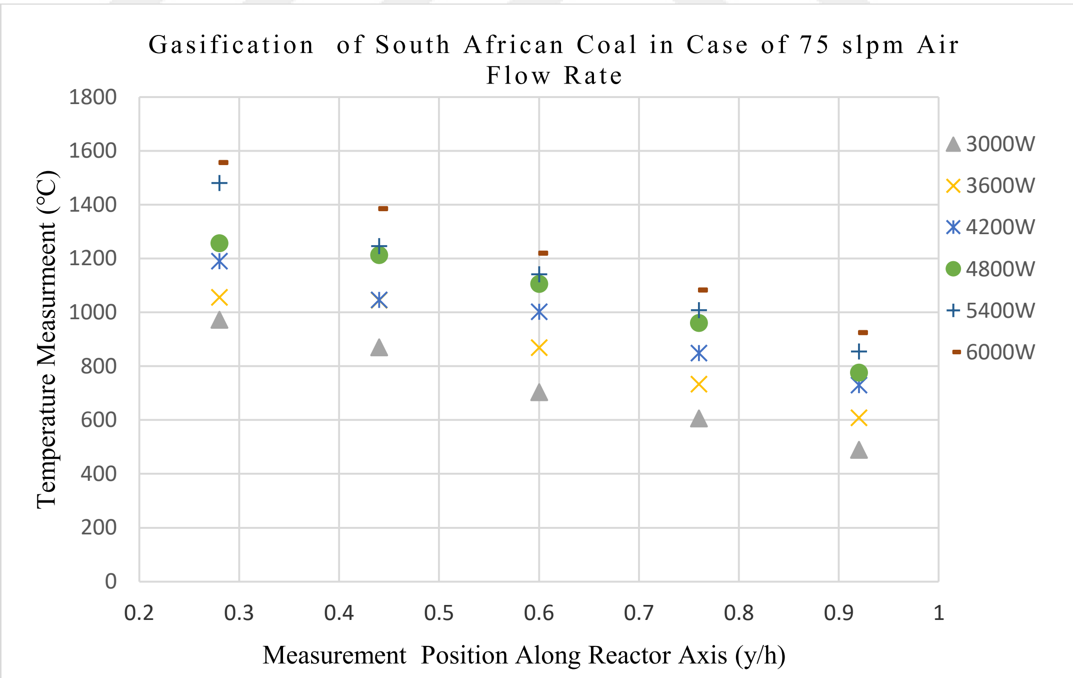

Figure 5.32 The temperature distribution for the gasification of South African coal (CSA) in case of 75 sL/min air flow rate

The average temperature goes down by increasing the flow rate from 50 to 75 sL/min. Because, the increment of air flow rate reduces the energy density in reactor. Meanwhile, the temperature in the reactor becomes more uniform. The difference of temperature at point y/h=0.28 ($T_{y/h=0.28}$) and y/h= 0.92 ($T_{y/h=0.92}$) at 6 kW and 50 sL/min is 690°C, while it is 631°C at 6 kW plasma power and 75 sL/min air flow rate.

The variation of temperature by changing power in case of 100 sL/min air flow rate input and initially 250 gr South African coal (CSA) dosed to the reactor is shown in Figure 5.33. The closest thermocouple to plasma flame which is located at y/h=0.28 has highest temperature $T_{y/h=0.28}$ = 908°C at 3 kW power. The temperature at this point goes up from 908 to 1534 °C by increasing the power from 3 kW to 6 kW. On the other hand, the temperature reduces gradually from region of the plasma flame to downward. The lowest measured temperature is 479 °C at the y/h=0.92 ($T_{y/h=0.92}$) and 3 kW power which is the outmost measurement point from the plasma flame. It varies from 479 to 918 °C by increasing the power from 3 kW to 6 kW. The average temperatures in the reactor (T_{syn}) are 658°C, 792°C, 914°C, 977°C, 1071°C and 1193°C at 3 kW, 3.6 kW, 4.2 kW, 4.8 kW, 5.4 kW and 6 kW plasma power respectively. The average temperature rises by increasing plasma power. Because, increasing plasma power rises the energy density in the reactor.

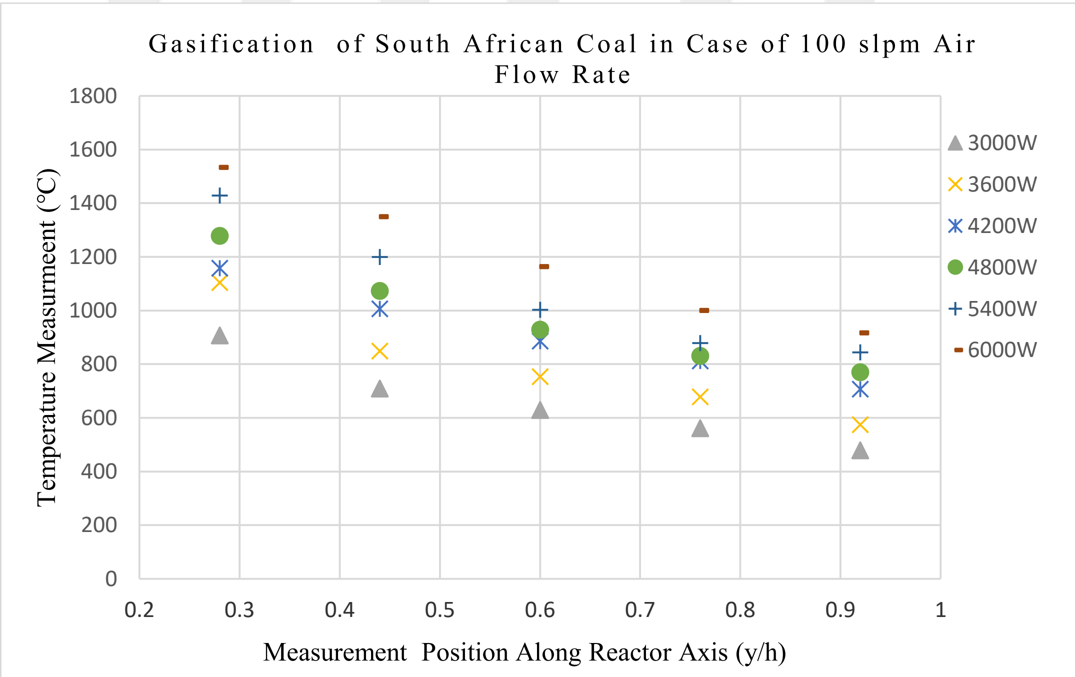

Figure 5.33 The temperature distribution for the gasification of South African coal (CSA) in case of 100 sL/min air flow rate

When the flow rate increase from 75 to 100 sL/min, the temperature in the gasifier reduces slightly. Because, the increment of air flow rate decreases the energy density in reactor. However, the temperature in the reactor at 100 sL/min air flow rate becomes slightly more uniform when it is compared with 75 sL/min air flow rate. The variation of temperature at point y/h=0.28 ($T_{y/h=0.28}$) and y/h= 0.92 ($T_{y/h=0.92}$) at 6 kW plasma power and 75 sL/min air flow rate is 631℃, while it is 616℃ at 6 kW plasma power and 100 sL/min air flow rate.

The syngas content distribution is given in case of gasification of South African coal (CSA) at 50 sL/min air flow rate and power levels between 3 kW - 6 kW in Figure 5.34. The CO_2 in syngas gradually goes down by increasing power from 25.47 % at 3 kW to 21.69 % at 6 kW. Also, The CH_4 reduces from 1.35 % to 1.01 % by increasing power from 3 kW to 6 kW. In contrast to that, The O_2 in syngas rises from 2.24 % at 3 kW to 2.56 % at 6 kW. Similarly, H_2 increases from 1.75 % to 2.18 % by increasing power from 3 kW to 6 kW. The CO in syngas mixture fluctuates between 38.67 %- 41.52 % by increasing power from 3 kW to 6 kW. Also, N_2 fluctuates between 30.01 %- 31.73 % by increasing power from 3 kW to 6 kW.

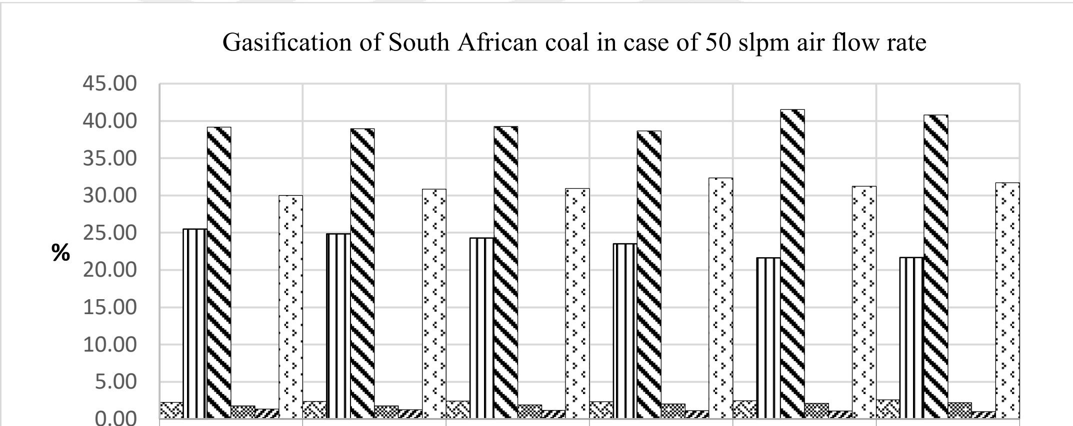

O2	2.24	2.35	2.42	2.31	2.44	2.56
CO2	25.47	24.86	24.30	23.52	21.62	21.69
CO	39.18	38.96	39.28	38.67	41.52	40.83
H2	1.75	1.76	1.89	2.04	2.10	2.18
CH4	1.35	1.23	1.19	1.10	1.09	1.01
N2	30.01	30.84	30.92	32.36	31.24	31.73

Figure 5.34 The produced syngas percentages for the gasification of South African coal (CSA) in case of 50 sL/min air flow rate

The syngas content distribution is shown in case of gasification of South African coal (CSA) at 75 sL/min air flow rate and power levels between 3 kW – 6 kW in Figure 5.35. The O_2 in syngas goes up from 2.92 % to 3.06 %, the CO_2 fluctuates in narrow range between 28.45 % and 31.20 %, the CO increases from 38.35 % to 42.84 %, H_2

increases from 1.81 % to 2.27 % and the CH_4 decreases from 1.37 % to 1.21 % by increasing power from 3 kW to 6 kW. The remainder of syngas, N_2 reduces from 24.8 % to 21.99 % by increasing power from 3 kW to 6 kW.

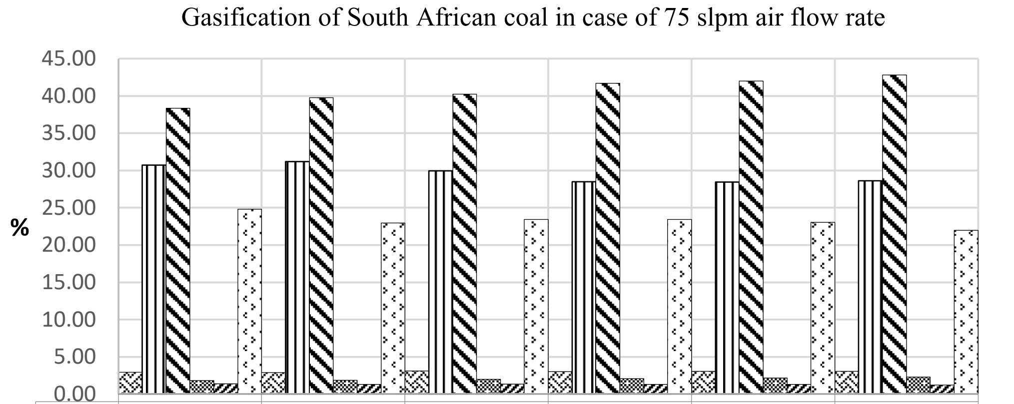

O2	2.92	2.88	3.09	3.02	3.05	3.06
CO2	30.75	31.20	29.93	28.50	28.45	28.61
CO	38.35	39.79	40.23	41.71	42.01	42.84
H2	1.81	1.87	1.97	2.05	2.14	2.27
CH4	1.37	1.31	1.34	1.30	1.28	1.21
N2	24.80	22.94	23.43	23.42	23.06	21.99

Figure 5.35 The produced syngas percentages for the gasification of South African coal (CSA) in case of 75 sL/min air flow rate

The syngas content distribution is presented in case of gasification of South African coal (CSA) at 100 sL/min air flow rate and power levels between 3 kW – 6 kW in Figure 5.36. The O_2 in syngas increases from 4.45 % to 4.91 % by changing power from 3 kW to 6 kW. Similarly, the CO goes up from 33.2 % to 38.24 % and H_2 rises from 1.73 % to 2.23 % by increasing power from 3 kW to 6 kW. On the other hand, the CO_2 gradually reduces by increasing power from 33.7 % at 3 kW to 29.91 % at 6 kW. Likewise, The CH_4 lowers from 1.37 % to 1.18 % by increasing power from 3 kW to 6 kW. The rest of the mixture, N_2 fluctuates between 25.54 % and 23.52 % in case of power levels between 3 kW and 6 kW.

The effects of air flow rate on syngas content distribution is revealed by comparing the results for 50, 75 and 100 sL/min flow rate in case of gasification of South African coal (CSA) at varied power level from 3 kW to 6 kW. The increase in flow rate has a reverse effect on CO. It goes down from 40.83 % to 38.24 % by increasing flow rate from 50 sL/min to 100 sL/min at 6 kW power. H_2 stays between 2.18 % and 2.27 % by raising the flow rate from 50 sL/min to 100 sL/min at 6 kW power.

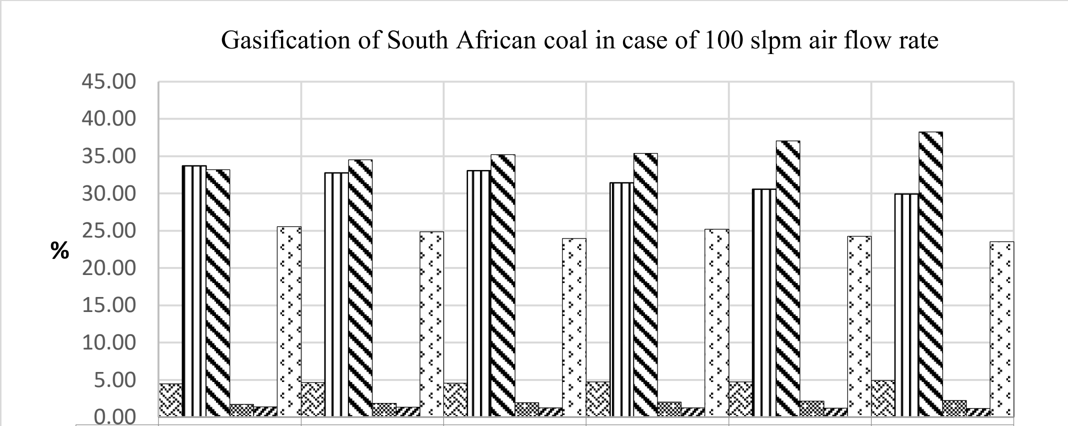

O2	4.45	4.64	4.54	4.72	4.73	4.91
CO2	33.70	32.77	33.07	31.42	30.56	29.91
CO	33.20	34.50	35.22	35.39	37.06	38.24
H2	1.73	1.85	1.94	2.03	2.17	2.23
CH4	1.37	1.36	1.26	1.24	1.20	1.18
N2	25.54	24.88	23.97	25.20	24.28	23.52

Power (W)

Figure 5.36 The produced syngas percentages for the gasification of South African coal (CSA) in case of 100 sL/min air flow rate

Meanwhile, the CO_2 in syngas rises from 21.69 % to 29.91 % by increasing flow rate from 50 to 100 sL/min at 6 kW power. Also, the CH_4 goes up from 1.01 % to 1.18 % by increasing flow rate from 50 to 100 sL/min at 6 kW power. The O_2 in syngas mixture rises from 2.56 % to 4.91 % by increasing flow rate from 50 to 100 sL/min at 6 kW power. The N_2 in syngas mixture fluctuates between 21.99 % and 31.73 % by increasing flow rate from 50 to 100 sL/min at 6 kW power. Syngas fraction change with similar way by increasing the flow rate in different power levels.

5.8 Gasification of Şırnak (Turkey) Coal (CTR)

The temperature distribution and the produced syngas content percentages for the gasification of Şırnak (Turkey) coal (CTR) are investigated in this section. The temperature distribution in gasifier are examined by changing the power level between 3 kW-6 kW in case of 50 sL/min, 75 sL/min and 100 sL/min air flow rate. Then the syngas content percentages are examined by changing the power level between 3 kW-6 kW in case of 50 sL/min, 75 sL/min and 100 sL/min air flow rate.

The temperature distributions for various power levels in case of 50 sL/min air flow rate input and initially 250 gr Şırnak (Turkey) coal (CTR) dosed to the reactor are presented in Figure 5.37. The closest thermocouple to the plasma flame which is located at y/h=0.28 has highest temperature $T_{y/h=0.28}$ = 972°C at 3 kW power. The temperature at y/h=0.28 ($T_{y/h=0.28}$) goes up from 972 °C to 1545 °C by increasing the power from 3 kW to 6 kW. Meanwhile, the temperature reduces gradually from region of the plasma flame to downward. The minimum temperature is 524°C at the y/h=0.92 ($T_{y/h=0.92}$) and 3 kW power which is the most distant measurement point from the plasma flame. It rises from 524 to 868 °C by increasing the power from 3 kW to 6 kW. The average temperatures in the reactor (T_{syn}) are 808°C, 884°C, 970°C, 1086°C, 1167°C and 1246°C at 3 kW, 3.6 kW, 4.2 kW, 4.8 kW, 5.4 kW and 6 kW plasma power respectively. The average temperature increases by increasing plasma power. Because, the increment of plasma power rises the energy density in the reactor.

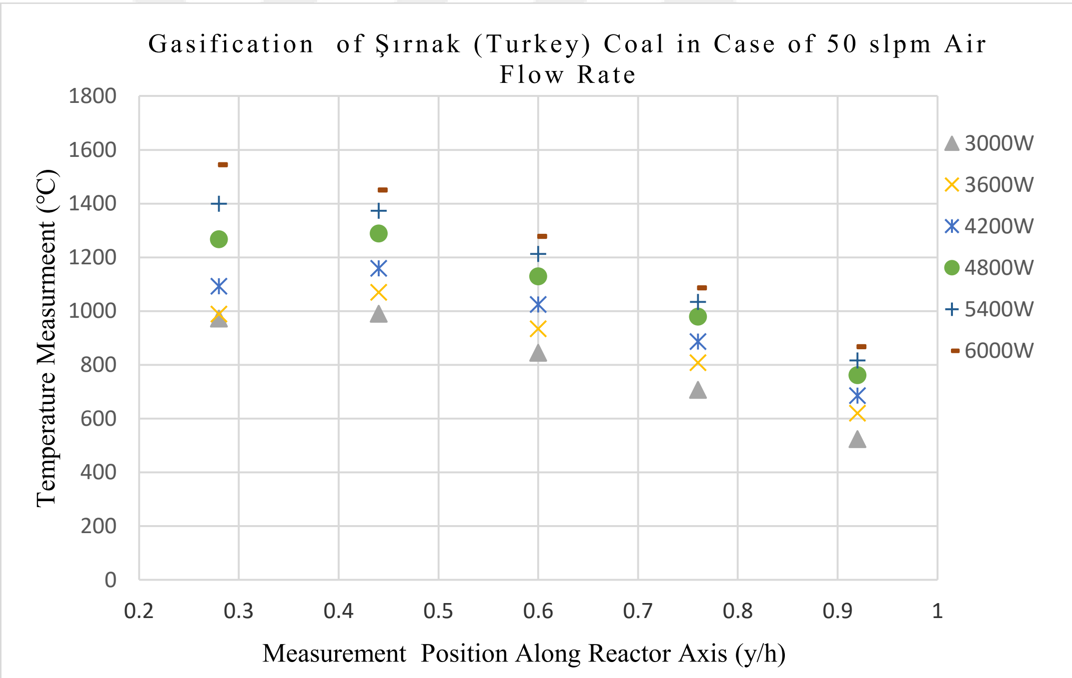

Figure 5.37 The temperature distribution for the gasification of Şırnak (Turkey) coal (CTR) in case of 50 sL/min air flow rate

The temperature distributions at power levels between 3kW and 6 kW are presented in Figure 5.38 in case of 75 sL/min air flow rate input and initially 250 gr Şırnak (Turkey) coal (CTR) dosed to the reactor. The nearest thermocouple to the plasma flame which is located at y/h=0.28 has highest temperature $T_{y/h=0.28}$ = 957°C at 3 kW power. The temperature at y/h=0.28 ($T_{y/h=0.28}$) rises from 957 to 1539°C by increasing the power from 3 kW to 6 kW. It goes down gradually from region of the plasma flame to downward. The lowest temperature is 480 °C at the y/h=0.92 ($T_{y/h=0.92}$) and 3 kW power which is the outmost measurement point from the plasma flame. It rises from 480 to 902 °C by increasing the power from 3 kW to 6 kW. The average temperatures in the reactor (T_{syn}) are 716°C, 844°C, 953°C, 1043°C, 1121°C and 1209°C at 3 kW, 3.6 kW, 4.2 kW, 4.8 kW, 5.4 kW and 6 kW plasma power respectively. The average temperature rises by increasing plasma power. Because, the increment of plasma power increases the energy density in the reactor.

The average temperature in gasifier reduces by increasing the flow rate from 50 to 75 sL/min. Because, the increment of air flow rate lowers the energy density in reactor. However, the temperature in the gasifier becomes more uniform when it is compared with 50 sL/min air flow rate. The gradient of temperature at point y/h=0.28 ($T_{y/h=0.28}$) and y/h= 0.92 ($T_{y/h=0.92}$) at 6 kW plasma power and 50 sL/min air flow rate is 677°C, while it is 638°C at 6 kW plasma power and 75 sL/min air flow rate.

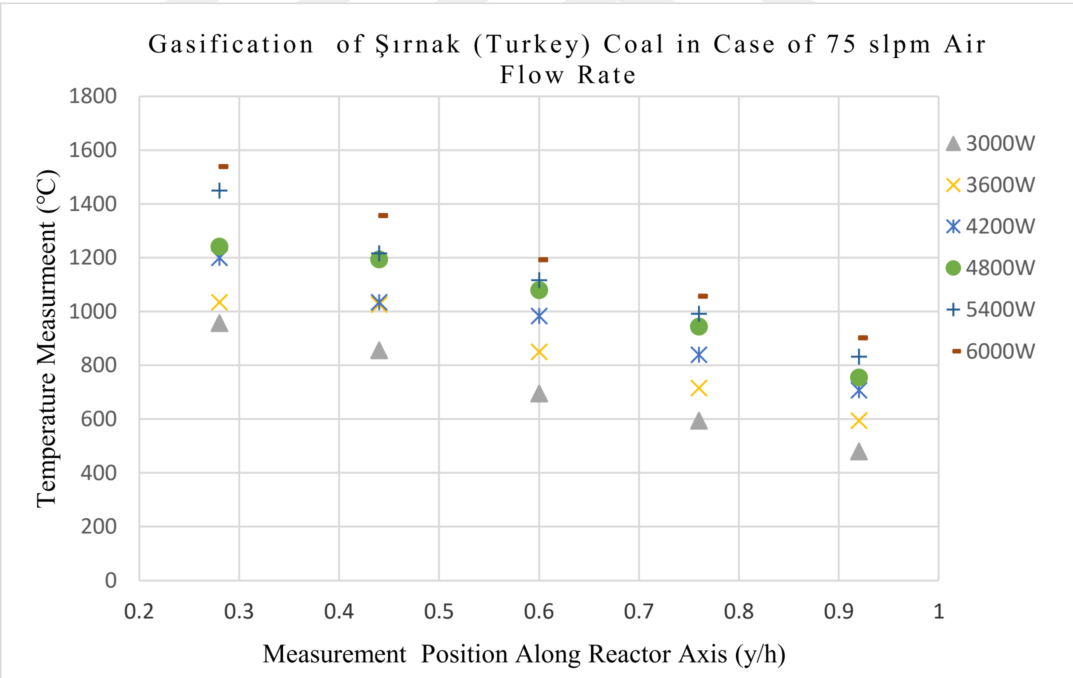

Figure 5.38 The temperature distribution for the gasification of Şırnak (Turkey) coal (CTR) in case of 75 sL/min air flow rate

The temperature distributions for various powers are presented in Figure 5.39, in case of 100 sL/min air flow rate input and initially 250 gr Şırnak (Turkey) coal (CTR) dosed to the reactor. The thermocouple which is located at y/h=0.28 (closest measurement point to plasma flame) has highest temperature $T_{y/h=0.28} = 885$°C at 3 kW power. The temperature at y/h=0.28 ($T_{y/h=0.28}$) rises from 885 to 1483 °C by increasing the power from 3 kW to 6 kW. It lowers gradually from region of the plasma flame to downward. The lowest temperature is 469 °C at the y/h=0.92 ($T_{y/h=0.92}$) and 3 kW power which is the furthest measurement point from the plasma flame. It rises from 469 to 887 °C by increasing the power from 3 kW to 6 kW. The average temperatures in the reactor (T_{syn}) are 641°C , 775°C, 891°C, 954°C, 1052°C and 1160°C at 3 kW, 3.6 kW, 4.2 kW, 4.8 kW, 5.4 kW and 6 kW plasma power respectively. The average temperature rises by increasing plasma power. Because, the increment of plasma power enhances the energy density in the reactor.

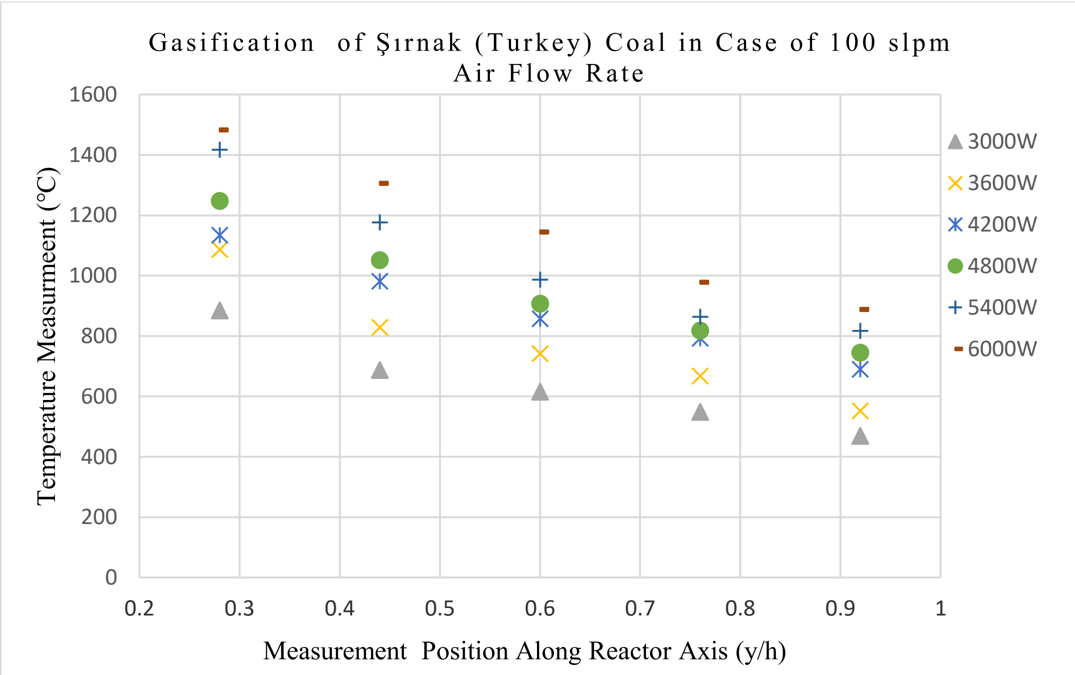

Figure 5.39 The temperature distribution for the gasification of Şırnak (Turkey) coal (CTR) in case of 100 sL/min air flow rate

The average temperature in gasifier goes down by increasing the flow rate from 75 to 100 sL/min. Because, the increment of air flow rate reduces the energy density in reactor. On the other hand, the temperature in the reactor at 100 sL/min air flow rate becomes more uniform when it is compared with 75 sL/min air flow rate. The variation of temperature at point y/h=0.28 ($T_{y/h=0.28}$) and y/h= 0.92 ($T_{y/h=0.92}$) at 6 kW plasma power and 75 sL/min air flow rate is 638°C, while it is 595°C at 6 kW plasma power and 100 sL/min air flow rate.

The syngas content distribution is presented in case of gasification of Şırnak (Turkey) coal (CTR) at 50 sL/min air flow rate and power levels between 3 kW -6 kW in Figure

5.40. The O_2 in syngas rises from 2.3 % to 2.59 %, the CO_2 goes down from 23.43 % to 19.95 %, the CO in syngas mixture fluctuates between 36.74 % and 37.78 %, H_2 rises from 1.54 % to 1.92 % and the CH_4 decreases from 1.57 % to 1.29 % by increasing power from 3 kW to 6 kW. The rest of the mixture, N_2 increases from 34.32 % to 37.50 % by increasing power from 3 kW to 6 kW.

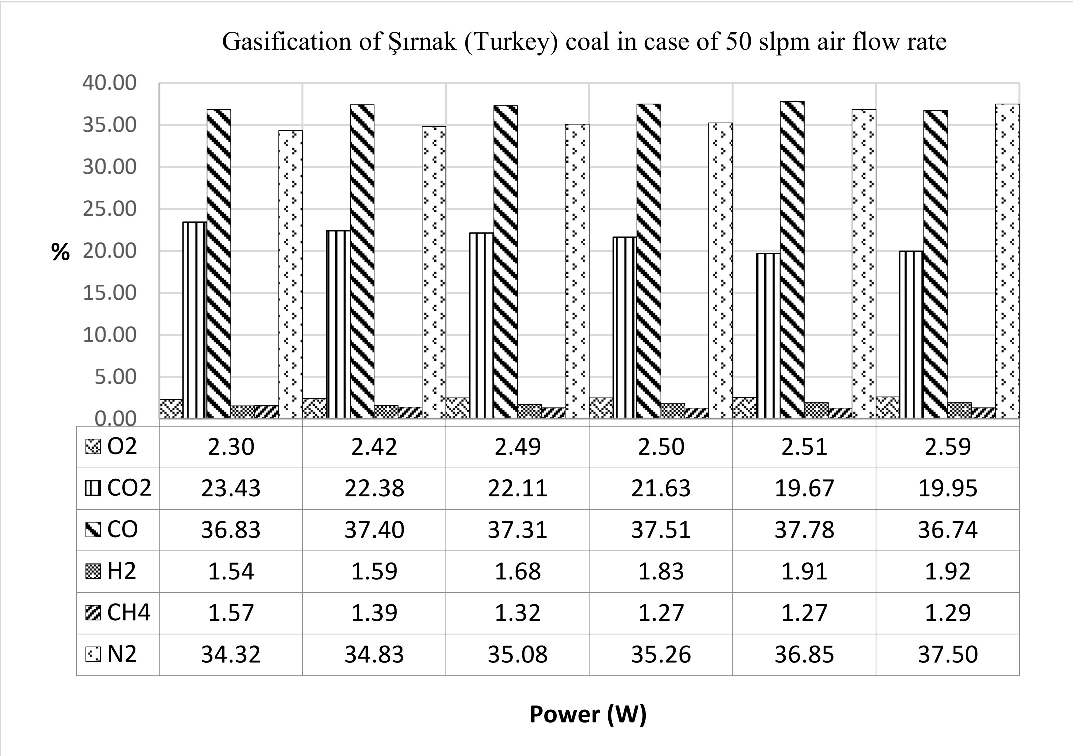

O2	2.30	2.42	2.49	2.50	2.51	2.59
CO2	23.43	22.38	22.11	21.63	19.67	19.95
CO	36.83	37.40	37.31	37.51	37.78	36.74
H2	1.54	1.59	1.68	1.83	1.91	1.92
CH4	1.57	1.39	1.32	1.27	1.27	1.29
N2	34.32	34.83	35.08	35.26	36.85	37.50

Figure 5.40 The produced syngas percentages for the gasification of Şırnak (Turkey) coal (CTR) in case of 50 sL/min air flow rate

The gasification results are shown in case of gasification of Şırnak (Turkey) coal (CTR) at 75 sL/min air flow rate and power levels between 3 kW – 6 kW in Figure 5.41. The O_2 in syngas rises from 3.11 % to 3.49 %, the CO_2 lowers from 28.59 % to 23.34 %, The CO fluctuates between 33.15 % and 34.41 %, H_2 rises from 1.58 % to 1.94 % and the CH_4 fluctuates between 1.52 % and 1.22 % by increasing power from 3 kW to 6 kW. The rest of the mixture, N_2 goes up from 32.04 % to 36.47 % by increasing power from 3 kW to 6 kW.

The fraction of syngas is given in case of gasification of Şırnak (Turkey) coal (CTR) at 100 sL/min air flow rate and power levels between 3 kW – 6 kW in Figure 5.42. The O_2 in syngas rises from 4.82 % to 5.59 %, the CO goes up from 26.52 % to 29.42 % and H_2 rises from 1.63 % to 1.96 % by increasing power from 3 kW to 6 kW. On the other hand, the CO_2 gradually reduces by increasing power from 34.31 % at 3 kW to 28.48 % at 6 kW. The CH_4 fluctuates between 1.55 % and 1.25 % by increasing power from 3 kW to 6 kW. The rest of the mixture, N_2 fluctuates between 30.14 % and 34.03 % in power levels between 3 kW and 6 kW.

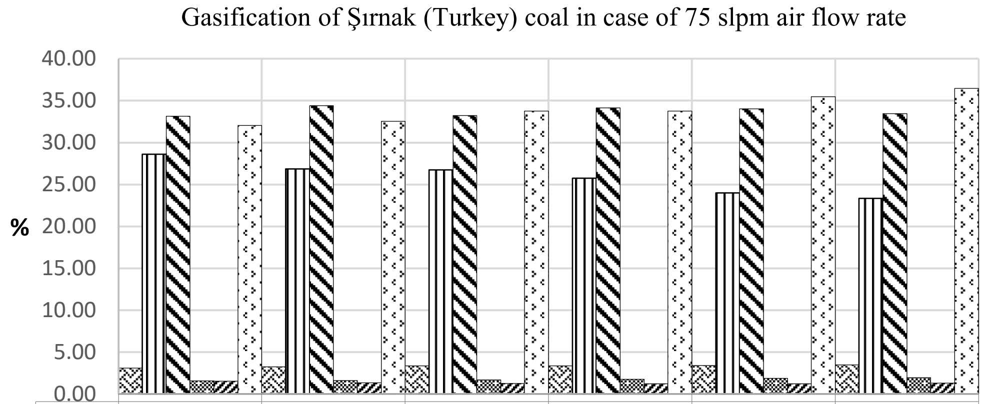

O2	3.11	3.26	3.36	3.37	3.39	3.49
CO2	28.59	26.85	26.76	25.74	24.00	23.34
CO	33.15	34.41	33.21	34.14	34.01	33.44
H2	1.58	1.60	1.67	1.78	1.89	1.94
CH4	1.52	1.34	1.25	1.22	1.23	1.32
N2	32.04	32.54	33.75	33.75	35.48	36.47

Figure 5.41 The produced syngas percentages for the gasification of Şırnak (Turkey) coal (CTR) in case of 75 sL/min air flow rate

The air flow rate effects the syngas content distribution essentially when the results compared for 50, 75 and 100 sL/min flow rate in case of gasification of Şırnak (Turkey) coal (CTR) for various powers from 3 kW to 6 kW.

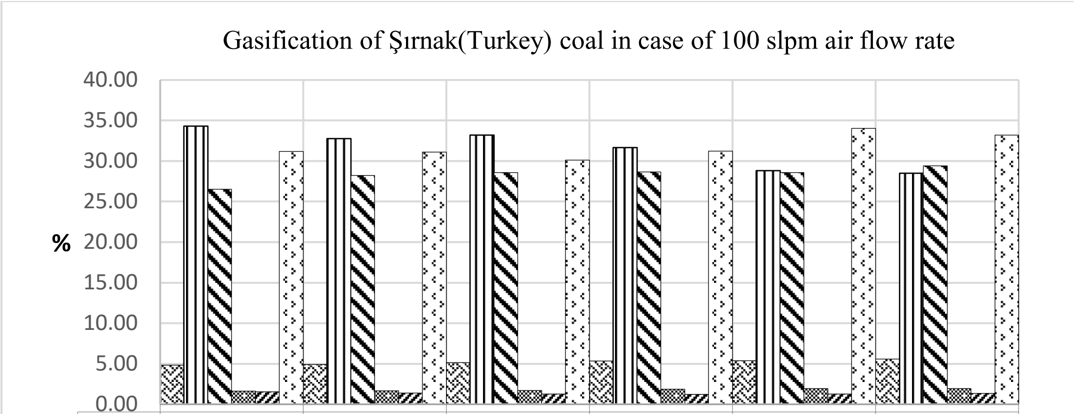

O2	4.82	4.89	5.14	5.32	5.39	5.59
CO2	34.31	32.76	33.18	31.67	28.80	28.48
CO	26.52	28.22	28.56	28.67	28.56	29.42
H2	1.63	1.67	1.70	1.85	1.95	1.96
CH4	1.55	1.38	1.28	1.25	1.26	1.35
N2	31.17	31.09	30.14	31.24	34.03	33.19

Figure 5.42 The produced syngas percentages for the gasification of Şırnak (Turkey) coal (CTR) in case of 100 sL/min air flow rate

The increment in flow rate has a reverse effect on CO. It goes down from 36.74 % to 29.42 % by increasing flow rate from 50 sL/min to 100 sL/min at 6 kW power. However, H_2 rises slightly from 1.92 % to 1.96 %, the CO_2 in syngas goes up from 19.95 % to 28.48 %, the CH_4 rises from 1.29 % to 1.35 % and the O_2 in syngas mixture rises from 2.59 % to 5.59 % by increasing flow rate from 50 to 100 sL/min at 6 kW power. The N_2 in syngas mixture reduces from 37.5 % to 33.19 % by increasing flow rate from 50 to 100 sL/min at 6 kW power. Syngas percentages change with similar way by increasing the flow rate in different power levels.

5.9 Gasification of Polyethylene (PP)

The temperature distribution in gasifier and the syngas mixture content for the gasification of Polyethylene (PP) are investigated in this section. The temperature variations are examined by changing the power level between 3 kW-6 kW in case of 50 sL/min, 75 sL/min and 100 sL/min air flow rate. Then the syngas content percentages are examined by changing the power level between 3 kW-6 kW in case of 50 sL/min, 75 sL/min and 100 sL/min air flow rate.

The temperature distribution in case of 50 sL/min air flow rate input and initially 250 gr Polyethylene (PP) dosed to the reactor is presented in Figure 5.43. The closest thermocouple to plasma flame which is located at y/h=0.28 has highest temperature $T_{y/h=0.28}$ = 956°C at 3 kW power. The temperature at y/h=0.28 ($T_{y/h=0.28}$) goes up from 956 °C to 1520 °C by increasing the power from 3 kW to 6 kW. The temperature lowers gradually from region of the plasma flame to downward. The lowest measured temperature is 516°C at the y/h=0.92 ($T_{y/h=0.92}$) and 3 kW power which is the outmost measurement point from the plasma flame. It varies from 516 to 847 °C by increasing the power from 3 kW to 6 kW. The average temperatures in the reactor (T_{syn}) are 793°C , 867°C, 949°C, 1070°C, 1147°C and 1218°C at 3 kW, 3.6 kW, 4.2 kW, 4.8 kW, 5.4 kW and 6 kW plasma power respectively. The average temperature goes up by increasing plasma power. Because, the increment of plasma power increases the energy density in the reactor.

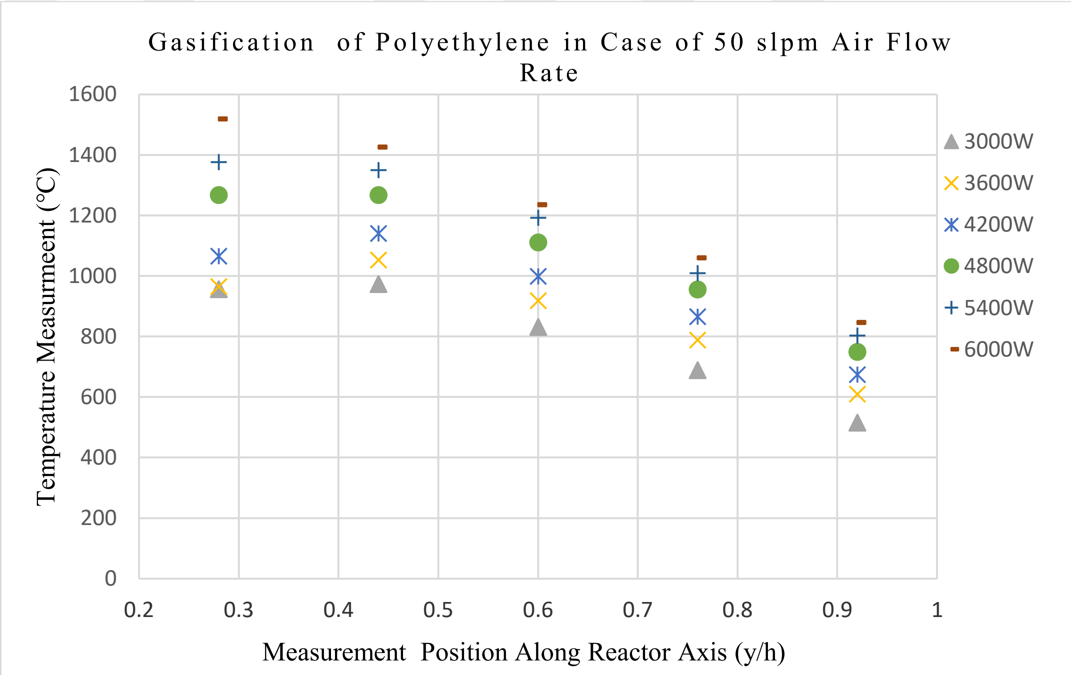

Figure 5.43 The temperature distribution for the gasification of Polyethylene (PP) in case of 50 sL/min air flow rate

The temperature distribution in case of 75 sL/min air flow rate input and initially 250 gr Polyethylene (PP) dosed to the reactor is given in Figure 5.44. The nearest thermocouple to plasma flame which is located at y/h=0.28 has highest temperature $T_{y/h=0.28}$ = 933°C at 3 kW power. The temperature at y/h=0.28 ($T_{y/h=0.28}$) rises from 933 to 1502°C by increasing the power from 3 kW to 6 kW. The temperature goes down gradually from region of the plasma flame to downward. The minimum temperature is 472 °C at the y/h=0.92 ($T_{y/h=0.92}$) and 3 kW power which is the farthest point from the plasma flame. It goes up from 472 to 887 °C by increasing the power from 3 kW to 6 kW. The average temperatures in the reactor (T_{syn}) are 700°C, 830°C, 935°C, 1024°C, 1101°C and 1183°C at 3 kW, 3.6 kW, 4.2 kW, 4.8 kW, 5.4 kW and 6 kW plasma power respectively. The average temperature rises by increasing plasma power. Because, the increment of plasma power enhances the energy density in the reactor.

The the average temperature in gasifier reduces by increasing the flow rate from 50 to 75 sL/min. Because, the increment of air flow rate decreases the energy density in reactor. However, the temperature in the reactor becomes more uniform. The variation of temperature at point y/h=0.28 ($T_{y/h=0.28}$) and y/h= 0.92 ($T_{y/h=0.92}$) at 6 kW plasma power and 50 sL/min air flow rate is 673°C, while it is 615°C at 6 kW plasma power and 75 sL/min air flow rate.

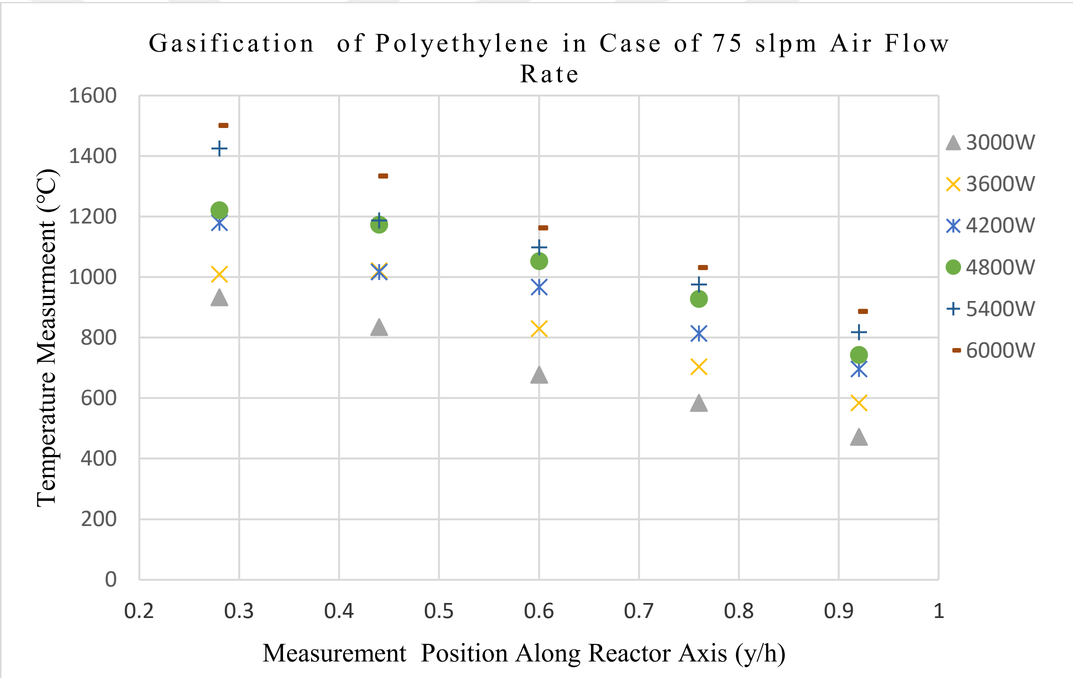

Figure 5.44 The temperature distribution for the gasification of Polyethylene (PP) in case of 75 sL/min air flow rate

The temperature distribution is shown in Figure 5.45 in case of 100 sL/min air flow rate input and initially 250 gr Polyethylene (PP) dosed to the reactor. The closest thermocouple to plasma flame which is located at y/h=0.28 has highest temperature $T_{y/h=0.28}$ = 870°C at 3 kW power. The temperature at y/h=0.28 ($T_{y/h=0.28}$) rises from 870 to 1445 °C by increasing the power from 3 kW to 6 kW. The temperature reduces gradually from region of the plasma flame to downward. The lowest temperature is measured 461 °C at the y/h=0.92 ($T_{y/h=0.92}$) and 3 kW power which is the outmost measurement point from the plasma flame. It rises from 461 to 872 °C by increasing the power from 3 kW to 6 kW. The average temperatures in the reactor (T_{syn}) are 629°C , 762°C, 876°C, 936°C, 1030°C and 1134°C at 3 kW, 3.6 kW, 4.2 kW, 4.8 kW, 5.4 kW and 6 kW respectively. The average temperature rises by increasing plasma power. Because, the increment of plasma power enhances the energy density in the reactor.

The average temperature reduces by increasing the flow rate from 75 to 100 sL/min too. Because, the increment of air flow rate lowers the energy density in reactor. The temperature in the reactor at 100 sL/min becomes more uniform when it is compared with 75 sL/min. The variation of temperature at point y/h=0.28 ($T_{y/h=0.28}$) and y/h= 0.92 ($T_{y/h=0.92}$) at 6 kW and 75 sL/min is 615°C, while it is 572°C at 6 kW and 100 sL/min.

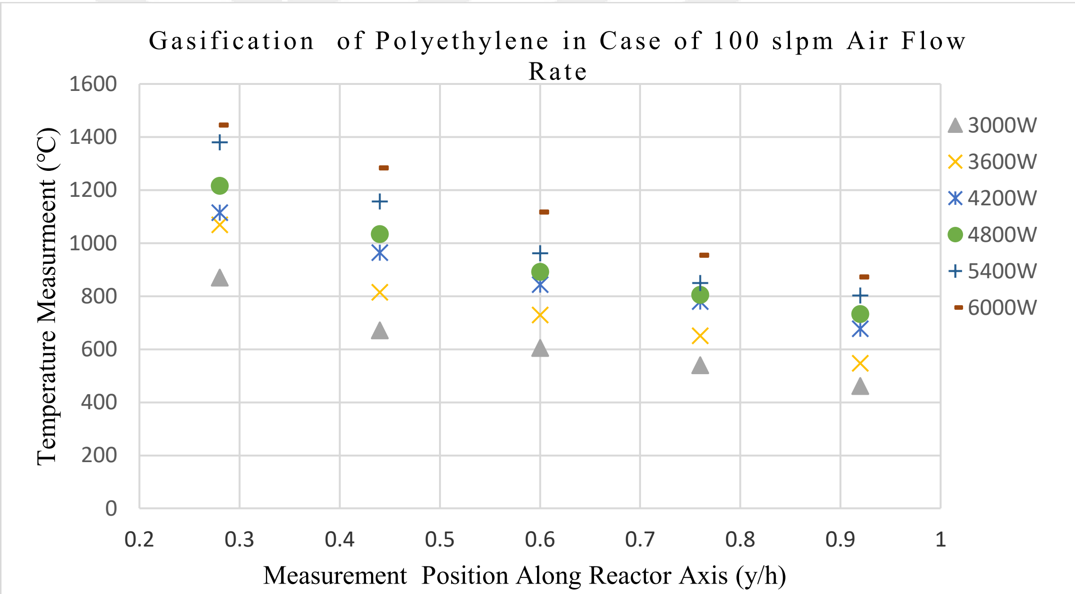

Figure 5.45 The temperature distribution for the gasification of Polyethylene (PP) in case of 100 sL/min air flow rate

The syngas content distribution is given in case of gasification Polyethylene (PP) at 50 sL/min air flow rate and power levels between 3 kW – 6 kW in Figure 5.46. The O_2 in syngas goes up from 1.12 % to 1.52 %, the CO_2 lowers from 16.21 % to 11.21 %, the CO goes up from 19.62 % to 22.27 %, H_2 rises from 9.8 % to 12.56 % by increasing power from 3 kW to 6 kW and CH_4 reduces from 2.12 % to 1.86 % by increasing power from 3 kW to 6 kW. The rest of the mixture, N_2 slightly decreases from 51.13 % to 50.58 % by increasing power from 3 kW to 6 kW.

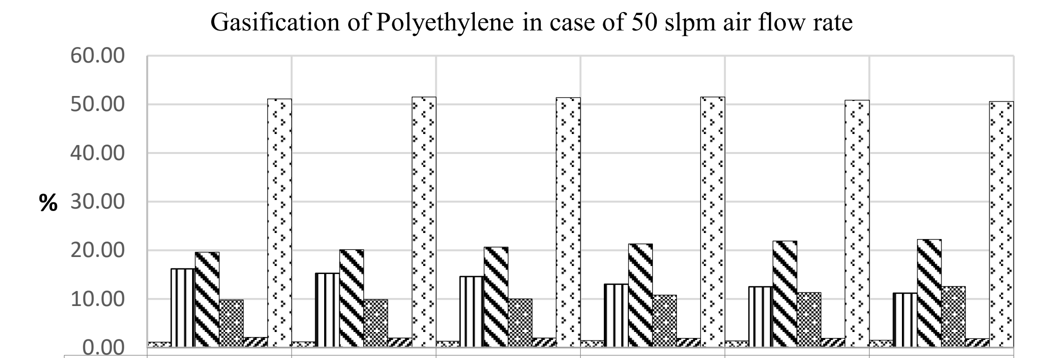

O2	1.12	1.18	1.32	1.44	1.43	1.52
CO2	16.21	15.30	14.62	13.01	12.54	11.21
CO	19.62	20.11	20.67	21.31	21.94	22.27
H2	9.80	9.91	10.03	10.80	11.32	12.56
CH4	2.12	2.01	1.98	1.94	1.95	1.86
N2	51.13	51.49	51.38	51.50	50.82	50.58

Power (W)

Figure 5.46 The produced syngas percentages for the gasification of polyethylene (PP) in case of 50 sL/min air flow rate

The syngas mixture content after gasification process is presented in case of gasification Polyethylene (PP) at 75 sL/min air flow rate and power levels between 3 kW – 6 kW in Figure 5.47.

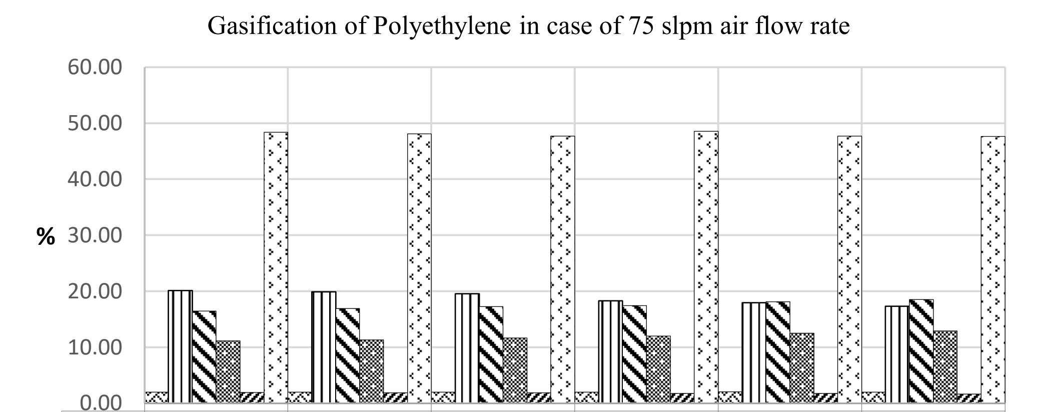

O2	1.99	1.96	1.98	1.97	2.03	2.01
CO2	20.12	19.88	19.56	18.27	17.94	17.32
CO	16.44	16.91	17.23	17.44	18.12	18.54
H2	11.12	11.28	11.67	12.01	12.51	12.89
CH4	1.95	1.88	1.89	1.77	1.73	1.63
N2	48.38	48.09	47.67	48.54	47.67	47.61

Power (W)

Figure 5.47 The produced syngas percentages for the gasification of polyethylene (PP) in case of 75 sL/min air flow rate

The O_2 in syngas fluctuates between 1.96 % and 2.03 %, the CO_2 reduces from 20.12 % to 17.32 %, the CO rises from 16.44 % to 18.54 %, H_2 goes up from 11.12 % to 12.89 % and CH_4 lowers from 1.95 % to 1.63 % by increasing power from 3 kW to 6 kW. The rest of the mixture, N_2 fluctuates between 47.61 % and 48.54 % by increasing power from 3 kW to 6 kW.

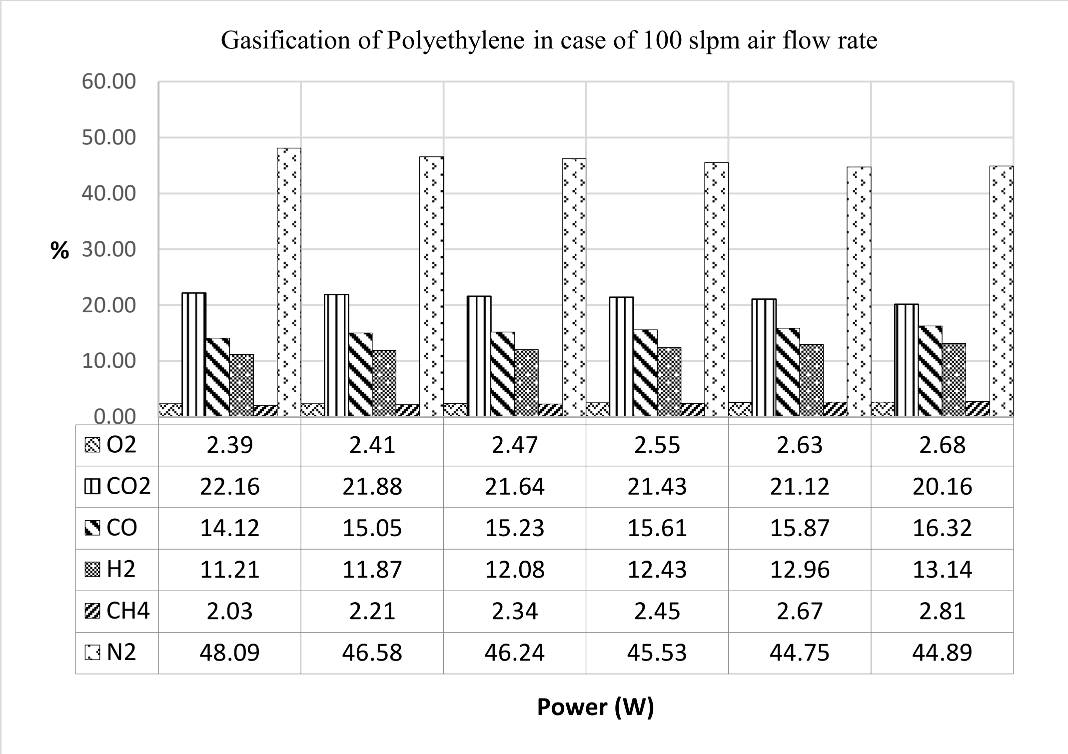

O2	2.39	2.41	2.47	2.55	2.63	2.68
CO2	22.16	21.88	21.64	21.43	21.12	20.16
CO	14.12	15.05	15.23	15.61	15.87	16.32
H2	11.21	11.87	12.08	12.43	12.96	13.14
CH4	2.03	2.21	2.34	2.45	2.67	2.81
N2	48.09	46.58	46.24	45.53	44.75	44.89

Figure 5.48 The produced syngas percentages for the gasification of polyethylene (PP) in case of 100 sL/min air flow rate

The syngas mixture content after the process is shown in case of gasification Polyethylene (PP) at 100 sL/min air flow rate and power levels between 3 kW – 6 kW in Figure 5.48. The O_2 in syngas rises from 2.39 % to 2.68 %, the CO_2 goes down from 22.16 % to 20.16 %, the CO rises from 14.12 % to 16.32 %, the H_2 goes up from 11.21 % to 13.14 % and CH_4 rises from 2.03 % to 2.81 % by increasing power from 3 kW to 6 kW. The rest of the mixture, N_2 decreases by increasing power from 48.09 % to 44.89 % by increasing power from 3 kW to 6 kW.

The effects of air flow rate on syngas content distribution is studied when the results compared for 50, 75 and 100 sL/min flow rate in case of gasification of polyethylene (PP) for various power level from 3 kW to 6 kW. The increment in flow rate has a reverse effect on CO. The CO reduces from 22.27 % to 16.32 % by increasing flow rate from 50 sL/min to 100 sL/min at 6 kW power. On the other hand, H_2 goes up slightly from 12.56 % to 13.14 %, the CO_2 in syngas rises from 11.21 % to 20.16 %, the CH_4 rises from 1.86 % to 2.81 % and the O_2 in syngas mixture rises from 1.52 % to 2.68 % by increasing flow rate from 50 to 100 sL/min at 6 kW power. The N_2 in syngas mixture reduces from 50.58 % to 44.89 % by increasing flow rate from 50 to 100 sL/min at 6 kW power. Syngas percentages change with similar way by increasing the flow rate in different power levels.

5.10 Evaluation of ash-reminder of fuel after gasification process

In this section, the ash of fuels after gasification process is evaluated. The amount of ash was measured by mass balance system and the ash content was examined by using EDX (Energy Dispersive X-ray) system. Even though the many elements are determined in very low level, carbon, oxygen and sulphur are considered for the evaluation because of their importance on the the gasification characteristics and environmental effects. The detailed content distributions (EDX analysis) and SEM anlysis results are given in Appendix-2. Because of low moleculer wieght of hydrogen, the EDX system could not detect the hydrogen.

The ash outputs from the reactor slightly decreases by increasing the plasma power while it increases by increasing the air flow rate regardless to fuel type. In case of gasification of 250 g Hornbeam sawdust (HSD) at 50 sL/min air flow rate, the ash amount decreases from 0.00216 kg to 0.00183 kg by increasing plasma power from 3 kW to 6 kW as given in Table 5.1. In case of 3 kW plasma power, the ash amount increases from 0.00216 kg to 0.0026 kg by rising the air flow rate from 50 sL/min to 100 sL/min. In case of gasification of 250 g pine tree sawdust (PSD) at 50 sL/min air flow rate, the ash amount decreases from 0.00282 kg to 0.00174 kg by increasing plasma power from 3 kW to 6 kW. In case of 3 kW plasma power, the ash amount increases from 0.00282 kg to 0.00482 kg by rising the air flow rate from 50 sL/min to 100 sL/min. In case of gasification of 250 g Russian coal (CR) at 50 sL/min air flow rate, the ash amount decreases from 0.05232 kg to 0.03927 kg by increasing plasma power from 3 kW to 6 kW. In case of 3 kW plasma power, the ash amount increases from 0.05232 kg to 0.0738 kg by rising the air flow rate from 50 sL/min to 100 sL/min. In case of gasification of 250 g South African coal (CSA) at 50 sL/min air flow rate, the ash amount decreases from 0.05621 kg to 0.04418 kg by increasing plasma power from 3 kW to 6 kW. In case of 3 kW plasma power, the ash amount increases from

0.05621 kg to 0.07767 kg by rising the air flow rate from 50 sL/min to 100 sL/min. In case of gasification of 250 g Şırnak (Turkey) coal (CTR) at 50 sL/min air flow rate, the ash amount decreases from 0.06947 kg to 0.04926 kg by increasing plasma power from 3 kW to 6 kW. In case of 3 kW plasma power, the ash amount increases from 0.06947 kg to 0.09177 kg by rising the air flow rate from 50 sL/min to 100 sL/min. In case of gasification of 250 g Polyethylene (PP) at 50 sL/min air flow rate, the ash amount decreases from 0.0021 kg to 0.00116 kg by increasing plasma power from 3 kW to 6 kW. In case of 3 kW plasma power, the ash amount increases from 0.0021 kg to 0.00613 kg by rising the air flow rate from 50 sL/min to 100 sL/min.

After gasification process, the content of ash outputs for the cases are presented in Table 5.5. The ash content is examined in case of varied powers and air flow rates. In case of gasification of Hornbeam sawdust (HSD) at 50 sL/min air flow rate, while the carbon (C) content before the gasification process is 49.3 %, it is 76.6 % for 3 kW plasma power and 77 % for the 6 kW plasma power. The oxygen (O) content before gasification is 47.5 %, it is 19.1 % for 3 kW plasma power and 19.3 % at 6 kW plasma power. The suphur (S) content before gasification is 0.39 %, it is 0.63 % for 3 kW plasma power and 0.59 % at 6 kW plasma power. The other elements before gasification is 2.8 %, it is 3.7 % for 3 kW plasma power and 3.2 % at 6 kW plasma power. The Carbon (C) content is 59.6 %, the Oxygen (O) content is 29.4 %, the Sulphur (S) content is 0.45 % and other elements are 10.5 % when the flow rate is increased to 100 sL/min.

In case of gasification of pine tree sawdust (PSD) at 50 sL/min air flow rate, while the carbon (C) content before the gasification process is 54 %, it is 70.7 % for 3 kW plasma power and 78.9 % for the 6 kW plasma power. The oxygen (O) content before gasification is 44.3 %, it is 21.9 % for 3 kW plasma power and 12.5 % at 6 kW plasma power. The suphur (S) content before gasification is 0.27 %, it is 0.94 % for 3 kW plasma power and 4.3 % at 6 kW plasma power. The other elements before gasification is 1.5 %, it is 6.5 % for 3 kW plasma power and 4.4 % at 6 kW plasma power. When the flow rate is increased to 100 sL/min, the Carbon (C) content is 75.3 %, the Oxygen (O) content is 20.7 %, the Sulphur (S) content is 0.33 % and other elements are 3.7 %.

In case of gasification of Russian coal (CR) at 50 sL/min air flow rate, while the carbon (C) content before the gasification process is 71.3 %, it is 43.2 % for 3 kW plasma power and 92.1 % for the 6 kW plasma power. The oxygen (O) content before gasification is 19.3 %, it is 28.6 % for 3 kW plasma power and 6.5 % at 6 kW plasma power. The suphur (S) content before gasification is 0.49 %, it is 0.55 % for 3 kW plasma power and it is not detected at 6 kW plasma power. The other elements before gasification is 8.9 %, it is 27.7 % for 3 kW plasma power and 1.4 % at 6 kW plasma power. When the flow rate is increased to 100 sL/min, the Carbon (C) content is 78.9 %, the Oxygen (O) content is 15.8 %, the Sulphur (S) content is 0.37 % and other elements are 4.9 %.

In case of gasification of South African coal (CSA) at 50 sL/min air flow rate, while the carbon (C) content before the gasification process is 71.6 %, it is 58.9 % for 3 kW plasma power and 46.3 % for the 6 kW plasma power. The oxygen (O) content before gasification is 19.1 %, it is 8.7 % for 3 kW plasma power and 32.4 % at 6 kW plasma power. The suphur (S) content before gasification is 0.7 %, it is 1.3 % for 3 kW plasma power and it is not detected at 6 kW plasma power. The other elements before gasification is 8.6 %, it is 31.1 % for 3 kW plasma power and 21.3 % at 6 kW plasma power. When the flow rate is increased to 100 sL/min, the Carbon (C) content is 69.6 %, the Oxygen (O) content is 20.7 %, the Sulphur (S) content is 1.5 % and other elements are 8.3 %.

In case of gasification of Şırnak (Turkey) coal (CTR) at 50 sL/min air flow rate, while the carbon (C) content before the gasification process is 60.7 %, it is 19.8 % for 3 kW plasma power and 63.4 % for the 6 kW plasma power. The oxygen (O) content before gasification is 20.5 %, it is 39.5 % for 3 kW plasma power and 11.7 % at 6 kW plasma power. The suphur (S) content before gasification is 6.5 %, it is 0.14 % for 3 kW plasma power and it is 5.4 % at 6 kW plasma power. The other elements before gasification is 12.3 %, it is 40.6 % for 3 kW plasma power and 19.5 % at 6 kW plasma power. When the flow rate is increased to 100 sL/min, the Carbon (C) content is 19.2 %, the Oxygen (O) content is 36.5 %, the Sulphur (S) content is 2.3 % and other elements are 42 %.

In case of gasification of Polyethylene (PP) at 50 sL/min air flow rate, while the carbon (C) content before the gasification process is 82.4 %, it is 25.6 % for 3 kW plasma power and 4.2 % for the 6 kW plasma power.

Table 5.5 Comparison of EDX analysis results of solid fuels and their ash

	Power (W)	Ash EDX analysis			
		C	**O**	**S**	Other elements
Hornbeam sawdust-before gasification	-	49.3	47.5	0.39	2.8
Hornbeam sawdust-50 sL/min	3000	76.6	19.1	0.62	3.7
	6000	76.9	19.3	0.59	3.2
Hornbeam sawdust-100 sL/min	3000	59.6	29.4	0.45	10.5
Pine tree sawdust-before gasification	-	54	44.3	0.27	1.5
Pine tree sawdust-50 sL/min	3000	70.7	21.9	0.94	6.5
	6000	78.9	12.5	4.3	4.4
Pine tree sawdust-100 sL/min	3000	75.3	20.7	0.33	3.7
Russian coal-before gasification	-	71.3	19.3	0.49	8.9
Russian coal-50 sL/min	3000	43.2	28.6	0.55	27.7
	6000	92	6.5	-	1.4
Russian coal-100 sL/min	3000	78.9	15.8	0.37	4.9
South African coal-before gasification	-	71.6	19.1	0.67	8.6
South African coal-50 sL/min	3000	58.9	8.7	1.3	31.1
	6000	46.3	32.4	-	21.3
South African coal-100 sL/min	3000	69.6	20.7	1.5	8.3
Şırnak (Turkey) coal-before gasification	-	60.7	20.5	6.5	12.3
Şırnak (Turkey) coal-50 sL/min	3000	19.8	39.5	0.14	40.6
	6000	63.4	11.7	5.4	19.5
Şırnak (Turkey) coal-100 sL/min	3000	19.2	36.5	2.3	42
Polyethylene-before gasification	-	82.4	11	0.14	6.4
Polyethylene-50 sL/min	3000	25.6	43.8	0.14	30.5
	6000	4.2	42.2	-	53.6
Polyethylene-100 sL/min	3000	9	50.3	0.15	40.5

The oxygen (O) content before gasification is 11 %, it is 43.8 % for 3 kW plasma power and 42.2 % at 6 kW plasma power. The suphur (S) content before gasification is 0.14 %, it is 0.14 % for 3 kW plasma power and it is not detected at 6 kW plasma power. The other elements before gasification is 6.4 %, it is 30.5 % for 3 kW plasma power and 53.6 % at 6 kW plasma power. When the flow rate is increased to 100 sL/min, the Carbon (C) content is 9 %, the Oxygen (O) content is 50.3 %, the Sulphur (S) content is 0.15 % and other elements are 40.5 %.

5.11 Conclusion

In this section, the plasma gasification characteristics of the solid fuels are presented. 6 different solid fuels, Russian coal (CR), South African coal (CSA), Şırnak coal (CTR), pine tree sawdust (PSD), hornbeam sawdust (HSD) and polyethylene (PP) are gasified at various powers between 3 kW and 6 kW, and various air flow rates at 50 sL/min, 75 sL/min and 100 sL/min. The temperature distribution in the gasifier is specified by measuring the temperature by thermocouples at y/h=0.28, 0.44, 0.6, 0.76 and 0.92 in each case. The 6 types of solid fuels are sorted according to type of them as follows; pine tree sawdust (PSD), hornbeam sawdust (HSD) are sawdust, Russian coal (CR), South African coal (CSA), Şırnak coal (CTR) are coals and polyethylene (PP) is polyethylene. According to this classification, the characteristics of each type of fuels are given in detail.

In case of gasification of sawdust, the average temperature in the reactor increases approximately 13.26 % when it is compared to without fuel (WF) case. The reactor temperature increases by raising the plasma power while it reduces by increasing the air flow rate. The increment in the syngas temperature is 53.76 % at 50 sL/min, 69.29 % at 75 sL/min and 80.46 % for 100 sL/min when the plasma power increases from 3kW to 6 kW. The reduction in the syngas temperature is 18 % for 3 kW and 3.75 % for 6 kW when the flow rate increases from 50 sL/min to 100 sL/min. The highest syngas temperature is 1175.23 ℃ at 6 kW plasma power, 50 sL/min and hornbeam sawdust (HSD) gasification for the gasification of sawdust. The lowest syngas temperature is 620.75 ℃ at 3 kW plasma power, 100 sL/min and hornbeam sawdust (HSD) gasification for the gasification of sawdust. In case of gasification of coals, the average temperature in the reactor increases approximately 18.55 % when it is compared to without fuel case. The reactor temperature increases by raising the plasma power while it reduces by increasing the air flow rate. The increment in the syngas temperature is 54.37 % at 50 sL/min, 69.37 at 75 sL/min and 81.5 % for 100 sL/min when the plasma power increases from 3kW to 6 kW. The reduction in the syngas temperature is 20.15 % for 3 kW and 6.12 % for 6 kW when the flow rate increases from 50 sL/min to 100 sL/min. The highest syngas temperature is 1276.14 ℃ at 6 kW plasma power, 50 sL/min and Russian coal (CR) gasification for the gasification of coal. The lowest syngas temperature is 640.89 ℃ at 3 kW plasma power, 100 sL/min and Şırnak (Turkey) coal (CTR) gasification for the gasification of coal. In case of gasification of polyethylene, the average temperature in the reactor increases approximately 15.65 % when it is compared to without fuel case. The reactor temperature increases by raising the plasma power while it reduces by increasing the air flow rate. The increment in the syngas temperature is 53.49 % at 50 sL/min, 68.98 at 75 sL/min and 80.31 % for 100 sL/min when the plasma power increases from 3kW to 6 kW. The reduction in the syngas temperature is 20.74 % for 3 kW and 6.88 % for 6 kW when the flow rate increases from 50 sL/min to 100 sL/min. The highest syngas temperature is 1217.91 ℃ at 6 kW plasma power, 50 sL/min for polyethylene (PP) gasification. The lowest syngas temperature is 628.94 ℃ at 3 kW plasma power, 100 sL/min for polyethylene (PP) gasification. In all the experimentation, the highest syngas temperature is 1276.14 ℃ at 6 kW plasma power, 50 sL/min and Russian coal (CR) gasification while the lowest syngas temperature is 620.75 ℃ at 3 kW plasma power, 100 sL/min and hornbeam sawdust (HSD) gasification.

In case of gasification of sawdust, the syngas production reduces by raising the power from 3 kW to 6 kW. The syngas production decreases approximately 24.69 % in case of 50 sL/min air flow rate, 24.64 % in case of 75 sL/min air flow rate and 23.48 % in case of 100 sL/min air flow rate by increasing the plasma power from 3 kW to 6 kW. Also, increasing air flow rate reduced the syngas production. The reduction in the syngas production is 21.33 % for 3 kW and 20.05 % for 6 kW when the flow rate increases from 50 sL/min to 100 sL/min. The highest syngas production is 1.116 kg at 3 kW plasma power, 50 sL/min and hornbeam sawdust (HSD) gasification for the sawdust gasification. The lowest syngas production is 0.662 kg at 6 kW plasma power, 100 sL/min air flow rate and hornbeam sawdust (HSD) gasification for the sawdust gasification. In case of gasification of coals, the syngas production lowers by raising the power from 3 kW to 6 kW. The syngas production decreases approximately 25.46 % in case of 50 sL/min air flow rate, 23.20 % in case of 75 sL/min air flow rate and 21.5 % in case of 100 sL/min air flow rate by increasing the plasma power from 3 kW to 6 kW. Increasing air flow rate reduced the syngas production too. The reduction in the syngas production is 22.98 % for 3 kW and 20.3 % for 6 kW when the flow rate increases from 50 sL/min to 100 sL/min. The highest syngas production is 1.204 kg at

3 kW plasma power, 50 sL/min air flow rate and Russian coal (CR) gasification for the coal gasification. The lowest syngas production is 0.72 kg at 6 kW plasma power, 100 sL/min air flow rate and Şırnak (Turkey) coal (CTR) gasification for the coal gasification. In case of gasification of polyethylene, the syngas production decreases by raising the power from 3 kW to 6 kW. The syngas production decreases approximately 15.26 % in case of 50 sL/min air flow rate, 11.32 % in case of 75 sL/min air flow rate and 9.19 % in case of 100 sL/min air flow rate by increasing the plasma power from 3 kW to 6 kW. Furthermore, increasing air flow rate reduces the syngas production. The reduction in the syngas production is 7.03 % for 3 kW and 0.37 % for 6 kW when the flow rate increases from 50 sL/min to 100 sL/min. The highest syngas production is 0.899 kg at 3 kW plasma power, 50 sL/min for the polyethylene (PP) gasification. The lowest syngas production is 0.759 kg at 6 kW plasma power, 100 sL/min for the polyethylene (PP) gasification. In all the experimentation, the highest syngas production is 1.204 kg at 3 kW plasma power, 50 sL/min air flow rate and Russian coal (CR) gasification while the lowest syngas production is 0.662 kg at 6 kW plasma power, 100 sL/min air flow rate and hornbeam sawdust (HSD) gasification. The syngas production changes depending on air flow rate and power. By raising the power, the gasification duration reduces. Because of the reduction in gasification time, the supplied air amount decreases. As a result, the produced syngas decreases. By raising the air flow rate, the supplied amount of mass to reactor increases. Because of increasing input mass to reactor, the syngas and ash outputs rise up.

As quantity of syngas production varies with plasma power and air flow rate, the quality of syngas varies by changing plasma power and air flow rate too. In case of gasification of sawdust, the O_2 percentage in syngas increases approximately 18 %, CO_2 percentage in syngas reduces approximately 31 %, CO percentage in syngas increases approximately 131 %, H_2 percentage in syngas increases approximately 195 %, CH_4 percentage in syngas increases approximately 1 % and N_2 percentage in syngas reduces approximately 11 % by increasing power from 3 kW to 6 kW. The O_2 percentage in syngas increases approximately 36 %, CO_2 percentage in syngas increases approximately 38 %, CO percentage in syngas decreases approximately 25 %, H_2 percentage in syngas reduces approximately 12 %, CH_4 percentage in syngas increases approximately 11 % and N_2 percentage in syngas reduces approximately 1 % by increasing air flow rate from 50 sL/min to 100 sL/min. In case of gasification of coals, the O_2 percentage in syngas increases approximately 10 %, CO_2 percentage in syngas reduces approximately 13.5 %, CO percentage in syngas increases approximately 8 %, H_2 percentage in syngas increases approximately 25 %, CH_4 percentage in syngas reduces approximately 16 % and N_2 percentage in syngas goes up approximately 2.5 % by increasing power from 3 kW to 6 kW. The O_2 percentage in syngas increases approximately 106 %, CO_2 percentage in syngas increases approximately 37 %, CO percentage in syngas decreases approximately 16 %, H_2 percentage in syngas reduces approximately 9 %, CH_4 percentage in syngas increases approximately 11 % and N_2 percentage in syngas reduces approximately 16 % by increasing air flow rate from 50 sL/min to 100 sL/min. In case of gasification of polyethylene, the O_2 percentage in syngas increases approximately 16 %, CO_2 percentage in syngas reduces approximately 18 %, CO percentage in syngas increases approximately 14 %, H_2 percentage in syngas increases approximately 20 %, CH_4 percentage in syngas increases approximately 3 % and N_2 percentage in syngas goes down approximately 3 % by increasing power from 3 kW to 6 kW. The O_2 percentage in syngas increases approximately 95 %, CO_2 percentage in syngas increases approximately 58 %, CO percentage in syngas decreases approximately 27 %, H_2 percentage in syngas increases approximately 9.5 %, CH_4 percentage in syngas increases approximately 23 % and N_2 percentage in syngas reduces approximately 8.5 % by increasing air flow rate from 50 sL/min to 100 sL/min.

The ash output reduces by raising the power from 3 kW to 6 kW in case of gasification of sawdust. The ash output decreases approximately 26.79 % in case of 50 sL/min air flow rate, 27.83 % in case of 75 sL/min air flow rate and 28 % in case of 100 sL/min air flow rate by increasing the plasma power from 3 kW to 6 kW. However, increasing air flow rate rises the ash output. The increment in the ash output is 45.65 % for 3 kW and 44.42 % for 6 kW when the flow rate increases from 50 sL/min to 100 sL/min. The highest ash output is 0.00482 kg at 3 kW plasma power, 100 sL/min and pine tree sawdust (PSD) gasification for the sawdust gasification. The lowest ash output is 0.00174 kg at 6 kW plasma power, 50 sL/min and pine tree sawdust (PSD) gasification for the gasification of sawdust. In case of gasification of coals, the ash output reduces by raising the power from 3 kW to 6 kW. The ash output decreases approximately 37.71 % in case of 50 sL/min air flow rate, 42.51 % in case of 75 sL/min air flow rate and 45.92 % in case of 100 sL/min air flow rate by increasing the plasma power from

3 kW to 6 kW. On the other hand, increasing air flow rate rises the ash output. The increment in the ash output is 37.11 % for 3 kW and 26.96 % for 6 kW when the flow rate increases from 50 sL/min to 100 sL/min. The highest ash output is 0.09177 kg at 3 kW plasma power, 100 sL/min and Şırnak (Turkey) coal (CTR) gasification for the coal gasification. The lowest ash output is 0.03927 kg at 6 kW plasma power, 50 sL/min and Russian coal (CR) gasification for the coal gasification. In case of gasification of polyethylene, the ash output reduces by raising the power from 3 kW to 6 kW. The ash output decreases approximately 44.76 % in case of 50 sL/min air flow rate, 40.55 % in case of 75 sL/min air flow rate and 34.58 % in case of 100 sL/min air flow rate by increasing the plasma power from 3 kW to 6 kW. However, increasing air flow rate rises the ash output significantly. The increment in the ash output is 191.9 % for 3 kW and 245.69 % for 6 kW when the flow rate increases from 50 sL/min to 100 sL/min. The highest ash output is 0.00613 kg at 3 kW plasma power, 100 sL/min for the polyethylene (PP) gasification. The lowest ash output is 0.00116 kg at 6 kW plasma power, 50 sL/min for the polyethylene (PP) gasification. The ash output varies depending on air flow rate and power. By raising the power, the conversion from fuel to syngas increases and the output ash decreases. However, increasing the air flow rate effects the fuel to syngas conversion adversely and increases the ash output.

CHAPTER VI

THERMODYNAMIC ANALYSIS

In this section, the thermodynamic analysis methodology is given in detail. The content conversion performance of syngas (CCP_{syn}), ash (CCP_{ash}) and hydrogen (CCP_{H_2}) are defined. Also, hydrogen quality (H_q) is introduced. Process energy efficiency (η_{EP}) and system energy efficiency (η_{ES}), hot gas efficiency (η_{HG}), process exergetic efficiency (η_{EXP}) and system exergetic efficiency (η_{EXS}) terms are described in detail. Then, the thermodynamic performance of solid fuels; Russian coal (CR), South African coal (CSA), Şırnak coal (CTR), pine tree sawdust (PSD), hornbeam sawdust (HSD) and polyethylene (PP) are examined in detail. The thermodynamic performance of each solid fuel gasification in case of 50, 75 and 100 sL/min air flow rate and varied powers between 3 kW and 6 kW are presented for each fuel type.

6.1 First Law Treatment Methodology

Overall theoretical system energy efficiency, η_E can be defined as the ratio of output (syngas and ash) energy to the input (fuel and plasma) energy from the thermodynamic point of view as defined in equation 6.1. The methodology presented here is based on the study of author (Ozdinc Carpinlioglu and Sanlisoy, 2018).

$$\eta_E[\%] = \frac{m_{syn}(kg).\,HHV_{syn}\left(^{kJ}/_{kg}\right) + m_{ash}(kg).\,HHV_{ash}\left(^{kJ}/_{kg}\right)}{m_{fuel}(kg).\,HHV_{fuel}\left(^{kJ}/_{kg}\right) + E_{plasma}\,(kJ)} \times 100 \qquad (6.1)$$

If syngas is at ambient condition, the higher heating value (HHV) is used. On the other hand, if the syngas is at operation condition that is usually higher than evaporation temperature of the water, the lower heating value (LHV) should be taken as heating value of fuel.

In order to determine the energy content of individual species the mass balance should be referred in equation 6.2:

$$m_{input} - m_{output} = (m_2 - m_1)_{CV} \;\; (kg) \qquad (6.2)$$

The mass balance defined above on a conceptual basis can be expressed in equation 6.3:

$$\mathrm{m_{air}} - \mathrm{m_{syn}} - \mathrm{m_{ash}} = \left(0 - m_{fuel}\right)_{CV} \ \text{(kg)} \tag{6.3a}$$

$$m_{\mathrm{fuel}} + \mathrm{m_{air}} = \mathrm{m_{syn}} + \mathrm{m_{ash}} \ \text{(kg)} \tag{6.3b}$$

A practical and meaningful efficiency term for mass balance is described by introducing a content conversion performance CCP. The process performance is directly related to the decomposition of fuel into its end products of syngas and ash. Since the profit or the required output is syngas, content conversion performance for the syngas (CCP_{syn}) can be defined in terms of syngas mass (m_{syn}) and mass of fuel,(m_{fuel}) as follows in equation 6.4a:

$$\mathrm{CCP_{syn}}[\%] = \frac{m_{\mathrm{syn}}}{\mathrm{m_{fuel}}} \times 100 \tag{6.4a}$$

Similarly the mass of ash (m_{ash}) generated as an output of plasma gasification can be expressed by content conversion performance of ash (CCP_{ash}) in equation 6.4b.

$$\mathrm{CCP_{ash}}[\%] = \frac{m_{\mathrm{ash}}}{\mathrm{m_{fuel}}} \times 100 \tag{6.4b}$$

$\mathrm{CCP_{syn}}$ and $\mathrm{CCP_{ash}}$ are expressed in percentages. The best performance is given with the case of $\mathrm{CCP_{syn}}$ which is close to 100 % in association with $\mathrm{CCP_{ash}}$ which is close to 0 %. Furthermore the hydrogen content of syngas as a function of fuel is another important measure. Content conversion performance for hydrogen ($\mathrm{CCP_{H_2}}$) can also be defined in equation 6.4c.

$$\mathrm{CCP_{H_2}}[\%] = \frac{m_{\mathrm{H_2}}}{\mathrm{m_{fuel}}} \times 100 \tag{6.4c}$$

Meanwhile hydrogen quality of syngas can be defined by the term $\mathrm{H_q}$ defined as follows in percentages in equation 6.4d:

$$\mathrm{H_q}[\%] = \frac{m_{\mathrm{H_2}}}{\mathrm{m_{syn}}} \times 100 \tag{6.4d}$$

Since the conversion of fuel to syngas is the aim; energy efficiency parameters for process and system can be defined disregarding the ash formation.

Energy efficiency of process, (η_{EP}) is defined as the ratio of syngas energy to the supplied fuel energy as given in equation 6.5a:

$$\eta_{EP}[\%] = \frac{m_{syn}(kg).\,\mathrm{HHV_{syn}}(^{\mathrm{kJ}}/_{\mathrm{kg}})}{\mathrm{m_{fuel}(kg).\,HHV_{fuel}}(^{\mathrm{kJ}}/_{\mathrm{kg}})} \times 100 \tag{6.5a}$$

The definition of syngas energy and fuel energy are given in equations 6.5b and 6.5c.

$$\mathrm{E_{syn}\ (kJ)} = m_{syn}\mathrm{(kg).\,HHV_{syn}}(^{\mathrm{kJ}}/_{\mathrm{kg}}) \tag{6.5b}$$

$$\mathrm{E_{fuel}\ (kJ) = m_{fuel}(kg).\,HHV_{fuel}}(^{\mathrm{kJ}}/_{\mathrm{kg}}) \tag{6.5c}$$

Energy efficiency of system (η_{ES}) is defined as the ratio of syngas energy to the supplied fuel energy and the input plasma energy, (E_{plasma}) as given in equation 6.6:

$$\mathrm{E_{plasma}\ (kJ) = W_{plasma}(\ kW).\,t_g\ (s)} \tag{6.6a}$$

$$\eta_{ES}[\%] = \frac{m_{syn}\mathrm{(kg).\,HHV_{syn}}\left(^{\mathrm{kJ}}/_{\mathrm{kg}}\right)}{m_{fuel}\mathrm{(kg).\,HHV_{fuel}}\left(^{\mathrm{kJ}}/_{\mathrm{kg}}\right) + \mathrm{E_{plasma}\ (kJ)}} \times 100 \tag{6.6b}$$

In these efficiency definitions, the temperature of the syngas (T_{syn}) or the sensible energy level of the syngas are the critical parameters. Hot gas efficiency (η_{HG}) is taken into account for the cases of syngas temperature (T_{syn}) is higher than the ambient temperature (T_0). The system hot gas efficiency (η_{HG}) is given in equation 6.7.

$$\eta_{HG}[\%] = \frac{m_{syn}\mathrm{(kg).}\left[\mathrm{HHV_{syn}}\left(^{\mathrm{kJ}}/_{\mathrm{kg}}\right) + \mathrm{c_{p(syn)}}\left(^{\mathrm{kJ}}/_{\mathrm{kg.\,K}}\right)\cdot(\mathrm{T_{syn}} - \mathrm{T_o})(K)\right]}{\mathrm{m_{fuel}(kg).\,HHV_{fuel}}\left(^{\mathrm{kJ}}/_{\mathrm{kg}}\right) + \mathrm{E_{plasma}(\ kJ)}} \times 100 \tag{6.7}$$

Process hot gas efficiency is defined with equation 6.7 disregarding input plasma energy (E_{plasma}). However adiabatic gasification reactor assumption results in 100 % hot gas efficiency. Therefore, it is meaningful to consider cold gas efficiency (Loha et al., 2011) as was done previously by other researchers (Table 2.2). Therefore efficiency parameters for process (η_{EP}) and system (η_{ES}) in equation 6.5 and equation 6.6 are referred as cold gas ones with assumption of $T_{syn} = T_0$.

Since energy efficiency parameters are based upon the determination of higher heating value (HHV) and lower heating value (LHV); HHV and LHV of the fuel can be calculated by using equation 6.8 described by Channiwala and Parikh, 2002 (Channiwala and Parikh, 2002) and by using equation 6.9 described by Finet, 1987 (Finet, 1987) respectively.

$$\mathrm{HHV} = 0.3491\mathrm{C} + 1.1783\mathrm{H} + 0.1005\mathrm{S} - 0.1034\mathrm{O} - 0.0151\mathrm{N} - 0.0211\mathrm{ash}\left(\frac{\mathrm{MJ}}{\mathrm{kg}}\right) \quad (6.8)$$

$$\mathrm{LHV} = \mathrm{HHV}(1 - \mathrm{H_2O}) - 2440(\mathrm{H_2O} + 9\mathrm{H})\left(\frac{\mathrm{MJ}}{\mathrm{kg}}\right) \quad (6.9)$$

Table 6.1 Heating values of gas species at 25°C (Çengel and Boles, 2007)

Substances	HHV (kJ/kg)	LHV (kJ/kg)
CO	10,100	10,100
H_2	141,800	120,000
CH_4	55,530	50,050
C_{2+}	50,900	48,000

Meanwhile, the heating value of a syngas mixture can be determined by taking the partial heating value of gas species. Heating value of some gases are given in Table 6.1 (Çengel and Boles, 2007).

6.2 Thermodynamic analysis of hornbeam sawdust (HSD) gasification process

In this section, thermodynamic performance of hornbeam sawdust (HSD) gasification process is handled. The content conversion performance of syngas ($\mathrm{CCP_{syn}}$), content conversion performance of ash ($\mathrm{CCP_{ash}}$), content conversion performance of hydrogen ($\mathrm{CCP_{H_2}}$), hydrogen quality of syngas ($\mathrm{H_q}$), process energy efficiency (η_{EP}), system energy efficiency (η_{ES}) and hot gas efficiency (η_{HG}) are calculated for each case of the gasification of hornbeam sawdust (HSD) for various powers from 3 kW to 6 kW and at 50 sL/min, 75 sL/min and 100 sL/min air flow rate. The results are presented in this section.

The $\mathrm{CCP_{syn}}$, $\mathrm{CCP_{ash}}$, $\mathrm{CCP_{H_2}}$, $\mathrm{H_q}$, syngas energy, fuel energy and plasma energy are given in the Table 6.2. The content conversion performance of syngas ($\mathrm{CCP_{syn}}$) decreases by increasing plasma power in 50, 75 and 100 sL/min air flow rate cases. Because, the increasing power reduces the gasification time (tg). The supplied air amount to the reactor reduces due to the reduction of supplying air flow rate duration.

As a result the produced syngas amount decreases while the supplied fuel amount is same. In case of 50 sL/min, it reduces from 446 % at 3 kW plasma power to 336 % at 6 kW plasma power. In case of 75 sL/min, it reduces from 525 % to 395 % by increasing plasma power from 3 kW to 6 kW. In case of 100 sL/min, it reduces from 604 % to 431 % by increasing plasma power from 3 kW to 6 kW. On the other hand, the increasing air flow rate causes the increment in the content conversion performance of syngas (CCP_{syn}). It goes up from 446 % to 604 % by increasing air flow rate from 50 sL/min to 100 sL/min at 3 kW power. Similarly, it increases from 336 % to 431 % by increasing air flow rate from 50 sL/min to 100 sL/min at 6 kW power.

The content conversion performance of ash (CCP_{ash}) decreases by increasing the plasma power in 50, 75 and 100 sL/min air flow rate cases because of the enhancement of solid fuel conversion to syngas by increasing plasma power. Higher solid fuel conversion to syngas means less ash output from the reactor. On the other hand, the air flow rate increases the content conversion performance of ash (CCP_{ash}). Because, increasing air flow reduces the temperature in reactor and the conversion of solid fuel to syngas. As a result, less syngas production and high ash are produced. In case of 50 sL/min, it goes down from 0.86 % at 3 kW power to 0.73 % at 6 kW power. In case of 75 sL/min, it decreases from 0.94 % to 0.76 % by increasing power from 3 kW to 6 kW. In case of 100 sL/min, it reduces from 1.04 % to 0.85 % by increasing power from 3 kW to 6 kW. On the other hand, the increasing air flow rate causes the increment of content conversion performance of ash (CCP_{ash}). It goes up from 0.86 % to 1.04 % by increasing air flow rate from 50 sL/min to 100 sL/min at 3 kW power. Similarly, it increases from 0.73 % to 0.85 % by increasing of air flow rate from 50 sL/min to 100 sL/min at 6 kW power.

The content conversion performance of hydrogen (CCP_{H_2}) increases by increasing the plasma power in 50, 75 and 100 sL/min air flow rate cases because of increment of syngas temperature and enhancement in conversion of solid fuel to syngas. Enhancement in syngas conversion increases the production of hydrogen. Also, the air flow rate increases the content conversion performance of hydrogen (CCP_{H_2}). Because, the increasing air flow rate also increases the syngas production. Higher production of syngas means the higher hydrogen production from the same amount of the fuel. In case of 50 sL/min, it increases from 0.7 % at 3 kW power to 2.13 % at 6 kW power.

In case of 75 sL/min, it goes up from 0.75 % to 2.03 % by increasing power from 3 kW to 6 kW. In case of 100 sL/min, it increases from 0.76 % to 2.05 % by increasing power from 3 kW to 6 kW. Also, the increasing air flow rate enhances the content conversion performance of hydrogen (CCP_{H_2}) in many cases. It goes up from 0.7 % to 0.76 % by increasing air flow rate from 50 sL/min to 100 sL/min at 3 kW power. However, it reduces slightly from 2.13 % to 2.05 % by increasing air flow rate from 50 sL/min to 100 sL/min at 6 kW power.

Hydrogen quality of syngas (H_q) goes up by increasing power in 50, 75 and 100 sL/min air flow rate cases. Because, the hydrogen production is proportional with the temperature in the reactor. The temperature increases by increasing plasma power. However, increasing air flow rate reduces the hydrogen quality of syngas (H_q). Because the air flow rate is inversely proportional with the temperature in the reactor. In case of 50 sL/min, it increases from 0.16 % at 3 kW power to 0.64 % at 6 kW power. In case of 75 sL/min, it goes up from 0.14 % to 0.51 % by increasing power from 3 kW to 6 kW. In case of 100 sL/min, it rises from 0.13 % to 0.48 % by increasing power from 3 kW to 6 kW. Nevertheless, the increasing air flow rate reduces the hydrogen quality of syngas (H_q). It decreases from 0.16 % to 0.13 % by increasing air flow rate from 50 sL/min to 100 sL/min at 3kW power. Also, it reduces from 0.64 % to 0.48 % by increasing air flow rate from 50 sL/min to 100 sL/min at 6 kW power.

Syngas energy increases by increasing plasma power in 50, 75 and 100 sL/min air flow rate cases. Because, the syngas energy depends on the syngas production and syngas content especially percentage of CO, H_2 and CH_4. Syngas production reduces by increasing plasma power. Percentage of CO and H_2 increases while CH_4 remains same or slightly reduces by increasing plasma power. As a result, the syngas energy increases by increasing the power. Also, syngas production reduces by increasing air flow rate and percentage of CO and H_2 reduces while percentage of CH_4 increases by increasing air flow rate. The production amount and the distribution of syngas effects the syngas energy. In case of 50 sL/min, syngas energy increases from 1644 kJ at 3 kW plasma power to 2903 kJ at 6 kW plasma power. In case of 75 sL/min, syngas energy increases from 1715 kJ at 3 kW plasma power to 2621 kJ at 6 kW plasma power. In case of 100 sL/min, syngas energy increases from 1936 kJ at 3 kW plasma power to 2479 kJ at 6 kW plasma power. The energy of 250 g hornbeam sawdust

(HSD) fuel is 5338 kJ. Similarly, the syngas energy increases from 1644 kJ to 1936 kJ by increasing air flow rate from 50 sL/min to 100 sL/min at 3 kW power. However, the syngas energy decreases from 2903 kJ to 2479 kJ by increasing air flow rate from 50 sL/min to 100 sL/min at 6 kW power.

Table 6.2 Presentation of the CCP_{syn}, CCP_{ash}, CCP_{H_2}, syngas energy, fuel energy and plasma energy results for the hornbeam sawdust (HSD) gasification process for various powers and flow rates

	Plasma Power (W)	CCP_{syn} (%)	CCP_{ash} (%)	CCP_{H_2} (%)	H_q (%)	Syngas energy (kJ)	Fuel energy (kJ)	Plasma energy (kJ)
Hornbeam sawdust-50sL/min	3000	446	0.86	0.70	0.16	1644	5338	2640
	3600	423	0.83	1.30	0.31	1985		2952
	4200	415	0.78	1.50	0.36	2078		3360
	4800	383	0.76	1.53	0.40	2465		3456
	5400	368	0.74	1.82	0.49	2603		3672
	6000	336	0.73	2.13	0.64	2903		3600
Hornbeam sawdust-75sL/min	3000	525	0.94	0.75	0.14	1715		2160
	3600	484	0.89	1.35	0.28	2021		2340
	4200	472	0.84	1.69	0.36	2094		2646
	4800	454	0.80	1.71	0.38	2196		2880
	5400	419	0.78	1.86	0.44	2319		2916
	6000	395	0.76	2.03	0.51	2621		3000
Hornbeam sawdust-100sL/min	3000	604	1.04	0.76	0.13	1936		1920
	3600	573	1.00	1.51	0.26	2227		2160
	4200	541	0.94	1.53	0.28	2204		2352
	4800	509	0.90	1.76	0.35	2242		2496
	5400	454	0.87	1.83	0.40	2280		2430
	6000	431	0.85	2.05	0.48	2479		2520

Process energy efficiency (η_{EP}) of hornbeam sawdust (HSD) in case of 50 sL/min, 75 sL/min and 100 sL/min for various plasma powers between 3 kW and 6 kW are presented in Figure 6.1. Process energy efficiency (η_{EP}) increases by increasing the plasma power while it remains almost constant by increasing air flow rate. The input energy is just the fuel energy in the case of process energy efficiency (η_{EP}). So, the syngas energy is the only one parameter which effects the process energy efficiency (η_{EP}). However, the relation between syngas energy, plasma power, and air flow rate are sophisticated to define the relation. Increasing power lowers the gasification duration and reduces the syngas production, but it enhances the conversion of fuel to syngas and rises the syngas temperature. Similarly, increasing air flow rate lowers the gasification duration and it reduces the syngas production. Also, it reduces the syngas temperature and the conversion of fuel to syngas. As a result, increment of plasma power rises the process energy efficiency (η_{EP}). However, increasing air flow rate has insignificant effect on the process energy efficiency (η_{EP}). In case of 50 sL/min air flow rate, process energy efficiency (η_{EP}) increases from 30.80 % to 54.39 % by increasing the plasma power from 3 kW to 6 kW. In case of 75 sL/min air flow rate, it increases from 32.12 % to 49.10 % by increasing the plasma power from 3 kW to 6 kW. In case of 100 sL/min air flow rate, it increases from 36.26 % to 46.44 % by increasing the plasma power from 3 kW to 6 kW. Increasing plasma power enhances the process energy efficiency (η_{EP}) in all cases. However, the effect of plasma power to the process energy efficiency (η_{EP}) decreases by increasing the flow rate. The increment in efficiency is 76.5 % by increasing plasma power from 3 kW to 6 kW in 50 sL/min and it is 28 % by increasing plasma power from 3kW to 6kW in 100 sL/min. While increasing air flow rate enhances the process energy efficiency (η_{EP}) at 3 kW plasma power, increasing air flow rate reduces the process energy efficiency (η_{EP}) at 6 kW plasma power. The process energy efficiency (η_{EP}) goes up from 30.8 % to 36.26 % by increasing the flow rate from 50 sL/min to 100 sL/min in case of 3 kW power and it reduces from 54.39 % to 46.44 % by increasing the flow rate from 50 sL/min to 100 sL/min in case of 6 kW plasma power.

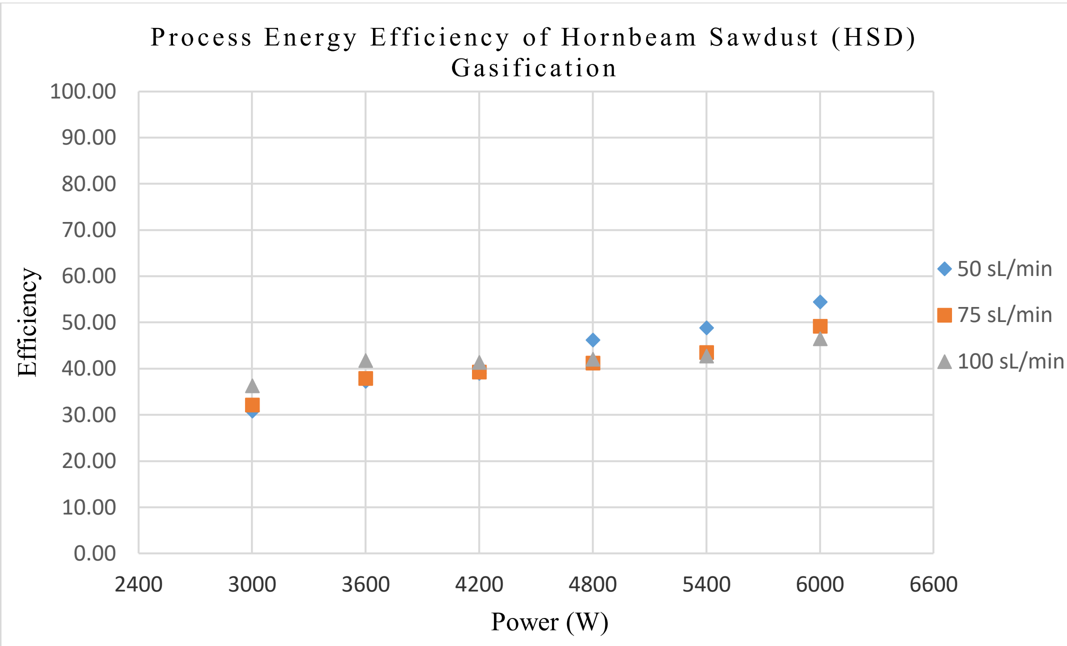

Figure 6.1 Process energy efficiency (η_{EP}) of hornbeam sawdust (HSD) gasification in the cases of 50-100 sL/min air flow rate and 3-6 kW plasma power

The system energy efficiency (η_{ES}) depends on the fuel energy, plasma energy and the syngas energy. The constant amount of fuel is dosed to the reactor in the each case. However, the plasma energy and syngas energy are varied depending on the plasma power and air flow rate. Increasing power lowers the gasification duration, reduces syngas production and increases the plasma energy consumption, but it enhances the conversion of fuel to syngas and rises the syngas temperature. Similarly, increasing air flow rate lowers the gasification duration, reduces syngas production and lowers the plasma energy consumption. On the other hand, it reduces the syngas temperature and the conversion of fuel to syngas. As a result, increment of plasma power rises the system energy efficiency (η_{ES}). However, increasing air flow rate has lighter effect on the system energy efficiency (η_{ES}). In case of 50 sL/min air flow rate, system energy efficiency (η_{ES}) increases from 20.61 % to 32.48 % by increasing the plasma power from 3 kW to 6 kW. In case of 75 sL/min air flow rate, it increases from 22.87 % to 31.43 % by increasing the plasma power from 3 kW to 6 kW. In case of 100 sL/min air flow rate, it increases from 26.67 % to 31.55 % by increasing the plasma power from 3 kW to 6 kW.

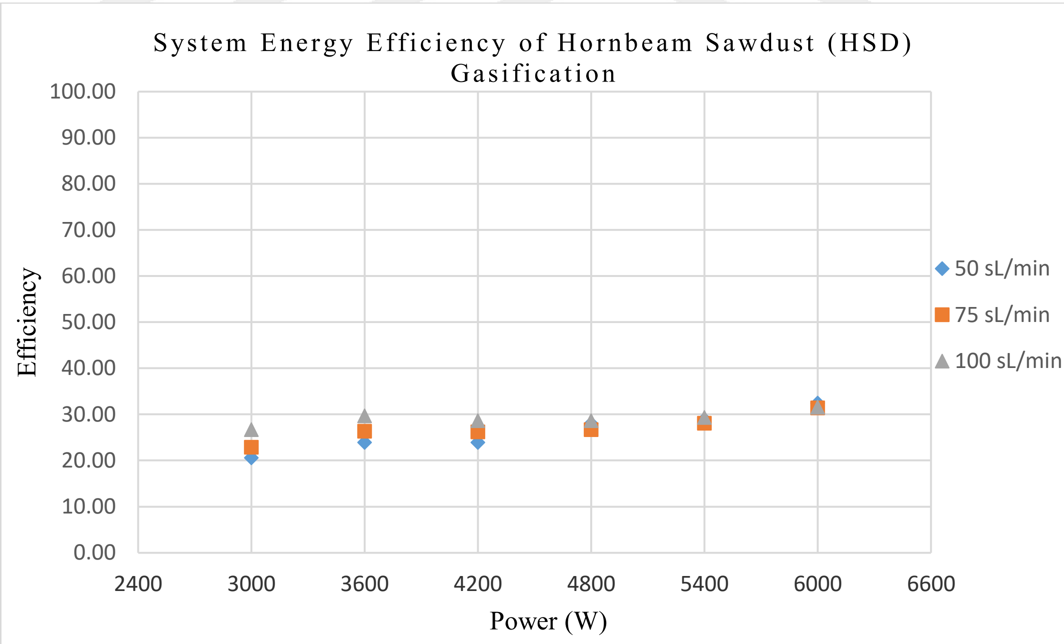

Figure 6.2 System energy efficiency (η_{ES}) of hornbeam sawdust (HSD) gasification in the cases of 50-100 sL/min air flow rate and 3-6 kW plasma power

The magnitude of the system energy efficiency (η_{ES}) is less than the process energy efficiency (η_{EP}). Because, the plasma power consumes energy and it has negative effects to system energy efficiency (η_{ES}). The increasing air flow rate rises the system energy efficiency (η_{ES}) at 3 kW plasma power. However, the increasing air flow rate reduces the system energy efficiency (η_{ES}) at 6 kW plasma power. The system energy efficiency (η_{ES}) goes up from 20.61 % to 26.67 % by increasing the flow rate from 50 sL/min to 100 sL/min in case of 3 kW power and it reduces from 32.48 % to 31.55 % by increasing the flow rate from 50 sL/min to 100 sL/min in case of 6 kW plasma power.

Hot gas efficiency (η_{HG}) of hornbeam sawdust (HSD) in case of 50 sL/min, 75 sL/min and 100 sL/min for various plasma powers between 3 kW and 6 kW is given in Figure 6.3. The hot gas efficiency (η_{HG}) depends on the fuel energy, plasma energy and the syngas energy similar to the system energy efficiency (η_{ES}). In addition to system efficiency parameters, the syngas energy includes both the chemical energy of the solid fuel and sensible energy as a result of its high temperature in the hot gas efficiency (η_{HG}). The variation of the hot gas efficiency (η_{HG}) is similar with the system energy efficiency (η_{ES}). The magnitude of the hot gas efficiency (η_{HG}) is higher than the system energy efficiency (η_{ES}). Because, the sensible energy of the syngas is also considered in calculations of hot gas efficiency (η_{HG}). As a result, increment of plasma power rises the hot gas efficiency (η_{HG}). However, increasing air flow rate has lighter effect on the hot gas efficiency (η_{HG}).

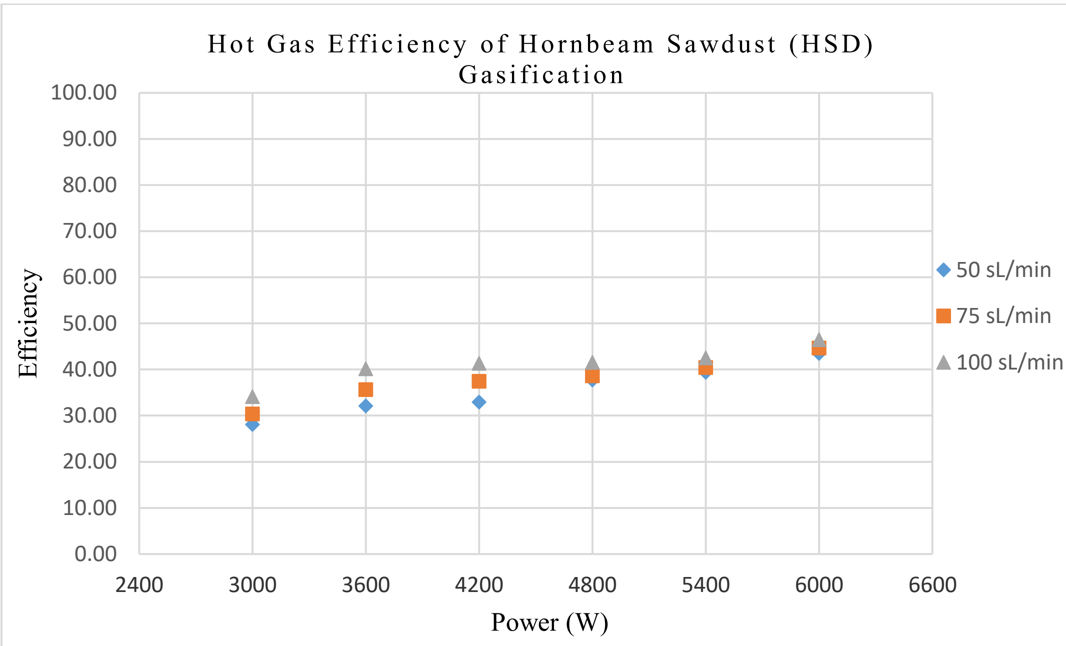

Figure 6.3 Hot gas efficiency (η_{HG}) of hornbeam sawdust (HSD) gasification in the cases of 50-100 sL/min air flow rate and 3-6 kW plasma power

In case of 50 sL/min air flow rate, hot gas efficiency (η_{HG}) increases from 28.06 % to 43.50 % by increasing the plasma power from 3 kW to 6 kW. In case of 75 sL/min air flow rate, it increases from 30.39 % to 44.68 % by increasing the plasma power from 3 kW to 6 kW. In case of 100 sL/min air flow rate, it increases from 34.11 % to 46.49 % by increasing the plasma power from 3 kW to 6 kW. The hot gas efficiency (η_{HG}) goes up from 28.06 % to 34.11 % by increasing the flow rate from 50 sL/min to 100 sL/min in case of 3 kW power and it also rises from 43.50 % to 46.49 % by increasing the flow rate from 50 sL/min to 100 sL/min in case of 6 kW plasma power.

6.3 Thermodynamic analysis of pine tree sawdust (PSD) gasification process

In this section, thermodynamic performance of pine tree sawdust (PSD) gasification process is handled. The content conversion performance of syngas (CCP_{syn}), content conversion performance of ash (CCP_{ash}), content conversion performance of hydrogen (CCP_{H_2}), hydrogen quality of syngas (H_q), process energy efficiency (η_{EP}), system energy efficiency (η_{ES}) and hot gas efficiency (η_{HG}) are calculated for each case of the gasification of pine tree sawdust (PSD) for various powers from 3 kW to 6 kW and at 50 sL/min, 75 sL/min and 100 sL/min air flow rate. The results are presented in this section.

The CCP_{syn}, CCP_{ash}, CCP_{H_2}, H_q, syngas energy, fuel energy and plasma energy are given in the Table 6.3. The content conversion performance of syngas (CCP_{syn}) decreases by increasing plasma power in 50, 75 and 100 sL/min air flow rate cases. Because, the increasing power reduces the gasification time (tg). The supplied air amount to the reactor reduces due to the reduction of supplying air flow rate duration. As a result the produced syngas amount decreases while the supplied fuel amount is same. In case of 50 sL/min, it reduces from 446 % at 3 kW plasma power to 336 % at 6 kW plasma power. In case of 75 sL/min, it reduces from 525 % to 371 % by increasing plasma power from 3 kW to 6 kW. In case of 100 sL/min, it reduces from 603 % to 446 % by increasing plasma power from 3 kW to 6 kW. On the other hand, the increasing air flow rate causes the increment of content conversion performance of syngas (CCP_{syn}). It goes up from 446 % to 603 % by increasing air flow rate from 50 sL/min to 100 sL/min at 3 kW power. Similarly, it increases from 336 % to 446 % by increasing air flow rate from 50 sL/min to 100 sL/min at 6 kW power.

The content conversion performance of ash (CCP_{ash}) decreases by increasing the plasma power in 50, 75 and 100 sL/min air flow rate cases because of the enhancement of solid fuel conversion to syngas by increasing plasma power. Higher solid fuel conversion to syngas means less ash output from the reactor. On the other hand, the air flow rate increases the content conversion performance of ash ($\mathrm{CCP_{ash}}$). Because, increasing air flow reduces the temperature in reactor and the conversion of solid fuel to syngas. As a result, less syngas production and high ash are produced. In case of 50 sL/min, it goes down from 1.13 % at 3 kW power to 0.7 % at 6 kW power. In case of 75 sL/min, it decreases from 1.35 % to 0.85 % by increasing power from 3 kW to 6 kW. In case of 100 sL/min, it reduces from 1.93 % to 1.20 % by increasing power from 3 kW to 6 kW. On the other hand, rising air flow rate causes the increment of content conversion performance of ash ($\mathrm{CCP_{ash}}$). It goes up from 1.13 % to 1.93 % by increasing air flow rate from 50 sL/min to 100 sL/min at 3 kW power. Similarly, it increases from 0.7 % to 1.2 % by increasing air flow rate from 50 sL/min to 100 sL/min at 6 kW power.

The content conversion performance of hydrogen ($\mathrm{CCP_{H_2}}$) increases by increasing the plasma power in 50, 75 and 100 sL/min air flow rate cases because of increment of syngas temperature and enhancement in conversion of solid fuel to syngas. Enhancement in syngas conversion increases the production of hydrogen. Also, the air flow rate increases the content conversion performance of hydrogen ($\mathrm{CCP_{H_2}}$). Because, the increasing air flow rate also increases the syngas production. Higher production of syngas means the higher hydrogen production from the same amount of the fuel. In case of 50 sL/min, it increases from 0.96 % at 3 kW power to 2.23 % at 6 kW power. In case of 75 sL/min, it goes up from 1.11 % to 2.07 % by increasing power from 3 kW to 6 kW. In case of 100 sL/min, it increases from 0.84 % to 2.01 % by increasing power from 3 kW to 6 kW. On the other hand, the content conversion performance of hydrogen ($\mathrm{CCP_{H_2}}$) is fluctuated by increasing air flow rate. It reduces from 0.96 % to 0.84 % by increasing air flow rate from 50 sL/min to 100 sL/min at 3 kW power. Similarly, it reduces from 2.23 % to 2.01 % by increasing air flow rate from 50 sL/min to 100 sL/min at 6 kW power.

Hydrogen quality of syngas ($\mathrm{H_q}$) rises by increasing power in 50, 75 and 100 sL/min air flow rate cases. Because, the hydrogen production is proportional with the temperature in the reactor. The temperature increases by increasing plasma power. However, increasing air flow rate reduces the hydrogen quality of syngas ($\mathrm{H_q}$).

Because the air flow rate is inversely proportional with the temperature in the reactor. In case of 50 sL/min, it increases from 0.21 % at 3 kW power to 0.66 % at 6 kW power. In case of 75 sL/min, it goes up from 0.21 % to 0.56 % by increasing power from 3 kW to 6 kW. In case of 100 sL/min, it rises from 0.14 % to 0.45 % by increasing power from 3 kW to 6 kW. However, the increment of air flow rate reduces the hydrogen quality of syngas (H_q). It decreases from 0.21 % to 0.14 % by increasing air flow rate from 50 sL/min to 100 sL/min at 3 kW power. Also, it reduces from 0.66 % to 0.45 % by increasing air flow rate from 50 sL/min to 100 sL/min at 6 kW power.

Table 6.3 Presentation of the CCP_{syn}, CCP_{ash}, CCP_{H_2}, syngas energy, fuel energy and plasma energy results for the pine tree sawdust (PSD) gasification process for various powers and flow rates

	Plasma Power (W)	CCP_{syn} (%)	CCP_{ash} (%)	CCP_{H_2} (%)	H_q (%)	Syngas energy (kJ)	Fuel energy (kJ)	Plasma energy (kJ)
Pine tree sawdust-50sL/min	3000	446	1.13	0.96	0.21	1936.		2640
	3600	430	1.04	1.27	0.29	2072		3024
	4200	415	0.98	1.62	0.39	2274		3360
	4800	383	0.90	1.58	0.41	2458		3456
	5400	368	0.79	1.63	0.44	2614		3672
	6000	336	0.70	2.23	0.66	2928		3600
Pine tree sawdust-75sL/min	3000	525	1.35	1.11	0.21	2121		2160
	3600	501	1.23	1.15	0.23	2374		2448
	4200	454	1.14	1.58	0.35	2540	4485	2520
	4800	430	1.11	1.65	0.38	2655		2688
	5400	407	0.98	1.87	0.46	2805		2808
	6000	371	0.85	2.07	0.56	3000		2760
Pine tree sawdust-100sL/min	3000	603	1.93	0.84	0.14	2271		1920
	3600	572	1.77	1.56	0.27	2592		2160
	4200	556	1.60	1.57	0.28	2625		2436
	4800	525	1.43	1.74	0.33	2715		2592
	5400	501	1.26	1.82	0.36	2722		2754
	6000	446	1.20	2.01	0.45	2735		2640

Syngas energy increases by increasing plasma power in 50, 75 and 100 sL/min air flow rate cases. Because, the syngas energy depends on the syngas production and syngas content especially percentage of CO, H_2 and CH_4. Syngas production reduces by increasing plasma power. Percentage of CO and H_2 increases while CH_4 remains same or slightly reduces by increasing plasma power. As a result, the syngas energy increases by increasing the power. Also, syngas production reduces by increasing air flow rate and percentage of CO and H_2 reduces while percentage of CH_4 increases by increasing air flow rate. The production amount and the distribution of syngas effects the syngas energy. In case of 50 sL/min, syngas energy increases from 1936 kJ at 3 kW plasma power to 2928 kJ at 6 kW plasma power. In case of 75 sL/min, syngas energy increases from 2121 kJ at 3 kW plasma power to 3000 kJ at 6 kW plasma power. In case of 100 sL/min, syngas energy increases from 2271 kJ at 3 kW plasma power to 2735 kJ at 6 kW plasma power. The energy of 250 g pine tree sawdust (PSD) fuel is 4485 kJ. Similarly, the syngas energy increases from 1936 kJ to 2271 kJ by increasing air flow rate from 50 sL/min to 100 sL/min at 3 kW power. However, the syngas energy goes down from 2928 kJ to 2735 kJ by increasing air flow rate from 50 sL/min to 100 sL/min at 6 kW power.

Process energy efficiency (η_{EP}) of the pine tree sawdust (PSD) in case of 50 sL/min, 75 sL/min and 100 sL/min for various plasma powers between 3 kW and 6 kW are presented in Figure 6.4. Process energy efficiency (η_{EP}) increases by increasing the plasma power while it fluctuates by increasing air flow rate. The input energy is just the fuel energy in the case of process energy efficiency (η_{EP}). So, the syngas energy is the only one parameter which effects the process energy efficiency (η_{EP}). However, the relation between syngas energy, plasma power, and air flow rate are sophisticated to define the relation. Increasing power lowers the gasification duration and reduces the syngas production, but it enhances the conversion of fuel to syngas and rises the syngas temperature. Similarly, increasing air flow rate lowers the gasification duration and it reduces the syngas production. Also, it reduces the syngas temperature and the conversion of fuel to syngas. As a result, increment of plasma power rises the process energy efficiency (η_{EP}). However, increasing air flow rate fluctuates the process energy efficiency (η_{EP}). In case of 50 sL/min air flow rate, process energy efficiency (η_{EP}) increases from 43.17 % to 65.29 % by increasing the plasma power from 3 kW to 6 kW. In case of 75 sL/min air flow rate, it increases from 47.28 % to 66.88 % by increasing the plasma power from 3 kW to 6 kW. In case of 100 sL/min air flow rate, it increases from 50.63 % to 60.98 % by increasing the plasma power from 3 kW to 6 kW. Increasing plasma power enhances the process energy efficiency (η_{EP}) in all cases. However, the effect of plasma power to the process energy efficiency (η_{EP}) decreases by increasing the flow rate. The increment in efficiency is 51.23 % by increasing plasma power from 3 kW to 6 kW in 50 sL/min and it is 20.44 % by increasing plasma power from 3 kW to 6 kW in 100 sL/min. While the increasing air flow rate increases the process energy efficiency (η_{EP}) at 3 kW plasma power, increasing air flow rate decreases the process energy efficiency (η_{EP}) at 6 kW plasma power. The process energy efficiency (η_{EP}) goes up from 43.17 % to 50.63 % by increasing the flow rate from 50 sL/min to 100 sL/min in case of 3 kW power and it reduces from 65.29 % to 60.98 % by increasing the flow rate from 50 sL/min to 100 sL/min in case of 6 kW plasma power.

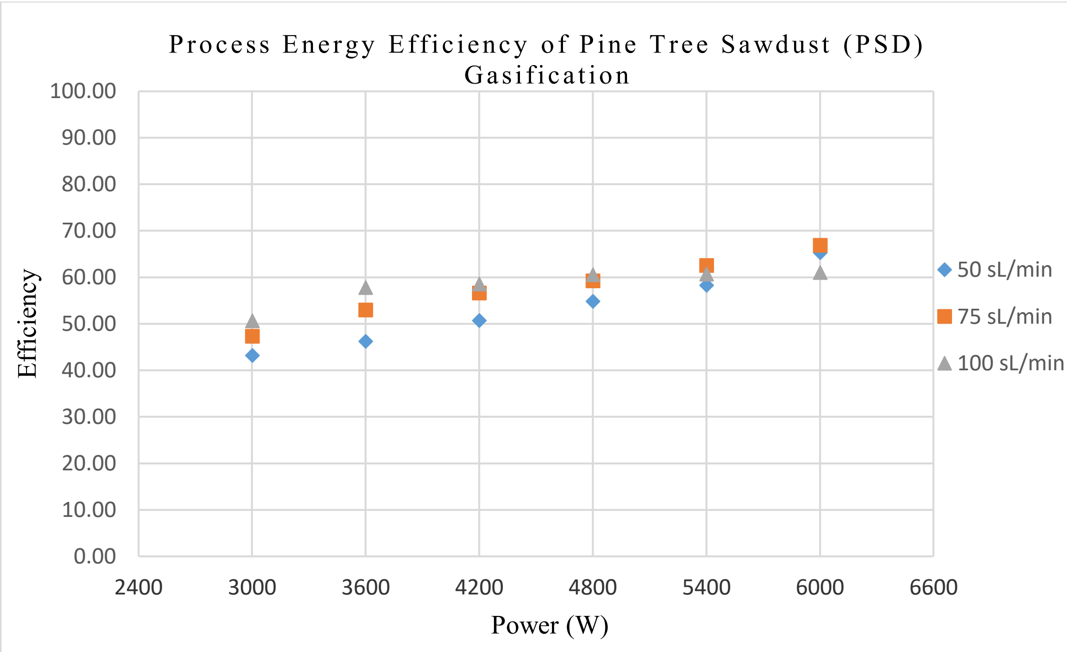

Figure 6.4 Process energy efficiency (η_{EP}) of pine tree sawdust (PSD) gasification in the cases of 50-100 sL/min air flow rate and 3-6 kW plasma power

System energy efficiency (η_{ES}) of the pine tree sawdust (PSD) in case of 50 sL/min, 75 sL/min and 100 sL/min for various plasma powers between 3 kW and 6 kW is presented in Figure 6.5. The system energy efficiency (η_{ES}) depends on the fuel energy, plasma energy and the syngas energy. The constant amount of fuel is dosed to the reactor in the each case. However, the plasma energy and syngas energy are varied depending on the plasma power and air flow rate. Increasing power lowers the gasification duration, reduces syngas production and increases the plasma energy consumption but it enhances the conversion of fuel to syngas and rises the syngas temperature. Similarly, increasing air flow rate lowers the gasification duration, reduces syngas production and lowers the plasma energy consumption. On the other hand, it reduces the syngas temperature and the conversion of fuel to syngas. As a result, increment of plasma power rises the system energy efficiency (η_{ES}). However, increasing air flow rate has lighter effect on the system energy efficiency (η_{ES}). In case of 50 sL/min air flow rate, system energy efficiency (η_{ES}) increases from 27.18 % to 36.22 % by increasing the plasma power from 3 kW to 6 kW. In case of 75 sL/min air flow rate, it increases from 31.91 % to 41.40 % by increasing the plasma power from 3 kW to 6 kW. In case of 100 sL/min air flow rate, it increases from 35.46 % to 38.38 % by increasing the plasma power from 3 kW to 6 kW. The system energy efficiency (η_{ES}) increases by increasing plasma power in all cases. However, the effect of plasma power to the system energy efficiency (η_{ES}) decreases by increasing the flow rate. The increment in efficiency is 33.25 % by increasing plasma power from 3 kW to 6 kW in 50 sL/min and it is 8.23 % by increasing plasma power from 3 kW to 6 kW in 100 sL/min. The magnitude of the system energy efficiency (η_{ES}) is less than the process energy efficiency (η_{EP}). Because, the plasma power increases the consumption of the system and it has negative effects to system energy efficiency (η_{ES}). Increasing air flow rate rises the system energy efficiency (η_{ES}) at 3 kW plasma power. However increasing air flow rate fluctuates the system energy efficiency (η_{ES}) at 6 kW plasma power. The system energy efficiency (η_{ES}) goes up from 27.18 % to 35.46 % by increasing the flow rate from 50 sL/min to 100 sL/min in case of 3 kW power and it fluctuates between 36.22 % and 41.40 % by increasing the flow rate from 50 sL/min to 100 sL/min in case of 6 kW plasma power.

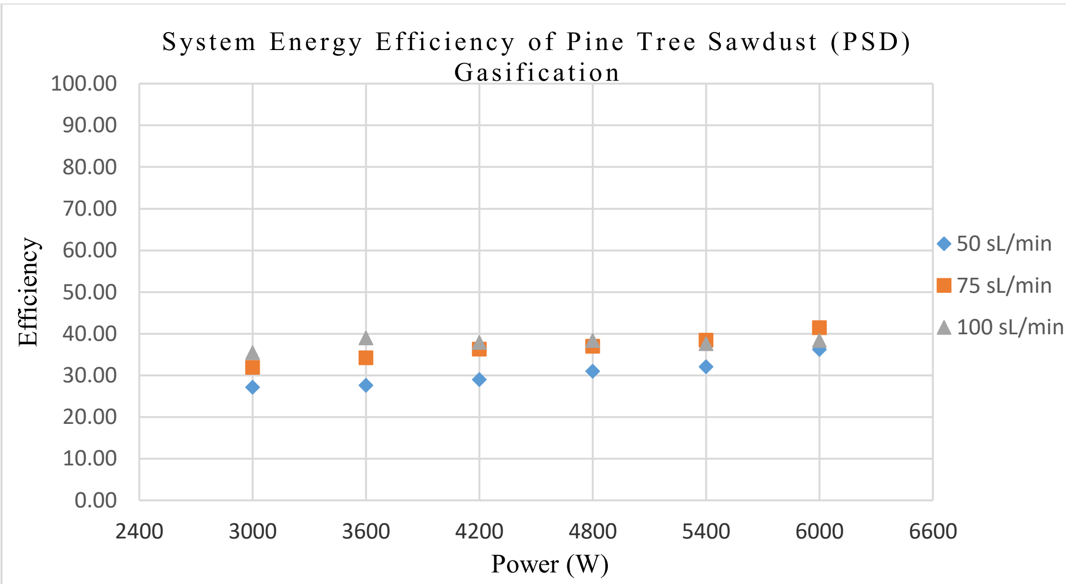

Figure 6.5 System energy efficiency of pine tree sawdust (PSD) gasification in the cases of 50-100 sL/min air flow rate and 3-6 kW plasma power

Hot gas efficiency (η_{HG}) of pine tree sawdust (PSD) in case of 50 sL/min, 75 sL/min and 100 sL/min for various plasma powers between 3 kW and 6 kW is given in Figure 6.6. The hot gas efficiency (η_{HG}) depends on the fuel energy, plasma energy and the syngas energy similar to the system energy efficiency (η_{ES}). In addition to system efficiency parameters, the syngas energy includes both the chemical energy of the solid fuel and sensible energy as a result of its high temperature in the hot gas efficiency (η_{HG}). The variation of the hot gas efficiency (η_{HG}) is similar with the system energy efficiency (η_{ES}). The magnitude of the hot gas efficiency (η_{HG}) is higher than the system energy efficiency (η_{ES}). Because, the sensible energy of the syngas is also considered in calculations of hot gas efficiency (η_{HG}). As a result, increment of plasma power rises the hot gas efficiency (η_{HG}). Also, increasing air flow rate increases the hot gas efficiency (η_{HG}).

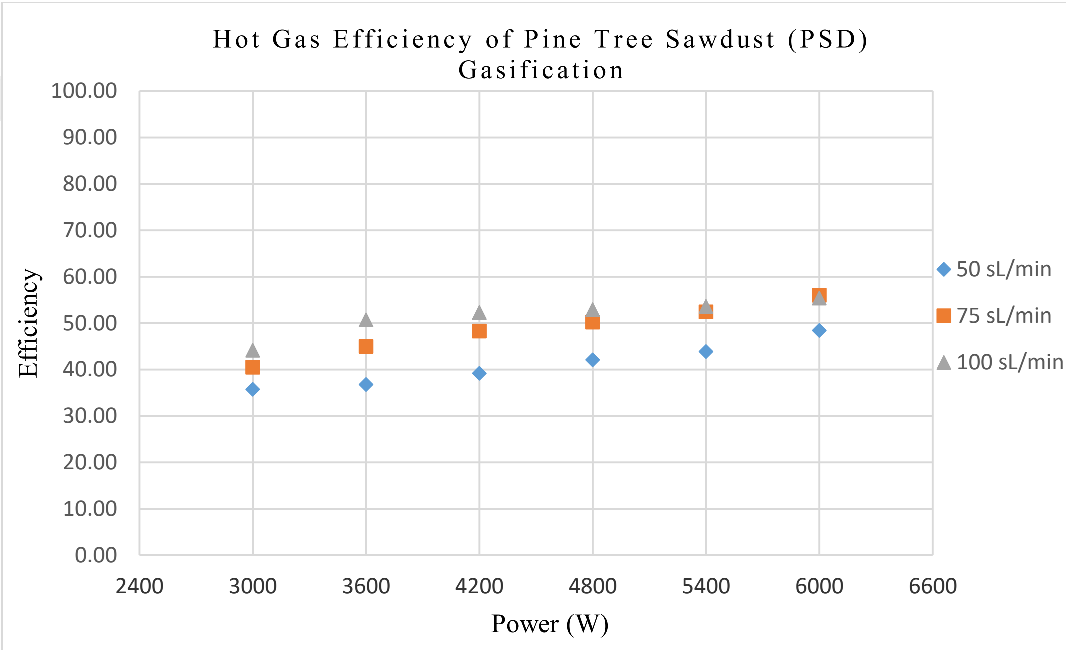

Figure 6.6 Hot gas efficiency (η_{HG}) of pine tree sawdust (PSD) gasification in the cases of 50-100 sL/min air flow rate and 3-6 kW plasma power

In case of 50 sL/min air flow rate, hot gas efficiency (η_{HG}) increases from 35.75 % to 48.41 % by increasing the plasma power from 3 kW to 6 kW. In case of 75 sL/min air flow rate, it goes up from 40.50 % to 56.01 % by increasing the plasma power from 3 kW to 6 kW. In case of 100 sL/min air flow rate, it increases from 44.16 % to 55.39 % by increasing the plasma power from 3 kW to 6 kW. Increasing plasma power rises the hot gas efficiency (η_{HG}) in all cases. Increasing air flow rate rises the hot gas efficiency (η_{HG}) in all plasma power levels. The hot gas efficiency (η_{HG}) goes up from 35.75 % to 44.16 % by increasing the flow rate from 50 sL/min to 100 sL/min in case of 3 kW power and it also rises from 48.41 % to 55.39 % by increasing the flow rate from 50 sL/min to 100 sL/min in case of 6 kW plasma power.

6.4 Thermodynamic analysis of Russian coal (CR) gasification process

In this section, thermodynamic performance of Russian coal (CR) gasification process is handled. The content conversion performance of syngas (CCP_{syn}), content conversion performance of ash (CCP_{ash}), content conversion performance of hydrogen (CCP_{H_2}), hydrogen quality of syngas (H_q), process energy efficiency (η_{EP}), system energy efficiency (η_{ES}) and hot gas efficiency (η_{HG}) are calculated for each case of the gasification of Russian coal (CR) for various powers from 3 kW to 6 kW and at 50 sL/min, 75 sL/min and 100 sL/min air flow rate. The results are presented in this section.

The CCP_{syn}, CCP_{ash}, CCP_{H_2}, H_q, syngas energy, fuel energy and plasma energy are given in the Table 6.4. The content conversion performance of syngas (CCP_{syn}) decreases by increasing plasma power in 50, 75 and 100 sL/min air flow rate cases. Because, the increasing power reduces the gasification time (tg). The supplied air amount to the reactor reduces due to the reduction of supplying air flow rate duration. As a result the produced syngas amount decreases while the supplied fuel amount is same. In case of 50 sL/min, it reduces from 482 % at 3 kW plasma power to 376 % at 6 kW plasma power. In case of 75 sL/min, it reduces from 560 % to 451 % by increasing plasma power from 3 kW to 6 kW. In case of 100 sL/min, it reduces from 655 % to 571 % by increasing plasma power from 3 kW to 6 kW. On the other hand, increasing air flow rate causes the increment of content conversion performance of syngas (CCP_{syn}). It goes up from 482 % to 655 % by increasing air flow rate from 50 sL/min to 100 sL/min at 3 kW power. Similarly, it increases from 376 % to 571 % by increasing air flow rate from 50 sL/min to 100 sL/min at 6 kW power.

The content conversion performance of ash (CCP_{ash}) decreases by increasing the plasma power in 50, 75 and 100 sL/min air flow rate cases because of the enhancement of solid fuel conversion to syngas by increasing plasma power. Higher solid fuel conversion to syngas means less ash output from the reactor. On the other hand, the air flow rate increases the content conversion performance of ash (CCP_{ash}). Because, increasing air flow reduces the temperature in reactor and the conversion of solid fuel to syngas. As a result, less syngas production and high ash are produced. In case of 50 sL/min, it goes down from 20.93 % at 3 kW power to 15.71 % at 6 kW power. In case of 75 sL/min, it decreases from 25.28 % to 16.34 % by increasing power from 3 kW to 6 kW. In case of 100 sL/min, it reduces from 29.52 % to 18.8 % by increasing power from 3 kW to 6 kW. On the other hand, increasing air flow rate causes the increment of content conversion performance of ash (CCP_{ash}). It goes up from 20.93 % to 29.52 % by increasing air flow rate from 50 sL/min to 100 sL/min at 3 kW power. Similarly, it increases from 15.71 % to 18.8 % by increasing air flow rate from 50 sL/min to 100 sL/min at 6 kW power.

The content conversion performance of hydrogen (CCP_{H_2}) stays almost constant by increasing the plasma power in 50, 75 and 100 sL/min air flow rate cases. Because the Russian coal (CR) has lack of hydrogen content. Even increasing plasma power or air flow rate change the syngas temperature and the conversion of solid fuel to syngas, hydrogen content in syngas is limited due to the lack of hydrogen in solid fuel. As a result, the hydrogen content is varied insignificantly. In case of 50 sL/min, it stays in level of 0.49 % - 0.52 % at plasma power between 3 kW and 6 kW. In case of 75 sL/min, it stays in level of 0.55 % - 0.57 % at plasma power between 3 kW and 6 kW. In case of 100 sL/min, it stays in level between 0.44 % and 0.51 % at plasma power between 3 kW and 6 kW. On the other hand, the content conversion performance of hydrogen (CCP_{H_2}) is fluctuated by increasing air flow rate. It fluctuates in level between 0.44 % and 0.55 % by change of air flow rate from 50 sL/min to 100 sL/min at 3 kW plasma power. In case of 6 kW plasma power, it fluctuates in level between 0.50 % and 0.57 % by change of air flow rate from 50 sL/min to 100 sL/min

Hydrogen quality of syngas (H_q) increases by increasing power in 50, 75 and 100 sL/min air flow rate cases. Because, the hydrogen production is proportional with the temperature in the reactor. The temperature increases by increasing plasma power. However, increasing air flow rate reduces the hydrogen quality of syngas (H_q). Because the air flow rate is inversely proportional with the temperature in the reactor. In case of 50 sL/min, it increases from 0.10 % at 3 kW power to 0.13 % at 6 kW power. In case of 75 sL/min, it goes up from 0.10 % to 0.13 % by increasing power from 3 kW to 6 kW. In case of 100 sL/min, it rises from 0.07 % to 0.09 % by increasing power from 3 kW to 6 kW. However, increasing air flow rate reduces the hydrogen quality of syngas (H_q). It decreases from 0.10 % to 0.07 % by increasing air flow rate from 50 sL/min to 100 sL/min at 3 kW power. Also, it reduces from 0.13 % to 0.09 % by increasing air flow rate from 50 sL/min to 100 sL/min at 6 kW power.

Table 6.4 Presentation of the CCP_{syn}, CCP_{ash}, CCP_{H_2}, syngas energy, fuel energy and plasma energy results for the Russian coal (CR) gasification process for various powers and flow rates

	Plasma Power (W)	CCP_{syn} (%)	CCP_{ash} (%)	CCP_{H_2} (%)	H_q (%)	Syngas energy (kJ)	Fuel energy (kJ)	Plasma energy (kJ)
Russian coal-50sL/min	3000	482	20.93	0.50	0.10	5421	7834	3060
	3600	459	20.07	0.49	0.11	5300		3456
	4200	444	19.29	0.51	0.11	5136		3864
	4800	413	18.15	0.51	0.12	4883		4032
	5400	399	16.46	0.52	0.13	4852		4320
	6000	376	15.71	0.50	0.13	4556		4440
Russian coal-75sL/min	3000	560	25.28	0.55	0.10	5821		2460
	3600	544	23.25	0.55	0.10	5840		2844
	4200	522	21.85	0.57	0.11	5710		3150
	4800	496	18.49	0.56	0.11	5614		3360
	5400	485	17.46	0.57	0.12	5553		3672
	6000	451	16.34	0.57	0.13	5250		3720
Russian coal-100sL/min	3000	655	29.52	0.44	0.07	6170		2220
	3600	633	27.50	0.46	0.07	6059		2556
	4200	612	24.50	0.47	0.08	6013		2856
	4800	598	22.48	0.48	0.08	5861		3168
	5400	585	20.52	0.50	0.09	5880		3456
	6000	571	18.80	0.51	0.09	5869		3720

Syngas energy goes down by increasing plasma power in 50, 75 and 100 sL/min air flow rate cases. Because, the syngas energy depends on the syngas production and syngas content especially percentage of CO, H_2 and CH_4. Syngas production reduces by increasing plasma power. Percentage of CO and H_2 increases while CH_4 remains same or slightly reduces by increasing plasma power. As a result, the syngas energy reduces by increasing the power. Also, syngas production reduces by increasing air flow rate and percentage of CO and H_2 reduces while percentage of CH_4 increases by increasing air flow rate. The production amount and the distribution of syngas effects the syngas energy. In case of 50 sL/min, syngas energy decreases from 5421 kJ at 3 kW plasma power to 4556 kJ at 6 kW plasma power. In case of 75 sL/min, syngas energy reduces from 5821 kJ at 3 kW plasma power to 5250 kJ at 6 kW plasma power. In case of 100 sL/min, syngas energy lowers from 6170 kJ at 3 kW plasma power to 5869 kJ at 6 kW plasma power. The energy of 250 g Russian coal (CR) fuel is 7834 kJ. On the other hand, the syngas energy increases from 5421 kJ to 6170 kJ by increasing air flow rate from 50 sL/min to 100 sL/min at 3 kW power. The syngas energy rises from 4556 kJ to 5869 kJ by increasing air flow rate from 50 sL/min to 100 sL/min at 6 kW power.

Process energy efficiency (η_{EP}) of Russian coal (CR) in case of 50 sL/min, 75 sL/min and 100 sL/min for various plasma powers between 3 kW and 6 kW are presented in Figure 6.7. Process energy efficiency (η_{EP}) reduces by increasing the plasma power while it increases by increasing air flow rate. The input energy is just the fuel energy in the case of process energy efficiency (η_{EP}). So, the syngas energy is the only one parameter which effects the process energy efficiency (η_{EP}). However, the relation between syngas energy, plasma power, and air flow rate are sophisticated to define the relation. Increasing power lowers the gasification duration and reduces the syngas production, but it enhances the conversion of fuel to syngas and rises the syngas temperature.

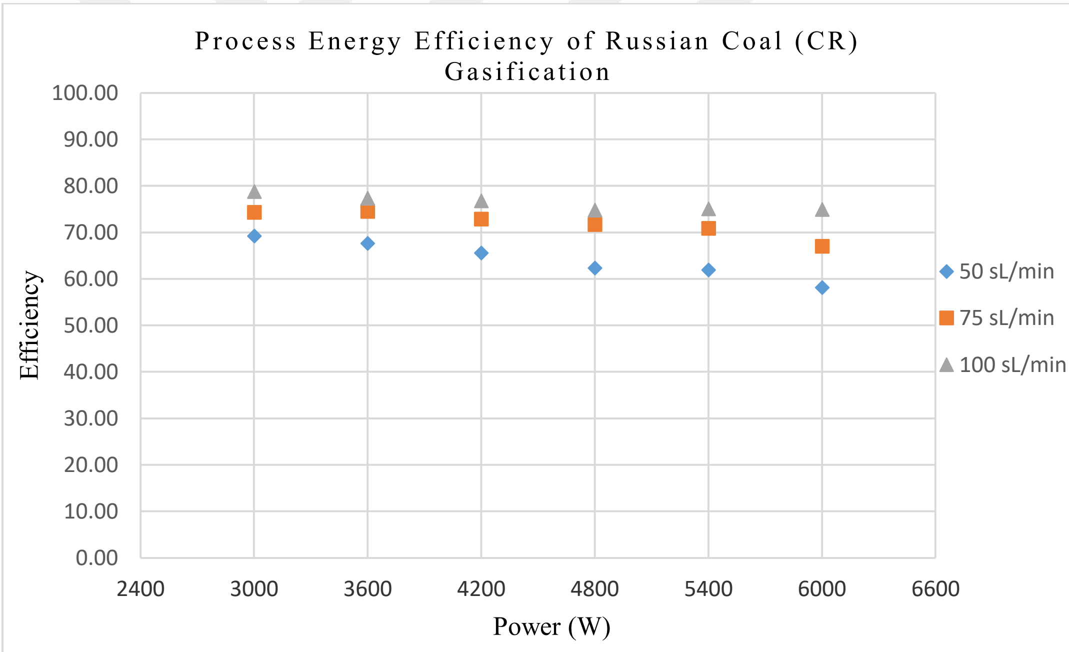

Figure 6.7 Process energy efficiency (η_{EP}) of Russian coal (CR) gasification in the cases of 50-100 sL/min air flow rate and 3-6 kW plasma power

Similarly, increasing air flow rate lowers the gasification duration and it reduces the syngas production. Also, it reduces the syngas temperature and the conversion of fuel to syngas. As a result, increment of plasma power lowers the process energy efficiency (η_{EP}). However, increasing air flow rate rises the process energy efficiency (η_{EP}). In case of 50 sL/min air flow rate, process energy efficiency (η_{EP}) goes down from 69.19 % to 58.16 % by increasing the plasma power from 3 kW to 6 kW. In case of 75 sL/min air flow rate, it slightly decreases from 74.31 % to 67.01 % by increasing the plasma power from 3 kW to 6 kW. In case of 100 sL/min air flow rate, it also slightly decreases from 78.76 % to 74.92 % by increasing the plasma power from 3 kW to 6 kW. Increasing plasma power reduces the process energy efficiency (η_{EP}). While the reduction in efficiency is 15.94 % by increasing plasma power from 3 kW to 6 kW in 50 sL/min, it is 4.87 % by increasing plasma power from 3 kW to 6 kW in 100 sL/min. The increment in air flow rate rises the process energy efficiency (η_{EP}) at 3 kW plasma power. Also, increasing air flow rate increases the process energy efficiency (η_{EP}) at 6 kW plasma power. The process energy efficiency (η_{EP}) goes up from 69.19 % to 78.76 % by increasing the flow rate from 50 sL/min to 100 sL/min in case of 3 kW power and it goes up from 58.16 % to 74.92 % by increasing the flow rate from 50 sL/min to 100 sL/min in case of 6 kW plasma power.

System energy efficiency (η_{ES}) of the Russian coal (CR) in case of 50 sL/min, 75 sL/min and 100 sL/min for various plasma powers between 3 kW and 6 kW are given in Figure 6.8. The system energy efficiency (η_{ES}) depends on the fuel energy, plasma energy and the syngas energy. The constant amount of fuel is dosed to the reactor in the each case. However, the plasma energy and syngas energy are varied depending on the plasma power and air flow rate. Increasing power lowers the gasification duration, reduces syngas production and increases the plasma energy consumption but it enhances the conversion of fuel to syngas and rises the syngas temperature. Similarly, increasing air flow rate lowers the gasification duration, reduces syngas production and lowers the plasma energy consumption. On the other hand, it reduces the syngas temperature and the conversion of fuel to syngas. As a result, increment of plasma power lowers the system energy efficiency (η_{ES}). However, increasing air flow rate reduces the system energy efficiency (η_{ES}). In case of 50 sL/min air flow rate, system energy efficiency (η_{ES}) reduces from 49.76 % to 37.12 % by increasing the plasma power from 3 kW to 6 kW. In case of 75 sL/min air flow rate, it goes down from 56.55 % to 45.43 % by increasing the plasma power from 3 kW to 6 kW. In case of 100 sL/min air flow rate, it decreases from 61.37 % to 50.80 % by increasing the plasma power from 3 kW to 6 kW. Increasing plasma power reduces the system energy efficiency (η_{ES}) in all cases. Also, the effect of plasma power to the system energy efficiency (η_{ES}) decreases by increasing the flow rate. The reduction in efficiency is 25.40 % by increasing plasma power from 3 kW to 6 kW in 50 sL/min and it is 17.22 % by increasing plasma power from 3 kW to 6 kW in 100 sL/min. The magnitude of the system energy efficiency (η_{ES}) is less than the process energy efficiency (η_{EP}). Because, the plasma power increases the consumption of the system and it has negative effects to system energy efficiency (η_{ES}). The increment of air flow rate rises the system energy efficiency (η_{ES}) at all plasma power levels. The system energy efficiency (η_{ES}) goes up from 49.76 % to 61.37 % by increasing the flow rate from 50 sL/min to 100 sL/min in case of 3 kW power and it rises from 37.12 % and 50.80 % by increasing the flow rate from 50 sL/min to 100 sL/min in case of 6 kW plasma power.

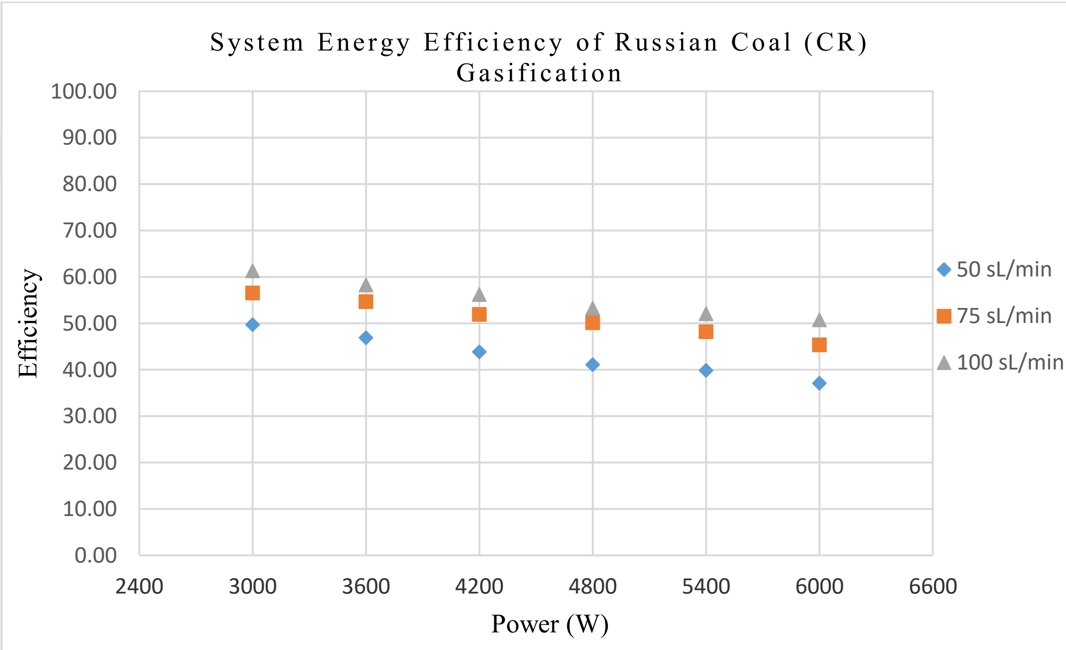

Figure 6.8 System energy efficiency of Russian coal (CR) gasification in the cases of 50-100 sL/min air flow rate and 3-6 kW plasma power

Hot gas efficiency (η_{HG}) of Russian coal (CR) in case of 50 sL/min, 75 sL/min and 100 sL/min for various plasma powers between 3 kW and 6 kW are given in Figure 6.9. The hot gas efficiency (η_{HG}) depends on the fuel energy, plasma energy and the syngas energy similar to the system energy efficiency (η_{ES}). In addition to system efficiency parameters, the syngas energy includes both the chemical energy of the solid fuel and sensible energy as a result of its high temperature in the hot gas efficiency (η_{HG}). The variation of the hot gas efficiency (η_{HG}) is similar with the system energy efficiency (η_{ES}). The magnitude of the hot gas efficiency (η_{HG}) is higher than the system energy efficiency (η_{ES}). Because, the sensible energy of the syngas is also considered in calculations of hot gas efficiency (η_{HG}). As a result, increment of plasma power lowers the hot gas efficiency (η_{HG}). However, increasing air flow rate increases the hot gas efficiency (η_{HG}). In case of 50 sL/min air flow rate, hot gas efficiency (η_{HG}) goes down from 56.59 % to 46.72 % by increasing the plasma power from 3 kW to 6 kW. In case of 75 sL/min air flow rate, it reduces from 63.32 % to 57.30 % by increasing the plasma power from 3 kW to 6 kW. In case of 100 sL/min air flow rate, it decreases from 67.92 % to 64.99 % by increasing the plasma power from 3 kW to 6 kW. Increasing plasma power cut down the hot gas efficiency (η_{HG}) in all cases. However, the reduction decreases by increasing the flow rate. While the reduction is 17.44 % by increasing power from 3 kW to 6 kW in case of 50 sL/min air flow rate, it is 4.31 % by increasing power from 3 kW to 6 kW in case of 100 sL/min air flow rate. The increment of air flow rate rises the hot gas efficiency (η_{HG}) in all plasma power levels. The hot gas efficiency (η_{HG}) goes up from 56.59 % to 67.92 % by increasing the flow rate from 50 sL/min to 100 sL/min in case of 3 kW power and it also rises from 46.72 % to 64.99 % by increasing the flow rate from 50 sL/min to 100 sL/min in case of 6 kW plasma power.

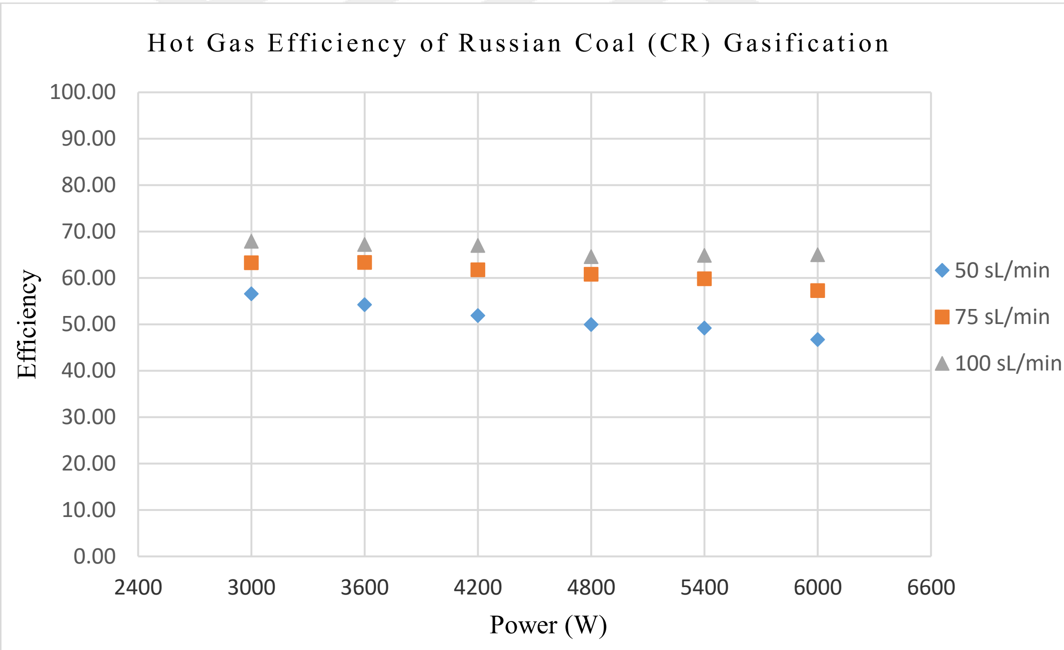

Figure 6.9 Hot gas efficiency (η_{HG}) of Russian coal (CR) gasification in the cases of 50-100 sL/min air flow rate and 3-6 kW plasma power

6.5 Thermodynamic analysis of South African coal (CSA) gasification process

In this section, thermodynamic performance of South African coal (CSA) gasification process is handled. The content conversion performance of syngas (CCP_{syn}), content conversion performance of ash (CCP_{ash}), content conversion performance of hydrogen

(CCP_{H_2}), hydrogen quality of syngas (H_q), process energy efficiency (η_{EP}), system energy efficiency (η_{ES}) and hot gas efficiency (η_{HG}) are calculated for each case of the gasification of South African coal (CSA) for various powers from 3 kW to 6 kW and at 50 sL/min, 75 sL/min and 100 sL/min air flow rate. The results are presented in this section.

The CCP_{syn}, CCP_{ash}, CCP_{H_2}, H_q, syngas energy, fuel energy and plasma energy are given in the Table 6.5. The content conversion performance of syngas (CCP_{syn}) decreases by increasing plasma power in 50, 75 and 100 sL/min air flow rate cases. Because, the increasing power reduces the gasification time (tg). The supplied air amount to the reactor reduces due to the reduction of supplying air flow rate duration. As a result the produced syngas amount decreases while the supplied fuel amount is same. In case of 50 sL/min, it reduces from 476 % at 3 kW plasma power to 382 % at 6 kW plasma power. In case of 75 sL/min, it reduces from 546 % to 435 % by increasing plasma power from 3 kW to 6 kW. In case of 100 sL/min, it reduces from 653 % to 511 % by increasing plasma power from 3 kW to 6 kW. On the other hand, the increment of air flow rate causes the increment of content conversion performance of syngas (CCP_{syn}). It goes up from 476 % to 653 % by increasing air flow rate from 50 sL/min to 100 sL/min at 3 kW power. Similarly, it increases from 382 % to 511 % by increasing air flow rate from 50 sL/min to 100 sL/min at 6 kW power.

The content conversion performance of ash (CCP_{ash}) decreases by increasing the plasma power in 50, 75 and 100 sL/min air flow rate cases because of the enhancement of solid fuel conversion to syngas by increasing plasma power. Higher solid fuel conversion to syngas means less ash output from the reactor. On the other hand, the air flow rate increases the content conversion performance of ash (CCP_{ash}). Because, increasing air flow reduces the temperature in reactor and the conversion of solid fuel to syngas. As a result, less syngas production and high ash are produced. In case of 50 sL/min, it goes down from 22.48 % at 3 kW power to 17.67 % at 6 kW power. In case of 75 sL/min, it decreases from 27.37 % to 19.91 % by increasing power from 3 kW to 6 kW. In case of 100 sL/min, it reduces from 31.07 % to 23.55 % by increasing power from 3 kW to 6 kW. On the other hand, the increment of air flow rate causes the increment of content conversion performance of ash (CCP_{ash}). It goes up from 22.48 % to 31.07 % by increasing air flow rate from 50 sL/min to 100 sL/min at 3 kW power. Similarly, it increases from 17.67 % to 23.55 % by increasing air flow rate from 50 sL/min to 100 sL/min at 6 kW power.

Table 6.5 Presentation of the CCP_{syn}, CCP_{ash}, CCP_{H_2}, syngas energy, fuel energy and plasma energy results for the South African coal (CSA) gasification process for various powers and flow rates

	Plasma Power (W)	CCP_{syn} (%)	CCP_{ash} (%)	CCP_{H_2} (%)	H_q (%)	Syngas energy (kJ)	Fuel energy (kJ)	Plasma energy (kJ)
South African coal-50sL/min	3000	476	22.48	0.53	0.11	4821		3030
	3600	461	21.29	0.52	0.11	4624		3492
	4200	439	20.46	0.53	0.12	4442		3822
	4800	424	19.34	0.55	0.13	4246		4176
	5400	389	18.49	0.53	0.14	4193		4212
	6000	382	17.67	0.54	0.14	4041		4560
South African coal-75sL/min	3000	546	27.37	0.61	0.11	5301		2400
	3600	524	25.72	0.60	0.12	5227		2736
	4200	502	23.72	0.61	0.12	5116	7690	3024
	4800	468	22.53	0.60	0.13	4951		3168
	5400	452	20.75	0.61	0.13	4819		3402
	6000	435	19.91	0.62	0.14	4711		3600
South African coal-100sL/min	3000	653	31.07	0.69	0.10	5498		2220
	3600	623	29.33	0.70	0.11	5459		2520
	4200	601	27.99	0.71	0.12	5324		2814
	4800	571	26.11	0.71	0.13	5127		3024
	5400	541	24.86	0.73	0.13	5080		3186
	6000	511	23.55	0.71	0.14	4945		3300

The content conversion performance of hydrogen (CCP_{H_2}) stays almost constant by increasing the plasma power in 50, 75 and 100 sL/min air flow rate cases. Because the South African coal (CSA) has lack of hydrogen content. Even increasing plasma power changes the syngas temperature and the conversion of solid fuel to syngas, hydrogen content in syngas is limited due to the lack of hydrogen in solid fuel. As a result, the hydrogen content is varied insignificantly. In case of 50 sL/min, it stays in level of 0.52 % - 0.55 % at plasma power between 3 kW and 6 kW. In case of 75 sL/min, it stays in level of 0.6 % - 0.62 % at plasma power between 3 kW and 6 kW. In case of 100 sL/min, it stays in level between 0.69 % and 0.73 % at plasma power between 3 kW and 6 kW. On the other hand, the content conversion performance of hydrogen (CCP_{H_2}) goes up by the increment of air flow rate. Because, increasing air flow rate rises the syngas production and it also increases the hydrogen production. It increases from 0.53 % to 0.69 % by increasing air flow rate from 50 sL/min to 100 sL/min at 3 kW plasma power. Also, it increases from 0.54 % to 0.71 % by increasing air flow rate from 50 sL/min to 100 sL/min at 6 kW plasma power.

Hydrogen quality of syngas (H_q) increases by increasing power in 50, 75 and 100 sL/min air flow rate cases. Because, the hydrogen production is proportional with the temperature in the reactor. The temperature increases by increasing plasma power. However, increasing air flow rate has insignificant effect on the hydrogen quality of syngas (H_q). In case of 50 sL/min, it increases from 0.11 % at 3 kW power to 0.14 % at 6 kW power. In case of 75 sL/min, it goes up from 0.11 % to 0.14 % by increasing power from 3 kW to 6 kW. In case of 100 sL/min, it rises from 0.10 % to 0.14 % by increasing power from 3 kW to 6 kW. However, the hydrogen quality of syngas (H_q) stays almost constant at varied flow rates at level of 0.11 % between 50 sL/min and 100 sL/min at 3kW plasma power. Similarly, it stays constant at varied flow rates at level of 0.14 % between 50 sL/min and 100 sL/min at 6 kW plasma power.

Syngas energy lowers by increasing plasma power in 50, 75 and 100 sL/min air flow rate cases. Because, the syngas energy depends on the syngas production and syngas content especially percentage of CO, H_2 and CH_4. Syngas production reduces by increasing plasma power. Percentage of CO and H_2 increases while CH_4 remains same or slightly reduces by increasing plasma power. As a result, the syngas energy reduces by increasing the power. Also, syngas production reduces by increasing air flow rate and percentage of CO and H_2 reduces while percentage of CH_4 increases by increasing air flow rate. The production amount and the distribution of syngas effects the syngas energy. In case of 50 sL/min, syngas energy decreases from 4821 kJ at 3 kW plasma power to 4041 kJ at 6 kW plasma power. In case of 75 sL/min, syngas energy reduces from 5301 kJ at 3 kW plasma power to 4711 kJ at 6 kW plasma power. In case of 100 sL/min, syngas energy reduces from 5498 kJ at 3 kW plasma power to 4945 kJ at 6 kW plasma power. The energy of 250 g South African coal (CSA) fuel is 7690 kJ. On the other hand, the syngas energy increases from 4821 kJ to 5498 kJ by increasing air flow rate from 50 sL/min to 100 sL/min at 3 kW power. The syngas energy rises from 4041 kJ to 4945 kJ by increasing air flow rate from 50 sL/min to 100 sL/min at 6 kW power.

Process energy efficiency (η_{EP}) of the South African coal (CSA) in case of 50 sL/min, 75 sL/min and 100 sL/min for various plasma powers between 3 kW and 6 kW are given in Figure 6.10. Process energy efficiency (η_{EP}) reduces by increasing the plasma power while it increases by increasing air flow rate. The input energy is just the fuel energy in the case of process energy efficiency (η_{EP}). So, the syngas energy is the only one parameter which effects the process energy efficiency (η_{EP}). However, the relation between syngas energy, plasma power, and air flow rate are sophisticated to define the relation. Increasing power lowers the gasification duration and reduces the syngas production, but it enhances the conversion of fuel to syngas and rises the syngas temperature. Similarly, increasing air flow rate lowers the gasification duration and it reduces the syngas production. Also, it reduces the syngas temperature and the conversion of fuel to syngas. As a result, increment of plasma power lowers the process energy efficiency (η_{EP}). However, increasing air flow rate rises the process energy efficiency (η_{EP}). In case of 50 sL/min air flow rate, process energy efficiency (η_{EP}) cut down from 62.69 % to 52.55 % by increasing the plasma power from 3 kW to 6 kW. In case of 75 sL/min air flow rate, it slightly declines from 68.94 % to 61.26 % by increasing the plasma power from 3 kW to 6 kW. In case of 100 sL/min air flow rate, it also slightly decreases from 71.5 % to 64.31 % by increasing the plasma power from 3 kW to 6 kW. Increasing plasma power lowers the process energy efficiency (η_{EP}). While the decrease in efficiency is 16.17 % by increasing plasma power from 3 kW to 6 kW in 50 sL/min, it is 10.05 % by increasing plasma power from 3 kW to 6 kW in 100 sL/min. The increment of air flow rate rises the process energy efficiency (η_{EP}) at 3 kW plasma power. Also, increasing air flow rate rises the process energy efficiency (η_{EP}) at 6 kW plasma power. The process energy efficiency (η_{EP}) goes up from 62.69 % to 71.50 % by increasing the flow rate from 50 sL/min to 100 sL/min in case of 3 kW power and it goes up from 52.55 % to 64.31 % by increasing the flow rate from 50 sL/min to 100 sL/min in case of 6 kW plasma power.

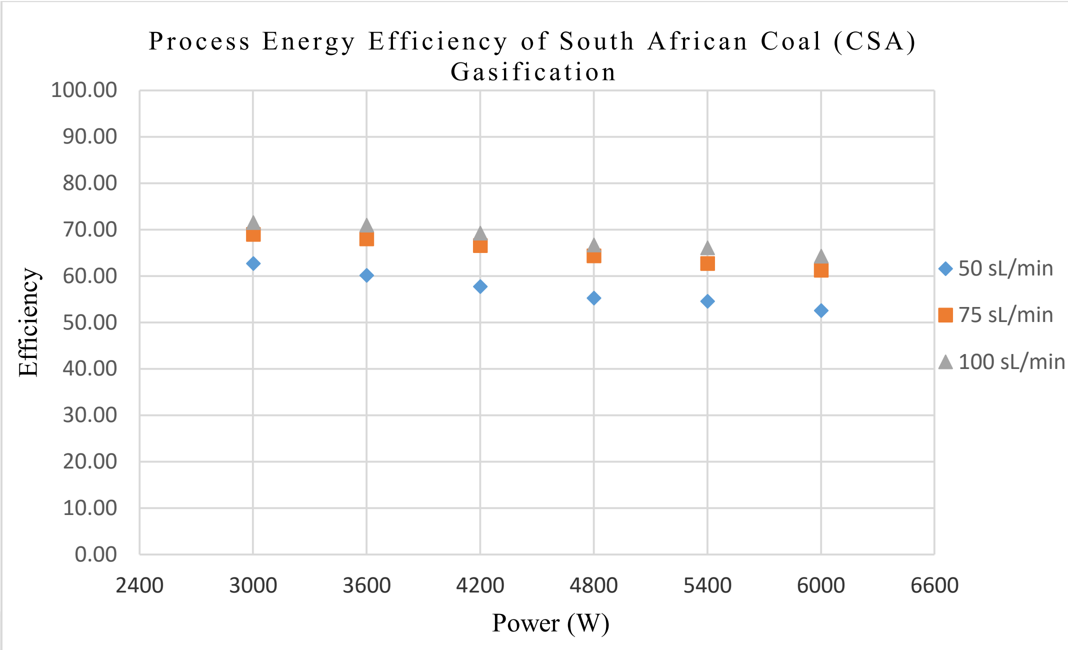

Figure 6.10 Process energy efficiency (η_{EP}) of South African coal (CSA) gasification in the cases of 50-100 sL/min air flow rate and 3-6 kW plasma power

System energy efficiency (η_{ES}) of the South African coal (CSA) in case of 50 sL/min, 75 sL/min and 100 sL/min for various plasma powers between 3 kW and 6 kW are given in Figure 6.11. The system energy efficiency (η_{ES}) depends on the fuel energy, plasma energy and the syngas energy. The constant amount of fuel is dosed to the reactor in the each case. However, the plasma energy and syngas energy are varied depending on the plasma power and air flow rate. Increasing power lowers the gasification duration, reduces syngas production and increases the plasma energy consumption but it enhances the conversion of fuel to syngas and rises the syngas temperature. Similarly, increasing air flow rate lowers the gasification duration, reduces syngas production and lowers the plasma energy consumption. On the other hand, it reduces the syngas temperature and the conversion of fuel to syngas. As a result, increment of plasma power lowers the system energy efficiency (η_{ES}). However, increasing air flow rate enhances the system energy efficiency (η_{ES}). In case of 50 sL/min air flow rate, system energy efficiency (η_{ES}) cut down from 44.97 % to 32.99 % by increasing the plasma power from 3 kW to 6 kW. In case of 75 sL/min air flow rate, it decreases from 52.54 % to 41.73 % by increasing the plasma power from 3 kW to 6 kW. In case of 100 sL/min air flow rate, it reduces from 55.48 % to 45.00 % by increasing the plasma power from 3 kW to 6 kW. Increasing plasma power declines the system energy efficiency (η_{ES}) in all cases. Also, the effect of plasma power to the system energy efficiency (η_{ES}) decreases by increasing the flow rate. The reduction in efficiency is 26.63 % by increasing plasma power from 3 kW to 6 kW in 50 sL/min and it is 18.88 % by increasing plasma power from 3 kW to 6 kW in 100 sL/min. The magnitude of the system energy efficiency (η_{ES}) is less than the process energy efficiency (η_{EP}). Because, the plasma power rises the consumption of the system and it has negative effects to system energy efficiency (η_{ES}). The increment of air flow rate increases the system energy efficiency (η_{ES}) at all plasma power levels. The system energy efficiency (η_{ES}) goes up from 44.97 % to 55.48 % by increasing the flow rate from 50 sL/min to 100 sL/min in case of 3 kW power and it rises from 32.99 % and 45.00 % by increasing the flow rate from 50 sL/min to 100 sL/min in case of 6 kW plasma power.

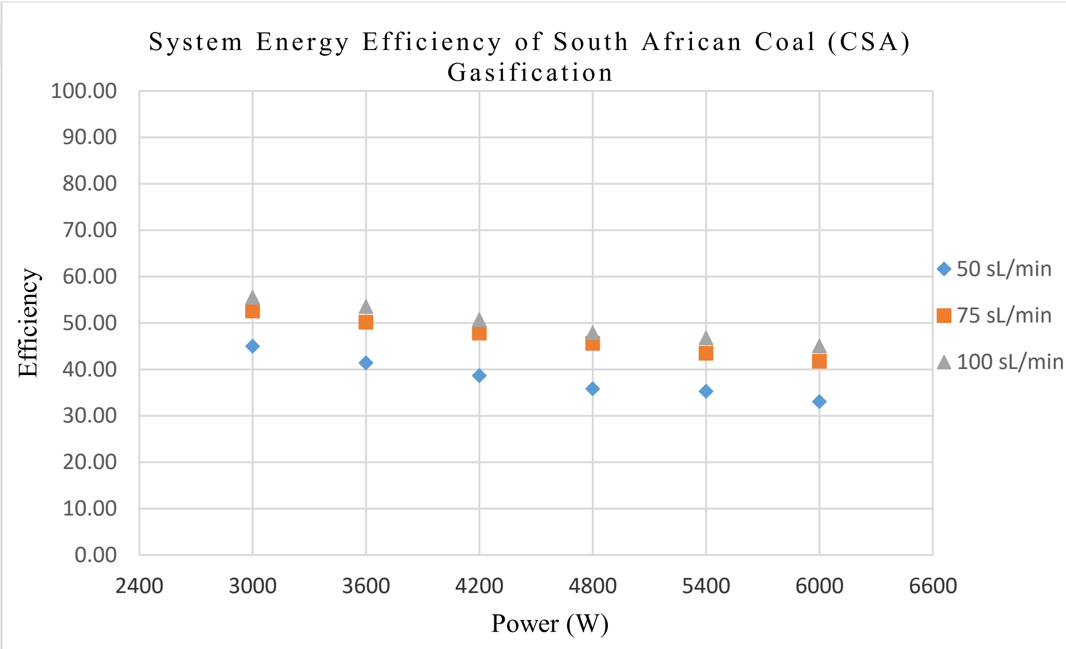

Figure 6.11 System energy efficiency of South African coal (CSA) gasification in the cases of 50-100 sL/min air flow rate and 3-6 kW plasma power

Hot gas efficiency (η_{HG}) of South African coal (CSA) in case of 50 sL/min, 75 sL/min and 100 sL/min for various plasma powers between 3 kW and 6 kW are given in Figure 6.12. The hot gas efficiency (η_{HG}) depends on the fuel energy, plasma energy and the syngas energy similar to the system energy efficiency (η_{ES}). In addition to system efficiency parameters, the syngas energy includes both the chemical energy of the solid fuel and sensible energy as a result of its high temperature in the hot gas efficiency (η_{HG}). The variation of the hot gas efficiency (η_{HG}) is similar with the system energy efficiency (η_{ES}). The magnitude of the hot gas efficiency (η_{HG}) is higher than the system energy efficiency (η_{ES}). Because, the sensible energy of the syngas is also considered in calculations of hot gas efficiency (η_{HG}). As a result, increment of plasma power reduces the hot gas efficiency (η_{HG}). However, increasing air flow rate increases the hot gas efficiency (η_{HG}). In case of 50 sL/min air flow rate, hot gas efficiency (η_{HG}) goes down from 51.77 % to 42.64 % by increasing the plasma power from 3 kW to 6 kW. In case of 75 sL/min air flow rate, it reduces from 59.19 % to 53.28 % by increasing the plasma power from 3 kW to 6 kW. In case of 100 sL/min air flow rate, it cut down from 62.06 % to 58.20 % by increasing the plasma power from 3 kW to 6 kW. Increasing plasma power reduces the hot gas efficiency (η_{HG}) in all cases. However, the reduction decreases by increasing the flow rate. While the reduction is 17.63 % by increasing power from 3 kW to 6 kW in case of 50 sL/min air flow rate, it is 6.22 % by increasing power from 3 kW to 6 kW in case of 100 sL/min air flow rate. The increment of air flow rate increases the hot gas efficiency (η_{HG}) in all plasma power levels. The hot gas efficiency (η_{HG}) goes up from 51.77 % to 62.06 % by increasing the flow rate from 50 sL/min to 100 sL/min in case of 3 kW power and it also rises from 42.64 % to 58.20 % by increasing the flow rate from 50 sL/min to 100 sL/min in case of 6 kW plasma power.

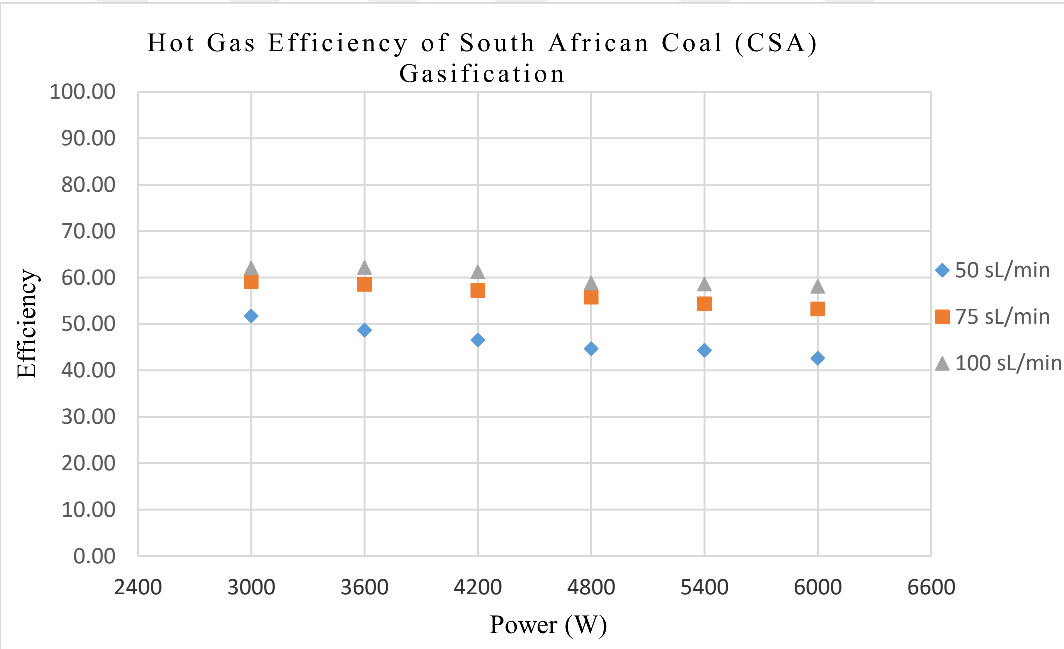

Figure 6.12 Hot gas efficiency (η_{HG}) of South African coal (CSA) gasification in the cases of 50-100 sL/min air flow rate and 3-6 kW plasma power

6.6 Thermodynamic analysis of Şırnak (Turkey) coal (CTR) gasification process

In this section, thermodynamic performance of Şırnak (Turkey) coal (CTR) gasification process is handled. The content conversion performance of syngas

(CCP_{syn}), content conversion performance of ash (CCP_{ash}), content conversion performance of hydrogen (CCP_{H_2}), hydrogen quality of syngas (H_q), process energy efficiency (η_{EP}), system energy efficiency (η_{ES}) and hot gas efficiency (η_{HG}) are calculated for each case of the gasification of Şırnak (Turkey) coal (CTR) for various plasma powers from 3 kW to 6 kW and at 50 sL/min, 75 sL/min and 100 sL/min air flow rate. The results are presented in this section.

The CCP_{syn}, CCP_{ash}, CCP_{H_2}, H_q, syngas energy, fuel energy and plasma energy are given in the Table 6.6. The content conversion performance of syngas (CCP_{syn}) decreases by increasing plasma power in 50, 75 and 100 sL/min air flow rate cases. Because, the increasing power reduces the gasification time (tg). The supplied air amount to the reactor reduces due to the reduction of supplying air flow rate duration. As a result the produced syngas amount decreases while the supplied fuel amount is same. In case of 50 sL/min, it reduces from 419 % at 3 kW plasma power to 380 % at 6 kW plasma power. In case of 75 sL/min, it reduces from 489 % to 431 % by increasing plasma power from 3 kW to 6 kW. In case of 100 sL/min, it reduces from 608 % to 501 % by increasing plasma power from 3 kW to 6 kW. On the other hand, the increment of air flow rate causes the increment of content conversion performance of syngas (CCP_{syn}). It goes up from 419 % to 608 % by increasing air flow rate from 50 sL/min to 100 sL/min at 3 kW power. Similarly, it increases from 380 % to 501 % by increasing air flow rate from 50 sL/min to 100 sL/min at 6 kW power.

The content conversion performance of ash (CCP_{ash}) decreases by increasing the plasma power in 50, 75 and 100 sL/min air flow rate cases because of the enhancement of solid fuel conversion to syngas by increasing plasma power. Higher solid fuel conversion to syngas means less ash output from the reactor. On the other hand, the air flow rate increases the content conversion performance of ash (CCP_{ash}). Because, increasing air flow reduces the temperature in reactor and the conversion of solid fuel to syngas. As a result, less syngas production and high ash are produced. In case of 50 sL/min, it goes down from 27.79 % at 3 kW power to 19.7 % at 6 kW power. In case of 75 sL/min, it decreases from 31.19 % to 24.22 % by increasing power from 3 kW to 6 kW. In case of 100 sL/min, it reduces from 36.71 % to 25.20 % by increasing power from 3 kW to 6 kW. On the other hand, the increment of air flow rate causes the increment of content conversion performance of ash (CCP_{ash}). It goes up from

27.79 % to 36.71 % by increasing air flow rate from 50 sL/min to 100 sL/min at 3 kW power. Similarly, it increases from 19.70 % to 25.20 % by increasing air flow rate from 50 sL/min to 100 sL/min at 6 kW power.

Table 6.6 Presentation of the CCP_{syn}, CCP_{ash}, CCP_{H_2}, syngas energy, fuel energy and plasma energy results for the Şırnak (Turkey) coal (CTR) gasification process for various powers and flow rates

	Plasma Power (W)	CCP_{syn} (%)	CCP_{ash} (%)	CCP_{H_2} (%)	H_q (%)	Syngas energy (kJ)	Fuel energy (kJ)	Plasma energy (kJ)
Şırnak (Turkey) coal-50sL/min	3000	419	27.79	0.41	0.10	4109	4989	2640
	3600	405	26.49	0.41	0.10	3993		3024
	4200	400	23.27	0.43	0.11	3933		3444
	4800	393	22.66	0.47	0.12	3893		3840
	5400	387	20.98	0.48	0.12	3906		4212
	6000	380	19.70	0.48	0.13	3748		4560
Şırnak (Turkey) coal-75sL/min	3000	489	31.19	0.48	0.10	4256		2130
	3600	473	29.25	0.48	0.10	4224		2448
	4200	469	27.67	0.49	0.10	4042		2814
	4800	452	26.57	0.51	0.11	4016		3072
	5400	441	25.50	0.53	0.12	3963		3348
	6000	431	24.22	0.54	0.12	3858		3600
Şırnak (Turkey) coal-100sL/min	3000	608	36.71	0.60	0.10	4292		2070
	3600	579	34.45	0.59	0.10	4261		2340
	4200	560	29.68	0.58	0.10	4121		2604
	4800	546	27.81	0.62	0.11	4072		2880
	5400	531	26.40	0.64	0.12	4028		3132
	6000	501	25.20	0.61	0.12	3931		3240

The content conversion performance of hydrogen (CCP_{H_2}) stays almost constant by increasing the plasma power in 50, 75 and 100 sL/min air flow rate cases. Because the Şırnak (Turkey) coal (CTR) has lack of hydrogen content. Even increasing plasma power changes the syngas temperature and the conversion of solid fuel to syngas, hydrogen content in syngas is limited due to the lack of hydrogen in solid fuel. As a result, the hydrogen content is varied insignificantly. In case of 50 sL/min, it stays in level of 0.41 % - 0.48 % at plasma power between 3 kW and 6 kW. In case of 75 sL/min, it stays in level of 0.48 % - 0.54 % at plasma power between 3 kW and 6 kW. In case of 100 sL/min, it stays in level between 0.58 % and 0.64 % at plasma power between 3 kW and 6 kW. On the other hand, the content conversion performance of hydrogen (CCP_{H_2}) goes up by the increment of air flow rate. . Because, increasing air flow rate rises the syngas production and it also increases the hydrogen production. It increases from 0.41 % to 0.6 % by increasing air flow rate from 50 sL/min to 100 sL/min at 3 kW plasma power. Also, it increases from 0.48 % to 0.61 % by increasing air flow rate from 50 sL/min to 100 sL/min at 6 kW plasma power.

Hydrogen quality of syngas (H_q) increases by increasing power in 50, 75 and 100 sL/min air flow rate cases. Because, the hydrogen production is proportional with the temperature in the reactor. The temperature increases by increasing plasma power. However, increasing air flow rate has insignificant effect on the hydrogen quality of syngas (H_q). In case of 50 sL/min, it increases from 0.10 % at 3 kW power to 0.13 % at 6 kW power. In case of 75 sL/min, it goes up from 0.11 % to 0.14 % by increasing power from 3 kW to 6 kW. In case of 100 sL/min, it rises from 0.10 % to 0.12 % by increasing power from 3kW to 6 kW. However, the hydrogen quality of syngas (H_q) stays almost constant at level of 0.1 % at varied flow rates between 50 sL/min and 100 sL/min at 3 kW plasma power. Similarly, it stays constant at varied flow rates at level of 0.12-0.13 % between 50 sL/min and 100 sL/min at 6 kW plasma power.

Syngas energy goes down by increasing plasma power in 50, 75 and 100 sL/min air flow rate cases. Because, the syngas energy depends on the syngas production and syngas content especially percentage of CO, H_2 and CH_4. Syngas production reduces by increasing plasma power. Percentage of CO and H_2 increases while CH_4 remains same or slightly reduces by increasing plasma power. As a result, the syngas energy increases by increasing the power. Also, syngas production reduces by increasing air flow rate and percentage of CO and H_2 reduces while percentage of CH_4 increases by increasing air flow rate. The production amount and the distribution of syngas effects the syngas energy. In case of 50 sL/min, syngas energy decreases from 4109 kJ at 3 kW plasma power to 3748 kJ at 6 kW plasma power. In case of 75 sL/min, syngas energy reduces from 4256 kJ at 3 kW plasma power to 3858 kJ at 6 kW plasma power. In case of 100 sL/min, syngas energy decreases from 4292 kJ at 3 kW plasma power to 3931 kJ at 6 kW plasma power. The energy of 250 g Şırnak (Turkey) coal (CTR) fuel is 4989 kJ. On the other hand, the syngas energy increases from 4109 kJ to 4292 kJ by increasing air flow rate from 50 sL/min to 100 sL/min at 3 kW power. The syngas energy rises from 3748 kJ to 3931 kJ by increasing air flow rate from 50 sL/min to 100 sL/min at 6 kW power.

Process energy efficiency (η_{EP}) of the Şırnak (Turkey) coal (CTR) in case of 50 sL/min, 75 sL/min and 100 sL/min for various plasma powers between 3 kW and 6 kW is presented in Figure 6.13. Process energy efficiency (η_{EP}) reduces by increasing the plasma power while it stays almost constant by increasing air flow rate. The input energy is just the fuel energy in the case of process energy efficiency (η_{EP}). So, the syngas energy is the only one parameter which effects the process energy efficiency (η_{EP}). However, the relation between syngas energy, plasma power, and air flow rate are sophisticated to define the relation. Increasing power lowers the gasification duration and reduces the syngas production, but it enhances the conversion of fuel to syngas and rises the syngas temperature. Similarly, increasing air flow rate lowers the gasification duration and it reduces the syngas production. Also, it reduces the syngas temperature and the conversion of fuel to syngas. As a result, increment of plasma power lowers the process energy efficiency (η_{EP}). Increasing air flow rate has almost no effect on the process energy efficiency (η_{EP}).

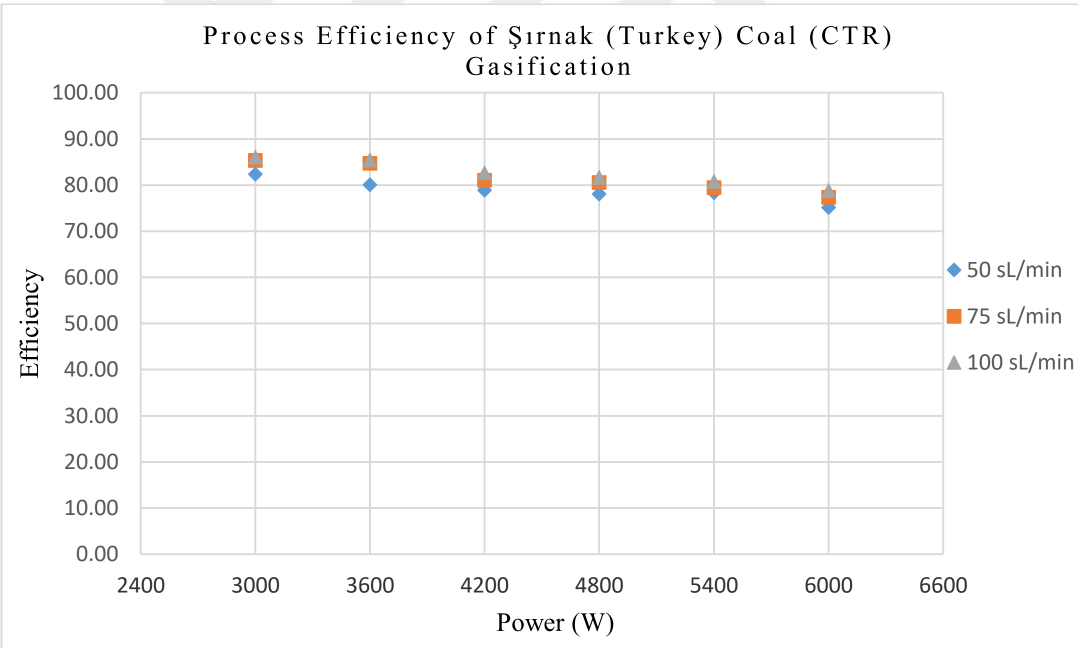

Figure 6.13 Process energy efficiency (η_{EP}) of Şırnak (Turkey) coal (CTR) gasification in the cases of 50-100 sL/min air flow rate and 3-6 kW plasma power

In case of 50 sL/min air flow rate, process energy efficiency (η_{EP}) goes down from 82.37 % to 75.14 % by increasing the plasma power from 3 kW to 6 kW. In case of 75 sL/min air flow rate, it slightly decreases from 85.32 % to 77.33 % by increasing the plasma power from 3 kW to 6 kW. In case of 100 sL/min air flow rate, it also slightly declines from 86.05 % to 78.81 % by increasing the plasma power from 3 kW to 6 kW. Increasing plasma power reduces the process energy efficiency (η_{EP}). While the reduction in efficiency is 8.77 % by increasing plasma power from 3 kW to 6 kW in 50 sL/min, it is 8.41 % by increasing plasma power from 3 kW to 6 kW in 100 sL/min. The increment of air flow rate increases the process energy efficiency (η_{EP}) at 3 kW plasma power. Also, increasing air flow rate increases the process energy efficiency (η_{EP}) at 6 kW plasma power. The process energy efficiency (η_{EP}) goes up from 82.37 % to 86.05 % by increasing the flow rate from 50 sL/min to 100 sL/min in case of 3 kW plasma power and it goes up from 75.14 % to 78.81 % by increasing the flow rate from 50 sL/min to 100 sL/min in case of 6 kW plasma power. The magnitude of the process energy efficiency (η_{EP}) is high because of the low heating value of the Şırnak (Turkey) coal (CTR). However, the produced syngas composition is similar with other coals.

System energy efficiency (η_{ES}) of the Şırnak (Turkey) coal (CTR) in case of 50 sL/min, 75 sL/min and 100 sL/min for various plasma powers between 3 kW and 6 kW are given in Figure 6.14. The system energy efficiency (η_{ES}) depends on the fuel energy, plasma energy and the syngas energy. The constant amount of fuel is dosed to the reactor in the each case. However, the plasma energy and syngas energy are varied depending on the plasma power and air flow rate. Increasing power lowers the gasification duration, reduces syngas production and increases the plasma energy consumption but it enhances the conversion of fuel to syngas and rises the syngas temperature. Similarly, increasing air flow rate lowers the gasification duration, reduces syngas production and lowers the plasma energy consumption. On the other hand, it reduces the syngas temperature and the conversion of fuel to syngas. As a result, increment of plasma power decreases the system energy efficiency (η_{ES}). However, increasing air flow rate reduces the system energy efficiency (η_{ES}). In case of 50 sL/min air flow rate, system energy efficiency (η_{ES}) reduces from 53.87 % to 39.25 % by increasing the plasma power from 3 kW to 6 kW. In case of 75 sL/min air flow rate, it cut down from 59.79 % to 44.92 % by increasing the plasma power from 3 kW to 6 kW. In case of 100 sL/min air flow rate, it goes down from 60.81 % to 47.78 % by increasing the plasma power from 3 kW to 6 kW. Increasing plasma power reduces the system energy efficiency (η_{ES}) in all cases. Also, the effect of plasma power to the system energy efficiency (η_{ES}) goes down by increasing the flow rate. The reduction in efficiency is 27.13 % by increasing plasma power from 3 kW to 6 kW in 50 sL/min and it is 21.42 % by increasing plasma power from 3 kW to 6 kW in 100 sL/min. The magnitude of the system energy efficiency (η_{ES}) is less than the process energy efficiency (η_{EP}). Because, the plasma power increases the consumption of the system and it has negative effects to system energy efficiency (η_{ES}). The increment of air flow rate enhances the system energy efficiency (η_{ES}) at all plasma power levels. The system energy efficiency (η_{ES}) goes up from 53.87 % to 60.81 % by increasing the flow rate from 50 sL/min to 100 sL/min in case of 3 kW power and it rises from 39.25 % and 47.78 % by increasing the flow rate from 50 sL/min to 100 sL/min in case of 6 kW plasma power. The magnitude of the system energy efficiency (η_{ES}) is high because of the low heating value of the Şırnak (Turkey) coal (CTR). However, the produced syngas composition is similar with other coals.

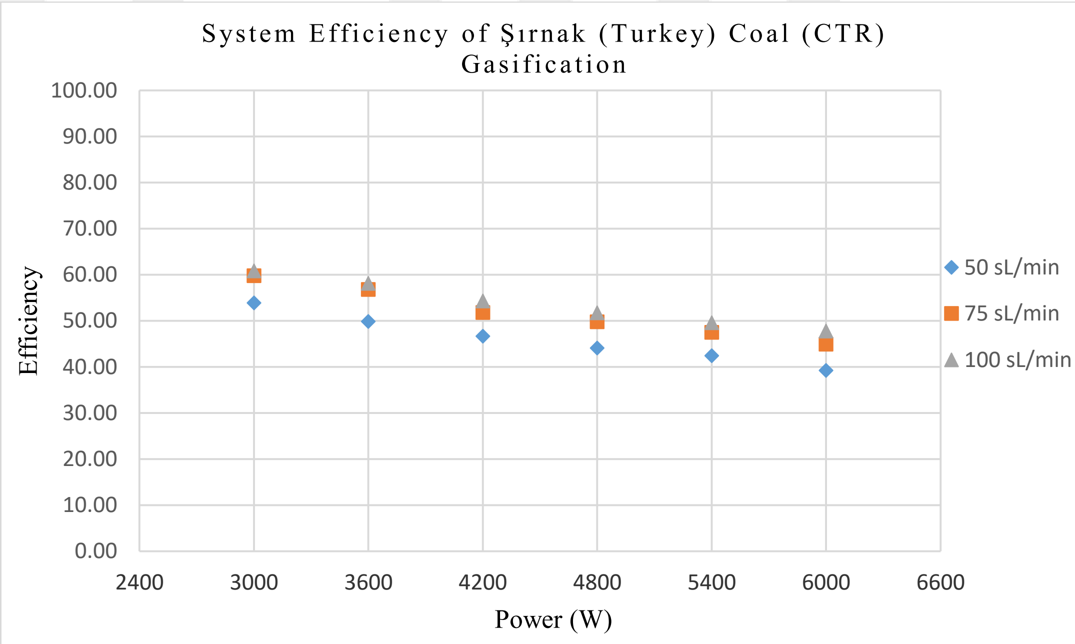

Figure 6.14 System energy efficiency (η_{ES}) of Şırnak (Turkey) coal (CTR) gasification in the cases of 50-100 sL/min air flow rate and 3-6 kW plasma power

Hot gas efficiency (η_{HG}) of Şırnak (Turkey) coal (CTR) in case of 50 sL/min, 75 sL/min and 100 sL/min for various plasma powers between 3 kW and 6 kW are given in Figure 6.15. The hot gas efficiency (η_{HG}) depends on the fuel energy, plasma energy and the syngas energy similar to the system energy efficiency (η_{ES}). In addition to system efficiency parameters, the syngas energy includes both the chemical energy of the solid fuel and sensible energy as a result of its high temperature in the hot gas efficiency (η_{HG}). The variation of the hot gas efficiency (η_{HG}) is similar with the system energy efficiency (η_{ES}). The magnitude of the hot gas efficiency (η_{HG}) is higher than the system energy efficiency (η_{ES}). Because, the sensible energy of the syngas is also considered in calculations of hot gas efficiency (η_{HG}). As a result, increment of plasma power lowers the hot gas efficiency (η_{HG}). However, increasing air flow rate increases the hot gas efficiency (η_{HG}). In case of 50 sL/min air flow rate, hot gas efficiency (η_{HG}) goes down from 62.04 % to 51.27 % by increasing the plasma power from 3 kW to 6 kW. In case of 75 sL/min air flow rate, it reduces from 67.94 % to 59.42 % by increasing the plasma power from 3 kW to 6 kW. In case of 100 sL/min air flow rate, it decreases from 68.96 % to 64.31 % by increasing the plasma power from 3 kW to 6 kW. Increasing plasma power reduces the hot gas efficiency (η_{HG}) in all cases. However, the reduction decreases by increasing the flow rate. While the reduction is 17.36 % by increasing power from 3 kW to 6 kW in case of 50 sL/min air flow rate, it is 6.74 % by increasing power from 3 kW to 6 kW in case of 100 sL/min air flow rate. The increment of air flow rate increases the hot gas efficiency (η_{HG}) in all plasma power levels. The hot gas efficiency (η_{HG}) goes up from 62.04 % to 68.96 % by increasing the flow rate from 50 sL/min to 100 sL/min in case of 3 kW power and it also rises from 51.27 % to 64.31 % by increasing the flow rate from 50 sL/min to 100 sL/min in case of 6 kW plasma power.

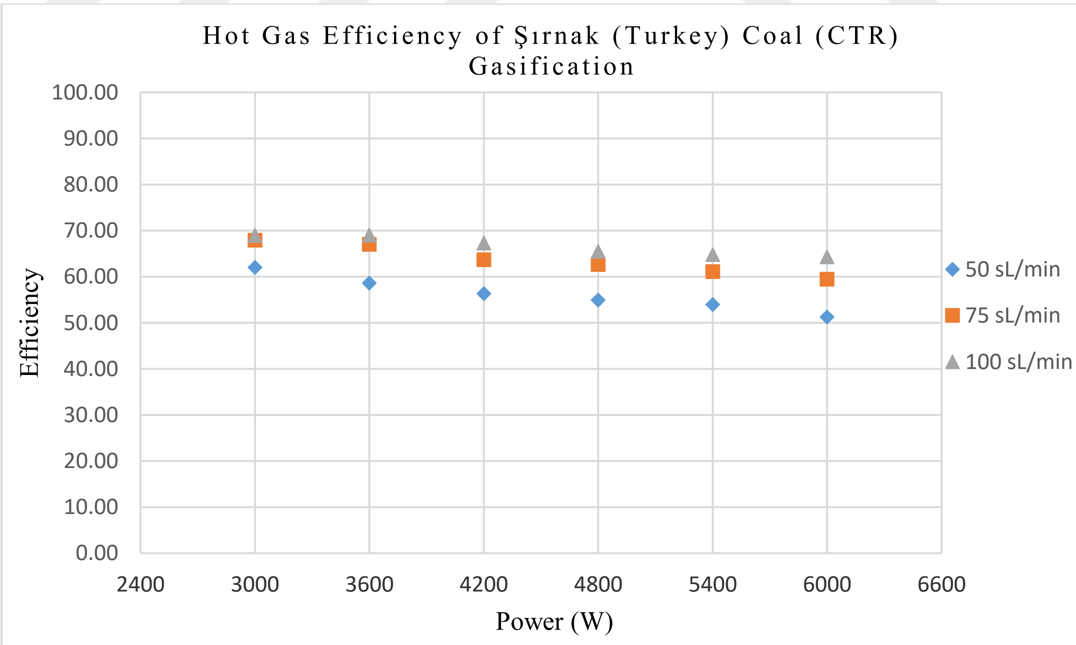

Figure 6.15 Hot gas efficiency (η_{HG}) of Şırnak (Turkey) coal (CTR) gasification in the cases of 50-100 sL/min air flow rate and 3-6 kW plasma power

6.7 Thermodynamic analysis of polyethylene (PP) gasification process

In this section, thermodynamic performance of polyethylene (PP) gasification process is handled. The content conversion performance of syngas (CCP_{syn}), content conversion performance of ash (CCP_{ash}), content conversion performance of hydrogen (CCP_{H_2}), hydrogen quality of syngas (H_q), process energy efficiency (η_{EP}), system energy efficiency (η_{ES}) and hot gas efficiency (η_{HG}) are calculated for each case of the gasification of polyethylene (PP) for various power from 3 kW to 6 kW and at 50 sL/min, 75 sL/min and 100 sL/min air flow rate. The results are presented in this section.

The CCP_{syn}, CCP_{ash}, CCP_{H_2}, H_q, syngas energy, fuel energy and plasma energy are given in the Table 6.7. The content conversion performance of syngas (CCP_{syn}) decreases by increasing plasma power in 50, 75 and 100 sL/min air flow rate cases. Because, the increasing power reduces the gasification time (tg). The supplied air amount to the reactor reduces due to the reduction of supplying air flow rate duration. As a result the produced syngas amount decreases while the supplied fuel amount is same. In case of 50 sL/min, it reduces from 360 % at 3 kW plasma power to 305 % at 6 kW plasma power. In case of 75 sL/min, it reduces from 465 % to 407 % by increasing plasma power from 3 kW to 6 kW. In case of 100 sL/min, it reduces from 571 % to 509 % by increasing plasma power from 3 kW to 6 kW. On the other hand, the increment of air flow rate causes the increment of content conversion performance of syngas (CCP_{syn}). It goes up from 360 % to 571 % by increasing air flow rate from 50 sL/min to 100 sL/min at 3 kW power. Similarly, it increases from 305 % to 509 % by increasing air flow rate from 50 sL/min to 100 sL/min at 6 kW power.

The content conversion performance of ash (CCP_{ash}) decreases by increasing the plasma power in 50, 75 and 100 sL/min air flow rate cases because of the enhancement of solid fuel conversion to syngas by increasing plasma power. Higher solid fuel conversion to syngas means less ash output from the reactor. On the other hand, the air flow rate increases the content conversion performance of ash (CCP_{ash}). Because, increasing air flow reduces the temperature in reactor and the conversion of solid fuel to syngas. As a result, less syngas production and high ash are produced. In case of 50 sL/min, it goes down from 0.84 % at 3 kW power to 0.46 % at 6 kW power. In case of 75 sL/min, it decreases from 1.61 % to 0.96 % by increasing power from 3 kW to 6 kW. In case of 100 sL/min, it reduces from 2.45 % to 1.6 % by increasing power from 3 kW to 6 kW. On the other hand, the increment of air flow rate causes the increment of content conversion performance of ash (CCP_{ash}). It goes up from 0.84 % to 2.45 % by increasing air flow rate from 50 sL/min to 100 sL/min at 3 kW power. Similarly, it increases from 0.46 % to 1.6 % by increasing air flow rate from 50 sL/min to 100 sL/min at 6 kW power.

The content conversion performance of hydrogen (CCP_{H_2}) increases by increasing the plasma power in 50, 75 and 100 sL/min air flow rate cases because of increment of syngas temperature and enhancement in conversion of solid fuel to syngas. Enhancement in syngas conversion increases the production of hydrogen. Also, the air flow rate increases the content conversion performance of hydrogen (CCP_{H_2}). Because, the increasing air flow rate also increases the syngas production. Higher production of syngas means the higher hydrogen production from the same amount of the fuel. In case of 50 sL/min, it increases from 2.53 % at 3 kW power to 2.9 % at 6 kW power. In case of 75 sL/min, it goes up from 3.67 % to 3.84 % by increasing power from 3 kW to 6 kW. In case of 100 sL/min, it increases from 4.5 % to 4.85 % by increasing power from 3 kW to 6 kW. Moreover, the increment of air flow rate increases the content conversion performance of hydrogen (CCP_{H_2}). It goes up from 2.53 % to 4.5 % by increasing air flow rate from 50 sL/min to 100 sL/min at 3 kW power. Also, it goes up from 2.9 % to 4.85 % by increasing air flow rate from 50 sL/min to 100 sL/min at 6 kW power.

Hydrogen quality of syngas (H_q) increases by increasing power in 50, 75 and 100 sL/min air flow rate cases. Because, the hydrogen production is proportional with the temperature in the reactor. The temperature increases by increasing plasma power. However, increasing air flow rate has insignificant effect on the hydrogen quality of syngas (H_q). In case of 50 sL/min, it increases from 0.7 % at 3 kW power to 0.95 % at 6 kW power. In case of 75 sL/min, it goes up from 0.79 % to 0.94 % by increasing power from 3 kW to 6 kW. In case of 100 sL/min, it rises from 0.79 % to 0.95 % by increasing power from 3kW to 6 kW. However, the hydrogen quality of syngas (H_q) stays almost constant at level of 0.7-0.79 % for various flow rates between 50 sL/min and 100 sL/min at 3 kW plasma power. Similarly, it stays constant for various flow rates at level of 0.94-0.95 % between 50 sL/min and 100 sL/min at 6 kW plasma power.

Table 6.7 Presentation of the CCP_{syn}, CCP_{ash}, CCP_{H_2}, syngas energy, fuel energy and plasma energy results for the polyethylene (PP) gasification process for various powers and flow rates

	Plasma Power (W)	CCP_{syn} (%)	CCP_{ash} (%)	CCP_{H_2} (%)	H_q (%)	Syngas energy (kJ)	Fuel energy (kJ)	Plasma energy (kJ)
Polyethylene-50sL/min	3000	360	0.84	2.53	0.70	3298	8658	1980
	3600	352	0.80	2.52	0.72	3267		2304
	4200	336	0.75	2.45	0.73	3187		2520
	4800	328	0.65	2.62	0.80	3274		2784
	5400	320	0.58	2.70	0.84	3321		3024
	6000	305	0.46	2.90	0.95	3327		3120
Polyethylene-75sL/min	3000	465	1.61	3.67	0.79	3938		1860
	3600	454	1.54	3.64	0.80	3895		2160
	4200	442	1.44	3.69	0.84	3898		2436
	4800	436	1.34	3.79	0.87	3905		2736
	5400	418	1.20	3.81	0.91	3885		2916
	6000	407	0.96	3.84	0.94	3854		3120
Polyethylene-100sL/min	3000	571	2.45	4.50	0.79	4499		1800
	3600	556	2.24	4.67	0.84	4713		2088
	4200	556	2.08	4.77	0.86	4844		2436
	4800	540	1.94	4.79	0.89	4877		2688
	5400	524	1.77	4.89	0.93	4970		2916
	6000	509	1.60	4.85	0.95	4999		3120

Syngas energy rises by increasing plasma power in 50, 75 and 100 sL/min air flow rate cases. Because, the syngas energy depends on the syngas production and syngas content especially percentage of CO, H_2 and CH_4. Syngas production reduces by increasing plasma power. Percentage of CO and H_2 increases while CH_4 remains same or slightly reduces by increasing plasma power. Also, syngas production reduces by increasing air flow rate and percentage of CO and H_2 reduces while percentage of CH_4 increases by increasing air flow rate. The production amount and the distribution of syngas effects the syngas energy. In case of 50 sL/min, syngas energy goes up from 3298 kJ at 3 kW plasma power to 3327 kJ at 6 kW plasma power. In case of 75 sL/min, syngas energy lowers from 3938 kJ at 3 kW plasma power to 3854 kJ at 6 kW plasma power. In case of 100 sL/min, syngas energy increases from 4499 kJ at 3 kW plasma power to 4999 kJ at 6 kW plasma power. The energy of 250 g Polyethylene (PP) fuel is 8658 kJ. On the other hand, the syngas energy increases from 3298 kJ to 4499 kJ by increasing air flow rate from 50 sL/min to 100 sL/min at 3 kW power. The syngas energy rises from 3327 kJ to 4999 kJ by increasing air flow rate from 50 sL/min to 100 sL/min at 6 kW power.

Process energy efficiency (η_{EP}) of polyethylene (PP) in case of 50 sL/min, 75 sL/min and 100 sL/min for various plasma powers between 3 kW and 6 kW are presented in Figure 6.16. Process energy efficiency (η_{EP}) remains almost constant by increasing the plasma power while it increases by increasing air flow rate. The input energy is just the fuel energy in the case of process energy efficiency (η_{EP}). So, the syngas energy is the only one parameter which effects the process energy efficiency (η_{EP}). However, the relation between syngas energy, plasma power, and air flow rate are sophisticated to define the relation. Increasing power lowers the gasification duration and reduces the syngas production, but it enhances the conversion of fuel to syngas and rises the syngas temperature. Similarly, increasing air flow rate lowers the gasification duration and it reduces the syngas production. Also, it reduces the syngas temperature and the conversion of fuel to syngas. As a result, increment of plasma power has insignificant effect on the process energy efficiency (η_{EP}). However, increasing air flow rate rises the process energy efficiency (η_{EP}). In case of 50 sL/min air flow rate, process energy efficiency (η_{EP}) slightly rises from 38.09 % to 38.42 % by increasing the plasma power from 3 kW to 6 kW. On the other hand, it slightly decreases from 45.48 % to 44.52 % by increasing the plasma power from 3 kW to 6 kW in case of 75 sL/min air flow rate. In case of 100 sL/min air flow rate, it increases from 51.96 % to 57.73 % by increasing the plasma power from 3 kW to 6 kW.

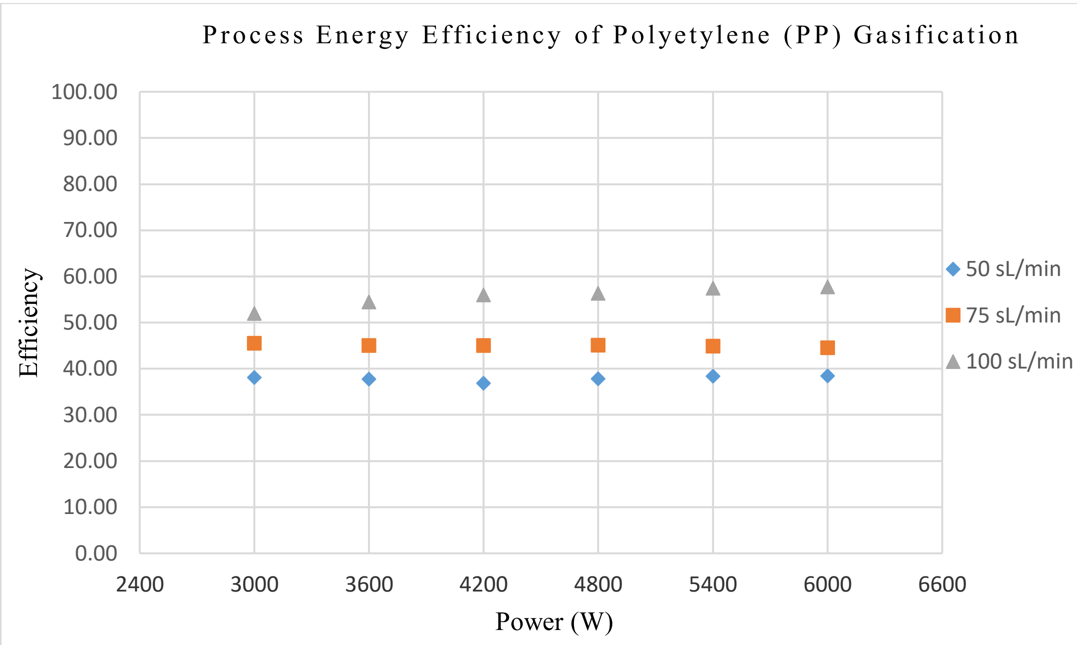

Figure 6.16 Process energy efficiency (η_{EP}) of polyethylene (PP) gasification in the cases of 50-100 sL/min air flow rate and 3-6 kW plasma power

The increment of air flow rate rises the process energy efficiency (η_{EP}) in all plasma power levels. The process energy efficiency (η_{EP}) goes up from 38.09 % to 51.96 % by increasing the flow rate from 50 sL/min to 100 sL/min in case of 3 kW plasma power and it goes up from 38.42 % to 57.73 % by increasing the flow rate from 50 sL/min to 100 sL/min in case of 6 kW plasma power.

System energy efficiency (η_{ES}) of the polyethylene (PP) in case of 50 sL/min, 75 sL/min and 100 sL/min for various plasma powers between 3 kW and 6 kW are given in Figure 6.17. The system energy efficiency (η_{ES}) depends on the fuel energy, plasma energy and the syngas energy. The constant amount of fuel is dosed to the reactor in the each case. However, the plasma energy and syngas energy are varied depending on the plasma power and air flow rate. Increasing power lowers the gasification duration, reduces syngas production and increases the plasma energy consumption but it enhances the conversion of fuel to syngas and rises the syngas temperature. Similarly, increasing air flow rate lowers the gasification duration, reduces syngas production and lowers the plasma energy consumption. On the other hand, it reduces the syngas temperature and the conversion of fuel to syngas. As a result, increment of plasma power reduces the system energy efficiency (η_{ES}). However, increasing air flow rate enhances the system energy efficiency (η_{ES}). In case of 50 sL/min air flow rate, system energy efficiency (η_{ES}) diminishes from 31.00 % to 28.24 % by increasing the plasma power from 3 kW to 6 kW. In case of 75 sL/min air flow rate, system energy efficiency (η_{ES}) decreases from 37.44 % to 32.72 % by increasing the plasma power from 3 kW to 6 kW. In case of 100 sL/min air flow rate, system energy efficiency (η_{ES}) goes down from 43.02 % to 42.44 % by increasing the plasma power from 3 kW to 6 kW. Increasing plasma power reduces the system energy efficiency (η_{ES}) in all cases. The reduction in efficiency is 8.9 % by increasing plasma power from 3 kW to 6 kW in 50 sL/min and it is 1.34 % by increasing plasma power from 3 kW to 6 kW in 100 sL/min. The magnitude of the system energy efficiency (η_{ES}) is less than the process energy efficiency (η_{EP}). Because, the plasma power increases the consumption of the system and it has negative effects to system energy efficiency (η_{ES}). The increment of air flow rate enhances the system energy efficiency (η_{ES}) at all plasma power levels. The system energy efficiency (η_{ES}) goes up from 31.00 % to 43.02 % by increasing the flow rate from 50 sL/min to 100 sL/min in case of 3 kW power and it goes up from 28.24 % to 42.44 % by increasing the flow rate from 50 sL/min to 100 sL/min in case of 6 kW plasma power.

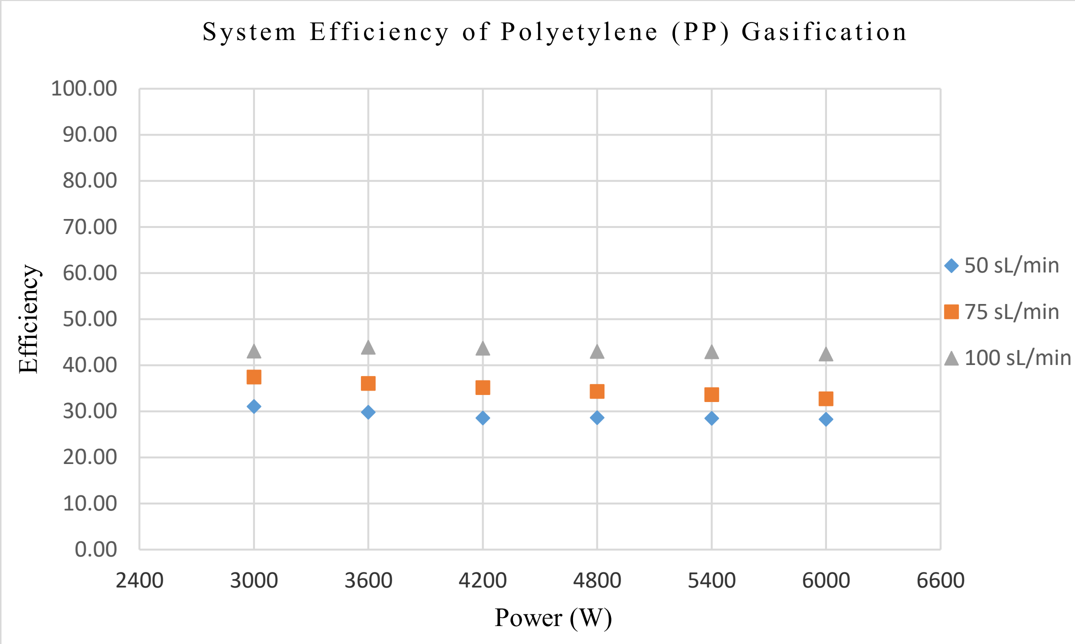

Figure 6.17 System energy efficiency (η_{ES}) of polyethylene (PP) gasification in the cases of 50-100 sL/min air flow rate and 3-6 kW plasma power

Hot gas efficiency (η_{HG}) of polyethylene (PP) in case of 50 sL/min, 75 sL/min and 100 sL/min for various plasma powers between 3 kW and 6 kW are given in Figure 6.18. The hot gas efficiency (η_{HG}) depends on the fuel energy, plasma energy and the syngas energy similar to the system energy efficiency (η_{ES}). In addition to system efficiency parameters, the syngas energy includes both the chemical energy of the solid fuel and sensible energy as a result of its high temperature in the hot gas efficiency (η_{HG}). The variation of the hot gas efficiency (η_{HG}) is similar with the system energy efficiency (η_{ES}). The magnitude of the hot gas efficiency (η_{HG}) is higher than the system energy efficiency (η_{ES}). Because, the sensible energy of the syngas is also considered in calculations of hot gas efficiency (η_{HG}). As a result, increment of plasma power rises the hot gas efficiency (η_{HG}). Also, increasing air flow rate increases the hot gas efficiency (η_{HG}). In case of 50 sL/min air flow rate, hot gas efficiency (η_{HG}) slightly rises from 36.23 % to 36.54 % by increasing the plasma power from 3 kW to 6 kW. In case of 75 sL/min air flow rate, it also slightly rises from 42.89 % to 43.32 % by increasing the plasma power from 3 kW to 6 kW. In case of 100 sL/min air flow rate, it goes up from 48.43 % to 55.12 % by increasing the plasma power from 3 kW to 6 kW. The hot gas efficiency (η_{HG}) goes up from 36.23 % to 48.43 % by increasing the flow rate from 50 sL/min to 100 sL/min in case of 3 kW power and it also rises from 36.54 % to 55.12 % by increasing the flow rate from 50 sL/min to 100 sL/min in case of 6 kW plasma power.

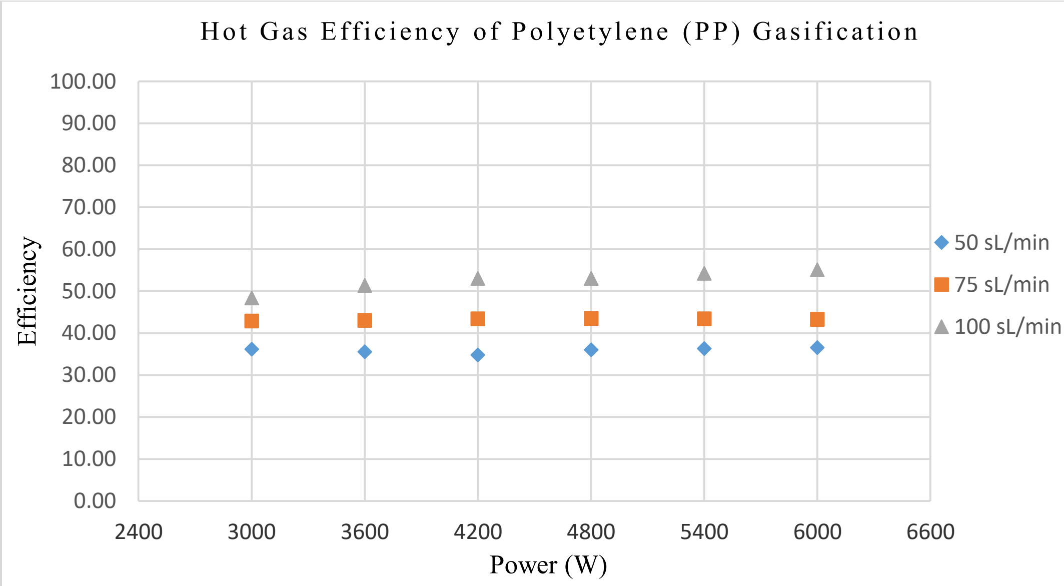

Figure 6.18 Hot gas efficiency (η_{HG}) of polyethylene (PP) gasification in the cases of 50-100 sL/min air flow rate and 3-6 kW plasma power

6.8 Conclusions

The thermodynamic analysis methodology of plasma gasification process is explained in detail. The content conversion performance of syngas (CCP_{syn}), content conversion performance of ash (CCP_{ash}), content conversion performance of hydrogen (CCP_{H_2}), hydrogen quality of syngas (H_q), process energy efficiency (η_{EP}) and system energy efficiency (η_{ES}), hot gas efficiency (η_{HG}), process exergetic efficiency (η_{EXP}) and system exergetic efficiency (η_{EXS}) are defined. The thermodynamic performance of solid fuels; Russian coal (CR), South African coal (CSA), Şırnak (Turkey) coal (CTR), pine tree sawdust (PSD), hornbeam sawdust (HSD) and polyethylene (PP) are examined regarding to defined terms. The thermodynamic performance of each solid fuel gasification in case of 50, 75 and 100 sL/min air flow rate and varied powers between 3 kW and 6 kW are presented for each fuel type. The conversion characteristics and thermodynamic performance of sawdust, coals and polyethylene are evaluated. The highlights of fuel gasification performances are presented.

In case of gasification of sawdust, the content conversion performance of syngas (CCP_{syn}) reduces approximately 24.7 % in case of 50 sL/min air flow rate, 27 % in case of 75 sL/min air flow rate and 27.38 % in case of 100 sL/min air flow rate by increasing the plasma power from 3 kW to 6 kW. On the other hand, the increasing air flow rate enhanced the content conversion performance of syngas (CCP_{syn}). The increment in the content conversion performance of syngas (CCP_{syn}) is 35.26 % for 3 kW and 30.44 % for 6 kW when the flow rate increases from 50 sL/min to 100 sL/min. The highest content conversion performance of syngas (CCP_{syn}) is 604 % at 3 kW plasma power, 100 sL/min and hornbeam sawdust (HSD) gasification. The lowest content conversion performance of syngas (CCP_{syn}) is 336 % at 6 kW plasma power, 50 sL/min and hornbeam sawdust (HSD) gasification. In case of gasification of coals, the content conversion performance of syngas (CCP_{syn}) reduces approximately 17 % in case of 50 sL/min air flow rate, 17.24 % in case of 75 sL/min air flow rate and 17.40 % in case of 100 sL/min air flow rate by increasing the plasma power from 3 kW to 6 kW. On the other hand, the increasing air flow rate enhanced the content conversion performance of syngas (CCP_{syn}). The increment in the content conversion performance of syngas (CCP_{syn}) is 41 % for 3 kW and 19.7 % for 6 kW when the flow rate increases from 50 sL/min to 100 sL/min. The highest content conversion performance of syngas (CCP_{syn}) is 655 % at 3 kW plasma power, 100 sL/min and Russian coal (CR) gasification. The lowest content conversion performance of syngas (CCP_{syn}) is 376 % at 6 kW plasma power, 50 sL/min and Russian coal (CR) gasification. In case of gasification of polyethylene, the content conversion performance of syngas (CCP_{syn}) reduces approximately 15.25 % in case of 50 sL/min air flow rate, 12.58 % in case of 75 sL/min air flow rate and 10.9 % in case of 100 sL/min air flow rate by increasing the plasma power from 3 kW to 6 kW. On the other hand, the increasing air flow rate enhanced the content conversion performance of syngas (CCP_{syn}). The increment in the content conversion performance of syngas (CCP_{syn}) is 58.8 % for 3 kW and 66.96 % for 6 kW when the flow rate increases from 50 sL/min to 100 sL/min. The highest content conversion performance of syngas (CCP_{syn}) is 571 % at 3 kW plasma power and 100 sL/min. The lowest content conversion performance of syngas (CCP_{syn}) is 305 % at 6 kW plasma power and 50 sL/min. In all the experimentation, the highest content conversion performance of syngas (CCP_{syn}) is 655 % at 3 kW plasma power, 100 sL/min and Russian coal (CR) gasification while the lowest content conversion performance of syngas (CCP_{syn}) is 305 % at 6 kW plasma power, 50 sL/min and Polyethylene (PP) gasification. The content conversion performance of syngas

(CCP_{syn}) decreases by increasing the plasma power at 50 sL/min, 75 sL/min and 100 sL/min. Because the increment of plasma power reduced the gasification time (t_g). By decreasing the gasification duration, less air is supplied to the reactor. As a result, the produced syngas amount decreases by increasing the plasma power. However, the increment of air flow rate increases the content conversion performance of syngas (CCP_{syn}). Supplying higher air flow rate causes higher syngas production rate. The content conversion performance of ash (CCP_{ash}) decreases by plasma power because of the enhancement of conversion of syngas by increasing plasma power. On the other hand, the air flow rate increases the content conversion performance of ash (CCP_{ash}). Because, the increment of air flow reduces the conversion of solid fuel to syngas.

In case of gasification of sawdust, the content conversion performance of hydrogen (CCP_{H_2}) goes up approximately 168.31 % in case of 50 sL/min air flow rate, 127.76 % in case of 75 sL/min air flow rate and 153.79 % in case of 100 sL/min air flow rate by increasing the plasma power from 3 kW to 6 kW. The reduction in the content conversion performance of hydrogen (CCP_{H_2}) is 1.79 % for 3 kW while it reduces 6.92 % for 6 kW when the flow rate increases from 50 sL/min to 100 sL/min. The highest content conversion performance of hydrogen (CCP_{H_2}) is 2.23 % at 6 kW plasma power, 50 sL/min and pine tree sawdust (PSD) gasification. The lowest content conversion performance of hydrogen (CCP_{H_2}) is 0.7 % at 3 kW plasma power, 50 sL/min and hornbeam sawdust (HSD) gasification. In case of gasification of coals, the content conversion performance of hydrogen (CCP_{H_2}) goes up approximately 5.87 % in case of 50 sL/min air flow rate, 4.96 % in case of 75 sL/min air flow rate and 6.75 % in case of 100 sL/min air flow rate by increasing the plasma power from 3 kW to 6 kW. Also, the increasing air flow rate enhanced the content conversion performance of hydrogen (CCP_{H_2}). The increment in the content conversion performance of hydrogen (CCP_{H_2}) is 20.89 % for 3 kW and 20.05 % for 6 kW when the flow rate increases from 50 sL/min to 100 sL/min. The highest content conversion performance of hydrogen (CCP_{H_2}) is 0.73 % at 5.4 kW plasma power, 100 sL/min and South African coal (CSA) gasification. The lowest content conversion performance of hydrogen (CCP_{H_2}) is 0.41 % at 3 kW plasma power, 50 sL/min and Şırnak (Turkey) coal (CTR) gasification. In case of gasification of polyethylene, the content conversion performance of hydrogen (CCP_{H_2}) increases approximately 14.66 % in case of 50 sL/min air flow rate, 4.56 %

in case of 75 sL/min air flow rate and 7.85 % in case of 100 sL/min air flow rate by increasing the plasma power from 3 kW to 6 kW. In addition, increasing air flow rate enhanced the content conversion performance of hydrogen (CCP_{H_2}). The increment in the content conversion performance of hydrogen (CCP_{H_2}) is 77.53 % for 3 kW and 66.99 % for 6 kW when the flow rate increases from 50 sL/min to 100 sL/min. The highest content conversion performance of hydrogen (CCP_{H_2}) is 4.85 % at 6 kW plasma power and 100 sL/min. The lowest content conversion performance of hydrogen (CCP_{H_2}) is 2.45 % at 4.2 kW plasma power and 50 sL/min. In all the experimentation, the highest content conversion performance of hydrogen (CCP_{H_2}) is 4.85 % at 6 kW plasma power, 100 sL/min and Polyethylene (PP) gasification while the lowest content conversion performance of hydrogen (CCP_{H_2}) is 0.41 % at 3 kW plasma power, 50 sL/min and Şırnak (Turkey) coal (CTR) gasification. The content conversion performance of hydrogen (CCP_{H_2}) increases by plasma power in case of gasification of sawdust and polyethylene and coals. Increasing the plasma power, enhances the conversion of fuel to syngas. Enhancement in syngas conversion also increases the production of hydrogen. The Hydrogen quality of syngas (H_q) increases in all the cases. Hydrogen quality of syngas (H_q) increases by plasma power because of the conversion enhancement at higher temperature. However, the air flow rate reduces the Hydrogen quality of syngas (H_q). Because the air flow rate is inversely proportional with the temperature in the reactor.

The process energy efficiency (η_{EP}) goes up approximately 63.92 % in case of 50 sL/min air flow rate, 47.15 % in case of 75 sL/min air flow rate and 24.24 % in case of 100 sL/min air flow rate by increasing the plasma power from 3 kW to 6 kW in case of gasification of sawdust. Similarly, the system energy efficiency (η_{ES}) goes up approximately 45.46 % in case of 50 sL/min air flow rate, 33.6 % in case of 75 sL/min air flow rate and 13.27 % in case of 100 sL/min air flow rate by increasing the plasma power from 3 kW to 6 kW in case of gasification of sawdust. While the increment in the process energy efficiency (η_{EP}) is 17.52 % for 3 kW plasma power, it reduces 29.95 % for 6 kW plasma power when the flow rate increases from 50 sL/min to 100 sL/min. Also, the increment in the system energy efficiency (η_{ES}) is 29.95 % for 3 kW plasma power and it rises 1.55 % for 6 kW plasma power when the flow rate increases from 50 sL/min to 100 sL/min. While the highest process energy efficiency (η_{EP}) is

66.88 % at 6 kW plasma power, 75 sL/min and pine tree sawdust (PSD) gasification, the lowest process energy efficiency (η_{EP}) is 30.8 % at 3 kW plasma power, 50 sL/min and hornbeam sawdust (HSD) gasification. Also, the highest system energy efficiency (η_{ES}) is 41.4 % at 6 kW plasma power, 75 sL/min and pine tree sawdust (PSD) gasification and the lowest system energy efficiency (η_{ES}) is 20.6 % at 3 kW plasma power, 50 sL/min and hornbeam sawdust (HSD) gasification. The process energy efficiency (η_{EP}) lowers approximately 13.63 % in case of 50 sL/min air flow rate, 10.11 % in case of 75 sL/min air flow rate and 7.78 % in case of 100 sL/min air flow rate by increasing the plasma power from 3 kW to 6 kW in case of gasification of coals. Similarly, the system energy efficiency (η_{ES}) decreases approximately 26.39 % in case of 50 sL/min air flow rate, 21.71 % in case of 75 sL/min air flow rate and 19.18 % in case of 100 sL/min air flow rate by increasing the plasma power from 3 kW to 6 kW in case of gasification of coals. The increment in the process energy efficiency (η_{EP}) is 10.77 % for 3 kW plasma and 18.69 % for 6 kW plasma power when the flow rate increases from 50 sL/min to 100 sL/min. Also, the increment in the system energy efficiency (η_{ES}) is 19.87 % for 3 kW plasma power and it rises 31.65 % for 6 kW plasma power when the flow rate increases from 50 sL/min to 100 sL/min. While the highest process energy efficiency (η_{EP}) is 86.04 % at 3 kW plasma power, 100 sL/min and Şırnak (Turkey) coal (CTR) gasification, the lowest process energy efficiency (η_{EP}) is 52.55 % at 6 kW plasma power, 50 sL/min and South African coal (CSA) gasification. Also, the highest system energy efficiency (η_{ES}) is 61.37 % at 3 kW plasma power, 100 sL/min air flow rate and Russian coal (CR) gasification and the lowest system energy efficiency (η_{ES}) is 32.99 % at 3 kW plasma power, 50 sL/min and South African coal (CSA) gasification. The process energy efficiency (η_{EP}) rises approximately 0.87 % in case of 50 sL/min air flow rate, lowers approximately 2.12 % in case of 75 sL/min air flow rate and rises approximately 11.1 % in case of 100 sL/min air flow rate by increasing the plasma power from 3 kW to 6 kW in case of gasification of polyethylene. Similarly, the system energy efficiency (η_{ES}) decreases approximately 8.9 % in case of 50 sL/min air flow rate, 12.59 % in case of 75 sL/min air flow rate and 1.35 % in case of 100 sL/min air flow rate by increasing the plasma power from 3 kW to 6 kW in case of gasification of polyethylene. The increment in the process energy efficiency (η_{EP}) is 36.42 % for 3 kW plasma and 50.27 % for 6 kW plasma power when the flow rate increases from 50 sL/min to 100 sL/min. Also, the increment in the system energy efficiency (η_{ES}) is 38.77 % for 3 kW plasma power and it rises 50.27 % for 6 kW plasma power when the flow rate increases from 50 sL/min to 100 sL/min. While the highest process energy efficiency (η_{EP}) is 57.73 % at 6 kW plasma power and 100 sL/min air flow rate, the lowest process energy efficiency (η_{EP}) is 36.8 % at 4.2 kW plasma power and 50 sL/min air flow rate. Also, the highest system energy efficiency (η_{ES}) is 43.86 % at 3.6 kW plasma power and 100 sL/min air flow rate, while the lowest system energy efficiency (η_{ES}) is 36.8 % at 4.2 kW plasma power and 50 sL/min air flow rate.

CHAPTER VII

CONCLUSIONS

In this chapter, general conclusions obtanied from the experimental study of microwave plasma gasification (MCw gasifier) are presented and the related future investigations are suggested.

As mentioned in introduction, recovery from waste has become significant because of the limited resources in nature and increasing amounts of waste due to increase in the population of the world. Furthermore the available energy demand increased rapidly by the technological developments and the improvements in human comfort. The plasma gasification systems which can dispose the waste and also produce a useful energy form (syngas) makes the method attractive for the waste to energy conversion.

An experimental set-up as shown in Figure 3.29 was constructed by referring to the available literature to investigate the microwave plasma gasification characteristics of solid fuels. Even there were several research in literature about MCw gasifier, the required data sets are missing for the performance evaluation. The performance were evaluated just with cold gas efficiency and content conversion efficiencies in literature. In this study, the temperature of syngas, the supplied air flow rate, fuel supply rate, plasma power and the ash outputs were measured and controlled. By knowing these independent parameters, it would be possible to investigate the thermodynamic performance of the gasification. The process and system energy efficiencies of the process are examined by measuring all these independent parameters.

In the operation of gasification system, there were several problems to feed the fuel to the reactor and the problems are solved by following ways.

-Solid fuel feeding method

The fuel supply system was isolated from the leakages of air in storage place. Also, the air flow is by-passed. By this way, the reactor and the feeder became in same pressure. The solid feeding location had to be changed by these modifications. As a result, the reversing of solid particles in the feeder is prevented.

-Solid fuel feeding location

The solid fuels were mixed with air and supplied to the system by plasma applicator air inlet port to satisfy equilibrium of pressure in reactor and solid fuel feeder. The new proposed system configuration is given in Figure 3.26.

-Gasification process and syngas production problem

In case of steady state operation, the syngas production was not achieved because of the air amount was much higher than the fuel in reactor. Although, the fuel feeding rate is adjusted to feed the maximum solid fuel and the air flow rate reduced to 50 sL/min, the syngas production was not achieved. In case of reducing air flow rate to the less than 50 sL/min, the swirling flow does not occur in plasma applicator. So, the quartz glass in the center of the applicator melt. It is caused because of high energy density in it. As a result, the minimum air flow rate and maximum fuel feeding rate were restricted.

To overcome these problems, the reactor is dosed by certain amount of solid fuel (250 g in this study) and then the plasma is activated instead of simultaneous feeding and plasma operation. In this case, the produced gas content is similar to the simultaneous solid fuel feeding and plasma operation. After a while of operation of plasma, the reactor were opened and the solid fuels were checked. It is observed that the plasma flame interact just the fuels at top of the reactor. The reaction was not occurred in whole reactor because the plasma was in contact just in the upper side of the gasifier. The plasma applicator and reactor assembly were reversed to spread the reaction to whole reactor. The gasifier connected from bottom and then the reactor and at the top the cyclone filter were located. The reactor were filled with solid fuel and then the reaction processes were performed by producing high amount of smoke. By this way, the solid feeder was just used to dose the reactor. The simultaneous solid fuel feeding and plasma gasification system operation were cancelled.

-The usage of steam as oxidant was cancelled because of problems occurred in the plasma generation system.

Solid fuels are examined by proximate and ultimate analysis methods, the heating value of the fuels are calculated through measurement of proximate and ultimate analysis and measured by the adiabatic bomb calorimeter test. Also, the solid fuels are examined by SEM and EDX analysis methods. While the Russian coal (CR) has the highest heating value of 26240 kJ/kg, the Hornbeam sawdust (HSD) has the lowest heating value with 14072 kJ/kg according to empirical calculations.

6 different solid fuels, Russian coal (CR), South African coal (CSA), Şırnak coal (CTR), pine tree sawdust (PSD), hornbeam sawdust (HSD) and polyethylene (PP) are gasified for powers between 3 kW and 6 kW, and flow rates between 50 sL/min and 100 sL/min. The temperature distribution in the gasifier is determined by measuring the temperature by thermocouples at y/h=0.28, 0.44, 0.6, 0.76 and 0.92 in each case. The 6 types of solid fuels are sorted according to type of them as follows; pine tree sawdust (PSD), hornbeam sawdust (HSD) are sawdust, Russian coal (CR), South African coal (CSA), Şırnak coal (CTR) are coals and polyethylene (PP) is polyethylene. According to this classification, the characteristics of each type of fuels are given.

The highest syngas temperature is 1175 ℃ at 6 kW plasma power, 50 sL/min and hornbeam sawdust (HSD) gasification in case of gasification of sawdust. The lowest syngas temperature is 621 ℃ at 3 kW plasma power, 100 sL/min air flow rate and hornbeam sawdust (HSD) gasification. In case of gasification of coals, the highest syngas temperature is 1276 ℃ at 6 kW plasma power, 50 sL/min air flow rate and Russian coal (CR) gasification. The lowest syngas temperature is 641 ℃ at 3 kW plasma power, 100 sL/min air flow rate and Şırnak (Turkey) coal (CTR) gasification. In case of gasification of polyethylene, the highest syngas temperature is 1218 ℃ at 6 kW plasma power, 50 sL/min air flow rate and polyethylene (PP) gasification. The lowest syngas temperature is 629 ℃ at 3 kW plasma power, 100 sL/min air flow rate and polyethylene (PP) gasification. In all the experimentation, the highest syngas temperature is 1276 ℃ at 6 kW plasma power, 50 sL/min air flow rate and Russian coal (CR) gasification while the lowest syngas temperature is 621 ℃ at 3 kW plasma power, 100 sL/min air flow rate and hornbeam sawdust (HSD) gasification.

The highest syngas production is 1.12 kg at 3 kW plasma power, 50 sL/min and hornbeam sawdust (HSD) gasification in case of gasification of sawdust. The lowest syngas production is 0.66 kg at 6 kW plasma power, 100 sL/min air flow rate and hornbeam sawdust (HSD) gasification. In case of gasification of coals, the highest syngas production is 1.2 kg at 3 kW plasma power, 50 sL/min air flow rate and Russian coal (CR) gasification. The lowest syngas production is 0.72 kg at 6 kW plasma power, 100 sL/min air flow rate and Şırnak (Turkey) coal (CTR) gasification. In case of gasification of polyethylene, the highest syngas production is 0.9 kg at 3 kW plasma power, 50 sL/min and Polyethylene (PP) gasification. The lowest syngas production is 0.76 kg at 6 kW plasma power, 100 sL/min and Polyethylene (PP) gasification. In all the experimentation, the highest syngas production is 1.2 kg at 3 kW plasma power, 50 sL/min air flow rate and Russian coal (CR) gasification while the lowest syngas production is 0.66 kg at 6 kW plasma power, 100 sL/min air flow rate and hornbeam sawdust (HSD) gasification. The syngas production changes depending on air flow rate and power. Because, the increasing power reduces the gasification time. The supplied air amount to the reactor reduces due to the reduction of supplying air flow rate duration. As a result the produced syngas amount decreases while the supplied fuel amount is same.

The highest process energy efficiency (η_{EP}) is 66.88 % at 6 kW plasma power, 75 sL/min and pine tree sawdust (PSD) gasification and the lowest process energy efficiency (η_{EP}) is 30.8 % at 3 kW plasma power, 50 sL/min and hornbeam sawdust (HSD) gasification in case of gasification of sawdust. Also, the highest system energy efficiency (η_{ES}) is 41.4 % at 6 kW plasma power, 75 sL/min and pine tree sawdust (PSD) gasification and the lowest system energy efficiency (η_{ES}) is 20.6 % at 3 kW plasma power, 50 sL/min and hornbeam sawdust (HSD) gasification in case of gasification of sawdust. While the highest process energy efficiency (η_{EP}) is 86.04 % at 3 kW plasma power, 100 sL/min and Şırnak (Turkey) coal (CTR) gasification, the lowest process energy efficiency (η_{EP}) is 52.55 % at 6 kW plasma power, 50 sL/min and South African coal (CSA) gasification in case of gasification of coals. Also, the highest system energy efficiency (η_{ES}) is 61.37 % at 3 kW plasma power, 100 sL/min and Russian coal (CR) gasification and the lowest system energy efficiency (η_{ES}) is 32.99 % at 3 kW plasma power, 50 sL/min and South African coal (CSA) gasification in case of gasification of coals. In case of gasification of polyethylene, while the highest process energy efficiency (η_{EP}) is 57.73 % at 6 kW plasma power and 100 sL/min air flow rate, the lowest process energy efficiency (η_{EP}) is 36.8 % at 4.2 kW plasma power and 50 sL/min air flow rate. The highest system energy efficiency (η_{ES}) is 43.86 % at 3.6 kW plasma power and 100 sL/min air flow rate, while the lowest system energy efficiency (η_{ES}) is 36.8 % at 4.2 kW plasma power and 50 sL/min air flow rate in case of gasification of polyethylene.

To sum up, in this experimental study, gasification of solid fuels at various flow rates and plasma power by microwave plasma gasification are investigated. All the independent parameters of the process; temperature, mass of syngas, fuel and ash; syngas, fuel and ash content are measured and the thermodynamic analysis of the process are performed.

In future studies, the following can be suggested to enhance and widen the knowledge about the microwave plasma gasification systems.

- The alternative reactor structure should be designed to overcome the problems occurred in operation. Instead of holding the plasma applicator parallel to reactor, the plasma applicator can be mounted to the reactor perpendicular or in angular positons. Mounting the applicator perpendicular or with an angle can eliminate the flame flashback and open possibilities to add steam to the reactor.
- In this current study, the process is transient process. The ways to operate the system steady should be investigated. The ways can be increasing the diameter of the reactor, eliminate the flashback, modify the reactor design.
- The waveguide should be pressurized by compress air to prevent the leakage of solid fuels and moisture to the magnetron.
- The steam should be supplied to the reactor to increase the outputs of Hydrogen. However, the leakage of steam to the magnetron should be solved to supply steam to the reactor. Usage of system for hydrogen production can be considered if the steam supply to the gasifier is achieved.
- The reactor can be isolated and the heat losses from the reactor can eliminate.
- The effects of solid fuel particle size on gasification characteristics can be examined.

- The cost analysis of the system can reveal the feasibility of the system for industrial applications.
- The durability of the reactor components should be tested for continues operation.

REFERENCES

Arena U. (2012). Process and Technological Aspects of Municipal Solid Waste Gasification. A Review., *Waste Management*, **32**, 625-639.

Bogaerts A., Neyts E., Gijbels R., van der Mullen J. (2002). Gas discharge plasmas and their applications, *Spectrochimica Acta Part B: Atomic Spectroscopy*, **57**, 609-658.

BP. British Petroleum. 2015. BP Statistical Review of World Energy June 2015. London, UK. availeble at: http://www.bp.com/content/dam/bp/pdf/energy-economics/statistical-review-2015/bp-statistical-review-of-world-energy-2015-full-report.pdf.

Çarpınlıoğlu M. Ö., Şanlısoy A. (2017). Katı Atıkların Enerji Dönüşümünde Plazma Gazlaştırma Kullanımı ile Çalışan Laboratuvar Ölçekli Bir Test Düzeneğinin (Mikrodalga Gazlaştırıcı) "Mcwgazlaştırıcı" Tasarım Üretim ve Performans Değerlendirilmesi-Plazma Gazlaştırma Teknolojisinin-Bilginin Üretilip Kullanılmasında Bir Vaka *TUBITAK 115M389 Interim report*, **1**.

Çarpınlıoğlu M. Ö., Şanlısoy A. (2017). Katı Atıkların Enerji Dönüşümünde Plazma Gazlaştırma Kullanımı ile Çalışan Laboratuvar Ölçekli Bir Test Düzeneğinin (Mikrodalga Gazlaştırıcı) "Mcwgazlaştırıcı" Tasarım Üretim ve Performans Değerlendirilmesi-Plazma Gazlaştırma Teknolojisinin-Bilginin Üretilip Kullanılmasında Bir Vaka *TUBITAK 115M389 Interim report*, **2**.

Çarpınlıoğlu M. Ö., Şanlısoy A. (2018). Katı Atıkların Enerji Dönüşümünde Plazma Gazlaştırma Kullanımı ile Çalışan Laboratuvar Ölçekli Bir Test Düzeneğinin (Mikrodalga Gazlaştırıcı) "Mcwgazlaştırıcı" Tasarım Üretim ve Performans Değerlendirilmesi-Plazma Gazlaştırma Teknolojisinin-Bilginin Üretilip Kullanılmasında Bir Vaka *TUBITAK 115M389 Interim report*, **3**.

Çengel Y. A., Boles M. A. 2007. Thermodynamics: an engineering approach. USA: McGraw-Hill.

Channiwala S. A., Parikh P. P. (2002). A unified correlation for estimating HHV of solid, liquid and gaseous fuels, *Fuel*, **81**, 1051-1063.

Coleman H. W., Steele W. G. 2009. Experimentation, Validaiton, and Uncertainty Analysis for Engineers. New Jersey: John Wiley&Sons.

Czylkowski D., Hrycak B., Miotk R., Jasiński M., Dors M., Mizeraczyk J. (2015). Hydrogen production by conversion of ethanol using atmospheric pressure microwave plasmas, *International Journal of Hydrogen Energy*, **40**, 14039-14044.

EERE. Office of Energy Efficiency & Renewable Energy. 2013. Biopower Basics. Washington DC. http://energy.gov/eere/energybasics/articles/biopower-basics. 04/12/2015.

Finet C. (1987). Heating value of municipal solid waste, *Waste Management & Research*, **5**, 141-145.

Gray L. 2014. Plasma Gasification as a Viable Waste-to-Energy Treatment of Municipal Solid Waste. Hartford, USA.

Hlina M., Hrabovsky M., Kavka T., Konrad M. (2014). Production of high quality syngas from argon/water plasma gasification of biomass and waste, *Waste Management*, **34**, 63-66.

Hong Y. C., Lee S. J., Shin D. H., Kim Y. J., Lee B. J., Cho S. Y., Chang H. S. (2012). Syngas production from gasification of brown coal in a microwave torch plasma, *Energy*, **47**, 36-40.

Hrycak B., Czylkowski D., Miotk R., Dors M., Jasinski M., Mizeraczyk J. (2014). Application of atmospheric pressure microwave plasma source for hydrogen production from ethanol, *International Journal of Hydrogen Energy*, **39**, 14184-14190.

Huang H., Tang L. (2009). Pyrolysis treatment of waste tire powder in a capacitively coupled RF plasma reactor, *Energy Conversion and Management*, **50**, 611-617.

Industrial Microwave P., RF and Control Systems M-Press Systems Sdn. Bhd. Industrial Microwave-, Plasma-, RF- and Control Systems. 2015. Magnetron Basics. http://www.m-press.com.my/en/technical_info/magnetron_basics.html. 05/12/2015.

ISRE. Biomass.net an Important Source of Reneweble Energy. 2015. A Brief Definition of Biomass. http://www.biomass.net/. 03/12/2015.

Jamróz P., Kordylewski W., Wnukowski M. (2018). Microwave plasma application in decomposition and steam reforming of model tar compounds, *Fuel Processing Technology*, **169**, 1-14.

Janajreh I., Raza S. S., Valmundsson A. S. (2013). Plasma Gasification Process: Modelling, Simulation and Comparasion with Conventional Air Gasification, *Energy Conversion and Management*, **65**, 801-809.

Kalinci Y., Hepbasli A., Dincer İ. (2011). Exergoeconomic Analysis of Hydrogen Production from Plasma Gasification of Sewage Sludge Using Specific Exergy Cost Method, *International Journal of Hydrogen Energy*, **36**, 11408-11417.

Knoef H. 2005. Practical Aspects of Biomass Gasification. Handbook on Biomass Gasification. Chapter 3. Enschede, Netherland: BTG.

Kotas T. J. 1985. Appendix A- Chemical exergy and enthalpy of devaluation. Butterworth-Heinemann.

Lee H. G., Park H.-W., Choi S., Park H.-S., Park D.-W. (2014). Production of Synthesis Gas from Coal by DC Non-Transferred Steam Plasma Gasification System, *Journal of Chemical Engineering of Japon*, **47**, 334-339.

Leins M. 2010. Development and spectroscopic investigation of a microwave plasma source for the decomposition of waste gases, Thesis type, Universität Stuttgart 04 Fakultät Energie-, Verfahrens- und Biotechnik.

Lin K. C., Lin Y.-C., Hsiao Y.-H. (2014). Microwave plasma studies of Spirulina algae pyrolysis with relevance to hydrogen production, *Energy*, **64**, 567-574.

Loha C., Chattopadhyay H., Chatterjee P. K. (2011). Thermodynamic Analysis of Hydrojen Rich Synthetic Gas Generation from Fluidized Bed Gasification of Rice Husk, *Energy*, **36**, 4063-4071.

Minutillo M., Perna A., Di Bona D. (2009). Modelling and performance analysis of an integrated plasma gasification combined cycle (IPGCC) power plant, *Energy Conversion and Management*, **50**, 2837-2842.

Moore M. E., McFarland A. R. (1990). Design of Stairmand-type sampling cyclones, *American Industrial Hygiene Association Journal*, **51**

NREL. National Renewable Energy Laboratory. 2014. Learning About Renewable Energy. http://www.nrel.gov/learning/re_biomass.html. 03/12/2015.

Ozdinc Carpinlioglu M., Sanlisoy A. (2018). Performance assessment of plasma gasification for waste to energy conversion: A methodology for thermodynamic analysis, *International Journal of Hydrogen Energy*, **43**, 11493-11504.

Prins M. J., Ptansinski K. J., Janssen F. J. J. G. (2007). From Coal to Biomass Gasification: Comparasion of Thermodynamic Efficiency, *Energy*, **32**, 1248-1259.

Roth J. R. 1994. Industrial Plasma Engineering. USA: Taylor & Francis.

Ruj B., Ghosh S. (2014). Technological aspects for thermal plasma treatment of municipal solid waste—A review, *Fuel Processing Technology*, **126**, 298-308.

Rutberg P. G., Bratsev A. N., Kuznetsov V. A., Popov V. E., Ufimtsev A. A., Shtengel S. V. (2011). On Efficiency of Plasma Gasification of Wood Residues, *Biomass and Bioenergy*, **35**, 495-504.

Sanlisoy A. 2013. Investigating the Effects of Plasma Actuator on the Flow Control Around NACA2415 Airfoil, Thesis type, Nigde University.

Sanlisoy A., Carpinlioglu M. O. 2016. Preliminary Measurements on Microwave Plasma Characteristics. Gaziantep,Turkey.

Sanlisoy A., Carpinlioglu M. O. 2016. Presentation of a Microwave Plasma Gasification System “MCw Gasifier” Istanbul.

Sanlisoy A., Carpinlioglu M. O. 2016. A Review on Plasma Gasification for Solid Waste Disposal. France.

Sanlisoy A., Carpinlioglu M. O. (2017). Preliminary measurements on microwave plasma flame for gasification, *Energy, Ecology and Environment*,

Sanlisoy A., Carpinlioglu M. O. (2017). A review on plasma gasification for solid waste disposal, *International Journal of Hydrogen Energy*, **42**, 1361-1365.

Sekiguchi H., Mori Y. (2003). Steam plasma reforming using microwave discharge, *Thin Solid Films*, **435**, 44-48.

Sekiguchi H., Orimo T. (2004). Gasification of polyethylene using steam plasma generated by microwave discharge, *Thin Solid Films*, **457**, 44-47.

Shie J.-L., Chen L.-X., Lin K.-L., Chang C.-Y. (2014). Plasmatron gasification of biomass lignocellulosic waste materials derived from municipal solid waste, *Energy*, **66**, 82-89.

Shie J.-L., Tsou F.-J., Lin K.-L., Chang C.-Y. (2010). Bioenergy and products from thermal pyrolysis of rice straw using plasma torch, *Bioresource Technology*, **101**, 761-768.

Shin D. H., Hong Y. C., Lee S. J., Kim Y. J., Cho C. H., Ma S. H., Chun S. M., Lee B. J., Uhm H. S. (2013). A pure steam microwave plasma torch: Gasification of powdered coal in the plasma, *Surface and Coatings Technology*, **228**, S520-S523.

Surov A. V., Popov S. D., Popov V. E., Subbotin D. I., Serba E. O., Spodobin V. A., Nakonechny G. V., Pavlov A. V. (2017). Multi-gas AC plasma torches for gasification of organic substances, *Fuel*, **203**, 1007-1014.

Szargut J., Styrylska T. (1964). Approximate evaluation of the exergy of fuels, *Brennst. Waerme Kraft*, **16**, 589-596.

Tang L., Huang H. (2007). Decomposition of polyethylene in radio-frequency nitrogen and water steam plasmas under reduced pressures, *Fuel Processing Technology*, **88**, 549-556.

Tang L., Huang H., Hao H., Zhao K. (2013). Development of Plasma Pyrolysis/Gasification Systems for Energy Efficient and Environmentally Sound Waste Disposal, *Journal of Electrostatics*, **71**, 839-847.

Tu W.-K., Shie J.-L., Chang C.-Y., Chang C.-F., Lin C.-F., Yang S.-Y., Kuo J. T., Shaw D.-G., You Y.-D., Lee D.-J. (2009). Products and bioenergy from the pyrolysis of rice straw via radio frequency plasma and its kinetics, *Bioresource Technology*, **100**, 2052-2061.

Uhm H. S., Kwak H. S., Hong Y. C. (2016). Carbon dioxide elimination and regeneration of resources in a microwave plasma torch, *Environmental Pollution*, **211**, 191-197.

Uhm H. S., Na Y. H., Hong Y. C., Shin D. H., Cho C. H. (2014). Production of hydrogen-rich synthetic gas from low-grade coals by microwave steam-plasmas, *International Journal of Hydrogen Energy*, **39**, 4351-4355.

Vaidyanathan A., Mulholland J., Ryu J., Smith M. S., Circeo Jr L. J. (2007). Characterization of fuel gas products from the treatment of solid waste streams with a plasma arc torch, *Journal of Environmental Management*, **82**, 77-82.

WCI. World Coal Institue. 2009. The coal resource a comprehensive overview of coal. London, UK. availeble at: http://www.worldcoal.org/sites/default/files/coal_resource_overview_of_coal_report%2803_06_2009%29.pdf.

Wheeler A. J., Ganji A. R. 2010. Introduction to Engineering Experimentation. Pearson.

Yokoyama S., Matsumura Y. 2008. The Assian Biomass Handbook A Guide for Biomass Production and Utilization. Tokyo: The Japon Institue of Energy.

Yoon S. J., Lee J.-G. (2012). Hydrogen-rich syngas production through coal and charcoal gasification using microwave steam and air plasma torch, *International Journal of Hydrogen Energy*, **37**, 17093-17100.

Yoon S. J., Yun Y. M., Seo M. W., Kim Y. K., Ra H. W., Lee J.-G. (2013). Hydrogen and syngas production from glycerol through microwave plasma gasification, *International Journal of Hydrogen Energy*, **38**, 14559-14567.

Zhang Q., Wu Y., Dor L., Yang W., Blasiak W. (2013). A thermodynamic analysis of solid waste gasification in the Plasma Gasification Melting process, *Applied Energy*, **112**, 405-413.

APPENDIX

A.1 System components technical specifications

In this section, the system components technical information is given and the measurement methodology is explained.

A1.1 Power supplier

The properties of the Muegge MX6000D-110K model power supplier are given in Table A.1.

Table A.1 Power Supplier technical specifications

Primary power circuit	208V AC, 3 phases, 50-60Hz, 27A
Primary control circuit	208V AC, 2 phases, 50-60Hz, 2.76A
Suitable for MW-output power	6 kW 2450MHz
Efficiency	Approx. % 90 at full output power
Interference	CAN-Bus, PLC, operating and display panel
Assembly	Fully closed aluminum housing, Solid encapsulated assembly
Dimensions	19 inch rack mount; Length 688mm, Width 483mm, Height 132.5mm
Conditions	Ambient temperature 5-45°C, Humidity % 80 at 30°C, subsequently linearly reduced to % 50 at 45°C, Cooling water 20-25°C
Connections	9pin Sub-D male (CAN BUS INTERFACE) 25 pin Sub-D female (PLC INTERFACE) Circ. Connector (Prim. Power circuit/primary control circuit) Circ. Connector (Sec. Heating Circuit) Circ. Connector (Magnetron head signal) BNC Connector (Reflected power measurement) Circ. Connector (Arc. Detection) HV socket (HV- output power Stud M6 (Ground/PE) 2xlock coupling G ¼”x 9mm (cooling water)
Weight	26kg

A1.2 Magnetron

Technical specification of the Muegge MH6000S-213BF model Magnetron is given in Table A.2.

Table A.2 Magnetron technical specifications

HF output power	6 kW
Frequency	2.45 GHz +/-20 MHz
Output flange	WR340
Magnetron	E327
Cooling water	6L/min 4 bar (inlet temp. 20-25℃
Interlock	Cover and Magnetron over-temperature
Assembly	Fully enclosed
Dimensions	Height 250 mm, Width 370 mm, Depth 460 mm
Conditions	Ambient temperature 5-45℃, Humidity % 80 at 30℃, subsequently linearly reduced to % 50 at 45℃, Cooling water 20-25℃
Cooling Connector	Hose connection nozzle 9mm
Weight	Approx. 22 kg

A1.3 Isolator

Muegge MW1006A-210EC model isolator which protects the magnetron from dummy load is given in Table A.3.

Table A.3 Technical specifications of isolator

Frequency	2.45 GHz +/-20 MHz
VSWR	Max 1.25 (matched load) Max 1.5 (output short circuited)
Insertion loss	0.2dB (max 0.3dB)
Isolation	26dB (min 20dB)
Power (forward)	6.5kW
Power (reflected)	6.5kW
Temperature range	10-50℃ ambient (max 40℃ water inlet)
Monitor coupling	65 dB +/-2dB (reflected power)
Connectors	Flange IEC PDR 26, Monitor N female
Dimensions	182 mm x 300 mm x 116 mm

A1.4 3-stub tuner

Mueege MW2010A-260EF model 3-stub tuner properties are given in Table A.4 which is used to provide signal matching and minimize the reflected power.

Table A.4 Technical specifications of 3-stub tuner

Frequency	2.45 GHz +/-50 MHz
Power	20kW max.
Tuning capacity	VSWR 10:1
Waveguide	WR340
Waveguide Flange	PDR 26
Weight	3.5kg (aluminum)
Length	260mm

A1.5 Plasma applicator

Muegge MA6000A-013BB model plasma applicator specifications are given in Table A.5.

Table A.5 Technical specifications of plasma applicator

Frequency	2.45 GHz +/-20 MHz
Power	6 kW max.
Waveguide	WR340
Waveguide Flange	UDR 26 (10xM6)
Reactor outlet	Quartz tube diameter 30mm, thickness 1.5mm, length 200mm
Cooling water	Min 4 L/min 4.5 bar at 20℃
Cooling connectors	Check valve $G^{1/4"}$*9mm
Igniter	Igniter pressurized cylinder
Igniter compressed air	Compressed air 6 bar
Air carrier gas connector	Threaded connector KF DN25-G1" (100-200L/min)
Working gas connector	Stainless hose fitting SS-6MO-1-2RP
Material	Aluminum/Brass
Dimensions	Approx. 479mmx210mmx140mm

A1.6 Compressor

Lupamat screw compressor is used to supply the required air flow rate to plasma generator. The technical properties of compressor is given in Table A.6.

Table A.6 Technical specifications of Lupamat screw compressor

Compressor type	1kV 30/8
Air efficiency	4.85 m^3/min
Operation pressure	8 bar
Max. pressure	8 bar
Motor power	30kW
Weight	800kg

A1.7 Water vapor generator

Malkan UP 100P2 model vapor generator is used to supply the required water vapor. The technical properties of vapor generator is given in Table A.7.

Table A.7 Technical specifications of Malkan UP100P2 model vapor generator

Type	UP100P2
Voltage-Frequency	400V-50Hz
Current	16.5A
Power	6.5kW
Moto pump	0.75kW
Resistance heater	4.5kW
Water volume	3 liters
Vapor pressure	3.7 bar (gauge)
Vapor capacity	5kg/h
IP code	IP 20
Net weight	50kg
Dimensions	55x43x110cm

A1.8 Mass flow meter

Alicat MCR-250SL/MIN-D model mass flow controller is used to measure and control the air flow rate supplied to the plasma generator. The technical properties of Mass flow meter is given in Table A.8. The calibration certificate of it is given in Figure A.1.

Table A.8 Alicat MCR-250SL/MIN-D mass flow controller technical specifications

MC-MCR Mass flow controller	
Accuracy at calibration conditions	Full scale% 0.2
Repeatability	Full scale % 0.2
Zero shift-span shift	Full scale % 0.02
Operational range	% 0.5- % 100
Maximum controllable flow rate	Full scale % 102.4
Maximum measurable flow rate	Full scale up to % 128
Response time	100ms
Heating time	1s
Working temperature	-10&60℃
Humidity rate	0 - % 100
Maximum internal pressure	145 psig
Power supplier	24-30V DC

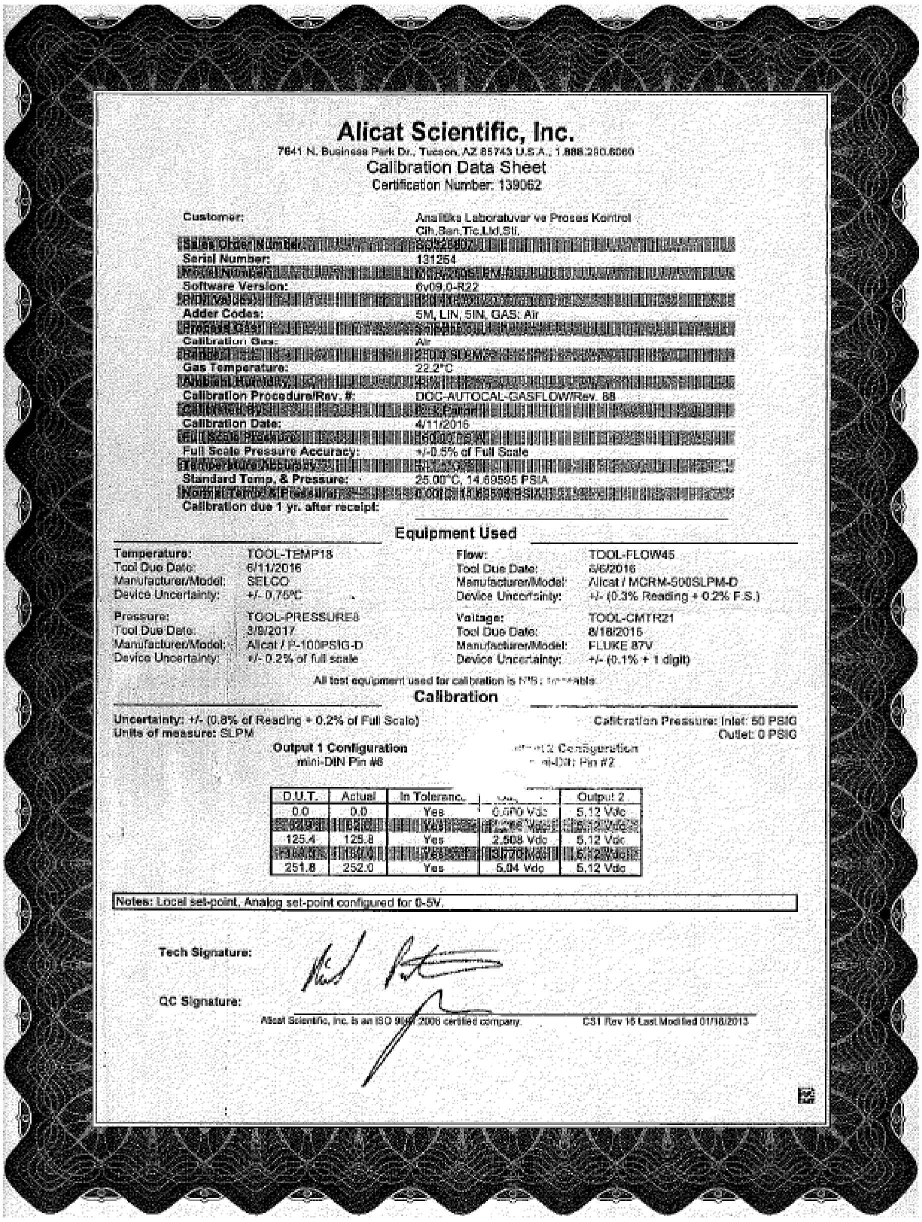

Alicat Scientific, Inc.

7641 N. Business Park Dr., Tucson, AZ 85743 U.S.A., 1.888.290.6060

Calibration Data Sheet

Certification Number: 139062

Customer:	Analitika Laboratuvar ve Proses Kontrol Cih.San.Tic.Ltd.Sti.
[redacted]	
Serial Number:	131254
[redacted]	
Software Version:	6v09.0-R22
[redacted]	
Adder Codes:	5M, LIN, 5IN, GAS: Air
[redacted]	
Calibration Gas:	Air
[redacted]	
Gas Temperature:	22.2°C
[redacted]	
Calibration Procedure/Rev. #:	DOC-AUTOCAL-GASFLOW/Rev. 88
[redacted]	
Calibration Date:	4/11/2016
[redacted]	
Full Scale Pressure Accuracy:	+/-0.5% of Full Scale
[redacted]	
Standard Temp. & Pressure:	25.00°C, 14.69595 PSIA
[redacted]	
Calibration due 1 yr. after receipt:	

Equipment Used

Temperature:	TOOL-TEMP18	**Flow:**	TOOL-FLOW45
Tool Due Date:	6/11/2016	Tool Due Date:	5/6/2016
Manufacturer/Model:	SELCO	Manufacturer/Model:	Alicat / MCRM-500SLPM-D
Device Uncertainty:	+/- 0.75°C	Device Uncertainty:	+/- (0.3% Reading + 0.2% F.S.)
Pressure:	TOOL-PRESSURE8	**Voltage:**	TOOL-CMTR21
Tool Due Date:	3/9/2017	Tool Due Date:	8/18/2016
Manufacturer/Model:	Alicat / P-100PSIG-D	Manufacturer/Model:	FLUKE 87V
Device Uncertainty:	+/- 0.2% of full scale	Device Uncertainty:	+/- (0.1% + 1 digit)

All test equipment used for calibration is NIST traceable.

Calibration

Uncertainty: +/- (0.8% of Reading + 0.2% of Full Scale)
Units of measure: SLPM

Calibration Pressure: Inlet: 50 PSIG
Outlet: 0 PSIG

Output 1 Configuration
mini-DIN Pin #6

Output 2 Configuration
mini-DIN Pin #2

D.U.T.	Actual	In Tolerance	Output 1	Output 2
0.0	0.0	Yes	0.000 Vdc	5.12 Vdc
[redacted]				
125.4	125.8	Yes	2.508 Vdc	5.12 Vdc
[redacted]				
251.8	252.0	Yes	5.04 Vdc	5.12 Vdc

Notes: Local set-point, Analog set-point configured for 0-5V.

Tech Signature:

QC Signature:

Alicat Scientific, Inc. is an ISO 9001:2008 certified company. CS1 Rev 15 Last Modified 01/18/2013

Figure A.1 ALICAT MCR-250sL/min-D mass flow meter calibration certificate

A1.9 Rotameter

YOKOGAVA RAMC01-A1SS-53L1-E90424/A16/SD model rotameter is used to measure the supplied water vapor flow rate to the reactor. The technical properties of the rotameter is given in Table A.9. Also, the calibration certificate of the rotameter is given in Figure A.2.

Table A.9 RAMC Rotameter technical specifications

YOKOGAVA RAMC rotameter	
Measuring range	4-40L/min
Measuring range ratio	10:1
Calibration state	5 bar absolute pressure and 152℃ saturated vapor
Wetted parts	Stainless steel -196&370℃
Accuracy	Full scale % 1.6
Linearity	Full scale % 0.2
hysteresis	Full scale % 0.1
Repeatability	Full scale % 0.1
Output signal	Full scale % 0.15
AC part of signal	Full scale % 0.15
Uncertainty	Full scale % 1.6
Electromagnetic compatibility	EN 61326 1-2-3
Transmitter output signal	4-20mA
Measurable fluids	Liquid, gas, vapor
Process connection	DN15 flange

ROTA YOKOGAWA

Kalibrier - Zertifikat
Calibration - Certificate

Allgemeine Daten / General Data

Produkt / Product:	ROTAMESSER / ROTAMETER
Modell / Model:	RAMC01-A1SS-53L1-E90424/A16/SD
P/O-No.:	BPY 16 020
Serien-Nr. / Serial-No.:	D1S402463
Messstelle / Tag:	

Schwebekörper / Float: D(s) = 18,00 mm M(s) = 33,3500 g rho(s) = 7,710 g/cm3

Abgleich Analog-Ausgang : Current Output Adjustment : 4 ... 20 mA = 0 - 45,00 l/min

Messbedingungen / Measuring Conditions

	Kalibrierung (i.K.) Calibration (i.K.)	Betriebszustand (i.B.) Customer Cond. (i.B.)
Medium	Luft	STEAM
Temp. / Temp.	20 °C	+ 150 °C
Druck / Pressure	1,000 bar abs.	3,750 bar g.
Dichte / Density	0,00119 kg/l	2,54800 kg/m³
Visk. / Visc.	0,0180 mPas	0,0140 mPas
Qmin - Qmax	417,0-4060,0 l/h	4,50-45,00 l/min

Durchflussprüfung / Actual Flow Test

Genauigkeit der Messnormale: < 1 % v.M.
Accuracy of master: < 1 % of rate

Messnormal / Master			Rotamesser / Rotameter	
Nr. No.	Qv i.K. [l/h]	Qv i.S. l/min	Skala Scale [mm]	Meßunsicherheit Uncertainty [% v.M.]
107	416,9	4,758	15,4	7,8
107	1011,0	11,510	23,0	3,2
107	1494,0	17,010	28,9	2,2
107	2017,0	22,960	35,3	1,6
107	2544,0	28,960	41,8	1,6
107	3034,0	34,540	49,3	1,6
107	4061,0	46,230	61,6	1,6

Die Skala des ROTAMESSERs wird bei ihrer Erstellung optimal der Durchflussanzeige des Messnormals angepasst. Deshalb reduziert sich die Abweichung zum Messnormal allein auf die Unsicherheit, die beim Ablesen und bei der Umrechnung in den Betriebszustand besteht. Weitere Abweichungen wie z.B. Linearitätsfehler sind wegen der verwendeten nicht-linearen Skala vernachlässigbar klein. Die angegebene Messunsicherheit entspricht den Berechnungsvorschriften nach VDI/VDE 3513 (2008).

At manufacturing the scale of the ROTAMETER is fitted optimally to the master's flow display. That is why the deviation to the master is reduced only to the uncertainty originated at reading and calculating to customer's conditions. Other deviations are neglectable by reason of using a non-linear scale. The above mentioned uncertainty is calculated according to VDI/VDE 3513 (2008).

Kalibrierergebnis / Calibration Result

Die Messunsicherheit des ROTAMESSERs entspricht unter Kalibrierbedingungen dem Fehlergrenzwert 1,6% bei einer Fehlergrenze von 50% Qmax nach VDI/VDE 3513/Blatt2 (2008). The uncertainty of the ROTAMETER is corresponding at calibration conditions to the max. permissable error of 1,6% at a limit of 50% Qmax according to VDI/VDE 3513/Part 2 (2008).

Wehr, 21.04.16

geprüft/approved
G. Giesen
Leiter /Head Calibration

T. Valva
Prüfer / Inspector

QIC-GC RA23g

Die Kalibrieranlagen ROTA YOKOGAWA sind ausnahmslos rückführbar auf die nationalen Normale der Europäischen Union. ROTA YOKOGAWA ist Mitglied des Deutschen Kalibrierdienstes (DKD-K-03901) und untersteht damit der direkten Aufsicht der Physikalisch-Technischen Bundesanstalt (PTB).
The calibration facilities of ROTA YOKOGAWA are completely traceable to the national standards of the Eurpean Union. ROTA YOKOGAWA is member of the German Calibration Service (DKD-K-03901) and is certified by Pysikalisch-Technische Bundesanstalt (PTB).

Figure A.2 RAMC rotameter calibration certificate

A1.10 Thermocouple (Elimko B type (Pt18Rh-Pt) Thermocouple)

The temperature measurement is performed by Elimko B type (PT18Rh-Pt) thermocouples. Thermocouple is consist of 2 different wire material that joined together. The joined point is called as hot junction point while the other ends are the cold junction (reference) points. As a result of temperature difference, the voltage in magnitude of mV generated across the cold junction points. The generated voltage is proportional with the temperature difference in hot and cold junction points. The B type thermocouple is measuring the temperature up to 1800°C. In Table A.10, the temperatures corresponding to measured voltage is presented.

Table A.10 B type platinum-% 18 rhodium thermocouple °C-mV conversion table.

°C	0	100	200	300	400	500	600	700	800	900	1,000	1,100	1,200	1,300	1,400	1,500	1,600	1,700	1,800	°C
0	0.000	0.033	0.178	0.431	0.786	1.241	1.791	2.430	3.154	3.957	4.833	5.777	6.783	7.845	8.952	10.094	11.257	12.426	13.585	0
10	-0.002	0.043	0.199	0.462	0.827	1.292	1.851	2.499	3.231	4.041	4.924	5.875	6.887	7.953	9.065	10.210	11.374	12.543	13.699	10
20	-0.003	0.053	0.220	0.494	0.870	1.344	1.912	2.569	3.308	4.126	5.016	5.973	6.991	8.063	9.178	10.325	11.491	12.659	13.814	20
30	-0.002	0.065	0.243	0.527	0.913	1.397	1.974	2.639	3.387	4.212	5.109	6.073	7.096	8.172	9.291	10.441	11.608	12.776		30
40	0.000	0.078	0.266	0.561	0.957	1.450	2.036	2.710	3.466	4.298	5.202	6.172	7.202	8.283	9.405	10.558	11.725	12.892		40
50	0.002	0.092	0.291	0.596	1.002	1.505	2.100	2.782	3.546	4.386	5.297	6.273	7.308	8.393	9.519	10.674	11.842	13.008		50
60	0.006	0.107	0.317	0.632	1.048	1.560	2.164	2.855	3.626	4.474	5.391	6.374	7.414	8.504	9.634	10.790	11.959	13.124		60
70	0.011	0.123	0.344	0.669	1.095	1.617	2.230	2.928	3.708	4.562	5.487	6.475	7.521	8.616	9.748	10.907	12.076	13.239		70
80	0.017	0.140	0.372	0.707	1.143	1.674	2.296	3.003	3.790	4.652	5.583	6.577	7.628	8.727	9.863	11.024	12.193	13.354		80
90	0.025	0.159	0.401	0.746	1.192	1.732	2.363	3.078	3.873	4.742	5.680	6.680	7.736	8.839	9.974	11.141	12.310	13.470		90
100	0.033	0.178	0.431	0.786	1.241	1.791	2.430	3.154	3.957	4.833	5.777	6.783	7.845	8.952	10.094	11.257	12.426	13.585		100

The measured temperature inputs recorded via Elimko E-PR-110 model data logger. It can log analog signal from the devices. It has 9 channels. Its accuracy for each channel is 0.5 % of reading data. It has 100 ms sampling period for each channels.

A1.11 Microwave power measurement

The Muegge MM1001B-110AB model microwave power detector is used for power measurement. The detector detects the microwave signal and converts to DC signal. The data is acquired and monitored by MUEGGE ME0220V-003AB model control software. The measured microwave signal in dBm can be converted to power signal by equation A.1.

$$dBm = 10\log_{10}\left(\frac{P}{1mW}\right) \qquad (A.1)$$

The transfer characteristics of microwave detector are given in Figure A.3 and the technical properties are given in Table A.11.

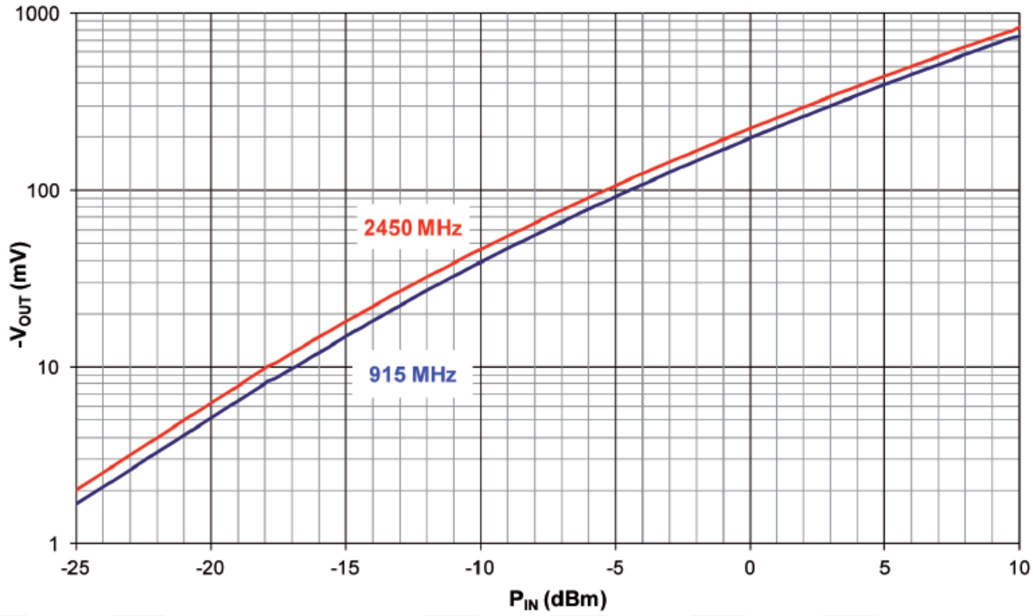

Figure A.3 Power detector transfer characteristics

Table A.11 Power detector technical properties

Frequency range	880-930MHz	2350-2550MHz
Frequency response variation (max.)	0.25dB	0.5dB
Output voltage	190mV	220mV
VSWR maximum	2	
VSWR typical	1.3	
Statistical spread of output voltage	1dB	
Output voltage polarity	Negative	
Output voltage temperature variation (5-65°C)	Maximum 3dB	
Maximum input working power	10mW	
Dimensions	58x26x26mm	
Input RF connector	N male	
Output DC connector	BNC female	

A1.12 Syngas Analysis

The MRU- AIR FAIR Varioplus model syngas monitoring system is used to measure the syngas components. The technical specifications of the system is given in Table A.12.

Table A.12 MRU-Varioplus model syngas monitoring system technical specifications

	Measurement range	Resolution	Method
Oxygen (O_2)	0-25	% 0.01	EC sensor
Carbon monoxide (CO)	0-100	% 0.01	NDIR (Nondispersive infrared sensor)
Carbon dioxide (CO_2)	0-100	% 0.01	NDIR (Nondispersive infrared sensor)
Methane (CH_4)	0-100	% 0.01	NDIR (Nondispersive infrared sensor)
Hydrogen (H_2)	0-100	% 0.01	TCD(Thermal conductivity)
Response time		30s	
Detection limit		% 0.05	
Linearity eror		Full scale % 1	
Repeatability		Full scale % 1	
Offset shift		negligible	
Span shift		Full scale %2	
Sample conditioning		Electrical gas cooling Teflon particle filter Monitored gas sample flow (60-80L/h) Sample input pressure -200hPa & 100hPa	
Dimensions		295x440x155mm	
Weight		7kg	
Ambient temperature		5-45 ℃	
Power supply		100-230V&47-63Hz	

CALIBRATION CERTIFICATE

Description of instrument *VARIO plus industrial*

Serial number 061481

We hereby confirm that the above-mentioned measuring system was calibrated conscientiously.

The adjustment and calibration of the flue gas analyser has been made with certified test gases. Other measuring procedures correspond with the technical regulations and norms valid at the time of the measurement.

Measuring installations:
Measurement with certified test gases

Measuring results:

	Nominal value	up./low. limits	Actual value of tested instrument
O2 / Vol.%	2,00	+/- 0,2 %	2,01
	10,10	+/- 0,2 %	10,08
CH4 / Vol.%	20,00	+/- 3,0 %	19,87
	40,00	+/- 3,0 %	40,08
	80,00	+/- 3,0 %	80,52
H2 / Vol.%	20,00	+/- 2,0 %	20,38
	40,00	+/- 2,0 %	40,06
	60,00	+/- 2,0 %	59,66
	80,00	+/- 2,0 %	79,54
CO2 / Vol.%	20,00	+/- 3,0 %	19,78
	40,00	+/- 3,0 %	39,92
	80,00	+/- 3,0 %	80,07
CO / Vol.%	20,00	+/- 3,0 %	20,18
	40,00	+/- 3,0 %	40,08
	80,00	+/- 3,0 %	79,94
Temperature	250°C	+/- 2°C	249,7
Draft mbar = hPa	meas. range in manual !	+/- 0,03 mbar	Values are between upper and lower limits !

*Special remarks:*______________________________________

Date of calibration: *10.11.14* Processed by:____________________________

MRU GmbH, Fuchshalde 8, D-74172 Neckarsulm-Obereisesheim Managing director: Erwin Hintz

Figure A.4 MRU- Air Fair Varioplus model syngas monitoring system calibration certificate

A1.13 Proximate analysis

Proximate analysis performed according to ASTM D 3172-89 method. The moisture content, volatile matter and ash content are measured according to ASTM D3173, D3175 and D3174 methods respectively.

A1.14 Ultimate analysis

The ultimate analysis of the fuels experiments is conducted in Bilecik Şeyh Edebali University central research laboratory by service procurement. The solid fuel samples were transferred to there. They use LECO CHN 628 model analyzer to perform the experiments. The experiments performed according to given standards in Table A.13.

Table A.13 Ultimate analyze measurement standards

Applied methods (ASME)	Measured parameters	Materials
D5291	C ,H, N	Oils
D5373/MTH A	C ,H, N	Coals
D1552	S	Oil and petroleum products
D4239	S	Coals
D5016	S	Coals and ashes
D1619	S	Carbon block
29541	C,H,N	Solid mineral fuels
19579	S	Solid mineral fuels

A1.15 Heating value of fuels

The heating value of the fuels are measured according to ASME D 5865 method.

A.2 Uncertainty Analysis

In this study, uncertainty of the measured and calculated parameters are defined by the methods proposed by Coleman and Steele, 2009 and Wheeler and Ganji, 2010. In this method, the general function is defined where experimental result which is denoted by r is function of variables which effect the experimental result and denoted by X_n as defined in equation A.2.

$$r = r(x_1, x_2, x_3, \dots x_n) \tag{A.2}$$

The uncertainty belong to this result is given in equation A.3.

$$\frac{U_r}{r} = \left[\left(\frac{x_1}{r}\frac{\partial r}{\partial x_1}\right)^2\left(\frac{U_{x_1}}{x_1}\right)^2 + \left(\frac{x_2}{r}\frac{\partial r}{\partial x_2}\right)^2\left(\frac{U_{x_2}}{x_2}\right)^2 + \cdots \left(\frac{x_n}{r}\frac{\partial r}{\partial x_n}\right)^2\left(\frac{U_{x_n}}{x_n}\right)^2\right]^{1/2} \tag{A.3}$$

If the result r is dependent only on product of measured variables as given in equation A.4, the equation A.3 can be reduced to equation A.5.

$$r = kx_1^a x_2^b x_3^c \dots . x_n^N \tag{A.4}$$

$$\frac{U_r}{r} = \left[a^2\left(\frac{U_{x_1}}{x_1}\right)^2 + b^2\left(\frac{U_{x_2}}{x_2}\right)^2 + c^2\left(\frac{U_{x_3}}{x_3}\right)^2 + \cdots c^2\left(\frac{U_{xn}}{x_n}\right)^2\right]^{1/2} \tag{A.5}$$

When result function has additive form as given in equation A.6, equation A.3 reduces to equation A.7.

$$r = a_1x_1 + a_2x_2 + \cdots a_nx_n \tag{A.6}$$

$$U_r = \left[\left(\frac{\partial r}{\partial x_1}\right)^2 (U_{x_1})^2 + \left(\frac{\partial r}{\partial x_2}\right)^2 (U_{x_2})^2 + \cdots \left(\frac{\partial r}{\partial x_n}\right)^2 (U_{x_n})^2\right]^{1/2} \tag{A.7}$$

The experiments include systematic errors caused by inaccuracy of each instruments and random errors because of quantities of measurements. The error types are classified as systematic (B) and random (R). Whereas the random errors depend on the number of measurement, the systematic errors are independent of measurement number. The random uncertainties can be calculated by the methodology explained below, If x variable is measured n times, the standard deviation can be determined by equation A.8.

$$S_x = \left(\sum_{i=1}^{n} \frac{(x_i - \bar{x})^2}{(n-1)} \right)^{1/2} \tag{A.8}$$

The mean of the variable can be estimated by using equation A.9.

$$\bar{x} = \frac{\sum_{i=1}^{n} x_i}{n} \tag{A.9}$$

For the given confidence level (usually 95 % for uncertainty analysis) and given degree of freedom ($v = n - 1$) t value can be determined by using equation A.10.

$$t = \frac{\bar{x} - \mu}{S/\sqrt{n}} \tag{A.10}$$

In this equation, $\bar{\mathbf{x}}$ denotes mean value, $\boldsymbol{\mu}$ denotes the population mean value, S denotes standard deviation and n denotes the number of samples. On the other hand, the number of samples are generally higher than 30 and the confidence level is 95 %. When these two conditions are satisfied t can be taken as 2. This simplifies the uncertainty analysis and the ASME recommends to hold the number of samples high for this reason.

The random uncertainty is then found by using equation A.11.

$$R_{\bar{x}} = \pm t \frac{S_x}{\sqrt{n}} \tag{A.11}$$

As a result of random and systematic uncertainties, the total uncertainty (U) can be determined by equation A.12.

$$U_x = \sqrt{(B_x)^2 + (R_x)^2} \tag{A.12}$$

ASME recommends to classify the uncertainty types to define and compare the source of uncertainties. According to ASME, the uncertainties can be classified into 5 groups which are calibration, data acquisition, data reduction, methods and others. The combined systematic uncertainties and random uncertainties can be estimated by using equation A.13 and A.14 respectively.

$$B_x = \sqrt{\sum_{i=1}^{k}(B_i)^2} \tag{A.13}$$

$$R_x = \sqrt{\sum_{i=1}^{k}(R_i)^2} \tag{A.14}$$

A2.1 Uncertainties of the measured parameters

<u>Uncertainty of mass flow meter:</u>

Measurement range: 0-250sL/min

Accuracy: reading value± 0.8 %, full scale ± 0.2 %

Repeatability: full scale ± 0.2 %

Zero shift and span shift: ± 0.02 %

Uncertainty: full scale ± 0.2 %

Equipment measures the flow rate at a range from 0 to 250 L/min. In this situation;

Accuracy: full scale ± 0.2 % - $250 \times 0.2/100 = 0.5\ \mathrm{sL/min}$

Repeatability: full scale ± 0.2 % -$250 \times 0.2/100 = 0.5\ \mathrm{sL/min}$

Zero shift and span shift:± 0.02 %- $250 \times 0.02/100 = 0.05\ \mathrm{sL/min}$

Table A.14 The errors in the measurement of mass flow rate

Errors	Systematic errors	Random errors
Accuracy	0.5	
Repeatability		0.5
Span shift		0.05

Total uncertainty;

$$U_x = \sqrt{((0.5)^2) + ((0.5)^2 + (0.05)^2)} = 0.7\mathrm{sL/min}$$

$$U_x/_x = \frac{0.7\mathrm{sL/min}}{250\ \mathrm{sL/min}} = 0.0028 = 0.28\ \%$$

<u>Uncertainty of Rotameter</u>

Accuracy: 1.6 %

Linearity: full scale 0.2 %

Hysteresis: full scale 0.1 %

Repeatability: full scale 0.1 %

Output signal (AC): full scale 0.15 %

Response time: 99 %

Effect of power supplier: full scale 0.15 %

Uncertainty: full scale 1.6 %

The equipment measures the flow rate between 0 and 40L/min in this situation;

Accuracy: 1.6 % - $40 \times 1.6/100 = 0.64$ L/min

Linearity: full scale 0.2 % - $40 \times 0.2/100 = 0.08$ L/min

Hysteresis: full scale 0.1 % - $40 \times 0.1/100 = 0.04$ L/min

Repeatability: full scale 0.1 %- $40 \times 0.1/100 = 0.04$ L/min

Output signal (AC): full scale 0.15 %- $40 \times 0.15/100 = 0.06$ L/min

Response time: 99 %

Effect of power supplier: full scale 0.15 % - $40 \times 0.15/100 = 0.06$ L/min

Table A.15 The errors in the measurement of water vapor flow rate

Errors	Systematic errors	Random errors
Accuracy	0.64	
Linearity	0.08	
Hysteresis	0.04	
Repeatability		0.04
Output signal (AC)	0.06	
Effect of power supplier	0.06	

Total uncertainty;

$$U_x = \sqrt{((0.64)^2 + (0.08)^2 + (0.04)^2 + (0.06)^2 + (0.06)^2) + ((0.04)^2)} = 0.65 \text{ L/min}$$

$$U_x/_x = \frac{0.65\text{sL/min}}{45 \text{ sL/min}} = 0.0144 = 1.44\ \%$$

Uncertainty of Temperature Measurements

B type Thermocouple

Calibration error: 0.5 %

Accuracy: 0.5 %

Data acquisition: reading value 0.5 %

Calculation of random errors;

It is determined by using 303 data that the average of the measurements are 1265°C . The standard deviation of them are 1.84°C. The calculated random uncertainty is 0.212°C.

The equipment measures the temperature between 500 and 1700°C. In this situation;

Calibration error: 0.5 % -$1700 \times 0.5/100 = 8.5$°C

Accuracy: 0.5 % -$1700 \times 0.5/100 = 8.5$°C

Data acquisition: reading value 0.5 % -$1265 \times 0.5/100 = 6.33$°C

It is determined by using 303 data that the average of the measurements are 1265°C . The standard deviation of them are 1.84°C. The calculated random uncertainty is 0.212°C.

Total uncertainty;

$$U_x = \sqrt{((8.5)^2 + (8.5)^2) + (6.33)^2 + ((0.212)^2)} = 13\ °C$$

$$\mathrm{U_x}/_x = \frac{13.58\ °C}{1850\ °C} = 0.00734 = 0.73\ \%$$

<u>Uncertainty of Gas Analyzer</u>

Accuracy: 2 %

Linearity: full scale 1 %

Repeatability: full scale 1 %

Response time: 30s

Span shift: 2 %

Resolution: 0.01 %

Table A.16 The errors in the gas analyzer

Errors	Systematic errors (%)	Random errors (%)
Accuracy	2	
Linearity	1	
Repeatability		1
Span shift	2	
Resolution		0.01

Total uncertainty;

$$U_x = \sqrt{((2)^2 + (1)^2 + (2)^2 +) + ((1)^2 + (0.01)^2)} = \ 3.16\ \%$$

$$\mathrm{U_x}/_x = 3.16\ \%$$

Uncertainty of gasification time (t_g)

During the experimentation, gasification time is varied between 420s and 1020s. As a result of 10 s error in measurement of gasification time, the uncertainty is;

$$\frac{U_x}{x} = \frac{10s}{1020s} = 0.0098 = 0.98\%$$

Uncertainty of mass measurement (mass of ash and fuel)

Linearity: 0.2 mg

Repeatability: 0.1 mg

Readability: 0.1 mg

Table A.17 The errors in the mass measurement

Errors	Systematic errors	Random errors
Linearity	0.2mg	
Repeatability		0.1mg
Readability	0.1mg	

Total uncertainty;

$$U_x = \sqrt{((0.2)^2 + (0.1)^2) + ((0.1)^2)} = 0.24 \text{ mg}$$

A2.2 Uncertainties of the calculated parameters

Mass of air calculation uncertainty

Mass of air is calculated by using equation 5.1. In equation 5.1, atmospheric pressure, ideal gas constant and air temperature are the standard values in standard conditions (101,325 kPa, 25℃ and 0.287 kJ/kgK). The volumetric flow rate and gasification time uncertainties are determined by using equation A.15.

$$\frac{U_{m_{air}}}{m_{air}} = \left[(1)^2\left(\frac{U_{\dot{\forall}}}{\dot{\forall}}\right)^2 + (1)^2\left(\frac{U_{t_g}}{t_g}\right)^2\right]^{1/2} \qquad A.15$$

$$\frac{U_{m_{air}}}{m_{air}} = [(1)^2(0.0028)^2 + (1)^2(0.0238)^2]^{1/2} = 0.024 = 2.4\ \%$$

$$U_{m_{air}} = 0.024\,.\,1kg = 0.024\ kg$$

Mass of syngas calculation uncertainty

Mass of syngas is calculated by using equation 5.2.

$$U_{m_{syngas}} = \left[\left(\frac{\partial m_{syngas}}{\partial m_{air}}\right)^2 (U_{m_{air}})^2 + \left(\frac{\partial m_{syngas}}{\partial m_{fuel}}\right)^2 (U_{m_{fuel}})^2 + \left(\frac{\partial m_{syngas}}{\partial m_{ash}}\right)^2 (U_{m_{ash}})^2\right]^{1/2}$$

$$U_{m_{syngas}} = 0.024 \text{ kg}$$

$$\frac{U_{m_{syngas}}}{m_{syngas}} = \frac{0.024 \text{ kg}}{1.2kg} = 2\ \%$$

<u>Syngas temperature calculation uncertainty</u>

$$U_{T_{syngas}} = \left[\left(\frac{\partial T_{syngas}}{\partial Ty/_{h=0.28}}\right)^2 \left(U_{Ty/_{h=0.28}}\right)^2 + \left(\frac{\partial T_{syngas}}{\partial Ty/_{h=0.44}}\right)^2 \left(U_{Ty/_{h=0.44}}\right)^2 + \right.$$

$$\left.\left(\frac{\partial T_{syngas}}{\partial Ty/_{h=0.6}}\right)^2 \left(U_{Ty/_{h=0.6}}\right)^2 + \left(\frac{\partial T_{syngas}}{\partial Ty/_{h=0.76}}\right)^2 \left(U_{Ty/_{h=0.76}}\right)^2 + \left(\frac{\partial T_{syngas}}{\partial Ty/_{h=0.92}}\right)^2 \left(U_{Ty/_{h=0.92}}\right)^2\right]^{1/2}$$

$$U_{T_{syngas}} = 30.36°C$$

<u>Syngas content (volumetric-molar based) calculation uncertainty</u>

$$\frac{U_{syngas\,(n\,\%)}}{syngas\ (n\ \%)} = \left[(-1)^2 \left(\frac{U_{t_g}}{t_g}\right)^2 + (1)^2 \left(\frac{U_{syngas\,\%\,(t)}}{syngas\ \%\ (t)}\right)^2\right]^{1/2}$$

$$\frac{U_{syngas\,\%}}{syngas\ \%} = 3.16\ \%$$

<u>Syngas molar weight calculation uncertainty</u>

$$U_{M_{syngas}} = \left[\left(\frac{\partial M_{syngas}}{\partial CO(n\,\%)}\right)^2 \left(U_{CO(n\,\%)}\right)^2 + \left(\frac{\partial M_{syngas}}{\partial CO_2\,(n\,\%)}\right)^2 \left(U_{CO_2\,(n\,\%)}\right)^2 + \left(\frac{\partial M_{syngas}}{\partial H_2(n\,\%)}\right)^2 \left(U_{H_2(n\,\%)}\right)^2 + \right.$$

$$\left.\left(\frac{\partial M_{syngas}}{\partial CH_4(n\,\%)}\right)^2 \left(U_{CH_4(n\,\%)}\right)^2 + \left(\frac{\partial M_{syngas}}{\partial O_2(n\,\%)}\right)^2 \left(U_{O_2(n\,\%)}\right)^2 + \left(\frac{\partial M_{syngas}}{\partial N_2(n\,\%)}\right)^2 \left(U_{N_2(n\,\%)}\right)^2\right]^{1/2}$$

$$U_{M_{syngas}} = 7.74\ \%$$

<u>Syngas content (mass based) calculation uncertainty</u>

$$\frac{U_{syngas\,(m\,\%)}}{syngas\ (m\ \%)} = \left[(1)^2 \left(\frac{U_{syngas\,(n\,\%)}}{syngas\ (n\ \%)}\right)^2 + (-1)^2 \left(\frac{U_{M_{syngas}}}{M_{syngas}}\right)^2\right]^{1/2}$$

$$\frac{U_{syngas\,(m\,\%)}}{syngas\ (m\ \%)} = 8.36\ \%$$

Uncertainty of Content conversion performance of syngas

$$\frac{U_{CCP_{syn}}}{CCP_{syn}} = \left[(1)^2\left(\frac{U_{m_{syn}}}{m_{syn}}\right)^2 + (-1)^2\left(\frac{U_{m_{fuel}}}{m_{fuel}}\right)^2\right]^{1/2}$$

$$\frac{U_{CCP_{syn}}}{CCP_{syn}} = \left[(1)^2(2)^2 + (-1)^2\left(\frac{0.24\text{mg}}{250\text{g}}\right)^2\right]^{1/2}$$

$$\frac{U_{CCP_{syn}}}{CCP_{syn}} = 2\ \%$$

Uncertainty of Content conversion performance of ash

$$\frac{U_{CCP_{ash}}}{CCP_{ash}} = \left[(1)^2\left(\frac{U_{m_{ash}}}{m_{ash}}\right)^2 + (-1)^2\left(\frac{U_{m_{fuel}}}{m_{fuel}}\right)^2\right]^{1/2}$$

$$\frac{U_{CCP_{ash}}}{CCP_{ash}} = \left[(1)^2\left(\frac{0.00024\text{ g}}{250\text{g}}\right)^2 + (-1)^2\left(\frac{0.00024\text{ g}}{250\text{g}}\right)^2\right]^{1/2}$$

$$\frac{U_{CCP_{ash}}}{CCP_{ash}} = 1.357\,.\,10^{-6} = 1.357\,.\,10^{-4}\ \%$$

Uncertainty of Content conversion performance of hydrogen

$$CCP_{H_2}[\%] = \frac{m_{H_2}}{m_{fuel}} \times 100$$

$$\frac{U_{CCP_{H_2}}}{CCP_{H_2}} = \left[(1)^2\left(\frac{U_{m_{syn}}}{m_{syn}}\right)^2 + (1)^2\left(\frac{U_{H_2\,(m\,\%)}}{H_2\,(m\,\%)}\right)^2 + (-1)^2\left(\frac{U_{m_{fuel}}}{m_{fuel}}\right)^2\right]^{1/2}$$

$$\frac{U_{CCP_{H_2}}}{CCP_{H_2}} = \left[(1)^2\left(\frac{0.00024\text{ g}}{250\text{g}}\right)^2 + (1)^2(8.36)^2 + (-1)^2\left(\frac{0.00024\text{ g}}{250\text{g}}\right)^2\right]^{1/2}$$

$$\frac{U_{CCP_{H_2}}}{CCP_{H_2}} = 8.36\ \%$$

Uncertainty of Hydrogen quality calculation

$$H_q[\%] = \frac{m_{H_2}}{m_{syn}} \times 100$$

$$\frac{U_{H_q}}{H_q} = \left[(1)^2\left(\frac{U_{H_2\,(m\,\%)}}{H_2\,(m\,\%)}\right)^2\right]^{1/2} = 8.36\ \%$$

Uncertainty of syngas energy calculation

$$E_{syn}\ (kJ) = m_{syn}(kg).\ HHV_{syn}(^{kJ}/_{kg})$$

$$\frac{U_{E_{syn}}}{E_{syn}} = \left[(1)^2\left(\frac{U_{m_{syn}}}{m_{syn}}\right)^2\right]^{1/2} = 2\ \%$$

Uncertainty of plasma energy calculation

$$E_{plasma}\ (kJ) = W_{plasma}(\ kW).\ t_g\ (s)$$

$$\frac{U_{E_{plasma}}}{E_{plasma}} = \left[(1)^2\left(\frac{U_{t_g}}{t_g}\right)^2\right]^{1/2} = 0.98\ \%$$

Uncertainty of fuel energy calculation

$$E_{fuel}\ (kJ) = m_{fuel}(kg).\ HHV_{fuel}(^{kJ}/_{kg})$$

$$\frac{U_{E_{fuel}}}{E_{fuel}} = \left[(1)^2\left(\frac{U_{m_{fuel}}}{m_{fuel}}\right)^2\right]^{1/2} = 0.96\ .\ 10^{-6} = 0.96\ .\ 10^{-4}\ \%$$

A.3 Scanning Electron Microscope (SEM) and Energy Dispersive X-ray (EDX) analysis results

In this section, the scaninng electron microscope and energy dispersive X-ray analysis results of each sample before gasification, ash of gasified fuels for various microwave power and air flow rate are presented.

A3.1 Scanning Electron Microscope (SEM) and Energy Dispersive X-Ray Analysis (EDX) On Fuel Samples

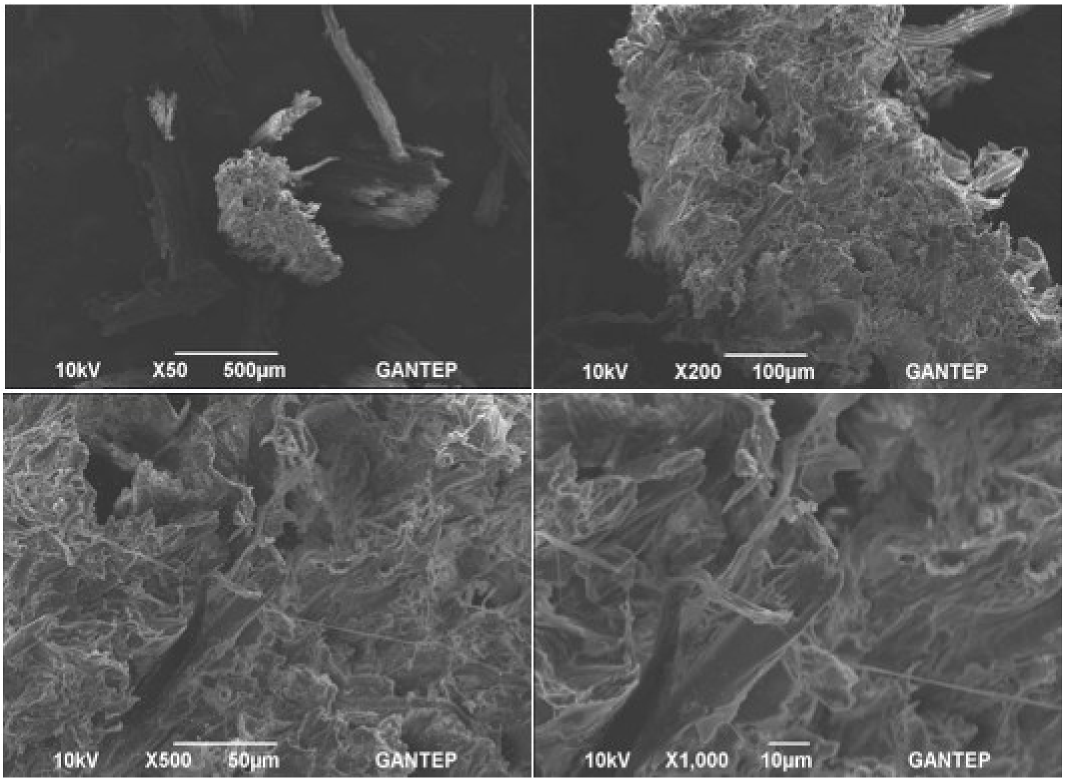

Figure A.5 Hornbeam sawdust (HSD) SEM analysis results

Table A.18 Hornbeam sawdust (HSD) EDX analysis results

Element	Concentration	Units
C	49.3	wt.%
O	47.5	wt.%
Mg	0.15	wt.%
Al	0.33	wt.%
Si	0.16	wt.%
S	0.38	wt.%
K	0.39	wt.%
Ca	0.43	wt.%
Ti	0.08	wt.%
Fe	0.56	wt.%
Cu	0.69	wt.%

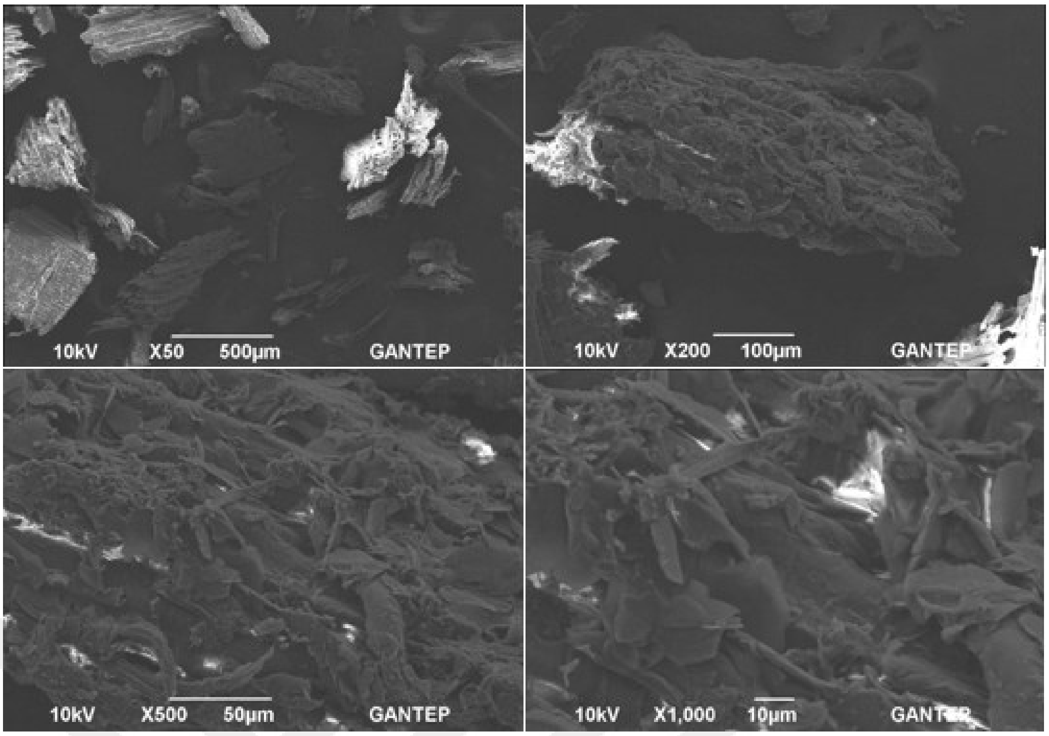

Figure A.6 Pine tree sawdust (PSD) SEM analysis results

Table A.19 Pine tree sawdust (PSD) EDX analysis results

Element	Concentration	Units
C	53.9	wt.%
O	44.3	wt.%
Mg	0.14	wt.%
Al	0.14	wt.%
Si	0.04	wt.%
S	0.27	wt.%
K	0.05	wt.%
Ca	0.41	wt.%
Ti	0.06	wt.%
Fe	0.09	wt.%
Cu	0.52	wt.%

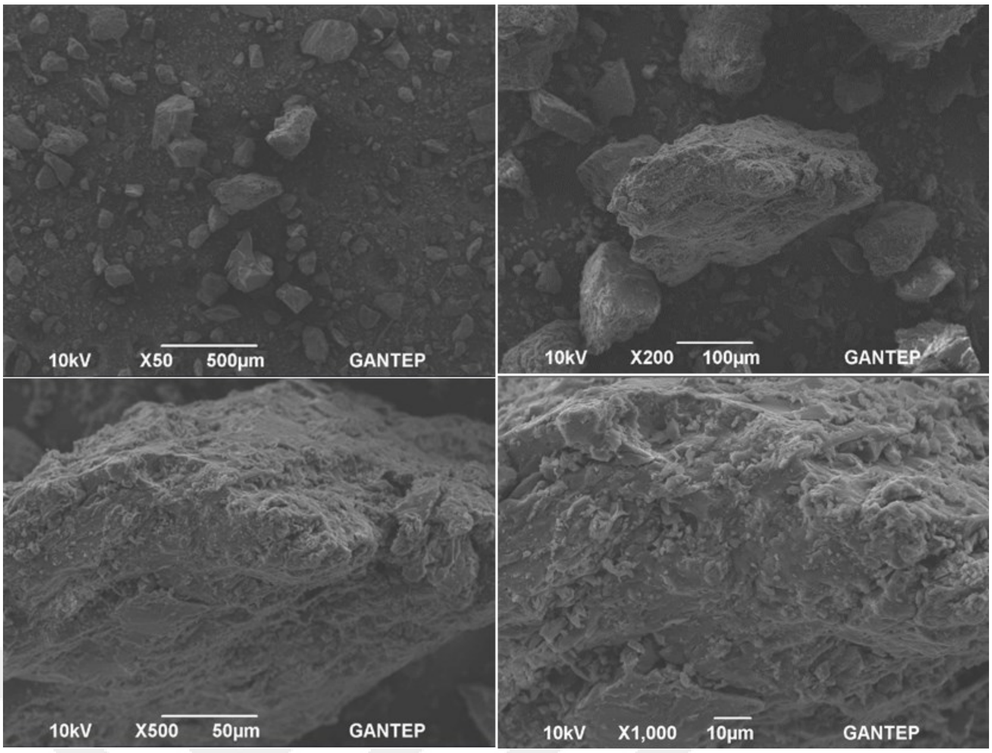

Figure A.7 Russian Coal (CR) SEM analysis results

Table A.20 Russian Coal (CR) EDX analysis results

Element	Concentration	Units
C	71.3	wt.%
O	19.3	wt.%
Mg	0.05	wt.%
Al	3.8	wt.%
Si	3.77	wt.%
S	0.49	wt.%
K	0.3	wt.%
Ca	0.1	wt.%
Ti	0.1	wt.%
Fe	0.4	wt.%
Cu	0.3	wt.%

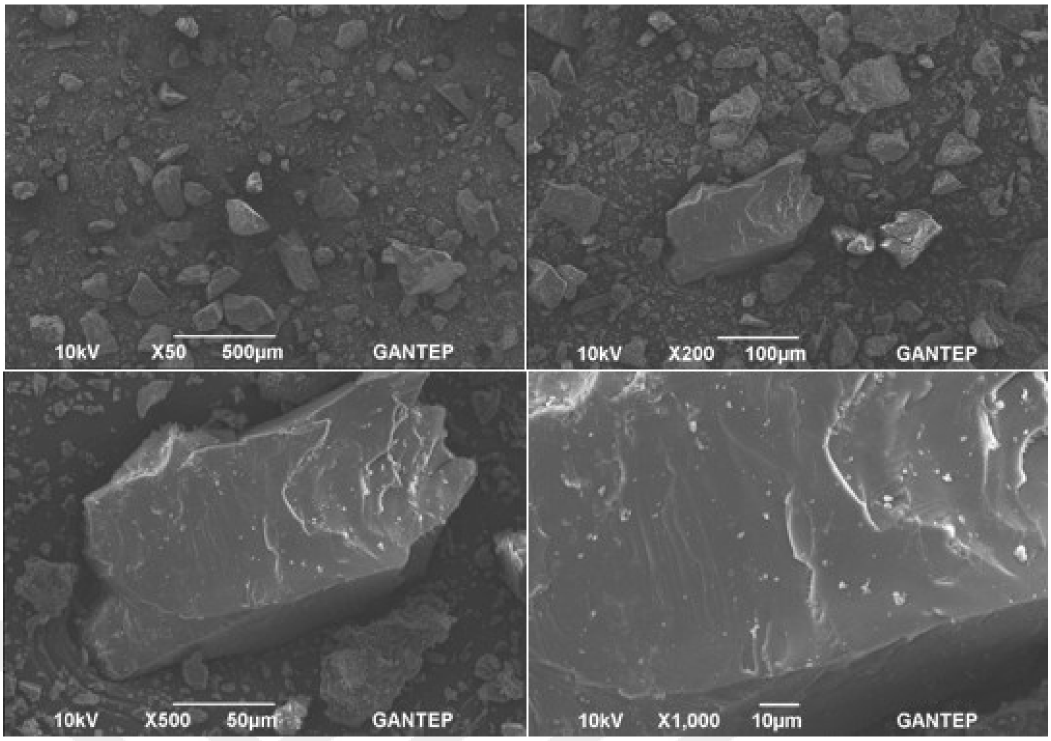

Figure A.8 South African coal (CSA) SEM analysis results

Table A.21 South African coal (CSA) EDX analysis results

Element	Concentration	Units
C	71.6	wt.%
O	19.1	wt.%
Mg	0.1	wt.%
Al	4.0	wt.%
Si	3.7	wt.%
S	0.7	wt.%
K	0.1	wt.%
Ca	0.1	wt.%
Ti	0.2	wt.%
Fe	0.16	wt.%
Cu	0.18	wt.%

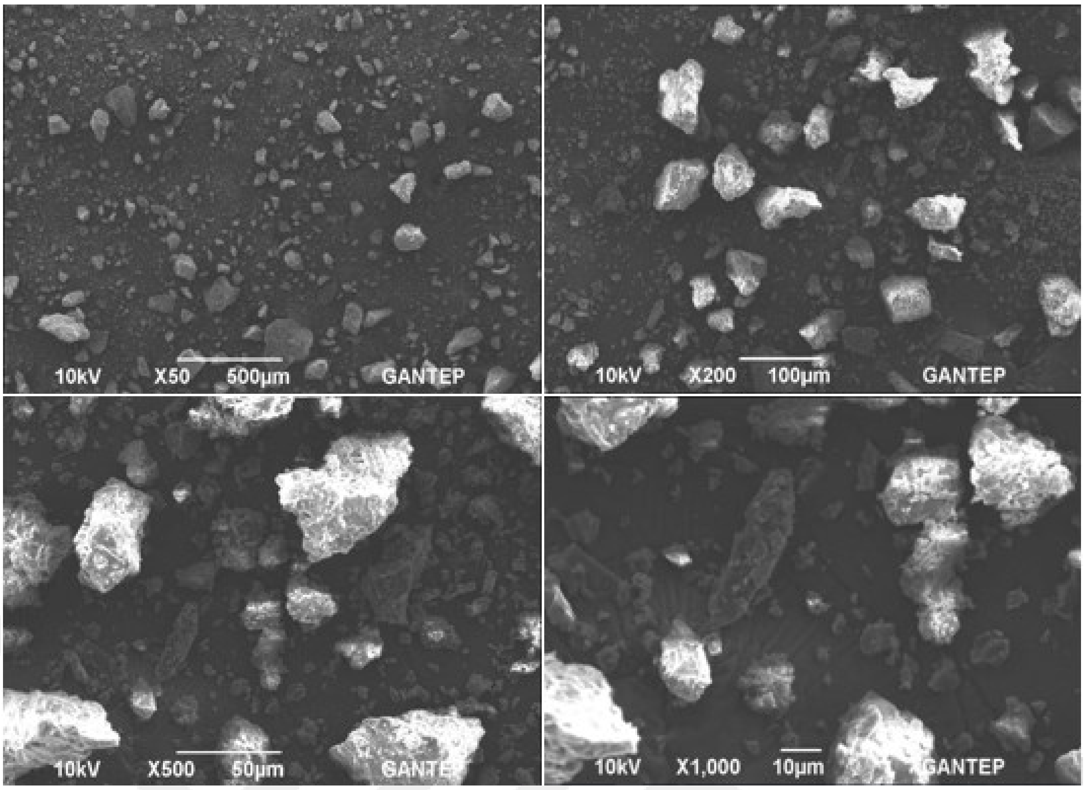

Figure A.9 Şırnak coal (CTR) SEM analysis results

Table A.22 Şırnak (Turkey) coal (CTR) EDX analysis results

Element	Concentration	Units
C	60.7	wt.%
O	20.5	wt.%
Mg	0.27	wt.%
Al	1.96	wt.%
Si	4.9	wt.%
S	6.5	wt.%
K	1	wt.%
Ca	2.8	wt.%
Ti	0.08	wt.%
Fe	0.7	wt.%
Cu	0.4	wt.%

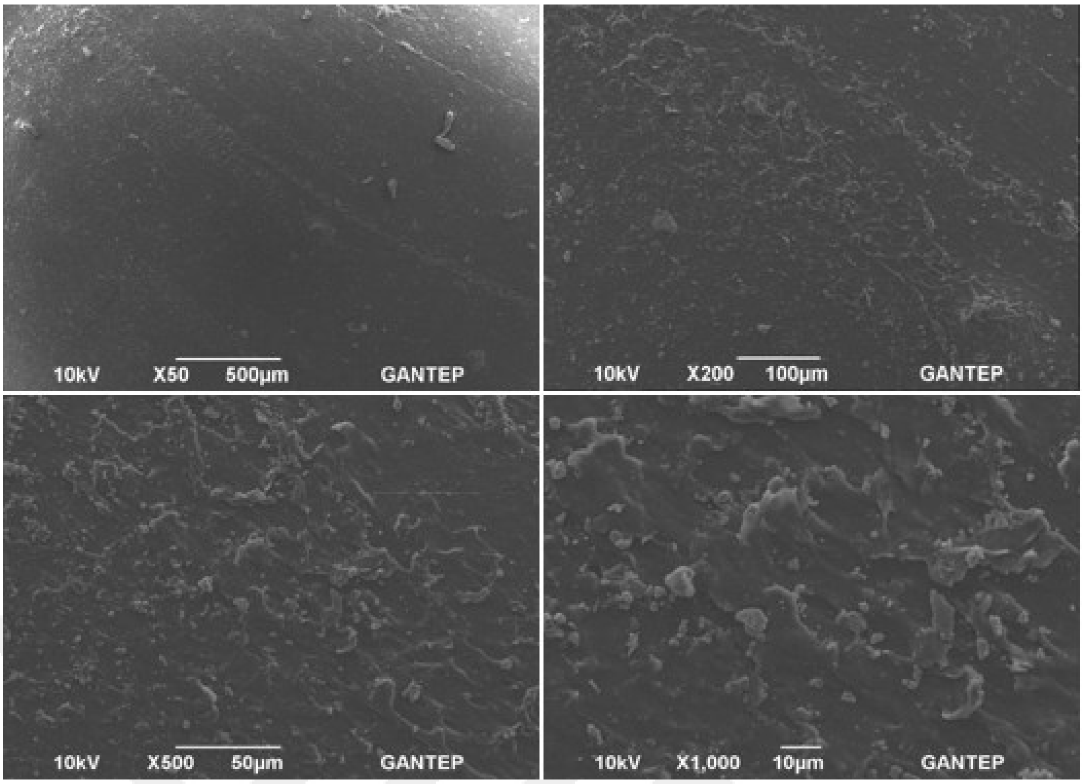

Figure A.10 Polyethylene (PP) SEM analysis results

Table A.23 Polyethylene (PP) EDX analysis results

Element	Concentration	Units
C	82.4	wt.%
O	11	wt.%
Mg	0.2	wt.%
Al	0.6	wt.%
Si	0.2	wt.%
S	0.14	wt.%
K	0.06	wt.%
Ca	2.9	wt.%
Ti	1.9	wt.%
Fe	0.2	wt.%
Cu	0.2	wt.%

A3.2 Scanning Electron Microscope (SEM) and Energy Dispersive X-ray (EDX) analysis results of Hornbeam Sawdust (HSD) ash after gasification

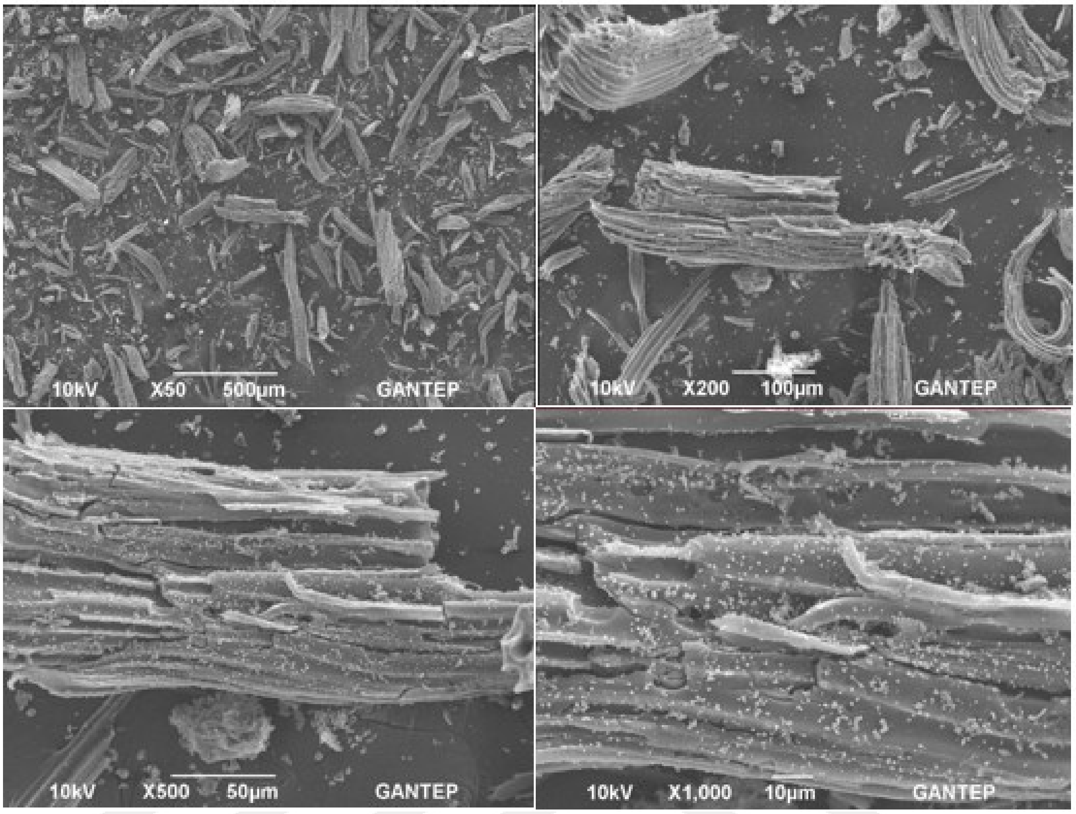

Figure A.11 SEM analysis results of ash of hornbeam sawdust (HSD) after gasification process in case of 50 sL/min air flow rate and 6kW plasma power

Table A.24 EDX analysis results of ash of hornbeam sawdust (HSD) after gasification process in case of 50 sL/min air flow rate and 6kW plasma power

Elt.	Concentration	Units
C	76.948	wt.%
O	19.269	wt.%
Mg	0.086	wt.%
Al	0.129	wt.%
Si	1.035	wt.%
S	0.583	wt.%
Ca	1.779	wt.%
Fe	0.171	wt.%

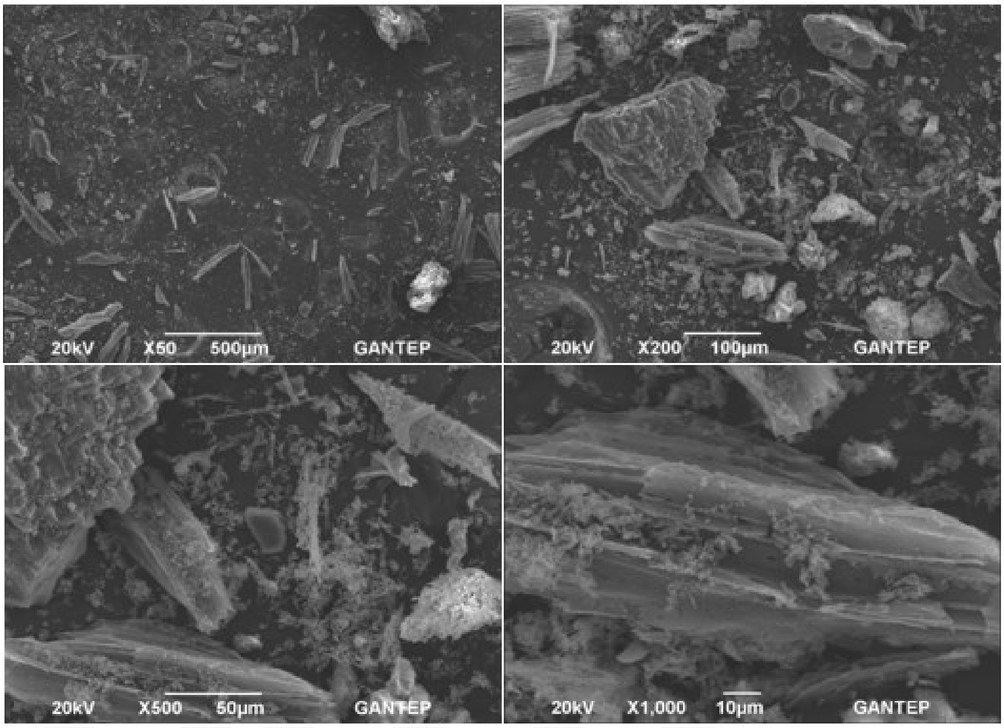

Figure A.12 SEM analysis results of ash of hornbeam sawdust (HSD) after gasification process in case of 50 sL/min air flow rate and 3 kW plasma power

Table A.25 EDX analysis results of ash of hornbeam sawdust (HSD) after gasification process in case of 50 sL/min air flow rate and 3 kW plasma power

Element	Concentration	Units
C	76.6	wt.%
O	19.1	wt.%
Mg	0.91	wt.%
Al	0.12	wt.%
Si	0.09	wt.%
S	0.63	wt.%
K	0.28	wt.%
Ca	1.39	wt.%
Ti	0.03	wt.%
Fe	0.06	wt.%
Cu	0.46	wt.%
Zn	0.33	wt.%

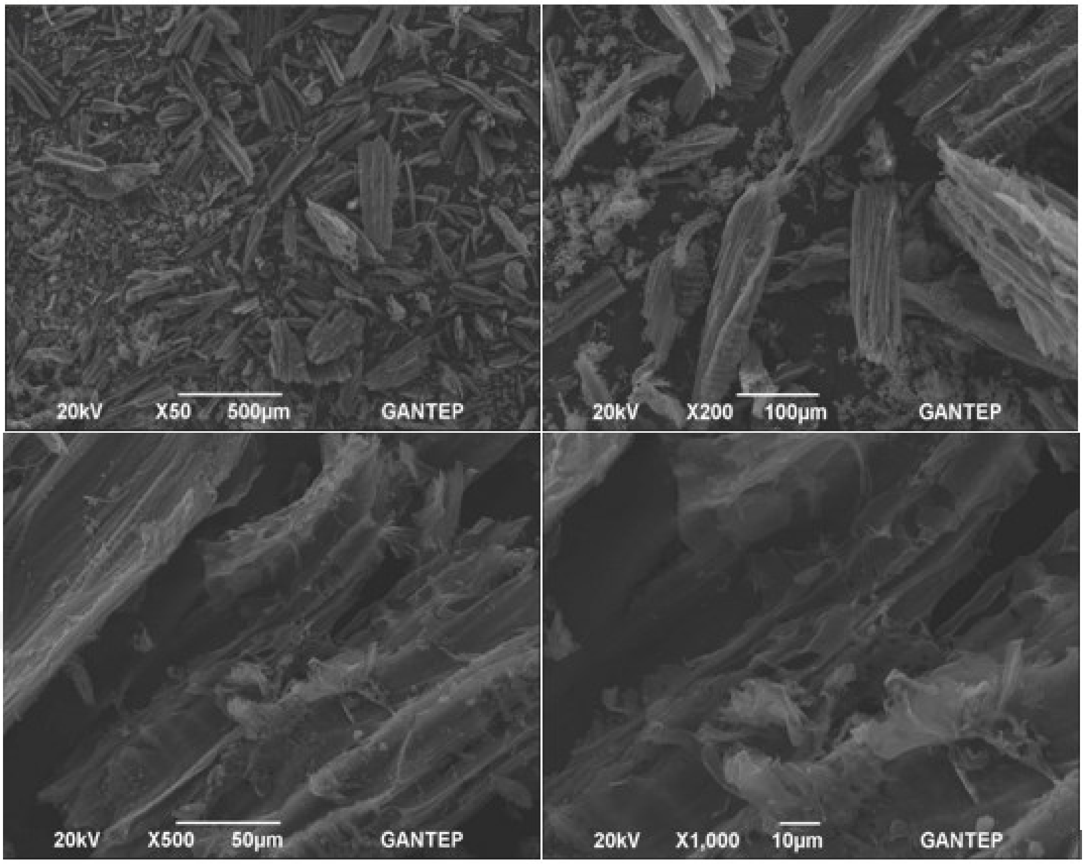

Figure A.13 SEM analysis results of ash of hornbeam sawdust (HSD) after gasification process in case of 100 sL/min air flow rate and 3 kW plasma power

Table A.26 EDX analysis results of ash of hornbeam sawdust (HSD) after gasification process in case of 100 sL/min air flow rate and 3 kW plasma power

Elt.	Concentration	Units
C	59.6	wt.%
O	29.4	wt.%
Mg	3.5	wt.%
Al	0.16	wt.%
Si	0.28	wt.%
S	0.45	wt.%
K	1	wt.%
Ca	5.1	wt.%
Ti	0.09	wt.%
Fe	0.2	wt.%
Cu	0.09	wt.%
Zn	0.1	wt.%

A3.3 Scanning Electron Microscope (SEM) and Energy Dispersive X-ray (EDX) analysis results of Pine Tree Sawdust (PSD) ash after gasification

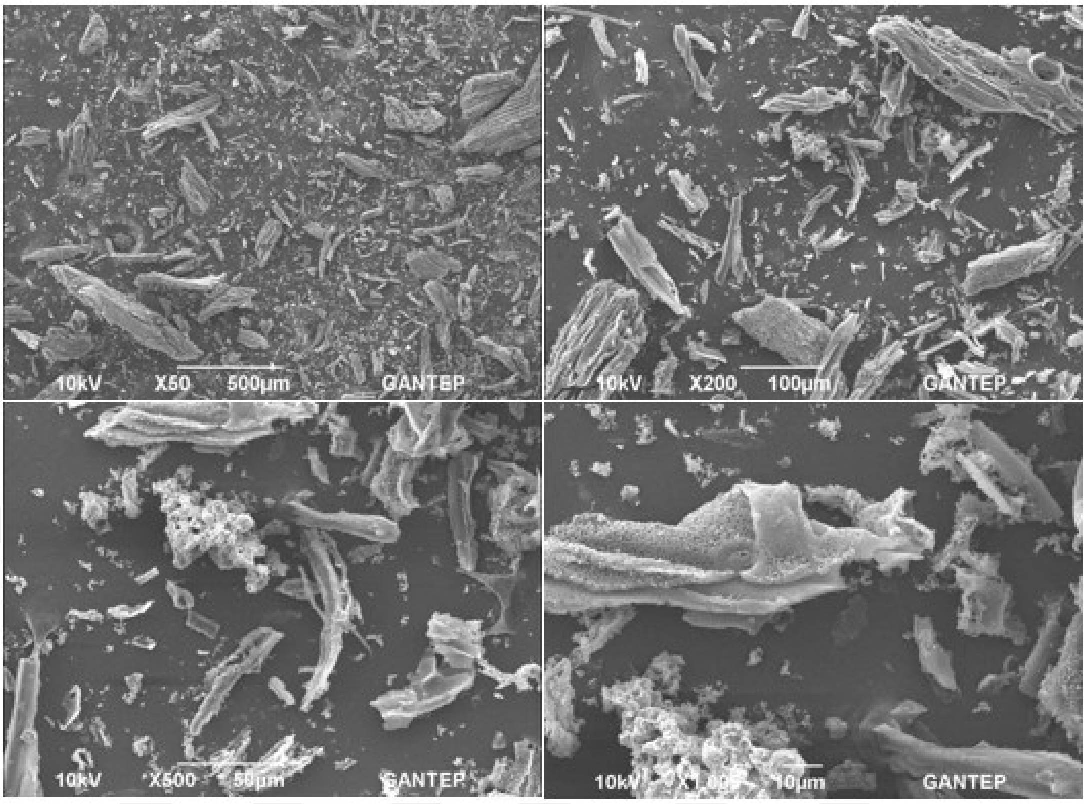

Figure A.14 SEM analysis results of ash of pine tree sawdust (PSD) after gasification process in case of 50 sL/min air flow rate and 6kW plasma power

Table A.27 EDX analysis results of ash of pine tree sawdust (PSD) after gasification process in case of 50 sL/min air flow rate and 6kW plasma power

Element	Concentration	Units
C	78.9	wt.%
O	12.5	wt.%
Mg	0.5	wt.%
Al	0.12	wt.%
Si	0.04	wt.%
S	4.3	wt.%
Ca	3.57	wt.%
Fe	0.13	wt.%

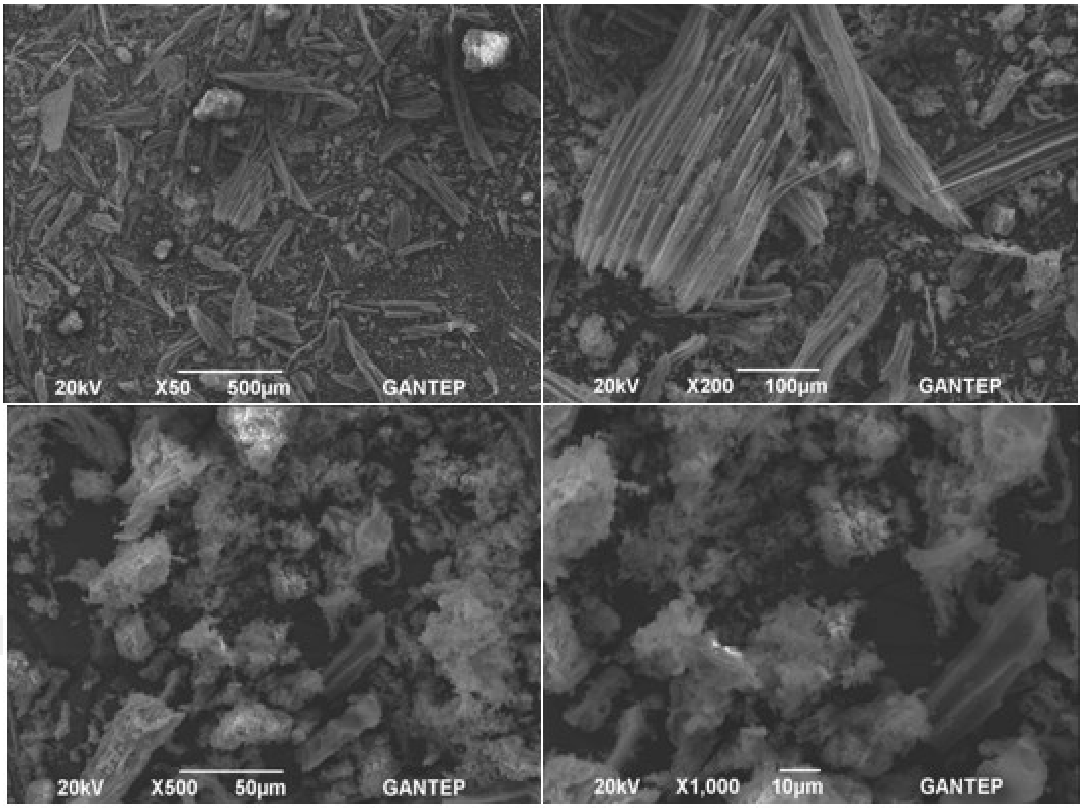

Figure A.15 SEM analysis results of ash of pine tree sawdust (PSD) after gasification process in case of 50 sL/min air flow rate and 3 kW plasma power

Table A.28 EDX analysis results of ash of pine tree sawdust (PSD) after gasification process in case of 50 sL/min air flow rate and 3 kW plasma power

Elt.	Concentration	Units
C	70.7	wt.%
O	21.9	wt.%
Mg	0.6	wt.%
Al	0.4	wt.%
Si	0.9	wt.%
S	0.9	wt.%
K	0.3	wt.%
Ca	3	wt.%
Ti	0.05	wt.%
Fe	0.28	wt.%
Cu	0.53	wt.%
Zn	0.38	wt.%

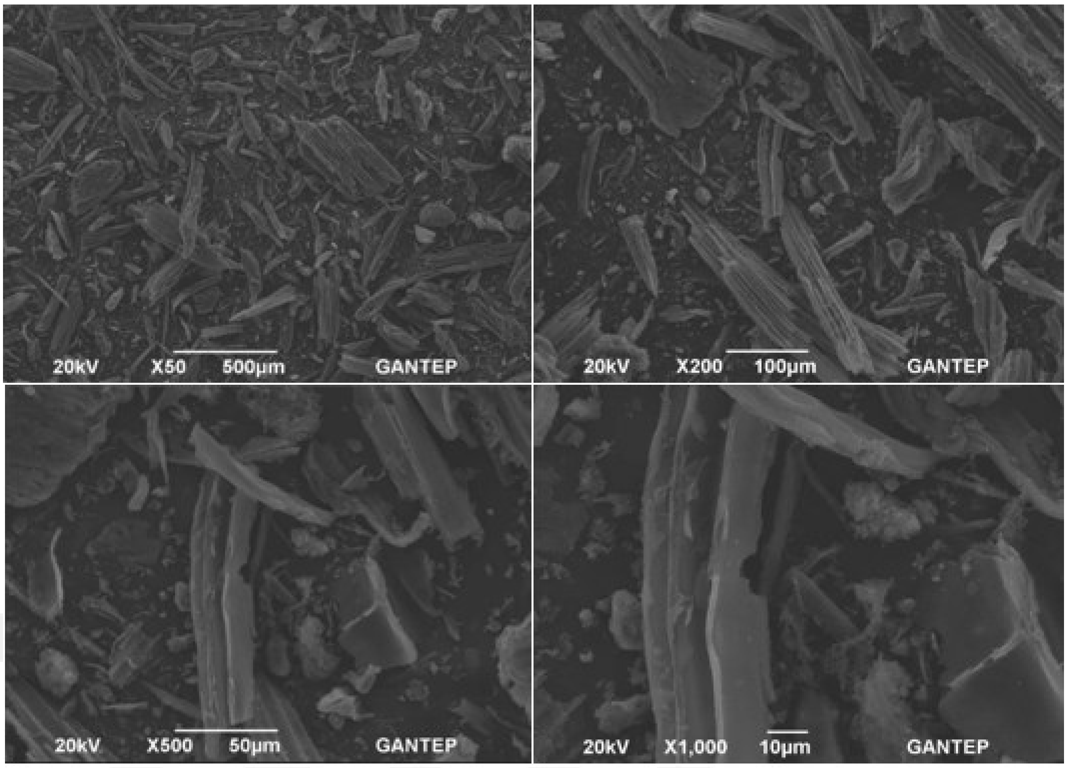

Figure A.16 SEM analysis results of ash of pine tree sawdust (PSD) after gasification process in case of 100 sL/min air flow rate and 3 kW plasma power

Table A.29 EDX analysis results of ash of pine tree sawdust (PSD) after gasification process in case of 100 sL/min air flow rate and 3 kW plasma power

Elt.	Concentration	Units
C	75.3	wt.%
O	20.7	wt.%
Mg	0.6	wt.%
Al	0.2	wt.%
Si	0.2	wt.%
S	0.3	wt.%
K	0.2	wt.%
Ca	2.1	wt.%
Ti	0.01	wt.%
Fe	0.12	wt.%
Cu	0.11	wt.%
Zn	0.12	wt.%

A3.4 Scanning Electron Microscope (SEM) and Energy Dispersive X-ray (EDX) analysis results of Russian coal (CR) ash after gasification

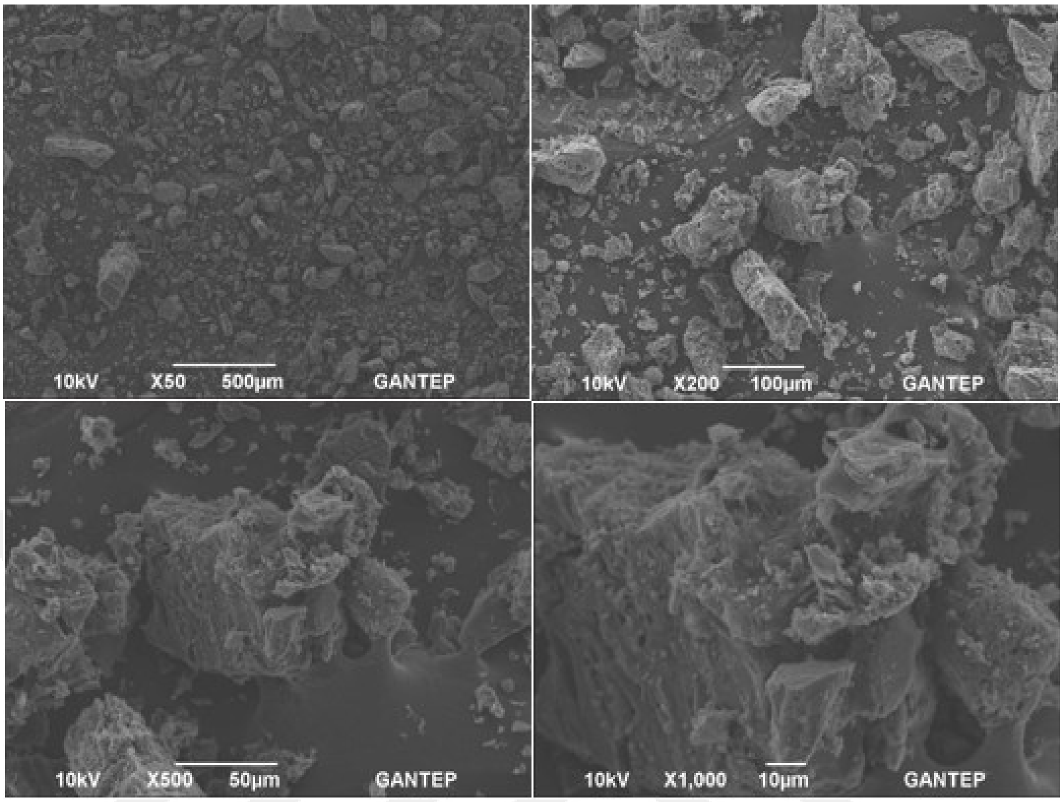

Figure A.17 SEM analysis results of ash of Russian coal (CR) after gasification process in case of 50 sL/min air flow rate and 6kW plasma power

Table A.30 EDX analysis results of ash of Russian coal (CR) after gasification process in case of 50 sL/min air flow rate and 6kW plasma power

Element	Concentration	Units
C	92	wt.%
O	6.6	wt.%
Mg	0.1	wt.%
Al	0.23	wt.%
Si	0.28	wt.%
Ca	0.14	wt.%
Ti	0.04	wt.%
Cu	0.5	wt.%

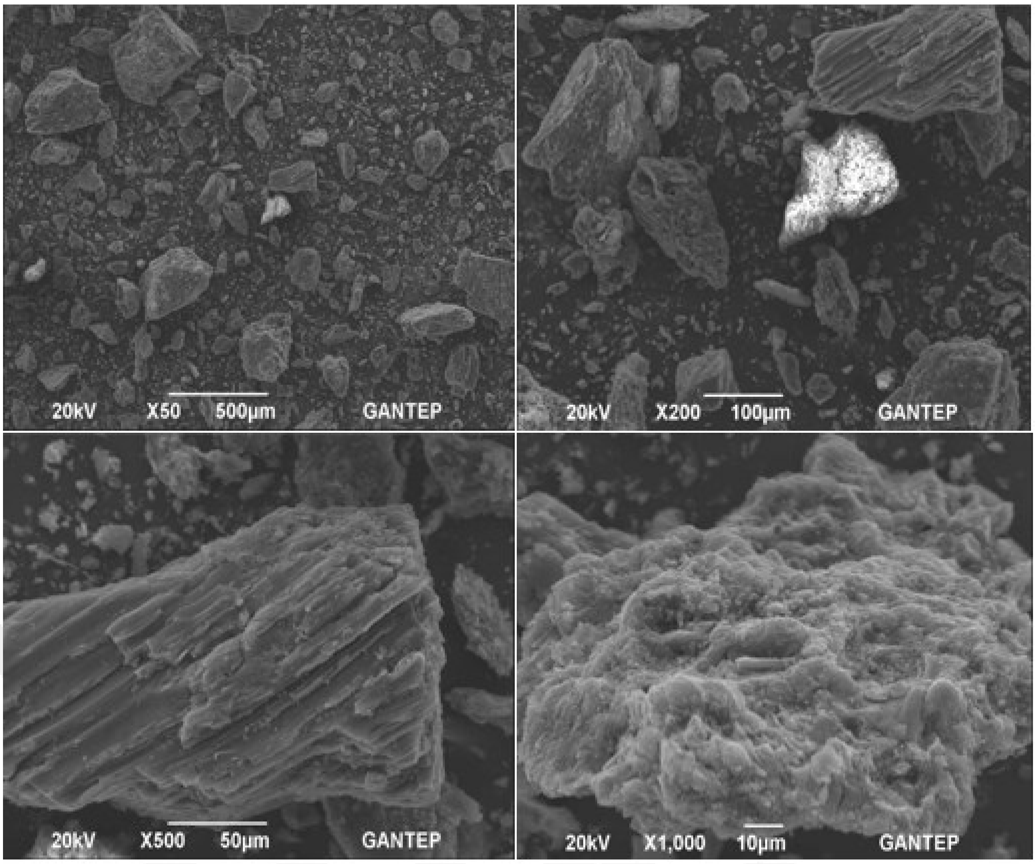

Figure A.18 SEM analysis results of ash of Russian coal (CR) after gasification process in case of 50 sL/min air flow rate and 3 kW plasma power

Table A.31 EDX analysis results of ash of Russian coal (CR) after gasification process in case of 50 sL/min air flow rate and 3 kW plasma power

Element	Concentration	Units
C	43.2	wt.%
O	28.6	wt.%
Mg	0.25	wt.%
Al	11.3	wt.%
Si	13.3	wt.%
S	0.55	wt.%
K	0.59	wt.%
Ca	0.22	wt.%
Ti	0.47	wt.%
Fe	0.33	wt.%
Cu	0.77	wt.%
Zn	0.46	wt.%

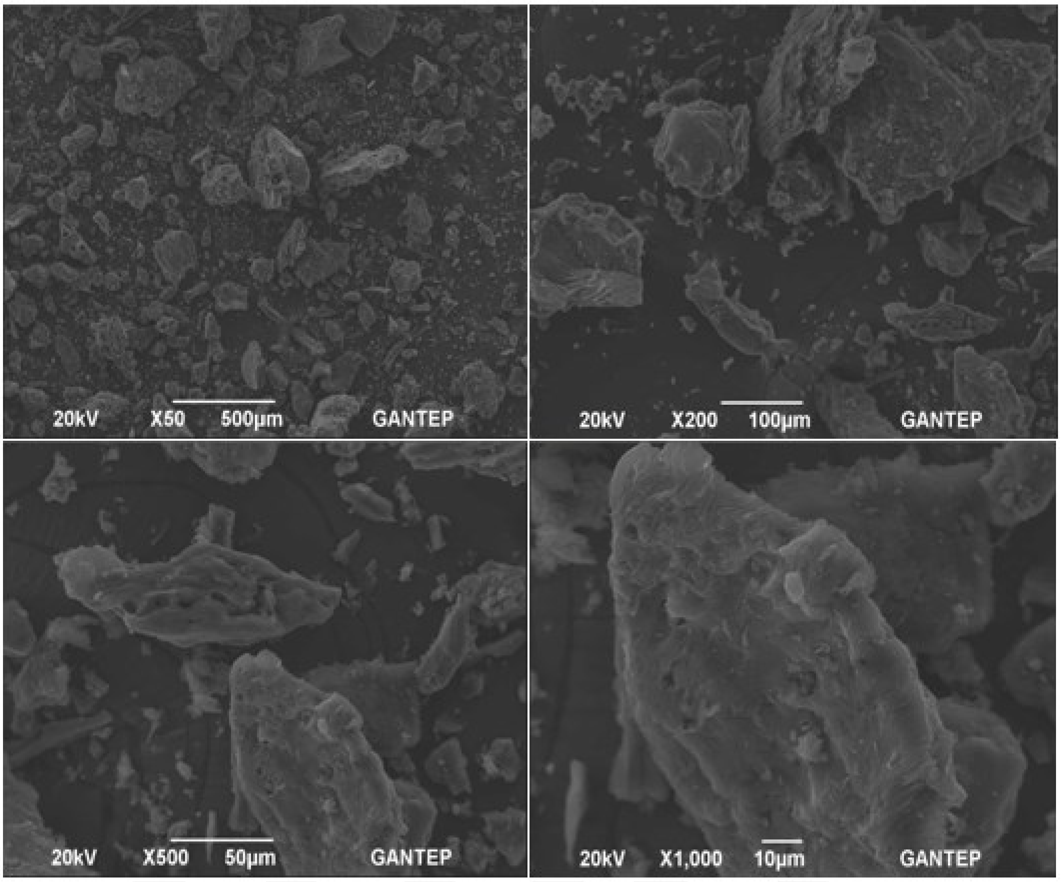

Figure A.19 SEM analysis results of ash of Russian coal (CR) after gasification process in case of 100 sL/min air flow rate and 3 kW plasma power

Table A.32 EDX analysis results of ash of Russian coal (CR) after gasification process in case of 100 sL/min air flow rate and 3 kW plasma power

Element	Concentration	Units
C	78.9	wt.%
O	15.8	wt.%
Mg	0.12	wt.%
Al	1	wt.%
Si	1.7	wt.%
S	0.37	wt.%
K	0.05	wt.%
Ca	0.53	wt.%
Ti	0.11	wt.%
Fe	0.27	wt.%
Cu	0.57	wt.%
Zn	0.44	wt.%

A3.5 Scanning Electron Microscope (SEM) and Energy Dispersive X-ray (EDX) analysis results of Russian coal (CR) ash after gasification

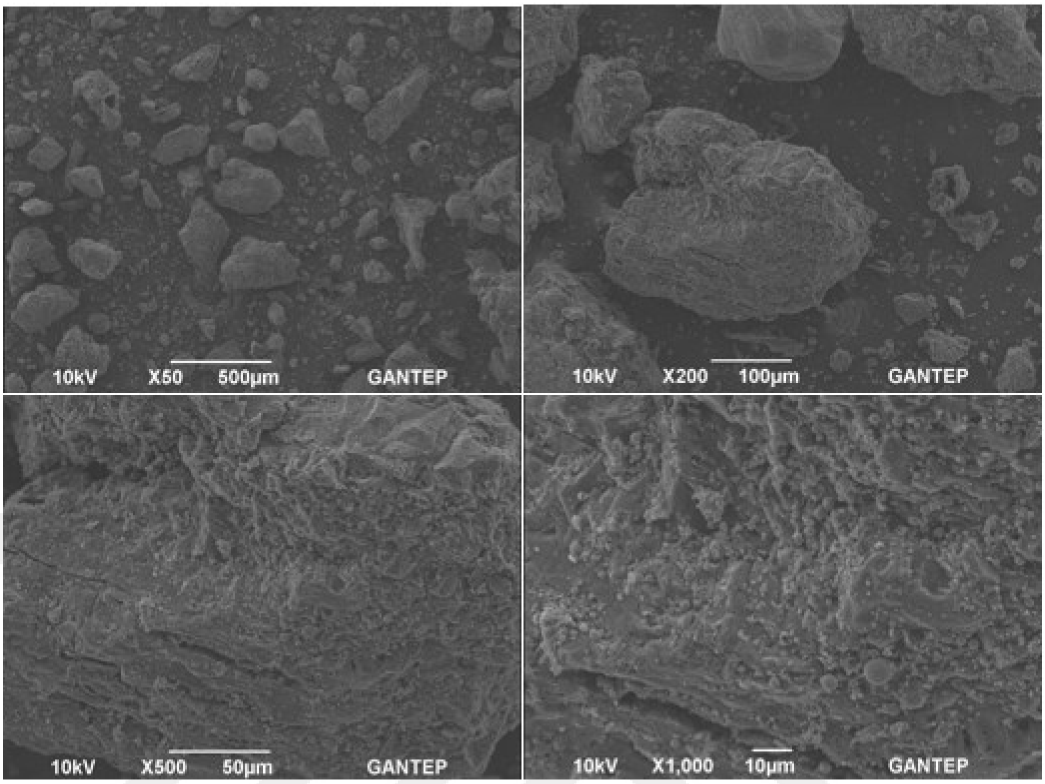

Figure A.20 SEM analysis results of ash of South African coal (CSA) after gasification process in case of 50 sL/min air flow rate and 6kW plasma power

Table A.33 EDX analysis results of ash of South African coal (CSA) after gasification process in case of 50 sL/min air flow rate and 6kW plasma power

Element	Concentration	Units
C	46.3	wt.%
O	32.4	wt.%
Mg	0.4	wt.%
Al	10.3	wt.%
Si	9.2	wt.%
K	0.4	wt.%
Ca	0.3	wt.%
Ti	0.3	wt.%
Cu	0.4	wt.%

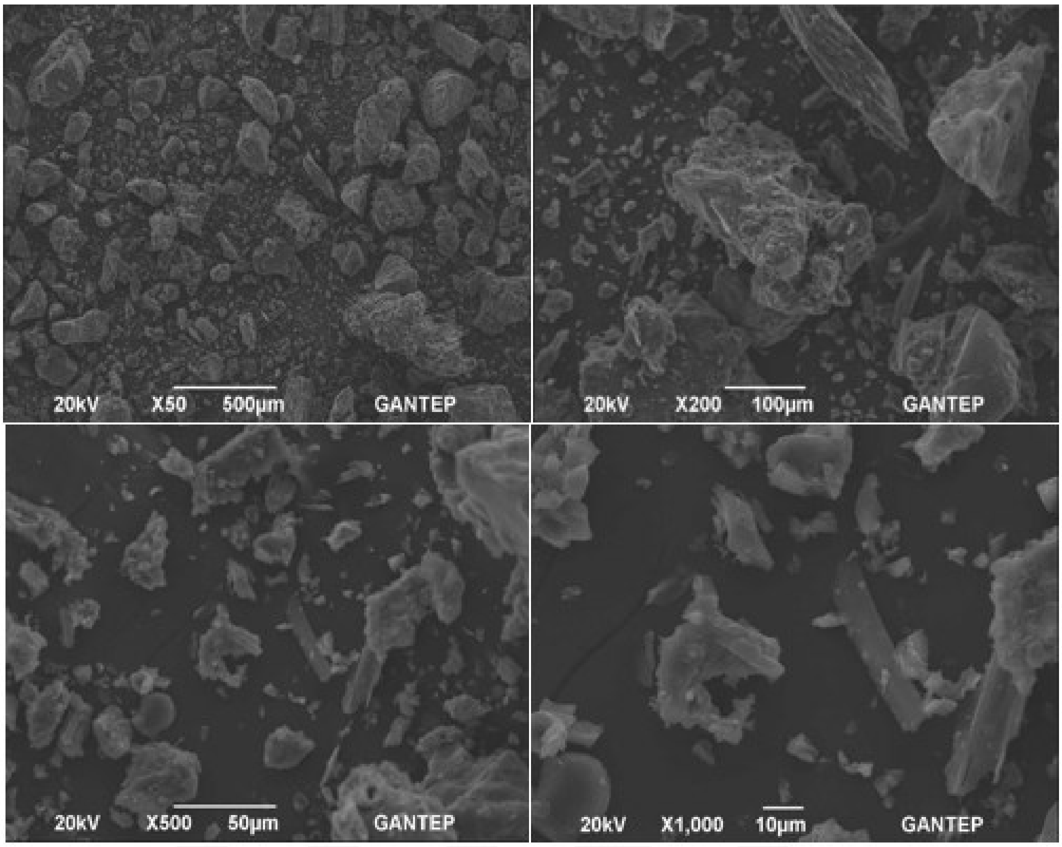

Figure A.21 SEM analysis results of ash of South African coal (CSA) after gasification process in case of 50 sL/min air flow rate and 3 kW plasma power

Table A.34 EDX analysis results of ash of South African coal (CSA) after gasification process in case of 50 sL/min air flow rate and 3kW plasma power

Element	Concentration	Units
C	58.9	wt.%
O	8.7	wt.%
Mg	0.16	wt.%
Al	1	wt.%
Si	0.8	wt.%
S	1.3	wt.%
Ca	9.6	wt.%
Fe	4.4	wt.%
Cu	9.1	wt.%
Zn	5.9	wt.%

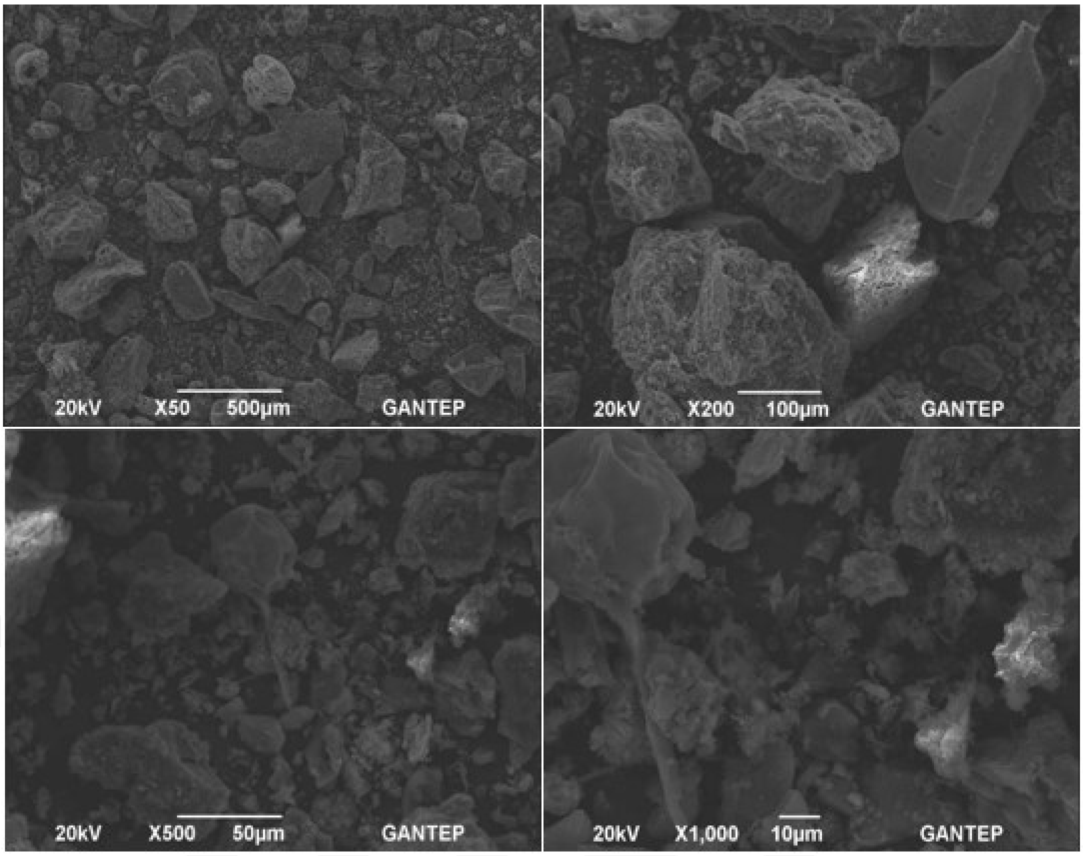

Figure A.22 SEM analysis results of ash of South African coal (CSA) after gasification process in case of 100 sL/min air flow rate and 3kW plasma power

Table A.35 EDX analysis results of ash of South African coal (CSA) after gasification process in case of 100 sL/min air flow rate and 3kW plasma power

Element	Concentration	Units
C	69.6	wt.%
O	20.7	wt.%
Mg	0.19	wt.%
Al	3.5	wt.%
Si	3.2	wt.%
S	1.5	wt.%
K	0.04	wt.%
Ca	0.41	wt.%
Ti	0.1	wt.%
Fe	0.1	wt.%
Cu	0.37	wt.%
Zn	0.27	wt.%

A3.6 Scanning Electron Microscope (SEM) and Energy Dispersive X-ray (EDX) analysis results of Şırnak (Turkey) (CTR) ash after gasification

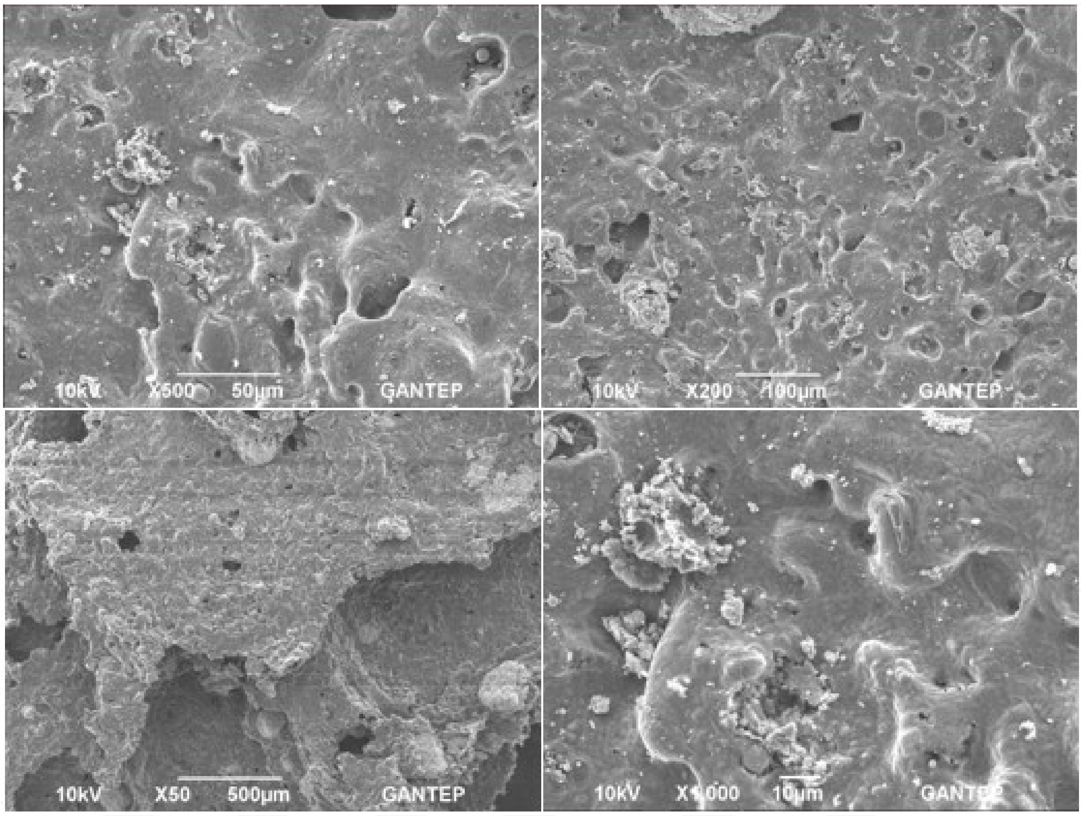

Figure A.23 SEM analysis results of ash of Şırnak (Turkey) coal (CTR) after gasification process in case of 50 sL/min air flow rate and 6kW plasma power

Table A.36 EDX analysis results of ash of Şırnak (Turkey) coal (CTR) after gasification process in case of 50 sL/min air flow rate and 6kW plasma power

Element	Concentration	Units
C	63.4	wt.%
O	11.7	wt.%
Mg	0.95	wt.%
Al	2.4	wt.%
Si	5.3	wt.%
S	5.4	wt.%
Ca	8.5	wt.%
Fe	2.2	wt.%

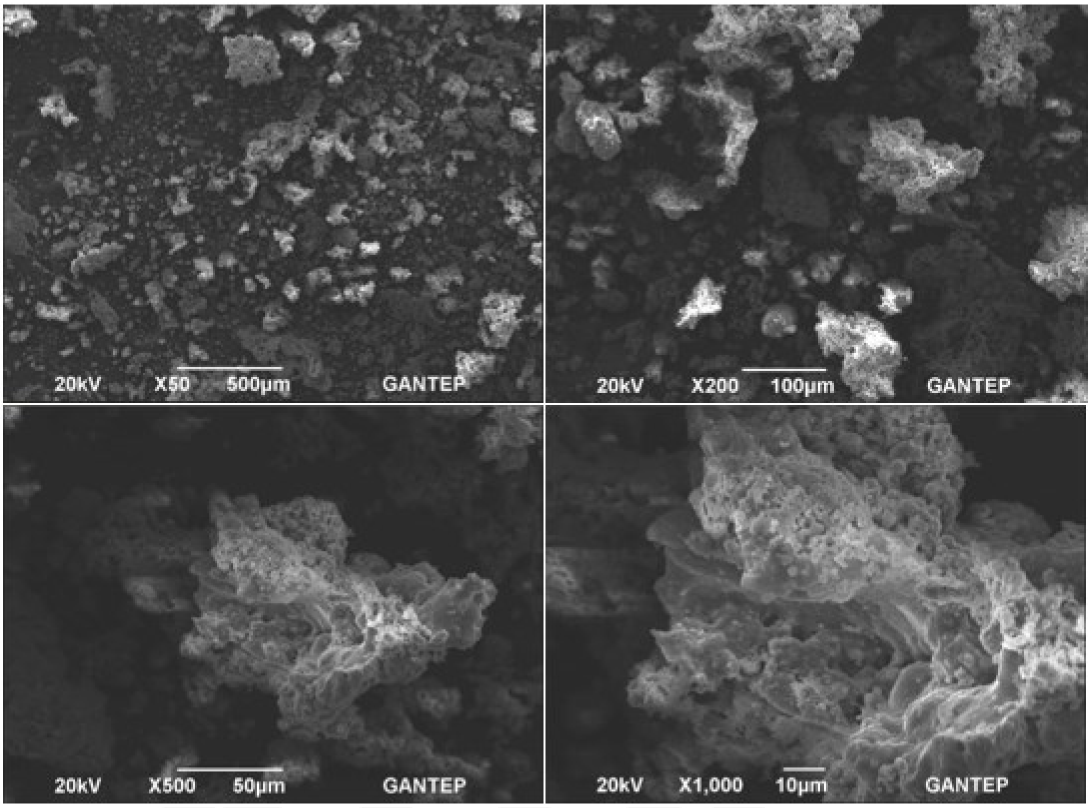

Figure A.24 SEM analysis results of ash of Şırnak (Turkey) coal (CTR) after gasification process in case of 50 sL/min air flow rate and 3 kW plasma power

Table A.37 EDX analysis results of ash of Şırnak (Turkey) coal (CTR) after gasification process in case of 50 sL/min air flow rate and 3 kW plasma power

Element	Concentration	Units
C	19.8	wt.%
O	39.5	wt.%
Mg	1.9	wt.%
Al	8.9	wt.%
Si	14	wt.%
S	0.14	wt.%
K	0.73	wt.%
Ca	9.8	wt.%
Ti	1.14	wt.%
Fe	3.8	wt.%
Cu	0.12	wt.%
Zn	0.12	wt.%

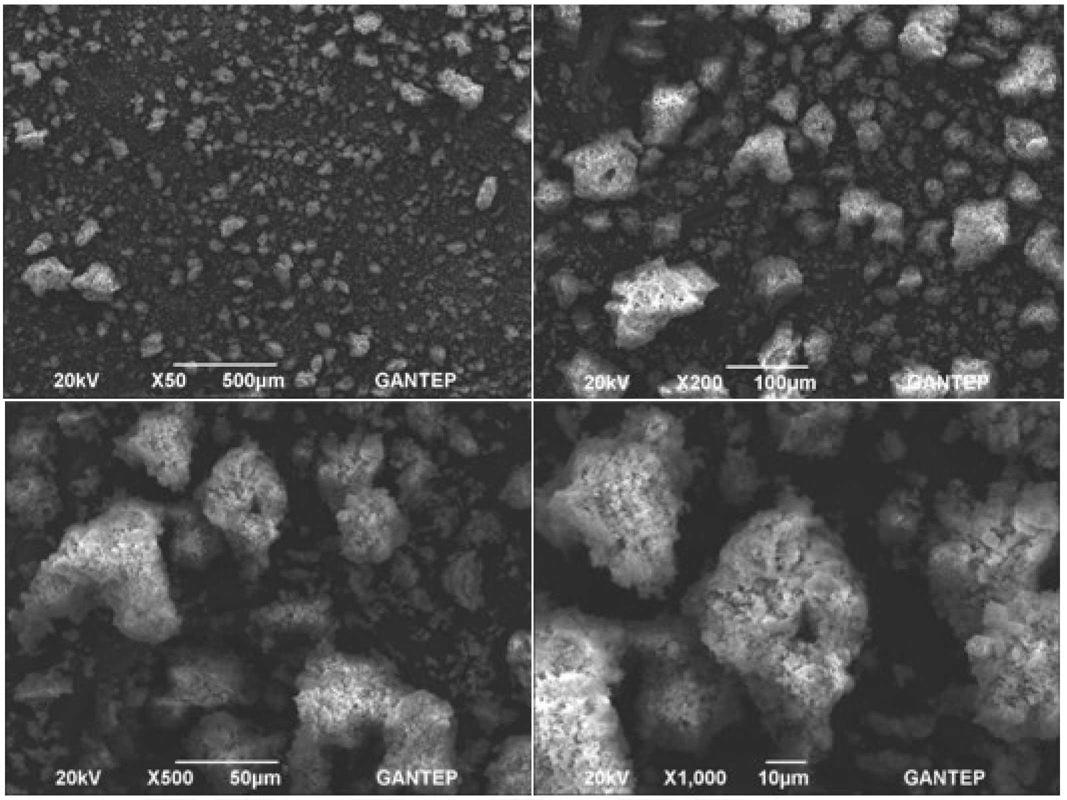

Figure A.25 SEM analysis results of ash of Şırnak (Turkey) coal (CTR) after gasification process in case of 100 sL/min air flow rate and 3 kW plasma power

Table A.38 EDX analysis results of ash of Şırnak (Turkey) coal (CTR) after gasification process in case of 100 sL/min air flow rate and 3 kW plasma power

Element	Concentration	Units
C	19.2	wt.%
O	36.5	wt.%
Mg	0.43	wt.%
Al	6.9	wt.%
Si	18	wt.%
S	2.3	wt.%
K	4.7	wt.%
Ca	8	wt.%
Ti	0.49	wt.%
Fe	1.4	wt.%
Cu	0.9	wt.%
Zn	0.78	wt.%

A3.7 Scanning Electron Microscope (SEM) and Energy Dispersive X-ray (EDX) analysis results of Polyethylene (PP) ash after gasification

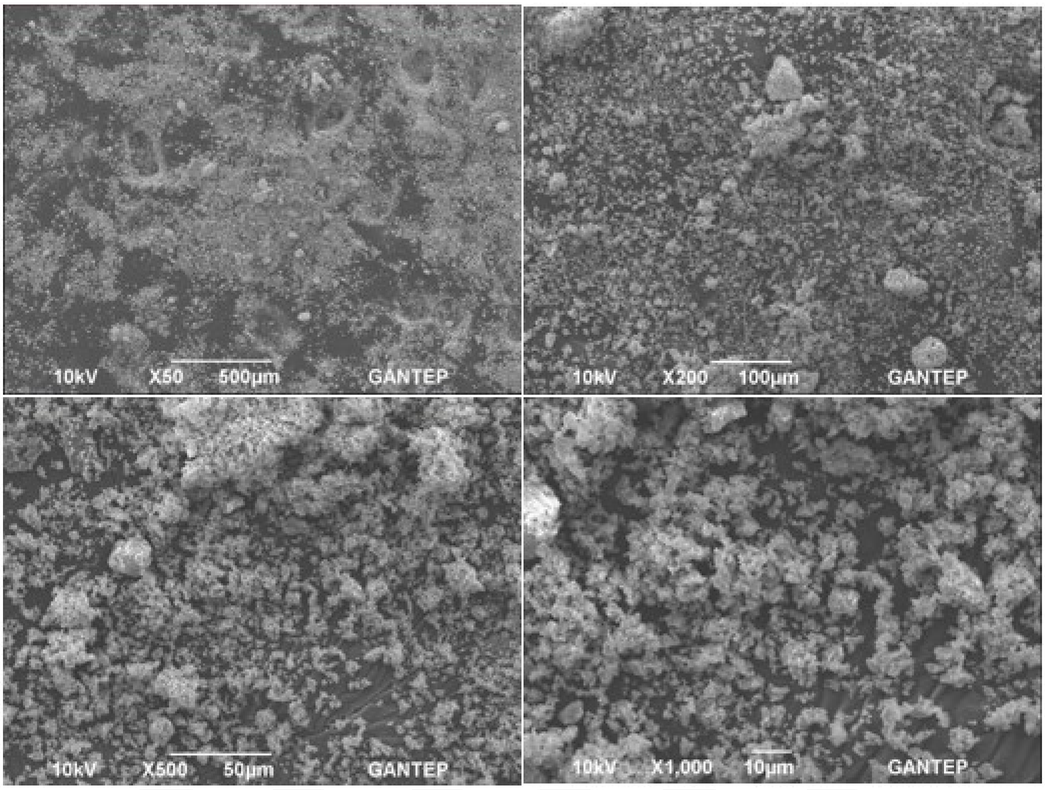

Figure A.26 SEM analysis results of ash of Polyethylene (PP) after gasification process in case of 50 sL/min air flow rate and 6kW plasma power

Table A.39 EDX analysis results of ash of Polyethylene (PP) after gasification process in case of 50 sL/min air flow rate and 6kW plasma power

Elt.	Concentration	Units
C	4.2	wt.%
O	42.2	wt.%
Mg	0.6	wt.%
Al	0.5	wt.%
Si	0.6	wt.%
Ca	34.5	wt.%
Ti	15.9	wt.%
Cu	1.4	wt.%

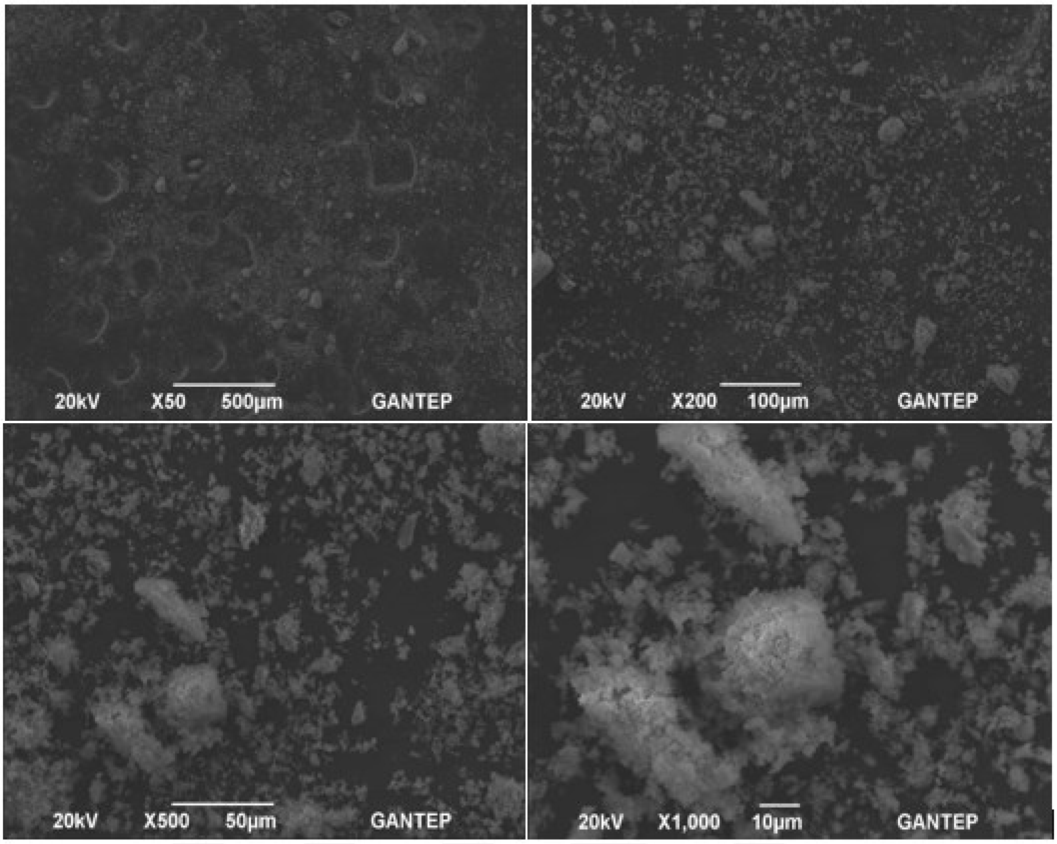

Figure A.27 SEM analysis results of ash of Polyethylene (PP) after gasification process in case of 50 sL/min air flow rate and 3 kW plasma power

Table A.40 EDX analysis results of ash of Polyethylene (PP) after gasification process in case of 50 sL/min air flow rate and 3 kW plasma power

Element	Concentration	Units
C	25.5	wt.%
O	43.8	wt.%
Mg	0.08	wt.%
Al	0.44	wt.%
Si	0.09	wt.%
S	0.14	wt.%
K	0.01	wt.%
Ca	28.2	wt.%
Ti	1.4	wt.%
Fe	0.04	wt.%
Cu	0.1	wt.%
Zn	0.12	wt.%

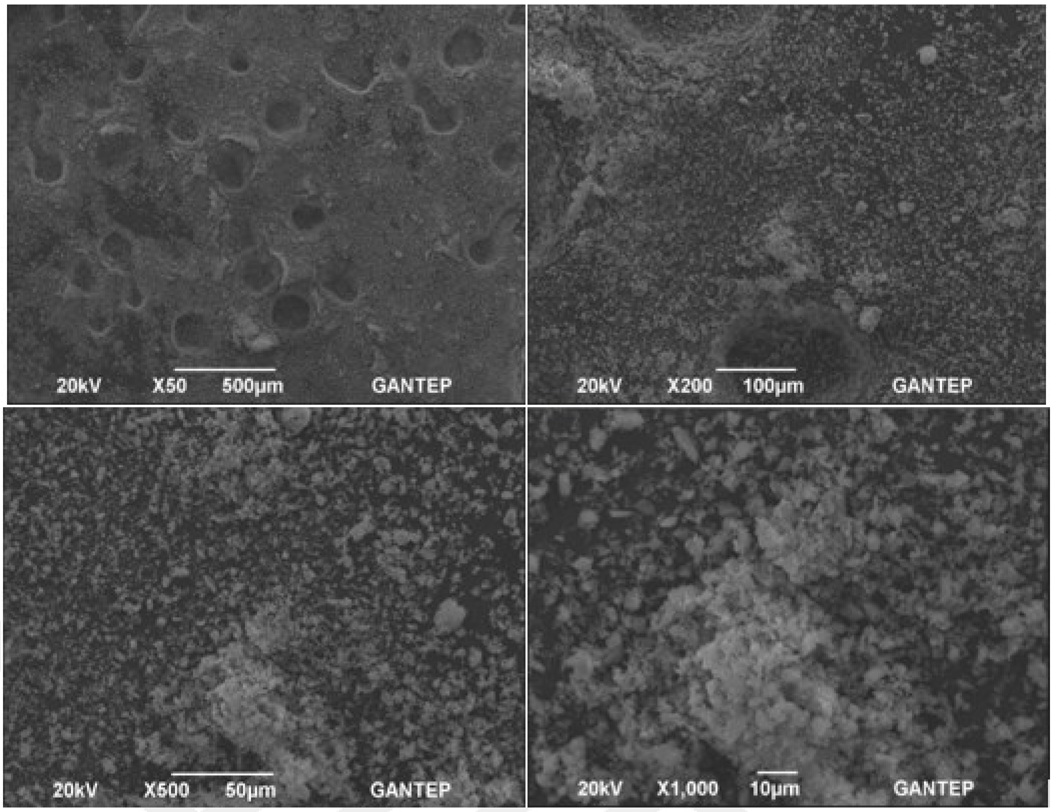

Figure A.28 SEM analysis results of ash of Polyethylene (PP) after gasification process in case of 100 sL/min air flow rate and 3 kW plasma power

Table A.41 EDX analysis results of ash of Polyethylene (PP) after gasification process in case of 100 sL/min air flow rate and 3 kW plasma power

Element	Concentration	Units
C	9	wt.%
O	50.3	wt.%
Mg	0.3	wt.%
Al	0.4	wt.%
Si	0.2	wt.%
S	0.15	wt.%
K	0.02	wt.%
Ca	29	wt.%
Ti	8.8	wt.%
Fe	0.1	wt.%
Cu	0.9	wt.%
Zn	0.67	wt.%

A-3 MRU- Varioplus gas analyzing unit sample results

Table A.42 MRU varioplus gas analyzing unit sample results

block	time	O_2,%	CO_2,%	CO,%	H_2,%	CH_4,%	N_2,%
1	4:03:06 PM	4.53	14.2	14.01	9.25	3.4	54.61
2	4:03:08 PM	4.38	15.1	15.69	9.3	3.33	52.2
3	4:03:10 PM	3.03	15.3	16.41	9.37	3.29	52.6
4	4:03:12 PM	2.55	15.7	16.19	9.48	3.25	52.83
5	4:03:14 PM	1.18	15.6	16.03	9.6	3.21	54.38
6	4:03:16 PM	1.03	15.5	16.97	10.66	3.2	52.64
7	4:03:18 PM	0.78	15.4	16.81	10.85	3.15	53.01
8	4:03:20 PM	0.64	15.3	16.73	10.95	3.14	53.24
9	4:03:22 PM	0.47	15.3	15.66	10.01	3.18	55.38
10	4:03:24 PM	0.38	15.3	15.62	10.02	3.19	55.49
11	4:03:26 PM	0.18	15.6	15.48	9.98	3.22	55.54
12	4:03:28 PM	0.11	15.9	15.37	9.9	3.24	55.48
13	4:03:30 PM	0.07	16.2	15.23	9.79	3.25	55.46
14	4:03:32 PM	0.06	16.3	14.14	9.72	3.25	56.53
15	4:03:34 PM	0.04	16.7	13.8	9.48	3.24	56.74
16	4:03:36 PM	0.04	16.8	14.56	9.28	3.22	56.1
17	4:03:38 PM	0.03	17	14.29	9.48	3.19	56.01
18	4:03:40 PM	0.03	17.2	12	9.85	3.18	57.74
19	4:03:42 PM	0.02	17.3	12.83	9.73	3.26	56.86
20	4:03:44 PM	0.03	17.7	12.29	9.41	3.42	57.15
21	4:03:46 PM	0.03	17.9	11.93	9.25	3.46	57.43
22	4:03:48 PM	0.04	17.9	11.56	9.12	3.67	57.71
23	4:03:50 PM	0.04	17.8	11.39	9.08	3.94	57.75
24	4:03:52 PM	0.03	17.6	10.93	8.98	3.85	58.61
25	4:03:54 PM	0.03	17.3	10.69	8.94	3.42	59.62
26	4:03:56 PM	0.03	18.1	10.5	8.71	3.21	59.45
27	4:03:58 PM	0.02	18.1	10.37	8.48	3.14	59.89
28	4:04:00 PM	0.02	18.1	10.3	8.17	2.98	60.43
29	4:04:02 PM	0.03	18.1	10.16	7.83	2.75	61.13
30	4:04:04 PM	0.08	18.1	10.08	7.8	2.72	61.22
31	4:04:06 PM	0.12	18.1	10.01	7.78	2.7	61.29
32	4:04:08 PM	0.18	18.1	9.94	7.75	2.7	61.33
33	4:04:10 PM	0.25	18.1	9.87	7.73	2.69	61.36
34	4:04:12 PM	0.27	16.7	11.24	7.26	2.68	61.85

35	4:04:14 PM	0.24	17	10.72	7.05	2.57	62.42
36	4:04:16 PM	0.14	17.1	10.42	6.98	2.55	62.81
37	4:04:18 PM	0.1	17.3	10.63	6.81	2.54	62.62
38	4:04:20 PM	0.12	17.5	10.22	6.71	2.49	62.96
39	4:04:22 PM	0.14	17.6	10.87	6.62	2.46	62.31
40	4:04:24 PM	0.17	17.7	10.57	6.54	2.51	62.51
41	4:04:26 PM	0.19	17.8	10.29	6.47	2.46	62.79
42	4:04:28 PM	0.21	17.8	10.08	6.4	2.44	63.07
43	4:04:30 PM	0.23	17.9	9.89	6.34	2.4	63.24
44	4:04:32 PM	0.23	17.9	9.71	6.28	2.47	63.41
45	4:04:34 PM	0.26	18	9.61	6.26	2.36	63.51
46	4:04:36 PM	0.29	18	9.36	6.19	2.41	63.75
47	4:04:38 PM	0.31	18.1	9.21	6.16	2.39	63.83
48	4:04:40 PM	0.33	18.1	8.89	6.14	2.36	64.18
49	4:04:42 PM	0.26	18.1	8.62	6.12	2.24	64.66
50	4:04:44 PM	0.3	18.1	8.48	6.1	2.23	64.79
51	4:04:46 PM	0.4	18.1	8.09	6.09	2.21	65.11
52	4:04:48 PM	0.44	18.1	8.09	6.09	2.2	65.08
53	4:04:50 PM	0.46	18.1	8.08	6.08	2.38	64.9
54	4:04:52 PM	0.47	18.1	8.08	6.08	2.18	65.09
55	4:04:54 PM	0.5	18.1	8.08	6.08	2.17	65.07
56	4:04:56 PM	0.51	18.1	8.08	6.08	2.17	65.06
57	4:04:58 PM	0.53	18.1	8.1	6.1	2.17	65
58	4:05:00 PM	0.54	18.1	8.16	6.16	2.17	64.87
59	4:05:02 PM	0.55	18.1	8.2	6.2	2.19	64.76
60	4:05:04 PM	0.59	18	8.35	6.35	2.24	64.47
61	4:05:06 PM	0.62	17.9	8	6.42	2.06	65
62	4:05:08 PM	0.65	17.8	8.15	6.47	2.09	64.84
63	4:05:10 PM	0.67	17.8	8.22	6.48	2.09	64.74
64	4:05:12 PM	0.7	17.7	8.35	6.5	2.09	64.66
65	4:05:14 PM	0.71	17.7	8.39	6.51	2.09	64.6
66	4:05:16 PM	0.71	17.6	8.4	6.51	2.07	64.71
67	4:05:18 PM	0.71	17.6	8.4	6.5	2.06	64.73
68	4:05:20 PM	0.7	17.6	8.39	6.5	2.06	64.75
69	4:05:22 PM	0.53	17.6	8.35	6.45	2.04	65.03
70	4:05:24 PM	0.37	17.6	8.31	6.38	2.01	65.33
71	4:05:26 PM	0.27	17.6	8.25	6.27	1.97	65.64

72	4:05:28 PM	0.24	17.7	8.12	6.16	1.93	65.85
73	4:05:30 PM	0.23	17.8	7.93	6.08	1.87	66.09
74	4:05:32 PM	0.27	17.9	7.75	6.01	1.86	66.21
75	4:05:34 PM	0.33	18	7.58	5.96	1.84	66.29
76	4:05:36 PM	0.41	18	7.44	5.92	1.81	66.42
77	4:05:38 PM	0.46	18.1	7.36	5.91	1.8	66.37
78	4:05:40 PM	0.42	18.1	7.16	5.87	1.76	66.69
79	4:05:42 PM	0.29	18.1	7.05	5.86	1.75	66.95
80	4:05:44 PM	0.15	18.1	6.98	5.86	1.75	67.16
81	4:05:46 PM	0.09	18.1	6.92	5.92	1.74	67.23
82	4:05:48 PM	0.03	18.1	6.92	5.99	1.75	67.21
83	4:05:50 PM	0.11	17.9	7.15	5.33	1.97	67.54
84	4:05:52 PM	0.27	17.7	7.56	5.59	2.16	66.72
85	4:05:54 PM	0.43	17.6	8.11	5.82	2.35	65.69
86	4:05:56 PM	0.57	17.5	8.41	5.93	2.42	65.17
87	4:05:58 PM	0.66	17.3	7.28	6.19	2.64	65.93
88	4:06:00 PM	0.73	17.2	7.76	6.35	2.71	65.25
89	4:06:02 PM	0.77	17.1	8.21	6.49	2.84	64.59
90	4:06:04 PM	0.86	17	8.65	6.61	2.95	63.93
91	4:06:06 PM	0.91	16.9	8.91	6.67	3	63.61
92	4:06:08 PM	0.94	16.8	9.65	6.79	3.14	62.68
93	4:06:10 PM	0.9	16.7	10.1	6.8	3.22	62.28
94	4:06:12 PM	0.74	16.7	10.45	6.7	3.27	62.14
95	4:06:14 PM	0.49	16.8	10.56	6.49	3.18	62.48
96	4:06:16 PM	0.25	16.9	10.35	6.26	3.01	63.23
97	4:06:18 PM	0.09	17	9.95	6.05	2.93	63.98
98	4:06:20 PM	0.04	17.1	9.44	6.88	2.77	63.77
99	4:06:22 PM	0.01	17.2	8.94	6.73	2.63	64.49
100	4:06:24 PM	0.06	17.3	8.66	6.67	2.57	64.74
101	4:06:26 PM	0.13	17.4	8.91	6.51	2.39	64.66
102	4:06:28 PM	0.19	17.5	8.5	6.42	2.3	65.09
103	4:06:30 PM	0.23	17.5	9.13	6.34	2.19	64.61
104	4:06:32 PM	0.34	17.6	8.81	6.27	2.11	64.87
105	4:06:34 PM	0.4	17.6	8.66	6.24	2.06	65.04
106	4:06:36 PM	0.46	17.6	8.27	6.16	1.98	65.53
107	4:06:38 PM	0.52	17.6	8.08	6.11	1.91	65.78
108	4:06:40 PM	0.58	17.6	7.91	6.06	1.86	65.99

109	4:06:42 PM	0.62	17.6	7.76	6.03	1.8	66.19
110	4:06:44 PM	0.64	17.5	7.61	6	1.75	66.5
111	4:06:46 PM	0.63	17.5	7.49	5.98	1.71	66.69
112	4:06:48 PM	0.63	17.4	7.41	5.95	1.67	66.94
113	4:06:50 PM	0.62	17.4	7.33	5.93	1.63	67.09
114	4:06:52 PM	0.63	17.4	7.29	5.91	1.62	67.15
115	4:06:54 PM	0.64	17.3	7.18	5.89	1.56	67.43
116	4:06:56 PM	0.65	17.3	7.22	5.88	1.53	67.42
117	4:06:58 PM	0.67	17.3	7.27	5.88	1.52	67.36
118	4:07:00 PM	0.68	17.3	7.35	5.9	1.52	67.25
119	4:07:02 PM	0.72	17.2	7.35	5.92	1.52	67.29
120	4:07:04 PM	0.73	17.2	7.41	6	1.53	67.13
121	4:07:06 PM	0.73	17.2	7.48	6.05	1.55	66.99
122	4:07:08 PM	0.73	17.2	7.69	6.14	1.55	66.69
123	4:07:10 PM	0.75	17.1	7.83	6.12	1.56	66.64
124	4:07:12 PM	0.78	17.1	7.85	6.17	1.58	66.52
125	4:07:14 PM	0.81	17.1	7.91	6.21	1.59	66.38
126	4:07:16 PM	0.83	17.1	8.55	6.24	1.59	65.69
127	4:07:18 PM	0.85	17.2	8.58	6.28	1.6	65.49
128	4:07:20 PM	0.94	17.1	8.59	6.29	1.6	65.48
129	4:07:22 PM	1.04	17.1	8.63	6.35	1.6	65.28
130	4:07:24 PM	1.15	17.1	8.65	6.37	1.6	65.13
131	4:07:26 PM	1.22	17.1	8.66	6.37	1.79	64.86
132	4:07:28 PM	1.13	17.1	8.65	6.37	1.78	64.97
133	4:07:30 PM	1.03	17.1	8.57	6.36	1.64	65.3
134	4:07:32 PM	0.93	17.1	9.47	6.36	1.62	64.52
135	4:07:34 PM	0.87	17	9.37	6.37	1.59	64.8
136	4:07:36 PM	0.84	17	9.29	6.38	1.67	64.82
137	4:07:38 PM	0.78	17.2	9.26	6.39	1.66	64.71
138	4:07:40 PM	0.75	16.7	9.2	6.4	1.65	65.3
139	4:07:42 PM	0.72	16.7	9.17	6.42	1.62	65.37
140	4:07:44 PM	0.71	16.5	9.15	6.43	1.62	65.59
141	4:07:46 PM	0.68	16.2	9.15	6.43	1.61	65.93
142	4:07:48 PM	0.67	15.6	9.14	6.44	1.59	66.56
143	4:07:50 PM	0.66	15.6	9.13	6.43	1.57	66.61
144	4:07:52 PM	0.65	15.8	9.12	6.44	1.56	66.43
145	4:07:54 PM	0.64	15.9	9.11	6.44	1.55	66.36

146	4:07:56 PM	0.63	15.9	9.1	6.43	1.55	66.39
147	4:07:58 PM	0.55	15.8	9.09	6.42	1.56	66.58
148	4:08:00 PM	0.59	15.7	9.07	6.39	1.56	66.69
149	4:08:02 PM	0.62	15.5	9.04	6.35	1.56	66.93
150	4:08:04 PM	0.65	15.4	8.01	6.32	1.56	68.06
151	4:08:06 PM	0.68	15.4	8.91	6.24	1.55	67.22
152	4:08:08 PM	0.72	15.4	8.82	6.18	1.54	67.34
153	4:08:10 PM	0.75	15.5	8.72	6.11	1.54	67.38
154	4:08:12 PM	0.95	15.6	8.62	6.07	1.53	67.23
155	4:08:14 PM	1.13	15.7	8.55	6.12	1.54	66.96
156	4:08:16 PM	1.32	15.8	8.54	6.24	1.59	66.51
157	4:08:18 PM	1.4	15.9	8.68	6.36	1.52	66.14
158	4:08:20 PM	1.62	16.1	8.92	6.41	1.59	65.36
159	4:08:22 PM	1.76	15.5	8.07	6.41	1.6	66.66
160	4:08:24 PM	1.89	15.4	8.38	6.37	1.62	66.34
161	4:08:26 PM	2.02	15.3	8.45	6.34	1.62	66.27
162	4:08:28 PM	2.13	15.3	8.65	6.31	1.61	66
163	4:08:30 PM	2.23	15.2	8.94	6.29	1.6	65.74
164	4:08:32 PM	2.31	15.1	9.41	6.28	1.59	65.31
165	4:08:34 PM	2.4	15	9.39	6.26	1.59	65.36
166	4:08:36 PM	2.44	14.9	9.37	6.22	1.59	65.48
167	4:08:38 PM	2.53	14.9	9.35	6.16	1.59	65.47
168	4:08:40 PM	2.56	14.8	9.34	6.01	1.59	65.7
169	4:08:42 PM	2.64	14.8	9.14	6.7	1.43	65.29
170	4:08:44 PM	2.84	14.9	9.83	6.58	1.31	64.54
171	4:08:46 PM	3.06	15.2	9.46	6.55	1.24	64.49
172	4:08:48 PM	3.25	15.4	9.15	6.71	1.21	64.28
173	4:08:50 PM	3.36	15.5	9.06	6.68	1.33	64.07
174	4:08:52 PM	3.42	15.3	9.31	6.46	1.59	63.92
175	4:08:54 PM	3.45	15.4	9.9	6.52	1.86	62.87
176	4:08:56 PM	3.47	15.5	9.72	6.84	2.06	62.41
177	4:08:58 PM	3.57	15.4	9.16	6.91	2.14	62.82
178	4:09:00 PM	3.65	15.4	9.38	7.06	2.29	62.22
179	4:09:02 PM	3.47	15.3	9.04	7.22	2.39	62.58
180	4:09:04 PM	3.18	15.1	9.62	7.34	2.45	62.31
181	4:09:06 PM	3.08	15.1	10.19	7.43	2.51	61.69
182	4:09:08 PM	3.3	14.9	10.48	7.47	2.55	61.3

183	4:09:10 PM	3.47	14.8	11.28	7.55	2.62	60.28
184	4:09:12 PM	3.63	14.8	11.79	7.45	2.65	59.68
185	4:09:14 PM	3.75	14.7	12.2	7.15	2.63	59.57
186	4:09:16 PM	3.82	14.7	12.28	6.96	2.55	59.69
187	4:09:18 PM	3.87	14.6	11.96	6.82	2.29	60.46
188	4:09:20 PM	3.92	14.6	11.55	6.89	2.28	60.76
189	4:09:22 PM	3.95	14.6	11.34	6.87	2.3	60.94
190	4:09:24 PM	4.14	14.5	11.38	7.04	2.31	60.63
191	4:09:26 PM	4.2	14.5	11.44	7.1	2.31	60.45
192	4:09:28 PM	4.22	14.4	11.7	7.2	2.29	60.19
193	4:09:30 PM	4.25	14.4	11.86	7.21	2.28	60
194	4:09:32 PM	4.27	14.4	11.97	7.19	2.26	59.91
195	4:09:34 PM	4.33	14.3	12	7.15	2.25	59.97
196	4:09:36 PM	4.37	14.3	11.94	7.11	2.34	59.94
197	4:09:38 PM	4.4	14.1	11.82	7.06	2.34	60.28
198	4:09:40 PM	4.46	14.1	11.66	6.9	2.31	60.57
199	4:09:42 PM	4.53	14	11.47	6.55	2.3	61.15
200	4:09:44 PM	4.57	14	11.32	6.32	2.23	61.56
201	4:09:46 PM	4.65	13.9	10.49	6.54	1.99	62.43
202	4:09:48 PM	4.7	13.9	9.6	6.15	1.79	63.86
203	4:09:50 PM	4.75	13.9	8.61	5.9	1.68	65.16
204	4:09:52 PM	4.72	13.2	7.74	5.75	1.62	66.97
205	4:09:54 PM	4.81	13	7.37	5.71	1.6	67.51
206	4:09:56 PM	4.87	11.2	7.53	5.64	1.58	69.18
207	4:09:58 PM	4.82	10.1	6.15	5.62	1.56	71.75
208	4:10:00 PM	4.86	9.9	5.9	5.62	1.48	72.24
209	4:10:02 PM	5.01	9	5.66	5.63	1.34	73.36
210	4:10:04 PM	5.08	8.1	5.61	5.63	1.32	74.26

CURRICULUM VITAE

PERSONAL INFORMATION

Name and surname: Aytaç Şanlısoy

Nationality: Turkish

Birth place and date: Tarsus – 16.07.1989

Marriage status: Married

Phone number: 00905349485684

Email: aytacsanlisoy@gmail.com / aytacsanlisoy@gantep.edu.tr

EDUCATION

Degree	Graduated school	Graduation year
Master	Ömer Halisdemir University (Niğde University),	2013
Bachelor	Ömer Halisdemir University (Niğde University),	2011
High School	Cumhuriyet High School	2006

WORK EXPERIENCE

Period	Place	Position
2015-	Gaziantep University, Mechanical. Engineering. Department	Project Assitant
2014-	Gaziantep University, Mechanical Engineering Department	Research Asistant
2012-2013	Ömer Halis Demir University (Niğde University), Mechatronic Engineering Department	Reserarch Assitant

2011-2013 Ömer Halis Demir University (Niğde University), Mechanical Engineering Department Project Assitant

CONFERANCES AND PUBLICATIONS

Akansu, Y. E., Karakaya, F., Şanlısoy, A. (2013) Active Control of Flow around NACA 0015 Airfoil by Using DBD Plasma Actuator EPJ Web of Conferances, 45, 01029.

Sanlisoy, A., & Carpinlioglu, M. (2015). Thermodynamic analysis of plasma gasification systems. Paper presented at the 18 th IFRF Members' Conference – Flexible and clean fuel conversion in industry, Germany.

Sanlisoy, A., & Carpinlioglu, M. O. (2016). Presentation of a microwave plasma gasification system "Mw gasifier" Paper presented at the Fourth European Conference on Renewable Energy Systems (ECRES2016), Istanbul.

Sanlisoy, A., & Carpinlioglu, M. O. (2016). A Review on Plasma Gasification for Solid Waste Disposal. Paper presented at the 4th International Conferance on Renewable Energy Generation and Application, France.

Sanlisoy, A., & Carpinlioglu, M. O. (2016). A review on plasma gasification for solid waste disposal. International Journal of Hydrogen Energy 2017:42:1361-5.

Sanlisoy, A., & Carpinlioglu, M. O. (2017). Preliminary measurements on microwave plasma flame for gasification. Energy, Ecology and Environment. 2018:3:32-8

Sanlisoy, A, & Carpinlioglu, M. O. (2017). A Case Study for the Gasification of Hornbeam Sawdust by an Atmospheric Air Microwave Discharge Plasma. Paper presented at the International Conference on Research and Applications of Plasmas (PLASMA 2017), Poland.

Carpinlioglu, M. O., & Sanlisoy, A. (2017). Performance of a Microwave Plasma Gasification System used for the Energy Conversion of Solid Wastes. Paper presented at the International Conference on Research and Applications of Plasmas (PLASMA 2017), Poland.

Sanlisoy, A, & Carpinlioglu, M. O. (2017). Characteristics of the Solid Fuels for the Plasma Gasification. Paper presented at the 4th International Conference on Power and Energy Systems Engineering, CPESE 2017, Germany.

Sanlisoy, A, & Carpinlioglu, M. O. (2017). Characteristics of the Solid Fuels for the Plasma Gasification. Energy Procedia 2017: 141: 282-6.

Carpinlioglu M, Sanlisoy A. Performance assessment of plasma gasification for waste to energy conversion: A methodology for thermodynamic analysis. International Journal of Hydrogen Energy 2018: 43: 11493-504

Sanlisoy, A, & Carpinlioglu, M. O. (2018). Microwave plasma gasification performance in case of handling coals. Paper presented at the 4th Anatolian Energy Symposium with International Participation, AES 2018, Edirne.

LANGUAGE SKILLS

English- Yokdil- grade 85

Czech - Beginner

HOBBIES

Trevelling, swimming and trekking.